GM 54950

EVALUATION REPORT, MANICOUAGAN PROPERTIES

Documents complémentaires

Additional Files



Licence

License

Cette première page a été ajoutée
au document et ne fait pas partie du
rapport tel que soumis par les auteurs.

Énergie et Ressources naturelles
Québec

MINERAUX MANIC INC.

EVALUATION REPORT

MANICOUAGAN PROPERTIES

MANICOUAGAN AREA, QUÉBEC
NTS 22N/07, 22N/10, 22N/02

Prepared by

Luciano Vendittelli, B.Sc., APGGQ

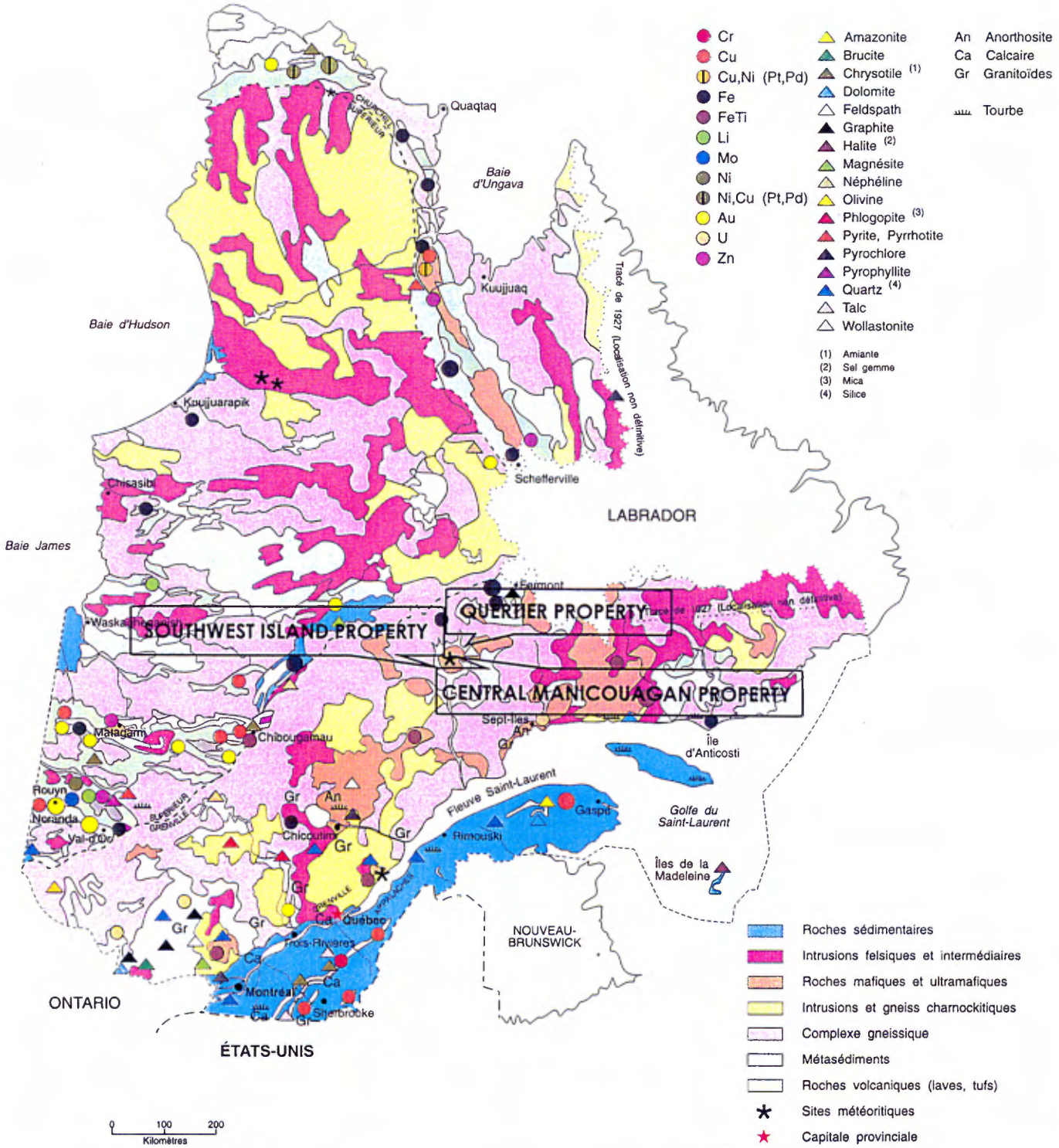
MRN - GÉOINFORMATION 1997
GM 54950

September 1997
Montreal, QC

'97 NOV 4 AM 11 03
BUREAU DU REGISTRAIRE
REÇU AU MRN
'97 NOV -3 15 :16

Gouvernement du Québec
Ministère de l'Énergie et des Ressources
Direction générale de l'Exploration géologique et minérale

CARTE MINÉRALE DU QUÉBEC, CANADA
MINERAL MAP OF QUÉBEC, CANADA



Représentation simplifiée de la carte originale à l'échelle de 1: 1 500 000

Centre de diffusion
5700, 4e Avenue ouest, local A-201
Charlesbourg (Québec) G1H 6R1
Téléphone: (418) 643-4601
Télécopieur: (418) 644-3814

FIGURE 1

Québec

Compilé par L. Avramtchev
Service d'information et de soutien à l'exploration minière

PRO 93-06
(Remplace le PRO 87-01)

Microfilm

PAGE DE DIMENSION HORS STANDARD

MICROFILMÉE SUR 35 MM ET

POSITIONNÉE À LA SUITE DES

PRÉSENTES PAGES STANDARDS

Numérique

PAGE DE DIMENSION HORS STANDARD

NUMÉRISÉE ET POSITIONNÉE À LA

SUITE DES PRÉSENTES PAGES STANDARDS

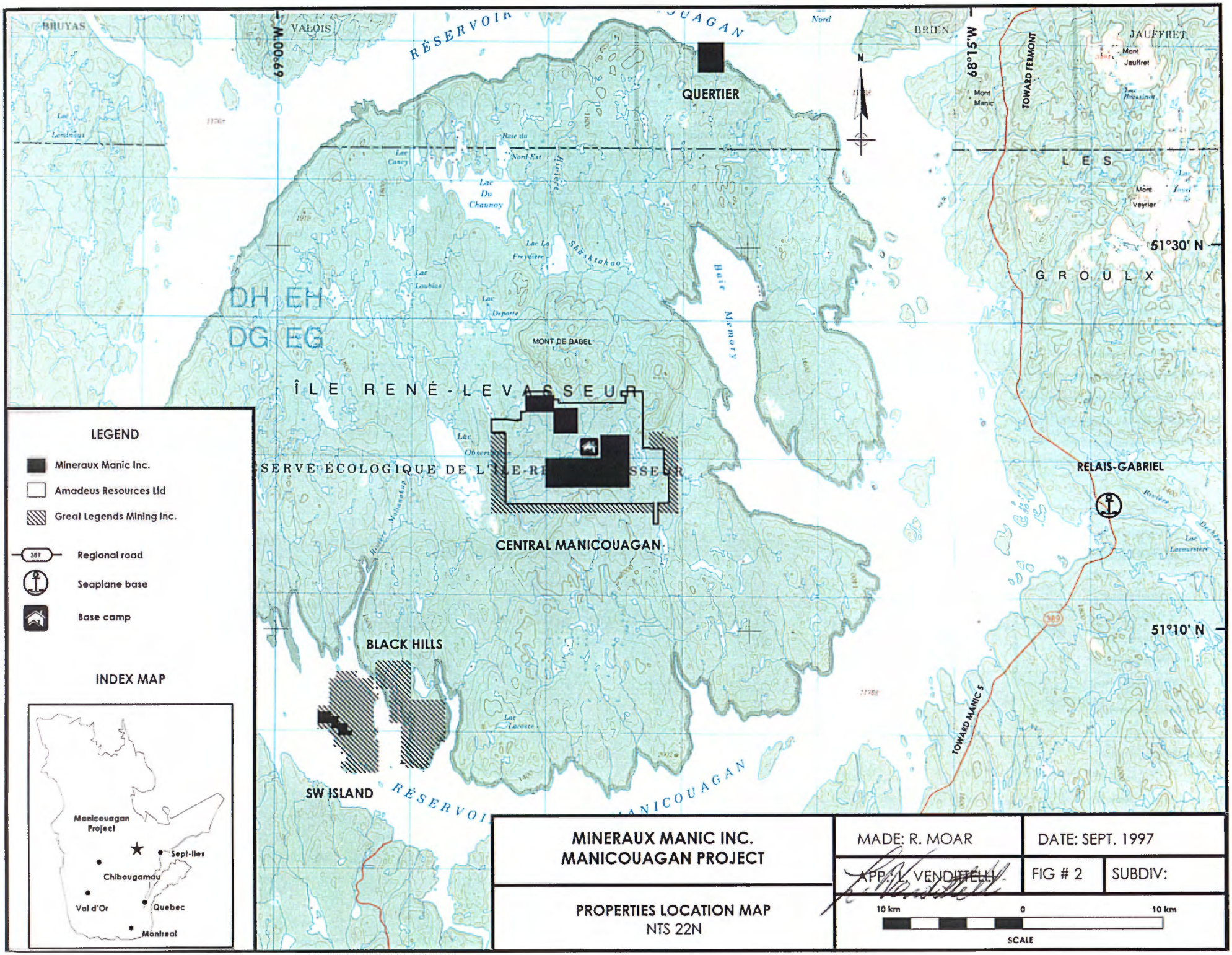

LEGEND
Mineraux Manic Inc.
Amadeus Resources Ltd
Great Legends Mining Inc.
389
Regional road
Seaplane base
Base camp
INDEX MAP
Manicouagan Project
Sept-Iles
Chibougamau
Val d'Or
Quebec
Montreal
QUERTIER
CENTRAL MANICOUAGAN
BLACK HILLS
SW ISLAND
MONT DE BABEL
ÎLE RENÉ-LEVASSEUR
RELAIS-GABRIEL
TOWARD FERMONT
TOWARD MANIC 5
68°15'W
69°00'W
51°30' N
51°10' N
N
10 km
0
10 km
SCALE
MINERAUX MANIC INC.
MANICOUAGAN PROJECT
PROPERTIES LOCATION MAP
NTS 22N
MADE: R. MOAR
DATE: SEPT. 1997
APP: L. VENDITTELLI
FIG # 2
SUBDIV:

TABLE OF CONTENTS

SUMMARY 6

1.0 LOCATION AND PHYSIOGRAPHY 9

2.0 PROPERTY DESCRIPTION 12
- 2.1 CENTRAL MANICOUAGAN PROPERTY 12
- 2.2 QUERTIER PROPERTY 15
- 2.3 SOUTHWEST ISLAND PROPERTY 17

3.0 REGIONAL GEOLOGY 19

4.0 PROPERTY GEOLOGY AND MINERALIZATION 27
- 4.1 CENTRAL MANICOUAGAN PROPERTY 27
- 4.2 QUERTIER PROPERTY 30
- 4.3 SOUTHWEST ISLAND PROPERTY 32

5.0 SOME PREVIOUS WORK BY OTHER WORKERS 34

6.0 PREVIOUS EXPLORATION WORK 39
- 6.1 CENTRAL MANICOUAGAN PROPERTY 40
- 6.2 QUERTIER PROPERTY 58
- 6.3 SOUTHWEST ISLAND PROPERTY 63

7.0 GENERAL DISCUSSION 66
- 7.1 GENERAL DISCUSSION OF THE MANICOUAGAN IMPACT 66
- 7.2 MINERALIZATION MODELS FOR THE MANICOUAGAN IMPACT SITE 67

8.0 CONCLUSIONS AND RECOMMENDATIONS 70
- 8.1 CENTRAL MANICOUAGAN PROPERTY 71
- 8.2 QUERTIER PROPERTY 72
- 8.3 SOUTHWEST ISLAND PROPERTY 73

9.0 RECOMMENDED WORK AND COSTS 74
9.1 CENTRAL MANICOUAGAN PROPERTY 74
9.2 QUERTIER PROPERTY 77
9.3 SOUTHWEST ISLAND PROPERTY 78

10.0 REFERENCES 80

LIST OF FIGURES

Fig. 1 Mineral map Of Quebec 2
Fig. 2 Properties location map 10
Fig. 3 Central Manicouagan Property - Claims map 13
Fig. 4 Quertier Property - Claims map 16
Fig. 5 Southwest Island Property - Claims map 18
Fig. 6 Simplified geologic map of the Manicouagan structure 24
Fig. 7 Total magnetic field Aerodat Ltd - Central Manicougan Property 41
Fig. 8 Compilation map - Quertier Property 60
Fig. 9 1991 VLF-EM (NSS) Survey - Quertier Property 61
Fig. 10 Sample location - Southwest Island Property 65

LIST OF TABLES

Table 1 Table of Formation 20
Table 2 Lines covered by the EM-MaxiProbe in 1990 - Central Manicouagan Property 44
Table 3 Results of the EM-MaxiProbe survey performed in 1990- Central Manicouagan Property 46
Table 4 Lines covered by the MaxiProbe-EM survey in 1996 - Central Manicouagan Property 49
Table 5 Results of EM-MaxiProbe survey performed in 1996 - Central Manicouagan Property 50
Table 6 Lines covered by the Melis survey in 1997 - Central Manicouagan Property .. 52
Table 7 Assay results on the original Cu-Ni-PGE showing - Quertier Property 58
Table 8 Assay results of prospecting and mapping work 1991- Quertier Property 59
Table 9 Lines covered by VLF(NSS)-EM survey in 1990 - Quertier Property 59
Table 10 Assay results of prospecting and mapping work 1990-1996- Southwest Island Property 63

ANNEXE I

CERTIFICATE OF QUALIFICATION

ANNEXE II

CORE LOG

ANNEXE III

CERTIFICATES OF ASSAYS

ANNEXE IV

SUPPLEMENTARY INFORMATION

Goodfellow, W., 1992. Giant Impacts : consequences for biological extinctions, global environments and ore formation; GEOS, Vol. 21, No. 1

Roest, W.R. and Pilkington, M., 1993. Identifying remanent magnetization effects in magnetic data; Geophysics, Vol. 58, No. 5

Information on iron meteorites

Grieve, R.A., and Masatitis, v.l., 1994. The Economic Potential of Terrestrial Impact Craters; International Geology Review, Vol. 36

ANNEXE V

SOME COMPANIES EXPLORATION RESULT

Boivin, L., 1990. Press Release: Manicouagan Crater - Ni/Cu Property

Boivin, L , 1994. Information Letter on the Manicouagan Project

Paterson, N.R., 1992. Communication on Modeling of the Magnetic Anomaly

Schultz, P. H., 1992. Communication on his assessment of the Manicouagan Property.

ANNEXE VI

INFORMATION ON THE MELIS METHOD

IN POCKET

COMPILATION MAP - CENTRAL MANICOUAGAN PROPERTY

SUMMARY

The Manicouagan crater area (100 km. wide) is the result of a hypervelocity meteorite impact which occurred about 200 million years ago when the area was located in the center of the only continent on earth. It can be considered in the same mega-size category as the Vredefort crater in South Africa (and the Bushveld complex as well, because evidence is mounting for its origins as a contemporaneous impact event with Vredefort) and the Sudbury crater in Canada. Both these craters are well-known for their world-class mining camp status and for the cratering event being largely responsible for the accumulation, if not the genesis of their mineral ores. A study of the inventory of terrestrial-based impact sites and their likelihood to host mineral deposits by Grieve and Masaitis in 1994 clearly indicates a much larger statistical probability of encountering economical mineral deposits in these contexts than in any other known general geological context. About 25 % of their inventory contain economic mineral deposits, half of which are being mined today or were mined in the past. We do not know how many of them have been explored. This study and its many implications are very little-known by today's exploration workers or geologists who are prospecting for ore deposits, but are very important, but not the most important considerations, in weighing the merits of the Manicouagan exploration play.

This report will serve as a descriptive outline of the geological environment of the Manicouagan crater area and as a summative evaluation of the relevant work done in the past in accumulating the data which is most pertinent to discuss the potential for finding economic mineralization. Recommendations and budgets for the next phases of exploration of Minéraux Manic Inc.'s (the Company) group of three claims blocks in the region is also provided. It is the opinion of the author that the claims groups have enormous merit for further evaluation considering the results of the more than $ 1,300,000 dollars worth of extremely conventional geological, geophysical, and reconnaissance and research work the Company has performed on its various claims blocks in the past.

The Company acquired the Central Manicouagan Property, 216 claims, in 1990, and then staked the northern Quertier claims group and the SW Island claims group, each of them located about 30 km. away in opposite directions from the central group, (but all of them in the interior limits of the crater) in subsequent years. This report covers all of the groups, collectively known for the purposes of this report, as the Manicouagan Property.

The Company acquired the Central Manicouagan claims group on the basis of a very unusual, extremely strong bulls-eye magnetic anomaly dead center in the crater, and this claims group (3 blocks) covers what appeared to be the best parts of the anomaly. Testing the cause of this anomaly,

which appears to be a buried body about 1.6 km. wide is the main focus of the Company's exploration program herein recommended. The remaining two claims blocks, Quertier and the SW Islands, were acquired on the basis of reconnaissance prospecting and the discovery of large surface areas of brecciated Cu-Ni-PGE mineralization on the Quertier claims, and massive sulphide veins (with Cu-Ni-PGE minerals) in post-impact ultra-mafic dykes on the SW Island claims. The similarity to the Sudbury Cu-Ni-PGE -bearing post-impact breccia dykes is obvious, although the impact was of different age and terrestrial conditions. Both the Sudbury region and the Manicouagan are similar in that they both were Grenvillean geological provinces already enriched in these elements prior to the impact.

QUERTIER PROPERTY

The Quertier Property presently consists of 42 contiguous claims of 16 hectares each covering a total surface area of 672 hectares in the Quertier Township (NTS Series 022N/10, Lac du Chaunoy) in the region of Manicouagan, Quebec. The property is located on the northeast shore of René-Levasseur Island in the Manicouagan crater approximately 30 km NNE of the company's base camp on its Central Property. All claims are owned 100% by Minéraux Manic Inc. and are in good standing.

The rocks making up the Quertier Property consist essentially of a series of garnetiferous paragneisses, of suevite and impact-brecciated mafic basement locally crosscut by a steeply dipping very fine grained ultramafic dyke with numerous tension fractures. This outcrop hosts the original nickel and copper showing, which precipitated the initial staking. Three grab samples were taken from the original showing and assayed for Au, Ag, Cu, Ni and PGE (Rh, Pt, Pd). The best values reported are 0.90% Cu, 0.27% Ni, 0.96 g/T Pt, 2.3 g/T Pd..

The interesting geological and metallogenic context of the property fully justifies a systematic exploration program in order to evaluate the economic potential of cupro-nickeliferous mineralization in impact-brecciated gneisses as well as in ultramafic intrusions crosscutting these gneisses. We recommend an exploration program for a total cost estimate of $181,220 aimed at studying and evaluating sulphide stringers cross-cutting the impact-breccias and the ultramafic intrusions from which mineralization seems to originate.

SOUTHWEST ISLAND PROPERTY

The Southwest Island Property is located in the southwestern part of the Manicouagan Reservoir, approximately 280 km from Baie-Comeau. Minéraux Manic Inc. holds 100% interest in a block of 11 mining claims. The property is located approximately 59 km north of Louise Lake seaplane base and 28 km southwest of the company's base camp on its Central Property. Minéraux Manic Inc.

holds 100% interest in a block of 11 contiguous mining claims (176 Ha). These claims were staked by the company in October 1996. All claims are in good standing. Reconnaissance work conducted in 1990 and in 1996 established the presence of ultramafic intrusive rocks mineralized in pyrrhotite (Po), pyrite (Py) and malachite (Ma). These intrusive rocks are devoid of impact related metamorphism. The presence of an ultramafic dyke on the property that does not show any evidence of shock metamorphism indicates post-impact magmatic activity suggesting the possibility of a magmatic cupro-nickeliferous (Cu-Ni) type of mineralization.

Therefore, with respect to the mineral potential of the Southwest Island Property, the author recommend that surface exploration work be undertaken on the Southwest Island Property adjacent to the Manicouagan Crater. A two-phased exploration program for a total cost of $96,235 is proposed. Exploration work will be aimed at determining the extent of the ultramafic dykes, their system of fractures and faults and associated sulfide mineralization

The exploration campaign on these properties and in this entire area is highly interesting and of definite merit.

I would like to thank Dr. Richard A.F. Grieve of the Geological Survey of Canada in Ottawa (GSC) for his useful comments and for access to his data base on the Manicouagan crater, Lauri Boivin, Roger Moar and Marlene MacKinnon for their help in the preparation of this report.

1.0 LOCATION AND PHYSIOGRAPHY

The Manicouagan Properties are divided into three groups, all of them located in the interior of the Manicouagan crater which is 300 km. due north form the city of Baie-Comeau on the northern shores of the St. Lawrence river in eastern Quebec. The groups are: the Central Manicouagan , the Quertier, and the Southwest Island properties (Fig. 2). All of the properties are accessible from the company's base camp situated in the the middle of René-Levasseur Island.

The regional highway 138 leads to Baie-Comeau, located at approximately 670 km from Montreal and at 400 km from Quebec. From Baie-Comeau, one takes the regional highway 389 north which links Baie-Comeau to Fermont, until one reaches the Manic 5 hydro dam, some 235 km. to the north of Baie-Comeau. A gravel road from there leads to a float plane and bush plane base 5 km. away. The Company's base camp is 80 km. from there, in the middle of the René-Levasseur Island and a flight would take about 40 minutes. If one prefers, one can drive all the way from the Manic 5 hydro dam, along the highway 389 to Relais-Gabriel, 120 km. away from Manic 5 and a short flight from this road would take about 15 minutes to reach the base camp.

The Central Manicouagan Property is located in the central part of the Province of Québec between latitude 51°20' N and 51°25' N and longitudes 68°45' W and 68°37' W (NTS 22N/07 Manicouagan Reservoir sheet).

The Quertier Property is located approximately 30 km NNE of the Company's base camp on its Central Property at Lac des Isles between latitude 51°36' and 51°38 and longitude 68°33' and 68°31'. (NTS 022N/10, Lac du Chaunoy).

The Southwest Island Property is located between latitude 51°11' and longitude 68°57' (NTS Series 022N/02, Lac Lacoste). The Southwest Island Property is located approximately 28 km SW of the company's base camp on its Central Property.

The crater interior is bounded by a circular reservoir created by the flooding of steep river beds surrounding one of the craters`rims after Hydro Quebec built the Manic 5 dam to the south.

Four physiographic features comprise the interior of the Manicouagan Impact Structure. An outer lowland lies just inside the reservoir. An annular plateau formed by nearly flat-lying Triassic igneous rocks is immediately inside, and topographically higher than, the outer highlands, and locally stepped, cliffs that culminate in bare vertical faces. The elevation of the highest parts of the plateau is about 715 m The third features is an inner lowland that lies between the annular plateau. The maximum elevation of the inner lowland is about 460 meters. The fourth feature is the central mountain, Mont de Babel. Mount rises about 460 m above the inner lowland with a highest peak at an elevation of 957 m above sea level

2.0 PROPERTY DESCRIPTION

2.1 CENTRAL MANICOUAGAN PROPERTY

Minéraux Manic Inc. holds 216 claims in the geographic center of René-Levasseur Island (Fig. 3) in the Manicouagan crater, approximately 300 kilometers North of Baie-Comeau (NTS Series 022N/07, Mont de Babel sheet). The claims are grouped in two blocks, one of 54 contiguous claims and another block of 162 contiguous claims. Each claim covers 16 hectares for a total of 4,391 Ha. The two blocks of claims are 2,400 meters apart. All claims are owned 100% by Minéraux Manic Inc. and are in good standing.

Expiry Date: 04 OCT 1997

Claim Numbers: TOTAL: 216

				5037519
5037520	5037521	5037522	5037523	5037524
5037525	5037526	5037527	5037528	5037529
5037530	5037531	5037532	5037533	5037534
5037535	5037536	5037537	5037538	5037539
5037540	5037541	5037542	5037543	5037544
5037545	5037546	5037547	5037548	5037549
5037550	5037551	5037552	5037553	5037554
5037555	5037556	5037557	5037558	5037559
5037560	5037561	5037562	5037563	5037564
5037565	5037566	5037567	5037568	5037569
5037570	5037571	5037572	5037573	5037574
5037575	5037576	5037577	5037578	5037579
5037580	5037581	5037582	5037583	5037584
5037585	5037586	5037587	5037588	5037589
5037590	5037591	5037592	5037593	5037594
5037595	5037596	5037597	5037598	5037599

5037600	5037601	5037602	5037603	5037604
5037605	5037606	5037607	5037608	5037609
5037610	5037611	5037612	5037613	5037614
5037615	5037616	5037617	5037618	5037619
5037620	5037621	5037622	5037623	5037624
5037625	5037626	5037627	5037628	5037629
5037630	5037631	5037632	5037633	5037634
5037635	5037636	5037637	5037638	5037639
5037640	5037641	5037642	5037643	5037644
5037645	5037646	5037647	5037648	5037649
5037650	5037651	5037652	5037653	5037654
5037655	5037656	5037657	5037658	5037659
5037660	5037661	5037662	5037663	5037664
5037665	5037666	5037667	5037668	5037669
5037670	5037671	5037672	5037673	5037674
5037675	5037676	5037677	5037678	5037679
5037680	5037681	5037682	5037683	5037684
5037685	5037686	5037687	5037688	5037689
5037690	5037691	5037692	5037693	5037694
5037695	5037696	5037697	5037698	5037699
5037700	5037701	5037702	5037703	5037704
5037705	5037706	5037707	5037708	5037709
5037710	5037711	5037712	5037713	5037714
5037715	5037716	5037717	5037718	5037719
5037720	5037721	5037722	5037723	5037724
5037725	5037726	5037727	5037728	5037729
5037730	5037731	5037732	5037733	5037734

2.2 QUERTIER PROPERTY

The Quertier Property (Fig. 4) presently consists of 42 contiguous claims of 16 hectares each covering a total surface area of 672 hectares in the Quertier Township (NTS Series, 022N/10, Lac du Chaunoy) in the region of Manicouagan, Quebec. In 1996, Minéraux Manic Inc. staked 12 claims bordering its block of 30 claims. All claims are owned 100% by Minéraux Manic Inc. and are in good standing.

QUERTIER PROPERTY (22N/10) CLAIMS.

Expiry Date: 08 OCT 1998

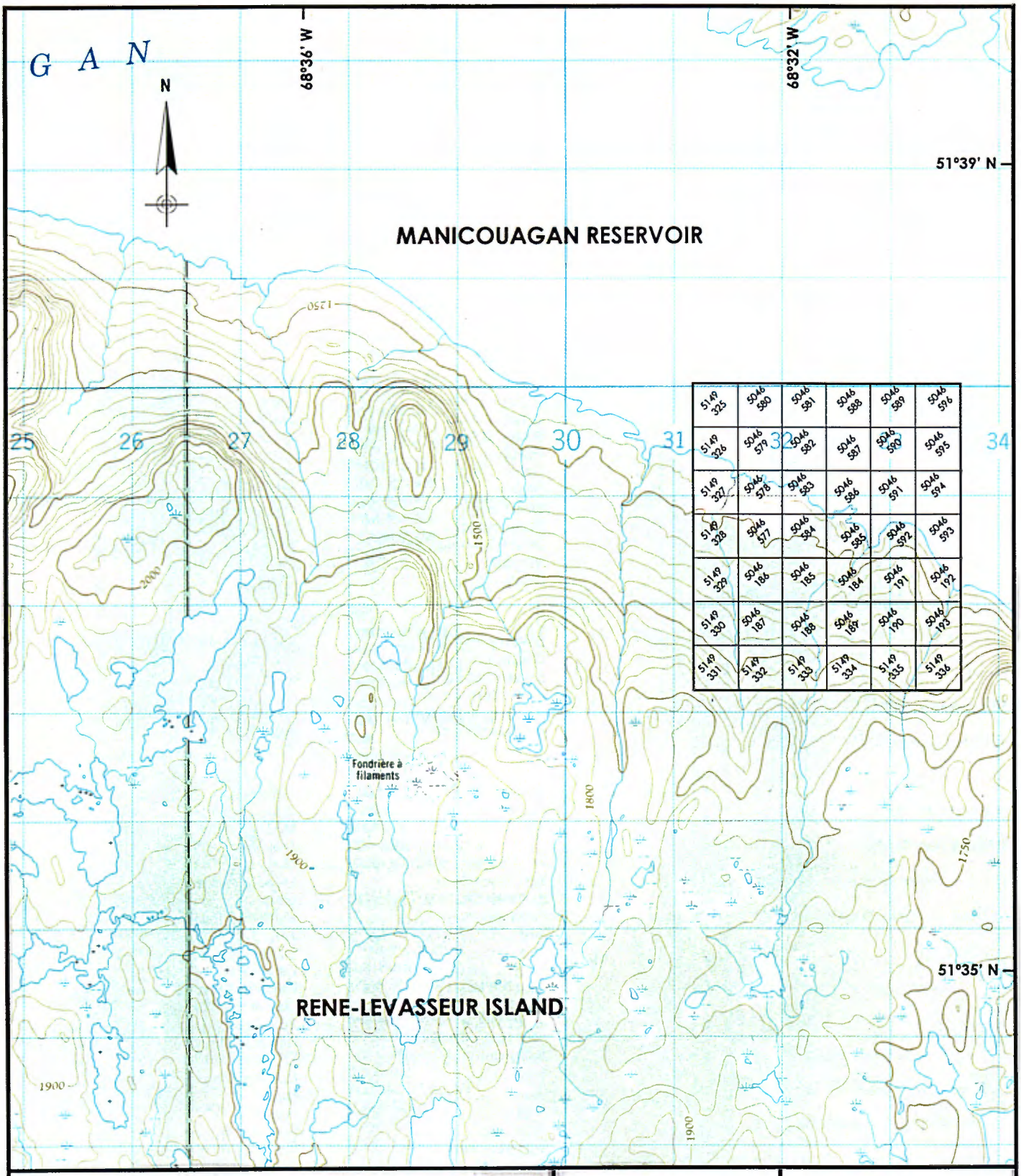
Claim Numbers: TOTAL: 30

5046184	5046185	5046186	5046187	5046188
5046189	5046190	5046191	5046192	5046193
5046577	5046578	5046579	5046580	5046581
5046582	5046583	5046584	5046585	5046586
5046587	5046588	5046589	5046590	5046591
5046592	5046593	5046594	5046595	5046596

Expiry Date: 20 OCT 1998

Claim Numbers: TOTAL: 12

5149325	5149326	5149327	5149328	5149329
5149330	5149331	5149332	5149333	5149334
5149335	5149326			



MINERAUX MANIC INC.
QUERTIER PROPERTY

MADE: R. MOAR

DATE: SEPT. 1997

APP'D: V. VENDITTELLI

FIG # 4

SUBDIV:

CLAIMS MAP
NTS 22N/10

1000 0 1000 2000 METRES

SCALE: 1:50 000

2.3 SOUTHWEST ISLAND PROPERTY

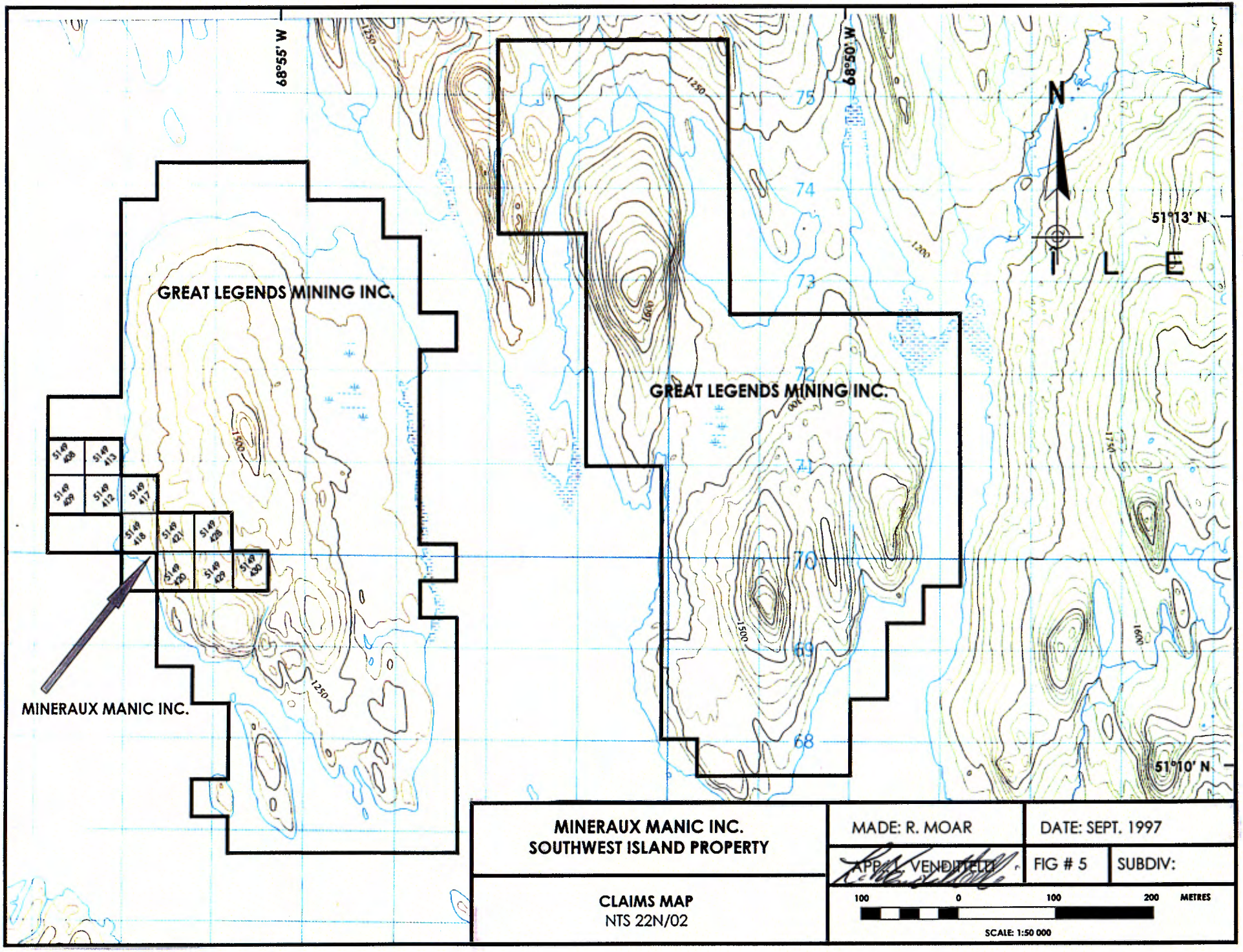
The Southwest Island Property (Fig. 5) presently consists of 11 contiguous claims of 16 hectares each covering a total surface area of 176 hectares in the southwestern part of Île René-Levasseur, region of Manicouagan (NTS Series, 022N/02, Lac Lacoste). These claims were first staked, prospected and sampled by the Company in 1990 and were staked again by the company in October 1996. All claims are owned 100% by Minéraux Manic Inc. and are in good standing

SOUTHWEST ISLAND PROPERTY (22N/02) CLAIMS

Expiry Date: 02 FEB 1999

Claims Numbers: TOTAL: 11

5149408	5149409	5149412	5149413	5149417
5149418	5149420	5149421	5149428	5149429
5149430				


68°55' W
68°50' W
51°13' N
51°10' N
N
GREAT LEGENDS MINING INC.
GREAT LEGENDS MINING INC.
MINERAUX MANIC INC.
75
74
73
72
71
70
69
68
1250
1500
1600
1750
1200
5149 408
5149 413
5149 409
5149 412
5149 417
5149 418
5149 421
5149 425
5149 420
5149 429
5149 400
MINERAUX MANIC INC.
SOUTHWEST ISLAND PROPERTY
CLAIMS MAP
NTS 22N/02
MADE: R. MOAR
DATE: SEPT. 1997
APP: L. VENDITTELLI
FIG # 5
SUBDIV:
100 0 100 200 METRES
SCALE: 1:50 000

3.0 REGIONAL GEOLOGY

The property is located within the Grenville structural province of the Canadian shield. On a regional scale the rocks are metamorphosed to upper amphibolite and locally granulite facies trending northeast-southwest. This structural fabric is interrupted by the Cretaceous-Tertiary meteor impact structure which created a unique suite of rocks.

Impacted rock consists of diverse Precambrian metamorphic and plutonic rocks; Ordovician sedimentary rocks; and their shock metamorphosed equivalents. Breccias (tagamites), impact melt, and suevite, and post-impact intrusive constitute the Triassic Manicouagan Complex.

According to Mu1taugh (1976), the relative ages of the Precambrian rocks as indicated in the Table of Formation (Table 1), is at best tentative. Problems arise from the polymetamorphic and multideformational history of the rocks; the reconnaissance nature of the geological mapping done; the abundant glacial and vegetative cover and consequent scarcity of good outcrops and exposures of contacts; the equivocal nature of contacts that were observed; and the paucity of absolute age dates available and the difficulty of interpreting those few dates.

The crater morphology and resultant geology is typical of large craters on Earth and on the Moon, and the reader may refer to a vast literature of expertise and research on the subject which is not usually in the scope of knowledge of most current workers in exploration, and which the author feels inadequate to represent with justice in the context of the present report. Suffice it to say that the regional stratigraphy underlying all the claims groups of the Manicouagan Properties are represented from top to bottom by:

1. Gradationally bedded suevite (fall-back breccia of basement rocks in fine-grained matrix)
2. Impact melt of monzonitic composition, also gradationally layered with larger fragments of basement rocks, and in some cases suevite, assimilated closer to the base units grading into finer more homogeneous grained higher units, which also may contain blocks or fragments of suevite.
3. Impact and post- impact mechanical brecciation of all units - tagamite
4. Post-impact ultramafic dykes and breccia dykes
5. Ordovician sedimentary rocks

Table 1 Table of Formation
(Modified after Murtaugh (1976))

AGE	UNIT	SUBUNIT AND LITHOLOGY
CENOZOIC (PLEISTOCENE, RECENT)	Glacial Deposits, Alluvium	Till, outwash, esker, glaciofluvial deposits; alluvium
MESOZOIC (TRIASSIC)	MANICOUAGAN COMPLEX	
	Contact metamorphosed country rocks	Contact metamorphosed by monzonite/latite. Rocks with decomposed mafic mineral, zeolitized rocks, hornfelsed anorthosite, melted and vesiculated gneissses
	Monzonite	Medium to coarse-grained brown, grey, or red massive rock with lath-shaped pyroxene phenocryst (may be younger than latite)
	Latite	Aphanitic to fine grained brown, red, or grey massive rocks; Medium-grained latite. May be part of mozonite unit or transitional between latite and monzonite.
	Basalt	Aphanitic black rock, locally glassy, locally vesicular. Red or greyish-black spherulitic rocks that grade to basalt, red breccia, and suevite
	Breccias	Autochthonous breccias. Rotated fragments in comminuted matrix. Suevite. Brown, green, or red polymict breccia with heterogeneous glasses and mixed shocked and unshocked fragments. Red breccia, nearly monomict breccia with heterogeneous glasses and shocked fragments. May be correlative with suevite. (pt) Pseudotachylite Rock of stage stages 0, I, II of Stoffler (1971) (See text)
PALEOZOIC (ORDOVICIAN)	Sedimentary rocks	Limestone; minor shale, siltstone.

Table 1 Table of Formation
(Modified after Murtaugh (1976))

AGE	UNIT	SUBUNIT AND LITHOLOGY
PRECAMBRIAN	Anorthosites	Metamorphosed garnetiferou anorthosites, minor gabbroic anorthosite including minor peridotites, pegmatites, and breccia pipe. Mont de Babel anorthosite
	Granitic gneiss	Undiffentiated granitic gneiss, minor granite, probably of several age. Mixed granitic gneiss and grey gneiss
	Grey gneiss complex	Hornblende-biotite-quartz-feldspar gneisses, commonly garnetiferous, locally with sillimanite or kyanite. Metamorphosed mafic and ultramafic rocks.

6. Basement Grenvillean gneisses and anorthositic 'uplifted' Rocks

All basements units have undergone various shock metamorphism and other processes from the impact event. The above units have been mapped and identified by L. Boivin during the past 5 field seasons. They differ somewhat from the regional geology as represented by figure 6 depicting very easily interpretative work on the following pages, mainly due to the reported absence in the field (as noted by L. Boivin) of any indication for the presence of mafic gneisses with the noted exception of the mafic gneisses located in the Black Hills on the Southwestern part of the crater island. The "tagamites" can be found on the eastern and northern shares of the crater island and the post-impact dykes and breccias can be found on the Quertier and Southwest Island Properties.

Physically, the impact structure is a 100 km circular basin with a central uplift of anorthositic composition (Mont de Babel) believed to be due to lithostatic rebound. The structure is evident on Landsat photographs. These anorthosites are surrounded by melt rock, rimmed by a margin of latite and suevite (fall back breccia). The ring of water was formed when two narrow crescent shaped rivers, Manicouagan and Mouchalagane, and surrounding incised lands were flooded in 1974 by Hydro-Québec dam Manic 5, to form the Manicouagan Reservoir.

3.1 MELT ROCKS

TAGAMITE

Autochthonous breccia, (see Property geology description), consisting of rotated fragments in a comminuted matrix, crops out sporadically near the bounding lakes.

SUEVITE

Suevite is an allochthonous polymict breccia containing shocked and unshocked fragments and heterogeneous glassy blebs in a matrix that can be clastic, cryptocrystalline, or glassy. Suevite crops out inside the René-Levasseur Island near the base of the outer edge of the annular plateau of igneous rocks. Dykes of suevite intrude both autochthonous breccia and unbrecciated country rocks, but locally grade into very fine grained suevite. Thin sheets of suevite locally overlie country rocks.

The suevite is red or green and grades locally into shocked and partly melted country rock, and may grade into the overlying latite in places.

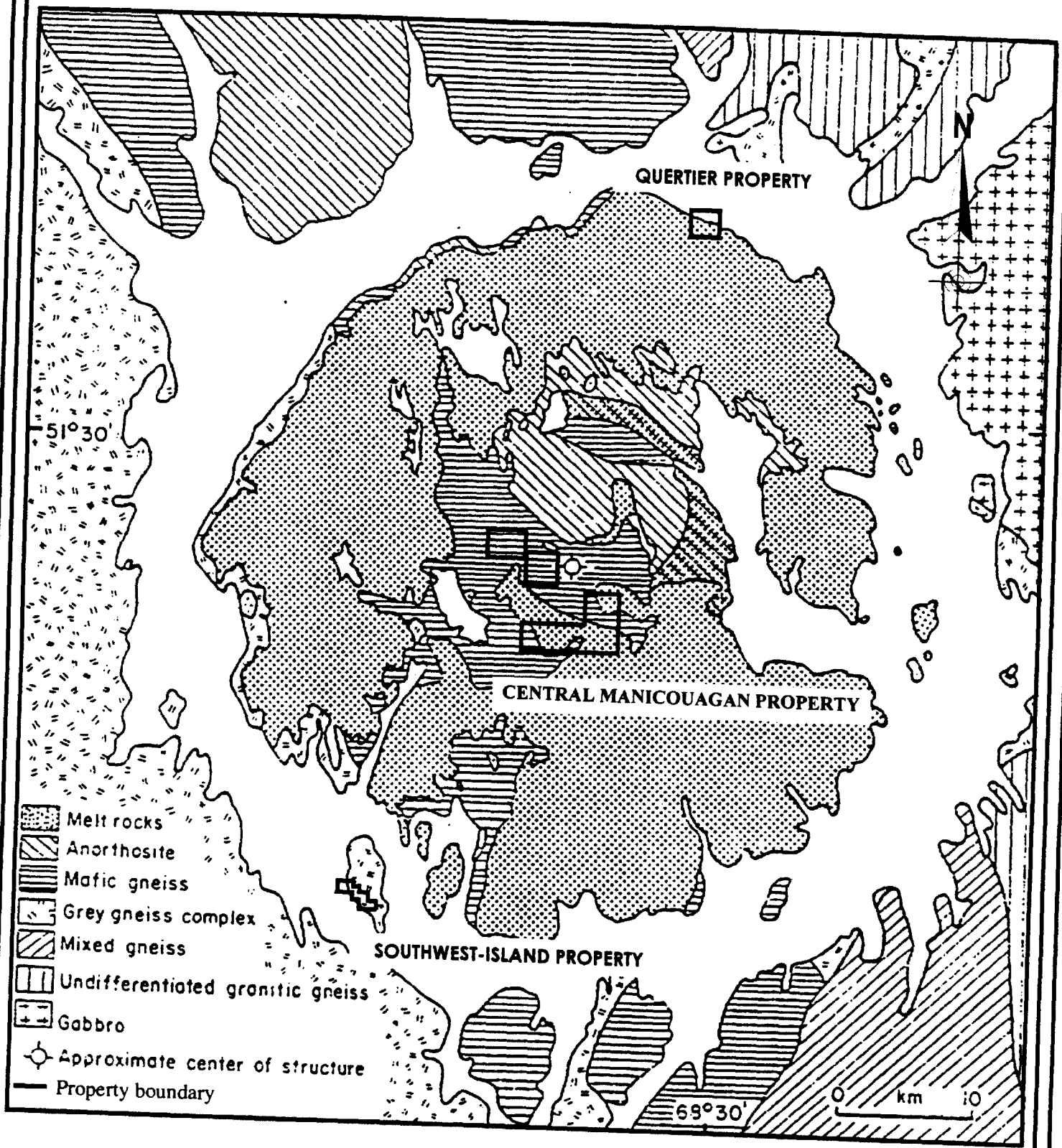
Pseudotachylite is a glassy rock, charged with small inclusions, that forms irregular veins, dykelets, and rootless pods in a country rocks inside the annular plateau of igneous rocks.

IMPACT MELT: LATITE / MONZONITE

The annular ring consits of an igneous subhorizontal sheet of latite and monzonite. The latite is the lower unit containing fragments of other rock grading abruptly upward into homogeneously red grained melt rock. No evidence of flow structure or individual units was found. Dikes and tabular subhorizontal bodies of latite and monzonite crop out in the interior of the structure. The latite contains inclusions of highly shocked and thermally metamorphosed country rocks. Both the heterogeneous (latite) and the homogeneous melt rock have identical monzonitic composition.

3.2 UNDIFFERENTIATED GRANITIC GNEISSES

Undifferentiated granitic gneisses and grey gneisses of different composition and textures, and probably of different ages were mapped as a single unit by Murtaugh (1976). Most of the different types were described by Kirsk (1968), and he did not map them separately. Granitic gneiss is abundant in the northeastern and southeastern parts of the area. Bassaget (1968) described the granitic gneiss in the southeast, and Kish (1968) described that in the northeast. The granitic gneiss is abundant in the southeast composed of a medium-grained pink rocks made up mostly of quartz, microcline microperthite, and plagioclase. Biotite, hornblende, chlorite, garnet, allanite, apatite, zircon, opaque minerals, and rare muscovite are accessory minerals. Kish (1968) distinguished three type of granite in the northeast on the basis of feldspar composition and feldspar ratios. He described two-feldspar granite, albite granite, and microcline granite, but did not mapped them separately. These rocks contain as much as 11 percent mafic mineral, and are therefore generally more mafic that the granitic gneiss in the southeast. The rocks range from slightly to well-foliated, or have flaser structure. Kish (1968) also described lit-par-lit mixtures of granitic and grey gneiss; These rock are shown on the Simplified geologic map of the Manicouagan structure as mixed gneiss.



MINERAUX MANIC INC.	**MADE: R. MOAR**	**DATE: MAY 1997**
SIMPLIFIED GEOLOGIC MAP OF THE MANICOUAGAN STRUCTURE AND PROPERTY OUTLINES MODIFIED AFTER GRIEVE AND FLORAN (1978)	**APP.: R. VENDITTELLI**	**FIG # 6** / **SUBDIV:**

3.3 GREY GNEISS COMPLEX

The grey gneiss complex consists of amphibolite facies gneisses and associated metamorphosed mafic and ultramafic rocks. The gneisses are predominantly quartz-plagioclase-biotite and hornblende rocks.

3.4 MAFIC GNEISS

Bodies of metamorphosed mafic and ultramafic gneisses in the central and in the southwestern part of the area range in size from a few meters to nearly a kilometer across. A typical specimen of the most common type weathers reddish-brown and is speckled reddish-black where fresh. Poorly defined foliation, or lineation, is formed by an inconspicuous layering or alignment of mafic mineral. Coarse granitic pegmatites cut these rocks in few places. A typical specimen of the most common type consists mainly of almandine garnet, clinopyroxene, hornblende and plagioclase. Accessory minerals are sphene, biotite, epidote, apatite, quartz, microclin, and opaque minerals.

3.5 ANORTHOSITE

The Mont de Babel is about 50 km long and 15 km wide and occupies the center of the Manicouagan Impact Structure. The Mont de Babel anorthosite differs from the Lake Tetepisca anorthosite to the northwest in that it contains only fine to medium-grained plagioclase with probably no mafic component.

3.6 ORDOVICIAN SEDIMENTARY ROCKS

Ordovician sedimentary rocks (not shown on Fig. 6) lie unconformably on, or are in fault contact with Precambrian rocks. They outcrop probably as slumped fragments (allochthonous) only within the Manicouagan Impact Structure, mostly along the shores of the René-Levasseur Island. The are predominantly limestones, but thin basal units of siltstone and shale are exposed in a few places.

3.7 SHOCK METAMORPHOSED ROCKS

Shock metamorphism is the progressive breakdown in the structural order of minerals and rocks due to the passage of a high-pressure shock wave. Effects of shock metamorphism in the country rocks

are: zeolitization of anorthosites and gneisses; transformation of mafic minerals to magnetite within the entire diameter of René-Levasseur Island; planar deformation features in tectosilicates and other such microscopic effects as catalogued extensively by previous workers in the Manicouagan Impact Structure (Dence (1964); Bunch *et Al* (1967); Dworak (1969)).

4.0 PROPERTY GEOLOGY AND MINERALIZATION

4.1 CENTRAL MANICOUAGAN PROPERTY

The circular structure is considered to be the product of a hypervelocity-meteorite impact with the Earth (astrobleme). Relatively few rocks outcrop on the crater structure called René-Lavasseur Island which hosts the crater geology and the Manic Central Property. The main lithology of the Manicouagan structure is a flat-lying sheet of clast bearing impact melt (Manicouagan melt rock) some 100 to 200 meters thick and 55 kilometers in diameter which is found within the central part of the structure (Fig. 6). The original thickness of this sheet may have been up to 400 meters. Plagioclase, sanidine and augite are the main minerals present in the matrix of the melted rocks while hypersthene, quartz, iron oxides and smectite are minor components.

The crater topography is a series of annular plateaus, and the highest part is the central uplift of anorthositic shock-metamorphosed massif to the north of the Central Manic Property, which is named the Mont de Babel, having little vegetation and no overburden. The Central Property contains no confirmed surface outcrops, which is typical of the geomorphology of the area. Outcrops in the crater are constrained to the northern and eastern section composed of suevite with impact melt in the rest of the crater interior, and the Grenvillean shock-metamorphosed basement exposed as flat outcrop along the beaches of the circular lake surrounding René-Levasseur Island.

Therefore, the geology of the Central Manic Property has heretofore been of an interpretive speculative nature , as depicted in map projects performed by such previous workers as Murtaugh (1969, 1972, 1976) and Grieve and Floran (1970) and Coles and Clark (1978). During the Company's first field season, extensive occurrences of buried boulders were mapped and subsequently reassessed in the field and eliminated as outcrop. The only remaining area where outcrop remains a possibility is in the southwestern part of the Property as indicated in the compilation map located in the Previous Work section of this report , series NC-10. The Company also performed compilation work in 1996 of the outcrop data located by previous workers Grieve et al, as collected by the GSC and has assured itself that this is true.

As to the property geology, the most reliable source of information remains the drill core extracted from one drill hole as described hereinafter. The drill core consists of shock-metamorphosed leucocratic Grenvillean gneisses with little or no mafic or magnetic component, typical of much of the Grenvillean geology surrounding the island. This was a surprise to the Company geologists (verbal communication L. Boivin) who expected to intercept rocks similar to those outcropping everywhere else in the middle of the crater, i.e. impact melt. After consultation with recognized crater geology experts (Grieve), the Company learned that this is indeed typical of impact geology, where most often the impact melt is "splashed" off center out of the middle part.

The drill hole mentioned above was begun in 1990-1991. Minéraux Manic Inc. drilled hole # MC-1 (at grid co-ordinates L14E, 28 + 00N) to a depth of 471.53 meters. The hole was capped at this point and will be continued in September of this year (1997). This hole was drilled to test the eastern part of the elliptical magnetic anomaly where it also coincides with a Maxi-Probe electromagnetic anomaly that possessed both the typical horizontal component so often detected in this property, as well as a rarer vertical component. This hole was designed to cross the entire width of the magnetic anomaly and explain the source of the magnetism. The log of the core obtained describes the rock as being mostly shock-metamorphosed Grenville leucocratic quartzofeldspathic gneisses cross-cut by occasional small veins of meteorite-caused tachylite. The core was further studied at the GSC in 1996 (see Sub-section 5.15 in the Previous Work section of this report).

The absence of a magnetic source rock at the depths this hole reached indicates the increased probability that the magnetic body is centered lower than the depths permissible for an intrusive model of origin (Paterson 1994 - work summarized in section 6.1.7 of this report and in the Annexe V.C). Certainly the airborne work performed by the Company over this property concurs with this in that no conductive rocks occur above about 125 meters deep. Please see the discussion of results later in this report

Otherwise, the Property can consist of rocks similar to those already identified elsewhere in the crater, as described below:

The Manicouagan melt rocks have been petrologically subdivided by Floran *et al.* (1978) into a lower, middle and upper unit.

MANICOUAGAN MELT ROCKS

The lower unit has a pseudoporphyritic texture in which abundant clasts of plagioclase, quartz and anorthosite reside in a very fine-grained matrix. At the base this unit is in unconformable contact with an undulating basement of Precambrian Grenville rocks. Here clasts/blocks up to 50 meters in size are noted.

The middle unit is characterized by a fine-grained, clast-bearing matrix and a poikilitic texture. This texture is described as being reminiscent of some lunar impact-melt rocks.

The upper unit is observed to be relatively coarse grained, but comparatively clast-poor. These units are overlain by suevite. Finally, suevite forms a very heterogeneous unit, consisting of 35% subangular partially digested gneiss fragments in a dark grey vesicular (10%) groundmass. The fragments vary greatly in size from a few millimeters up to 10 centimeters. The groundmass is siliceous with 5% felsic laths (up to 2 mm) and 2% angular glass-like shards.

PRECAMBRIAN BASEMENT ROCKS

Precambrian rocks include anorthosite, gabbro and a variety of gneissic rocks. Gneissic rocks can be grouped into quartz-feldspar (grey) gneiss and a series of mafic, charnokitic and transitional gneisses. The anorthosites occupy a prominent uplifted block within the center of the Manicouagan structure.

Remains of sedimentary rocks of Paleozoic-age (Ordovician) may occur locally on a regional scale and can be found as rare inclusions within the melt. This could provide the source of carbon for the formation of VD or normal diamonds in the area.

In an inward traverse from the outer limits of the impact zone toward the center of the crater, the intensity of the impact fracturing increases within the paragneiss basement suite. It commences with three moderately spaced (10 to 15 cm) planes of brittle fracture, resulting in blocky outcrops, and within a space of less than ten meters the blockiness increases significantly due to narrowly spaced fractures and occasional narrow shears.

4.2 QUERTIER PROPERTY

IMPACT-AFFECTED BASEMENT ROCKS

The basement suite grades into a brecciated gneiss with a continued increase in brittle deformation. These outcrops are characterized by one half to one meter of saprolite covering a crumbly oxidized surface. This breccia is crosscut by narrow continuous steeply dipping shears subparallel to the gneissosity at 110° to 125°. **Sulphide mineralization,** as identified on the Company's Quertier Property, located in the Manicouagan crater some 30 kilometers to the north of the Central Property described in this report, can accompany this brittle-ductile deformation pattern (Please see following paragraph). Pyrrhotite and up to 3% of pyrite can occur as discontinuous drusy stringers along fracture and shear planes within a groundmass of crushed gneiss and "rubbleized rock" (field term) i.e. tagamite (see Regional geology).

Along several fractures on the rock one can find traces to 2% disseminated fine grained pyrite. Interestingly, this sulphide mineralization, though minor, is also found plating late brittle fractures, which can be interpreted as postmetamorphic sulphide mineralization.

Another significant unit within the basement suite is the brecciated mafic gneiss. This unit's relative position with respect to the banded gneiss is uncertain, but from preliminary field observations (Kenwood, 1991) it likely lies between the brecciated gneiss and the suevite. This unit is chiefly composed of weakly foliated pyroxene-rich rounded fragments in a very fine grained black matrix. The mafic fragments vary in size from 0.5 cm to 20 cm, and are often slightly elliptical or tear drop shaped with their long axis oriented downdip. The matrix is aphanitic and locally contains dull black tachylite veinlets. Mineralization is irregular, with traces of pyrite (up to 2%), magnetite and probably ilmenite.

This unit can be very mineralized (Quertier Property- description below) and may be quite extensive. Mineral occurrence of copper-nickel - PGE have been assayed from surface outcrops and there is potential for finding an orebody in this area. The Company has determined there is a strong likelihood that post-impact mineralized intrusive mafic dykes are associated with this mineralized brecciation (L. Boivin).

The initial property was mapped by Kenwood in 1991. Outcrop density on the property is controlled by topography. Only a few small islands outcrop in the northern part of the property. Two of these islands are of interest. The rocks on these islands are part of the brecciated mafic basement. One island is crosscut by a steeply dipping very fine grained ultramafic dyke with numerous tension fractures. This outcrop hosts the original nickel and copper showing, which precipitated the initial staking. During prospecting and reconnaissance work in the Manicouagan Crater performed by Minéraux Manic Inc in 1990, three grab samples were taken from the original showing and assayed for Au, Ag, Cu, Ni and PGE (Rh, Pt, Pd). The best values reported are 0.90% Cu, 0.27% Ni, 0.96 g/T Pt, 2.3 g/T Pd, 0.50 g/T Au and a few traces of Rh and Ag (L2-6-3).

There is approximately 30% outcrop in the southern part of the property. The outcrops are located mainly in the hills proximal to the shoreline as well as in the steeply cut river valleys and bedrock lithology consists of garnetiferous paragneisses, brecciated gneisses, and suevite. The garnetiferous paragneisses are characterized by their predominantly felsic banding interbanded with minor (25%) mafic bands. These rocks have been metamorphosed to the upper amphibolite grade. They have a well developed foliation often enclosing an amphibolite mineral lineation. Locally, certain bands include trace to 2% disseminated fine grained pyrite along fractures. This sulphide mineralization also plates late brittle fractures, suggesting post-metamorphic sulphide crystallization.

The basement suite of rocks grades into a brecciated gneiss showing continued brittle deformation. These outcrops are characterized by saprolite covering a crumbly oxidized surface. Narrow continuous steeply dipping shears crosscut this brecciated gneiss sub-parallel to the gneissosity at 110^0 to 125^0. Sulphide mineralization up to 3% Po ±Py accompanies the deformation occurring as discontinuous drusy stringers along fractures and shear planes within a groundmass of crushed gneiss.

The brecciated mafic gneiss unit within the basement suite appears to lie between the brecciated gneiss and the suevite. This unit is composed of weakly foliated pyroxene-rich rounded fragments in a very fine grained black matrix. The mafic fragments are slightly elliptical or tear drop shaped with their long axis oriented downdip. The matrix is aphanitic and locally contains dull black tachylite veinlets. Irregular mineralization consists of trace to 2% Py, trace to 2% Cp, trace Mt and possibly ilmenite. The brecciation is believed to be directly due from the meteorite impact, and the sulphide mineralization may result from the remobilization fluids within the brecciation event.

Outcrops on the southern part of the property proximal to the centre of the crater form a series of frost heaved ridges of suevite. These rocks consist of 35% subangular partially digested gneiss fragments in a dark grey vesicular (10%) groundmass. The groundmass is siliceous with 5% felsic laths and 2% glass-like shards.

4.3 SOUTHWEST ISLAND PROPERTY

GREY GNEISS COMPLEX

The most abundant Precambrian rocks in the property are medium-grained to coarse grained grey gneisses. Large isolated lenses of metamorphosed mafic and ultramafic rocks are intersperse with the grey gneisses. Outcrops are generally sparse and small, and large cliff-forming outcrops are partially covered with moss. A well developed foliation formed by oriented biotite grains is common, parallel or subparallel to banding formed by concentrations of mafic minerals. In places the foliation is inclined at high angle to the banding. Banding is irregular and rapid changes in thickness of banding along strike are common. Pink pegmatitic material forms rootless lenses, knots, and stringers that are generally conformable with, but locally crosscut, the banding. Plagioclase, quartz, biotite, and hornblende are the essential minerals. Sillimanite and kyanite are rare. Garnet and potassic feldspar are locally abundant. Sericite, chlorite, and calcite are local alteration products.

POST-IMPACT INTRUSIVES

The post-impact ultramafic dykes are fresh, undeformed and contain no metamorphic minerals such is typical of the Grenville region (e.g. garnet). Unlike surrounding rocks, there is also no evidence of shock-metamorphism due to the meteoritic impact. All rocks in this area of similar composition and subjected to the impact would have been transformed into magnetite units. This is interpreted as being evidence for post-impact emplacement (Boivin, 1994). These dykes are fresh, unmetamorphosed and unaltered coarse-grained peridotite-pyroxenite. Owing to their ultramafic composition and apparent lack of zircons, age-dating these dykes will be difficult. The petrographic examination of a sample collected in 1990 reveals that the rock is a plagioclase bearing pyroxene hornblendite consisting of 90% amphiboles and pyroxenes and 5% plagioclase, 3% iron bearing biotite and 1-2% opaques (Chabot, 1990).

Sulphide mineralization which occurs as veins is associated with these dykes, and interesting values of nickel, copper, and PGE elements have been obtained in grab samples on the Company's SW Island Property, located 30 kilometers SW of the central property. Company geologist, Roger Moar, has indicated through field work performed in 1996 a relationship to brecciation of these dykes, a brecciation heretofore only before seen in the Company's mineralized Quertier Property, located 30 kilometers to the north of the property described in this report, in the Manicouagan crater.

The Southwest Property is underlain by a gneiss unit of the Grenville Province and Triassic rocks of the Manicouagan complex. Regional prospecting work conducted in 1990 led to the discovery of weakly mineralized ultramafic intrusive rocks cross-cutting the Grenville and Manicouagan complex units. These intrusive rocks do not exhibit impact related metamorphism.

5.0 SOME PREVIOUS WORK BY OTHER WORKERS

A.P. Low (1897), was the first geologist to give a geological description of the Manicouagan area. Hammond (1945) briefly described the geology along the shores of Lake Mouchalagane and suggested that the apparently flay-lying igneous rocks along the inner shores were late Precambrian or Early Paleozoic in age. Rose (1957), of the GSC, worked in the area and published a geologic reconnaissance map showing the major geology features. Bérard (1962), of the Department of Natural Resources, Quebec, mapped the perimeter of the Manicouagan impact structure and a small part of the interior. His work was confined below an elevation of 1 200 feet, an area that would be flooded upon the completion of Manic 5 dam. Kirsh (1962, 1963, 1968), of the Department of Natural Resources, Quebec, mapped the northeastern corner of bounded by latitudes 51°30' and 51°45', and longitudes 68°00' and 68°30'. Kirsh was primarily concerned with the rocks east of the Manicouagan impact structure. During an expedition in 1963, Dence of the Dominion Observatory of Canada discovered the first evidence of shock metamorphism in the structure. Currie (1964) of the GSC was the first geologist to begin detailed mapping of the Manicouagan Impact Structure and subsequently proposed a volcanic-tectonic origin. Murtaugh and Currie collaborated to produce a preliminary report and map in 1969.

5.1 PRELIMINARY STUDY OF THE MANICOUAGAN STRUCTURE. By J.G. Murtaugh and K.L. Currie (1969)
STUDY OF THE GEOLOGY AND PETROLOGY OF THE MANICOUAGAN RESURGENT CALDERA. By K.L. Currie (1972)

Currie interpreted the Manicouagan structure as a resurgent caldera and proposed a volcanic-tectonic model as its mode of origin. In this model, Currie proposes the updoming of an area larger than the present structure followed by radial explosions along marginal radial fractures then by explosions in voids in the interior of the structure. He interprets these explosions as having been chemical in nature caused by detonation of water-poor, hydrogen-rich gas emanating from a magma at depth. Such detonations everywhere caused the shock metamorphism and, in voids in the fractured center of the dome, produced the shatter cones. Degassing caused the collapse of the dome. This collapse was followed by the intrusion and eruption of alkali basalt and intrusion of larvikite (Murtaugh's monzonite) and at the base of this, trachyandesite (Murtaugh's latite). Currie interprets the pseudotachylite as a mixture of droplets of magma mixed with rock powder from the walls of the fractures. Currie proposes Mont de Babel rose on subterranean igneous rocks. This was followed by normal faulting which downdropped parts of the Manicouagan Complex.

This theory has since fallen into disfavor with the subsequent evidence and scientific evolution of knowledge of the Sudbury and other impact features. Murtaugh himself converted with the times as

his subsequent work indicates. As one of the few existing references on the impact site at the time, it is not surprising that elements of Currie's musing with respect to magnetization and structural events were constructed and built upon by later workers who adopted some of the ideas and applied them to geophysical models and studies written by geophysicists.

5.2 GEOLOGY OF THE MANICOUAGAN IMPACT STRUCTURE. By J.G. Murtaugh (1976)

Murtaugh (1976) fully mapped and described the geology of the Manicouagan structure and proposed an alternate model for its origin. He proposes that a hypervelocity impact of a cosmic body formed the structure. According to him, the breccias of the Manicouagan Complex were formed by or were related to the impact melt. Murtaugh also states that the igneous rocks of the Manicouagan Complex may be of endogenous origin, but that field relations suggest they were impact melt.

Murtaugh classified the rocks of the Manicouagan Complex into four categories: shock metamorphosed rocks, breccias, igneous rocks and contact metamorphosed country rocks. He also classified the shock metamorphosed rocks into six shock stages based on the extent of shock effects observed.

Based on the presence of diaplectic glass, Murtaugh determined the rocks were shocked to pressures of 350 kb which are beyond the pressures generated by known volcanic explosions. Also, shock metamorphism in the country rocks indicates that Manicouagan is an impact structure. He suggests it is unlikely a magma could produce, mix, disperse and quench the different types of heterogeneous glasses observed.

Local suevite selvages on basalt suggest that the two rocks may have been formed contemporaneously. Murtaugh describes the ellipsoids and lenticles of glass, devitrified glass or recrystallized material in tachylite at Manicouagan as similar to the spheroids from the West Clearwater Lake impact crater. He interprets the basalt as being impact melt from a totally vaporized or fused part of a turbulent cloud of volatilized, fused and fragmented country rock that deposited the suevite.

Murtaugh points out that the contact metamorphic aureoles around some tabular bodies of igneous rock are of extraordinary widths. In order to account for the observed contact metamorphic effects, he proposes the country rocks were preheated to high temperatures, as evidenced by a thin vein of pseudotachylite bordered by altered hypersthene and vitrified scapolite. The pseudotachylite alone could not have contained sufficient heat to have caused vitrification of scapolite and then cooled to a glass. Murtaugh proposes the source of preheating was the residual shock heat from the hypervelocity impact of an extraterrestrial body. He suggests that the rocks near the surface of the primary crater would be intruded and overlain by impact melt before the residual shock heat could dissipate.

The hills around Mont de Babel and in its meridian valley are interpreted by Murtaugh as blocks that became detached from the mountain at the time of uplift. He interprets the observation that rocks at the summit of Mont de Babel show decomposition of mafic minerals only near veins of pseudotachylite as suggesting that Mont de Babel rose above the main body of the impact melt. Zeolitization of the anorthosite on the mountain suggests Mont de Babel was at one time covered by fallback melt.

5.3 CENTRAL MAGNETIC ANOMALY STUDY. By R.L. Coles and J.F. Clark (1978)

The basis for this study by Coles and Clark (1978) was a 1969 GSC aeromagnetic survey flown with a nominal spacing of 800 meters at altitudes of 300 meters, which yielded the signature of a wide elliptical magnetic anomaly. Coles and Clark concluded that highly magnetic rocks occur close to the surface over an area of about 8 x 12 km with a depth to the base of the magnetic body at not more than 3 km. They suggested that the cause of the anomaly could be the impact-generated magnetization of a mafic body which was subsequently uplifted.

From systematic sampling and measuring of the magnetic susceptibility of the country and melt rocks, Coles and Clark concluded that none of the samples, with the exception of two shocked ultra-mafic rocks, is sufficiently magnetic to form any significant portion of the causative body of the central anomaly.

Coles and Clark discuss the cause of the proposed mafic or ultra-mafic body perhaps underlying the central anomaly. They suggest it is unlikely that thermal magnetization could have caused the remanent magnetization as there is little evidence that the temperature below the melt rock would be as high as the Curie temperature over a large enough volume. They believe that a shock pressure-induced magnetization is adequate to produce the magnetization of the mafic minerals, as such an impact can produce an order of magnetization of 20 to 30 GPa, which decreases rapidly downward and outward. Coles and Clark are of the opinion that the steep vertical gradient of the central magnetic anomaly can be explained by the rapid decrease in pressure downward and outward and would be further delineated by rapid uplift of the affected area.

With respect to the Coles and Clark interpretation, L. Boivin (1994) concludes that the mafic body which would have been magnetized would have had to be the only plug-like mafic geological unit in a rather large region and that these rocks would have had to be ultra-mafic in order to produce 100% magnetite equivalent. To her knowledge, there are no ultra-mafic units of that size in this Grenville region, although there are occurrences of mafic gabbroic gneisses in the NE region of the crater. These mafic gabbroic gneisses do not demonstrate the high magnetization gradient of the central rocks, despite the fact that virtually all mafic minerals within the confines of the crater have been transformed to magnetite. The central rocks could not have produced a higher magnetization than other rocks of similar composition especially when created by the same event at the same geological time.

5.4 CHEMICAL STUDIES OF THE MANICOUAGAN IMPACT MELT

CHEMICAL INTERPRETATION OF THE MANICOUAGAN IMPACT MELT BY GRIEVE AND FLORAN (1978)

The Triassic melt rocks at the Manicouagan structure have been interpreted both as volcanic (Currie, 1972) and as the product of impact melting (Dense, 1971; Murtaugh, 1976; Floran *et al,* 1976). The data base for this study consists of earlier major element data from the GSC study (Currie, 1972) and major and trace element analysis performed at the Johnson Space Center in Houston (Floran *et al* 1976, 1978). In this study, Grieve and Floran favor the impact melting interpretation and present chemical arguments compatible with the impact origin. They comment on the composition of the melt and its relationship to the underlying basement units. In addition, Grieve and Floran used the chemical and petrographic data to constrain a model for the formation of the melt and the Manicouagan structure in a hypervelocity impact event.

Grieve and Floran conclude that the melt sheet is compositionally homogeneous in relation to the underlying and surrounding basement rocks. They have successfully modeled the melt for both major and trace elements as a mixture of chemically distinct lithologies, a property considered characteristic of impact melts. The mixture of diverse target lithologies to form a generally homogeneous melt composition is a result of the dynamic conditions accompanying melt genesis.

Their model for the generation of the Manicouagan structure and melt sheet in a hypervelocity impact event proposes that compositional homogeneity results from the melted portion of the target containing internal velocity gradients of several kilometers per second and the melt being driven into the expanding cavity as a high velocity turbulent flow of superheated silicate liquid. During movement the silicate liquid incorporates crystalline inclusions the number and type of which are a function of the path travelled by the melt. In general, the number of inclusions decreases upward and toward the center of the structure establishing a lateral and vertical stratigraphy in an otherwise coherent melt sheet. These internal relationships derived from the cratering model are consistent with the detailed stratigraphy of the melt sheet described by Floran *et al,* 1978.

STUDY OF THE STRATIGRAPHY, PETROLOGY AND CHEMISTRY OF THE MANICOUAGAN IMPACT MELT BY FLORAN *ET AL* (1978)

Floran *et al* (1978) studied a sheet of clast-laden impact melt that forms an annular plateau surrounding an uplift of shocked anorthosite. The researchers analysed 24 representative melt rocks. Based on internal stratigraphy, petrology and major and trace element geochemistry, they present a three-dimensional model for the crystallization history of the Manicouagan melt rocks.

Floran *et al* determined the bulk composition of the melt rocks to resemble that of terrestrial andesites and monzonites. They also found chemical homogeneity to be a major characteristic of the Manicouagan impact melt and suggest that homogenization was achieved early in the melt's history.

They attribute the undifferentiated nature of the impact melt to the extreme sheetlike form of the melt body and to the viscosity of the clast-laden melt during crystallization. These researchers also found that textural heterogeneity is a major feature of the Manicouagan impact site. This textural diversity in the melt sheet reflects variation in pyroxene and feldspar morphology, matrix grain size and clast content. Superimposed on the dominant chemical and textural features of the melt are second-order effects leading to chemical heterogeneity on a local scale and textural homogeneity on a limited regional scale.

Based on decreasing clast abundance and on coarsening of the melt above the base, Floran *et al* divide the melt sheet into three vertically gradational units; a lower unit, a middle unit and an upper unit. The mineralogy of the three units is similar. The upper unit contains inverted pigeonite and pseudomorphs after olivine while the middle and lower units contain rare biotite and hornblende.

The lower unit is very fine-grained, clast-rich and dominated by a pseudoporphyritic texture. This unit contains a local facies called Subunit A, which is found only as dykes and pods of melt rock adjacent to large basement rocks or inclusions. This subunit forms a spherulitic to basaltic textural sequence with skeletal crystal morphologies indicative of extreme undercooling.

The middle unit is fine-grained, clast-rich and consists of a variety of textural types including microophitic, poikilitic and transitional. Development of the poikilitic texture within this unit can be modeled by a two stage cooling history in which the mafic composition of the melt permitted augite to be the liquidus phase. Supercooling caused by a high clast content initiated nucleation of augite adjacent to plagioclase clasts which then preferentially nucleated on relict clasts and enveloped earlier formed augite during growth. A similar model is applicable to some of the aluminous Apollo 17 poikilitic-textured impact melt rocks.

The upper unit is medium-grained and clast-poor with a hypidiomorphic granular texture. Textural homogeneity is most typical of this unit. It is similar in grain size and texture to hypabyssal intrusions. The continuous nature of this unit and its consistent texture indicate a more uniform and slower cooling history than that experienced by the bulk of the clast laden melt.

All three melt units are variable in thickness with the coarser-grained middle and upper units becoming more prominent closer to the center of the structure. According to Floran *et al*, this suggests the melt cooled more slowly in the central region, possibly due to the high post-shock residual temperature of the basement and included clasts.

6.0 PREVIOUS EXPLORATION WORK

No other mining company or prospecting outfit has performed mineral or conventional exploration in the crater region other than Minéraux Manic Inc.

The following is a summary of all the exploration work performed by Minéraux Manic Inc. since 1990 on the Manicouagan Properties.

CENTRAL MANICOUAGAN PROPERTY

YEAR	EXPLORATION WORK
1990	Airborne geophysics survey (Aerodat Limited)
1990	Line cutting, 340.6 km of lines cut
1990	Mapping and geological survey (L. Boivin)
1990	Geological survey (T. Podolsky)
1990-1991	Diamond drilling (DDH MC-1, 471 m)
1991	Ground magnetic survey
1991	MaxiProbe geophysical survey
1992	Study of the Manicouagan magnetics (Schultz)
1992	Computer modeling of the Manicouagan magnetic data (Paterson)
1992-1993	Study of the remanent magnetization in the Manicouagan Crater (Roest and Pilkington)
1994	Shadow mapping of the Manicouagan magnetic data
1994	Mapping of the surficial geology of the Manicouagan Crater (644 km^2) at 1:50,000 scale
1994	Lithochemical study (Siriunas)
1994	Petrography and rock magnetic properties study of the drill core from DDH MC-1
1996	MaxiProbe geophysical survey
1997	Generation of a Manicouagan database and associated mineral potential data products
1997	MELIS survey

QUERTIER PROPERTY

YEAR	EXPLORATION WORK
1990	Prospecting and Claim Staking (30 claims)
1991	Mapping and Prospecting (J. Kenwood)
1991	MAG-VLF Ground Geophysical Survey (J. Kenwood)
1991	Chemical Analysis of Grab Samples
1991-1992	Diamond Drilling (DDH MM-91-01 to a depth of 9.41 meters, DDH MM-91-02 to a depth of 29.57 meters and DDH MM-91-03 to a depth of 35.66 meters)
1996	Claim Staking (12 claims)
1996	Line cutting, 37.8 km lines cut
1996	Prospecting (R. Moar)

SOUTHWEST ISLAND PROPERTY

YEAR	EXPLORATION WORK
1996	Prospecting, staking, sampling and mapping (11 claims)
1996	Chemical Analysis of Grab Samples

A compilation map showing previous work done by Minéraux Manic Inc. in the Central Manicouagan Property and the Quertier Property is provided in the back pocket of this report and in the Previous work section respectively.

6.1 CENTRAL MANICOUAGAN PROPERTY

6.1.1 1990 WINTER SEASON EXPLORATION

AIRBORNE SURVEY

This airborne survey carried out by Aerodat Limited, Toronto, Ontario, over the Central Manicouagan Property was flown during the period of July 3 to 5, 1990. Nine flights were required to complete the survey with flight lines oriented at azimuths of 030-210 degrees and flown at a nominal spacing of 200 meters at a mean terrain clearance of 60 meters. A total of approximately 1000 line kilometers, including tie lines, of the recorded data were compiled in map form. Equipment operated included a four frequency electromagnetic system, a high sensitivity cesium vapour magnetometer, a two-frequency VLF-EM system, a power line monitor, a video tracking camera, an electronic positioning. Electromagnetic, magnetic, and altimeter data were recorded both in digital

and analog form. Positioning data were stored in digital form. Visual check of position were also recorded on the flight path navigation by the operator during the flight. Subsequently, Aerodat produced a derivative gradient map of the central anomaly. This survey was done with hopes of providing the means for an interpretation of the depth to the summit of the magnetic body. The results obtained from this survey do not give this information but the survey confirms and enhances the previous GSC survey of the area (i.e. 0.2 km line spacing and sensor height of 45 m above ground level compared to the 0.8 km and 300 m of the prior federal survey) (Fig. 7).

Aerodat Limited interprets the form of the magnetic anomaly as conforming to the response from a thick plate, slightly dish shaped along its top surface. They state that the upper surface of a large intrusive body would create a similar response but would require the intrusive to be more magnetic at this surface. A separate, surficial or near surface sheet-like body overlies the main magnetic structure. This surficial sheet produces narrow, northwesterly magnetic trends that complicate the magnetic response from the main body.

6.1.2 1990 SUMMER FIELD WORK

GEOLOGICAL MAPPING

Field reconnaissance mapping work commenced in the summer of 1990. This work was performed for the purposes of mapping of lithological units on the property and the evaluation of the economic mineral potential, which at the time was represented to a large degree by seeking the cause of the strong magnetic anomaly situated in the centre of the Manicouagan impact crater. Particular attention was paid to boulders found on the Property, in order to evaluate the likelihood of finding mineralization.

The mapping work referred to here was mostly concentrated on the Central Manicouagan Property, on a grid of lines oriented North-South at a spacing of 200 meters which was chained every 25 meters. 220 km. were cut with a 200 meters spacing on the larger claims group of 162 claims and a total of 400 meters was cut on the smaller claims group containing 54 claims. Areas believed more likely to contain outcrops were prospected by foot and compass between the lines in supplementary traverses. Outcrops were localized using air photos to the scale of 1:15,840 and were compiled on base maps at a scale of 1:20,000 (see compilation map in pocket).

There are very few outcrops on the property, which is generally covered by thick overburden of glacial deposits. Rocks generally outcrop only if they form part of vertical cliffs. A total of about 30 outcrops were mapped on the Property. The two principal lithologies encountered were: Precambrian rocks (gneiss and anorthosite) which had undergone shock metamorphism and/or Triassic age rocks resulting from the melting in situ of the basement during the impact (latite and monzonite). The melt rocks have a monzonitic composition and these represent the most common rocks found on the Central Property.

No explanation for the central magnetic anomaly was found from the geological mapping.

FIELD OBSERVATION ON THE MANICOUAGAN IMPACT SITE by L. Boivin (1990)

Field observations indicate that all mafic minerals in pre-existing basement rocks were transformed to magnetite within the confines of the crater delineated by the water reservoir. Post-impact ultra-mafic dykes were not transformed, are totally fresh, unaltered and unmetamorphosed large-grained peridotite-pyroxenites.

The suevite (fall-back breccia) is uniformly highly magnetic, covers scattered regions around the crater zone and does not reflect the high magnetic signature found in the center. It is possible the oxidation of an iron-nickel meteorite could have created the highly magnetic microcrystalline dust of the suevite matrix.

A hill-sized blasted fragment of mafic basement rocks has been injected and cross-cut with tachylitic stockwerk of highly magnetic microcrystalline black material (magnetic dust?) and veins of transparent silica glass melt. L. Boivin postulates that the impact blast blew this mega-fragment into the air, limiting to a minimum the usual impact magnetization of the mafic minerals typically found in the in-situ basement rocks and in the smaller gneissic fragments caught up in the impact melt and the suevite.

The stockwork could either be an impact tachylite of oxidized meteoritic composition or its derivative or the result of a chimney of magnetic hydrothermal fluids, such as might be found in a vent near a caldera. Company geologists confirmed the presence of Ni/Cu/PGE mineralization in older pre-impact mafic rocks in the crater and in very young ultra-mafic dykes cross-cutting older rocks in the crater.

EXAMINATION OF THE GEOLOGICAL SETTING OF THE MAGNETIC ANOMALY. By T. Podolsky

Terry Podolsky made field visits and a geological tour of the crater and surrounding areas in Company with Minéraux Manic Inc. in August,1990. Subsequently, Podolsky provided conclusions to the Company in a brief report which included microscopic petrography on which these assumptions are based.

The objective of this study conducted by T. Podolsky was to interpret the geological setting of the oval-shaped magnetic anomaly (Fig. 7).

Podolsky interprets the Triassic igneous rocks at Manicouagan as being part of an intrusive, the lower exposed portion of which has been modified by the assimilation of matrix and fragments of breccia (suevite). The parent melt formed in a deep-seated magma chamber where magmatism was triggered

by an instantaneous decrease in lithostatic pressure as brecciated rock was ejected from the impact site to form the crater.

MAXIPROBE HORIZONTAL LOOP ELECTROMAGNETIC SURVEY

During the month of August until October 1990, a MaxiProbe horizontal loop EM survey was performed on the South-West bloc in order to determine whether or not deep seated conductors were present on the Property. The work was performed over the areas of high magnetism by the geophysical consulting company Geoprobe Limited of Toronto. The table below summarizes the lines covered.

Table 2 Lines covered by the EM-MaxiProbe in 1990 - Central Manicouagan Property

LINES	STATIONS	DISTANCE (km)
L 9+00 E	10+25S-14+00N	2.425
L10+00E	10+00S-35+00N	4.5
L11+00E	10+25S-35+00N	4.525
L12+00E	20+00N-35+00N	1.5
L13+00E	10+25S-35+00N	4.525
L14+00E	10+00S-35+00N	4.5
L16+00E	10+25S-15+75N	2.6
L18+00E	10+00S-2+00S	0.8
L24+00W	10+50S-1+50N	1.2
L28+00W	8+00S-4+00N	1.2
L32+00W	7+00S-5+00N	1.2
L36+00W	4+00S-8+00N	1.2
L40+00W	2+00S-10+50N	1.25
	TOTAL	**31.425**

The equipment used in this survey was a portable version of the MaxiProbe EMR-16. There is no physical connection between the transmitter and the receiver. The transmitter is activated by two batteries of 12 volts, the transmitter loop has a length of 50 meters and is laid-out in a circular fashion on the ground. At each station, the receiver measures the vertical magnetic electromagnetic field and the horizontal field simultaneously on about 12 different frequencies varying from 0.22 to 17.57 kHz. For each frequency, measurements were taken of the difference in amplitude of the

vertical electromagnetic field with respect to the horizontal electromagnetic field, as well as the phase difference between these two. During this survey, the distance between the transmitter and the receiver was 500 m during the entire survey. Readings were taken at 25 meters stations on each line. The depth of penetration was estimated to be about 610 meters vertical. In addition, it is important to note that the MaxiProbe system is an asymetrical system that is, best results are obtained if the transmitter is positioned down dip with respect to the receiver. Results are presented in the form of tilt angle and depth section (apparent resistivity as a function of depth). The tilt angle parameter is indicative of the conductivity in the ground. The tilt angle response is weak when a conductor is weak at low frequencies and it increases progressively towards higher frequencies. The peak in intermediate frequency ranges corresponds to the position of the conductor. A migration of peaks starting from high frequencies towards low frequencies indicates a conductor that is dipping. The peak of an anomaly in high frequencies moves towards the up-dip side of the conductor. With respect to the depth-section, it indicates the source and the depths of the anomaly. It also helps in distinguishing anomalies originating from overburden and adjacent rocks. In effect, a more or less horizontal contour in the shallow parts of the depth-section generally represents an anomaly caused by conductive overburden.

The MaxiProbe EM survey detected many EM conductors which could be grouped into two main types; basin or sub-horizontal types (type 1) and the second type (type 2) with a more vertical component, i.e. having a root, (type 2).

Type 1 anomalies generally cover distances of hundreds of meters and are continuous from one line to another. Anomalous zones are often situated either underneath the highly magnetic regions of the Property or close to their borders and could indicate either a lithological change or potential mineralization. Type 2 anomalies are stronger, smaller in physical size and are situated deeper or underneath anomalies of type 1. Their relationship with the magnetic anomalies already present on the Property is less obvious. Many type 2 anomalies coincide with magnetic highs that are locally very strong thereby constituting favourable targets for the discovery of mineralization, especially where these are also associated with or coinciding with much larger horizontal type or lake type anomalies (type 1).

As mentioned previously, the airborne survey performed by Aerodat Limited did not locate any conductors on the Property other than very superficial items such as lakes, swamps or streams. Therefore, there is no correlation between the results of the airborne survey and the results of the MaxiProbe survey. Consequently the MaxiProbe survey revealed EM anomalies at greater depths than the airborne survey was capable of obtaining.

The following table presents the location and the type of EM anomalies located by the MaxiProbe electromagnetic survey in 1990. The location of these anomalies have been transferred to the compilation to the 1:20,000 scale compilation map in the accompanying pocket of this report

Table 3 Results of the EM-MaxiProbe survey performed in 1990- Central Manicouagan Property

LINES	STATIONS	AXIS	TYPE
L9+00E	?10+00S - 4+00 S	9+00S 7+30S 6+00S	Irregular basin 3 vertical roots
	0+50N - 4+25N	2+75N 3+85N	large; 2 vertical roots
	7+50N - 10+00N	9+50N	Large, 1 vertical root
L10+00E	10+00S - 5+50S	9+75S 8+25S 5+75S	Irregular
	1+25N - 4+00N	3+00N	Large, 1 vertical root
	7+00N - 8+50N	8+10N	Large, 1 vertical root, incomplete
	?9+75 - 10+25N		Incomplete
	12+75N - 13+75N		Incomplete
	?14+75 - 27+00N	27+50N	Large basin
	29+75N - 35+00N		2 basins
L11+00E			
	10+25S - 700S	7+25S	Extensive anomaly with 1 vertical root
	3+00S-2+25S	2+70S	Weak anomaly, 1 vertical root
	0+75N-3+75S	2+50N	Extensive anomaly with 1 vertical root
	7+50N - 3+75N	9+00N; 11+00N	Large basin
	15+00N - 20+50N		Very large basin
	23+00N -26+50N	25+00N	large, 1 vertical root
	32+50N - 35+00N		Basin
L12+00E	23+00N - 26+75N	25+75N	1 vertical root
	28+00N - 30+00N		basin
	32+90N - 35+00N		basin

Table 3 Results of the EM-MaxiProbe survey performed in 1990- Central Manicouagan Property

LINES	STATIONS	AXIS	TYPE
L13+00E	10+25S - 1+50S	6+50S; 7+75S	Large basin
	2+00N - 4+75N	2+85N	1 vertical root
	7+50N - 10+25N	8+25N; 10+00N	2 vertical roots
	12+90N - 13+35N	13+15N	weak, 1 vertical root
	15+00N - 17+25N	15+60N	basin, 1 vertical root
	19+25N - 21+25N	19+65N	1 vertical root
	24+00N - 24+50N?	24+25N?	1 vertical root; incomplete
L14+00E	10+00S - 1+90S	5+30S; 7+10S	Basin; 2 vertical root
	0+90S - 13+40N	0+70S 3+70S 6+30N 8+40N 12+80N	Very large basin with several vertical roots
	19+00N - 21+25N	20+80N	1 vertical root
	22+50N - 23+50N	22+70N	weak anomaly ; 1 vertical root
	24+50N - 26+75N	26+25N	1 vertical root
	28+60N - 33+75N		weak anomaly; basin
L16+00E	10+25S - 3+75S	5+50S 9+50S	Basin; 2 vertical roots
	0+50S - 9+00N	1+75N 5+50N 7+25N	Basin; 3 vertical roots
L18+00E	10+00S - 6+75S	8+70S 7+50S	2 vertical roots
	5+50S - 4+25S	4+75S	1 vertical root
L28+00W	5+20S - 8+00S	6+00S	weak; 1 vertical root
	1+00N - 4+20N		Basin
L 32+00W	0+50S - 3+60S	1+70S	1 vertical root

Table 3 Results of the EM-MaxiProbe survey performed in 1990- Central Manicouagan Property

LINES	STATIONS	AXIS	TYPE
	4+00N - 5+00N		weak
L36+00W	3+10S - 0+70N	0+60S	1 vertical root
	3+60N - 7+70N	7+30N	1 vertical root
L 40+00W	0+20S - 3+00N	1+70N	1 vertical root
	3+60N - 7+10N	3+80N	1 vertical root
	8+30N - 9+90N	5+80N	1 vertical root
	8+30N - 9+90N	5+80N	1 vertical root

6.1.3 1990-91 WINTER FIELD WORK

DIAMOND DRILLING: 1990-1991

Hole # MC-1 was collared on line 14+00E / 28+00N on the azimuth 215°N dipping 60°. This hole was drilled to test a Maxi-Probe electromagnetic anomaly that coincides with the axis of an airborne magnetic anomaly. The log of the core obtained describes the rock as being mostly shock-metamorphosed Grenville leucocratic quartzofeldspathic gneisses cross-cut by occasional small veins of meteorite-caused tachylite. The hole was drilled to a final depth of 471.53 meters whereupon it was temporarily halted. The casing was left in place and the hole capped in order to allow the drilling to continue at a future date. The complete description of the drill hole is present in Annex II of this report.

6.1.4 SUMMER EXPLORATION WORK 1991

GROUND MAGNETIC SURVEY

Ground magnetic survey was performed during summer 1991 to verify some of the magnetic anomalies revealed by the airborne survey conducted by Aerodat Limited in winter 1990.

With respect to the ground work, total field magnetometer measurements were taken in the central part of the Property. A total of 340.6 km of line was cut and cut/rechained. A total of 322.1 km of measurements at 25 meters spacings were made.

Results were presented in magnetic contours drawn every 50 nanoteslas. The presence of the strong magnetic signatures in this part of the region influenced the staking position of property mining

claims. It became apparent from the ground work and the subsequent digitalization and compilation of the field data that certain claim blocks are askew of the targeted magnetic highs. As a result, professional surveying of all claim block boundaries will be performed and will resolve all question of the proper location of boundaries.

The results of these surveys confirmed the rather unique geophysical nature of this structure. The results also reflect the homogeneity of a 200 million year old impact melt as well as the absence of conductors in any shocked metamorphosed Grenville basement rocks which may occur above depths of 400 vertical feet in the center of the crater. The absence of such conductors could be due to the absence of such rocks, or possibly to shock metamorphism erasure of such geophysical signatures.

6.1.5 AUTUMN EXPLORATION WORK 1996

EM MAXIPROBE SURVEY

During the month of October 1996, a small additional EM horizontal loop MaxiProbe survey was effected on the South-West block in order to verify the correct interpretation of the previous survey done in the same place. Due to the seemingly horizontal nature of the strata and of the conductors previously discovered by MaxiProbe, the geophysical consulting firm recommended that we proceed with an additional test, only this time from a North to South direction i.e. the opposite direction previously performed. This was done in order to ascertain whether a different direction of approach of the transmitter and receiver would or would not affect the localization of the EM conductors. The table below indicates the lines covered by this survey. Readings were taken every 25 meters on lines 12+00E et 14+00E, and at every 50 meters on lines 16+00E.

Table 4 Lines covered by the MaxiProbe-EM survey in 1996 - Central Manicouagan Property

LINES	STATIONS	DISTANCE (km)
L12+00E	10+00S-39+75N	4.975
L14+00E	10+00S-38+50N	4.85
L16+00E	10+00S-38+00N	4.8
	TOTAL	**14.625**

The equipment used for this survey was the same as that used in 1990. However, certain parameters such as the separation between the receiver and the transmitter, as well as the range of frequencies used was modified. The separation between the receiver and the transmitter was fixed at 300 meters and the readings were taken on 15 frequencies varying from 0.11 to 39.06 kHz. The depth of penetration was evaluated at about 500 m vertical. In addition, considering that the MaxiProbe

System is asymetrical, the survey was executed in a direction North to South, opposite to that done in 1990, in order to compare the results of both surveys.

The MaxiProbe EM survey permitted the detection of several EM anomalies that could be again regrouped into two principal types; the basin type (type 1) and the root type, having a vertical component (type 2).

The following table indicates the localization and the type, as well as the quality of the EM anomalies indicated by the MaxiProbe EM survey in 1996. These anomalies have been indicated on the 1:20,000 scale compilation map in the pocket in the present report.

Table 5 Results of EM-MaxiProbe survey performed in 1996 - Central Manicouagan Property

LINES	STATIONS	AXIS	TYPE / QUALITY
L12+00E	10+00S - 2+00N		Large basin
	4+00N - 6+50N	4+75N	Excellent
	7+00N - 8+25N	7+87.5N	Poor
	8+75N - 12+00N	10+00N	Mediocre
	17+25N - 19+25N	18+75N	Excellent
	21+25N - 22+75N	22+00N	Mediocre
	23+25N - 26+50N	25+50N	Excellent
L14+00E	10+00S - 1+90S		Large basin; 4 vertical roots
		9+25S	Weak
		7+75S	Weak
		6+50S	Excellent
		3+00S	Excellent
		0+37.5S	Mediocre
	1+75N - 5+25N	4+00N	Mediocre
	7+00N - 8+50N	7+75N	Excellent
	10+00N - 20+00N	11+00N	Mediocre
	18+25N - 20+00N	19+25N	Excellent
	24+00N - 26+75N	25+00N	Excellent
	36+75N - 38+50N	37+50N	Excellent
L16+00E	10+00S - 5+00S	9+50S	Basin; 2 vertical roots
		5+50S	

Table 5 Results of EM-MaxiProbe survey performed in 1996 - Central Manicouagan Property

LINES	STATIONS	AXIS	TYPE / QUALITY
	1+00S - 4+50N		Basin
		1+00N	Excellent
		2+50N	Mediocre
		6+00N	Weak
		7+50N	Weak
		10+00N	Weak
		19+00N	Mediocre
		21+50N	Excellent
		26+00N	Weak
		30+00N	Weak
		35+25N	Weak

The analysis of the results of the 1996 survey with respect to the survey done in 1990 concluded that it was not necessary to perform this type of survey in both directions and that the results of the 1996 survey were close enough to those of the 1990, such that they confirmed the relative accuracy of the interpreted location of conductors at depth.

6.1.6 SUMMER FIELD WORK 1997

MELIS HORIZONTAL LOOP EM SURVEY (PRESENTLY UNDER WAY)

In May 1997, Minéraux Manic Inc. commissioned SAGAX Géophysique Inc., Val d'Or, Quebec, to carry out an electromagnetic loop ρ' mode survey (Melis system) over its north-western of the central Manicouagan Property. The purpose of this survey was to detect and delimit electromagnetic anomalies at depth as well as determine potential drill targets. This survey method was chosen because of its patent-based technology identical to MaxiProbe. The Company wished to compare the survey techniques, costs and interpretative results. Previous extensive geophysical work had led the Company to select a system suited to finding low resistivity, but not necessarily strong conductive bodies. The depth of investigation of any EM techniques is strongly related to the conductivity and size of the target. The depth of investigation of the MELIS survey should be at last 600 m for vertical conductors and 1 000 m for sub-horizontal targets in such environment. A full description of the method, field operations, interpretation principles, depth of investigation including case histories is present in Annexe VII of the present report.

The MELIS survey was conducted over a total of 18 km lines. The lines are parallel to each other and are spaced 400 m apart. Stations are spaced every 75 meters. The lengths of the individual surveyed lines are listed in Table 7 hereinafter.

Table 6 Lines covered by the Melis survey in 1997 - Central Manicouagan Property

LINES	STATIONS	DISTANCE (km)
L20+00E	TL 12+00S-TL 9+00N	2.1
L16+00E	TL 12+00S-TL 9+00N	2.1
L12+00E	TL 12+00S-TL 9+00N	2.1
L8+00E	TL 12+00S-TL 9+00N	2.1
L4+00E	TL 12+00S-TL 9+00N	2.1
L4+00W	TL 8+00N-TL 24+00N	1.6
L8+00W	TL 8+00N-TL 24+00N	1.6
L12+00W	TL 8+00N-TL 24+00N	1.6
L16+00W	TL 8+00N-TL 24+00N	1.6
L20+00W	TL 8+00N-TL 24+00N	1.6
	TOTAL	**18.5**

The data obtained during the MELIS survey on the Central Manicouagan Property of Minéraux Manic Inc. is currently being interpreted by SAGAX Geophysics. The results will be available during the next few months.

6.1.7 OTHER STUDIES PERFORMED ON THE MANICOUAGAN PROPERTY

COMPUTER MODELLING OF MANICOUAGAN MAGNETIC DATA (See ANNEXE V.C)

In 1992, Paterson of the geophysics consulting firm Paterson, Grant and Watson Limited, Toronto, generated several computer models of the Manicouagan magnetic anomaly and concluded that two possible models can explain this anomaly.

1. A relatively shallow emplacement of a body of mafic composition, the center of which is not below 560 m, and having a magnetic susceptibility of about 4% Fe_2O_3 or less which corresponds to a fairly well mineralized magnetic mafic intrusion.

2. A relatively deeper body, the center of which is at approximately 1,000 m deep, with a susceptibility equivalent to roughly 80% Fe_2O_3 or less which, according to Mark Pilkington

of the GSC, is seven times higher than that for iron formation indicating the body may be the remnant of an iron-nickel meteorite.

Paterson also concluded that the body causing the anomaly could have a minimum width of 600 meters, but more likely is 1,800 meters wide.

STUDY ON MANICOUAGAN MAGNETICS (See ANNEXE V.D)

In 1992, Peter Schultz, an expert on meteorite impacts in general and the Sudbury and Manicouagan structures in particular from Brown University, produced a study of the magnetic data from Manicouagan, and examined means and methods to determine the cause of the central magnetic anomaly.

Schultz hypothesizes that the differences in the crater diameter and magnetic anomaly diameter ratios between Manicouagan and other large impact sites may be due to the greater speed or smaller size and increased density of the object that hit at Manicouagan.

IDENTIFICATION OF REMANENT MAGNETIZATION EFFECTS IN MAGNETIC DATA FROM THE MANICOUAGAN CRATER (See ANNEXE IV.B)

Remanent magnetization can have a significant influence on the shape of the magnetic anomalies in the areas characterized by induced magnetization. This approach was applied to the magnetic anomaly in the center of the Manicouagan crater in 1992/1993 by Roest and Pilkington of the GSC.

The study consisted of proposing a method to determine the possible contribution of remanent magnetization to a particular anomaly and in measuring and re-aligning the remanent magnetization to magnetic north, thereby separating and distinguishing the total field magnetics from the magnetic field reduced to pole, the latter of which reflects more accurately the 'real' magnetic intensity and dimensions of the central anomaly.

The results of this study, based only on the magnetic anomaly observations, are in agreement with constraints on the direction of remanent magnetization from rock samples. The results are significant in the debate concerning the identity and cause of the body producing the magnetic anomaly. This study suggests the anomaly was caused by the impact, in other words it was not present beforehand and did not happen after the time of impact. The magnetic anomaly, therefore cannot be a large chunk of displaced iron formation nor the topographical expression of shallow basement rocks, as had been speculated by various geologists in the past.

SHADOW MAPPING OF MAGNETIC DATA

In 1994, the Geophysics division of the GSC produced a 1:50,000 scale shadow map of the Manicouagan crater in its regional Grenville context. The relative magnetic highs and troughs are represented with respect to each other as textural features on a regional scale.

The results indicate the overall inhomogeneous pattern and variations in texture and smoothness of the magnetic signature covering the Grenvillean region to the exterior of the crater perimeters.

In contrast, the Manicouagan crater rocks, with the exception of the central anomaly which has different proportions, has a homogeneously rippled texture throughout the entire crater interior. This reflects a uniform magnetic background to the impact melt rocks overlying a shock metamorphosed and perhaps geophysically transformed basement.

REPORT ON THE SURFICIAL GEOLOGY OF THE MANICOUAGAN STRUCTURE.

In 1994, The Manicouagan impact structure was mapped at 1:50,000 scale by Geovision International, Boucherville, Quebec, in the hopes that the nature, extent and thickness of surficial deposits would provide information useful for planning further exploration activity and subsequent property development.

The surficial deposits and the estimated thickness of the deposits over local bedrock subcrops were interpreted from stereo sets of 1:50,000 scale airphotos taken in 1976 covering a study area of 644 km^2. Twelve types of surficial deposits and four depth classes were mapped and characterized. Results were presented as nine annotated airphotos and the interpretations were transferred to a 1:50,000 digitized planimetric map base.

LITHOCHEMICAL STUDY OF THE MANICOUAGAN IMPACT SITE. By J.M. Siriunas.

In 1994, Minéraux Manic Inc. commissioned J.M. Siriunas of NR & J Resource Associates Limited, Toronto to produce a study involving the re-evaluation of samples collected in the vicinity of the Manicouagan structure and analysed for whole rock and trace elements. This re-examination attempted to seek lithologic evidence for the nature of the meteoric body at the Manicouagan site and/or any lithochemical anomalies that may be of economic significance.

Siriunas observed the Manicouagan melt rocks to be intermediate in the sense that they are compositionally intermediate (andesite) and that their bulk composition lies intermediate to the country rocks of the region. The composition of the melt rocks is very homogeneous. Only three samples vary chemically from the bulk composition of the melt-rock samples. Two of these samples have higher lime and magnesia contents. According to Grieve and Floran (1978), this local heterogeneity may be due to the assimilation of mafic clasts in the immediate vicinity of these samples. Siriunas notes that since the iron oxide content of these samples matches that of the bulk

content, the additional lime and magnesium could have been supplied by local inclusions of limestone.

This study was inconclusive in showing that the Manicouagan melt rocks have any affinity for an extraterrestrial body, but nickel and the platinum group metals (including iridium) were not included in the data analysed. The geochemistry of melt rocks is not expected to reflect any association with spatially-related magmatic base metal deposits since ore-forming processes are not directly linked to the formation of an impact melt.

Siriunas suggests that continued exploration work on the Property, especially in the form of diamond drilling, may intersect additional igneous lithologies on which lithochemical studies can be performed and evaluated for their PGE potential.

PETROGRAPHY AND ROCK MAGNETIC PROPERTIES OF DRILL CORE FROM THE CENTRAL MAGNETIC ANOMALY

In 1996, in the framework of an industrial partners' program of the CGC (GSC IPP Project #930022) Minéraux Manic Inc. obtained the participation of the GSC in research work concerning the petrography, as well as the magnetic properties of the drill core from hole MC-1 drilled by Minéraux Manic. Inc. on the central magnetic anomaly in 1990-1991.The purpose of this study was to investigate the origin of the localized magnetic anomaly high observed in the Manicouagan impact structure by determining the lithologic, mineralogical and magnetic characteristics of the core. The core was analysed for magnetic susceptibility and its anisotropy, and for natural remanent magnetization characteristics.

The following conclusions were drawn from this study. The most important conclusion of the GSC was that the magnetism of the drill core itself was very feeble, not obtaining a magnetic susceptibility of more than 2%, with a very low content (less than 1%) of fine grained magnetite that was the result of metamorphism of mafic minerals in the drill core. The GSC concluded that there were no other minerals in the drill core that could have produced magnetism, i.e. for instance sulfide mineralization. The GSC also informed the Company that in its view the drill hole had simply not yet reached the source of the magnetism and that furthermore, the core susceptibility test indicated that the Company had not missed its target by either drilling underneath the magnetic body or beside it. The Company also wishes me to enclose in this report its comment that it has no opinion with respect to the possibility that the Central Manicouagan Property overlies part of the central uplift area of the meteorite impact crater. The Company notes that the topography, the lack of graben and horst type up to the features which are so outstanding in the case of the anorthositic uplifted regions to the North of the Property, demonstrate that the area underlying the Central Property may or may not be part of a central uplift area. The GSC conclusions were as follows.

> The core is composed of granulite grade basement rocks uplifted some ten kilometers by the structural rebound of the central uplift during the impact event. The formation

of secondary magnetite from pyroxenes and garnets resulted from the combination of the uplift of hot, high grade rocks and mechanical and thermal shock effects. The intensity of magnetization of the granulitic gneisses may have increased due to the acquisition of a new natural remanent magnetization by the shocked and heated rocks. This study determined that sulphides are present only in trace amounts. Therefore the magnetic character of the granulite gneiss sampled by the drill core and analysed cannot be due to sulphide-type magnetic minerals such as pyrrhotite, but must be due to other magnetic minerals such as magnetite. This study also determined that alteration increases with depth which suggests that hydrothermal alteration and shock decomposition of mafic minerals extends to a greater depth than that sampled by drilling to date.

This study concludes that three-dimensional modelling of the observed magnetic field at Manicouagan and comparison with drill core measurements suggests that the high magnetizations of the causative body have not been reached by the borehole.

GENERATION OF A MANICOUAGAN DATABASE AND ASSOCIATED MINERAL POTENTIAL DATA PRODUCTS. IN PROGRESS

In December 1996, in response to common scientific interest, Great Legends Mining Inc., Minéraux Manic Inc., First Mark Technologies Limited, Ottawa and the GSC entered into a intellectual partnership to study the regional context and details of the Manicouagan impact structure.

The primary goal of the effort is to construct a Manicouagan database, using a Geo-referenced Information System (GIS) based toolset, which will allow for the generation of thematic and interpretive maps to support the mineral exploration of the Manicouagan impact site. The secondary objective, and the motivating factor for the GSC participation, is the evaluation of Radarsat data as a correlative data source for the analysis of mineral potential analysis. The output from the exercise will be utilized, in cooperation with the claims holders in the publication of research results by Richard Grieve of GSC.

The database covers all of NTS 22N (Manicouagan Reservoir sheet), half of the 22O (Lac Fouquet sheet) and 22K (Berté Lake sheet) and a quarter of the 22J (XXXX sheet). The equivalent UTM (Zone 19, NAD 83) are:

Maximum Northing:	5770000 mN	Maximum Easting:	627000 mE
Mimimum Northing:	5590000 mN	Minimum Easting:	420000 mE

The primary tools to be used are remote sensing data. The GSC contributed remote sensing data including: Radarsat I Synthetic Aperture Radar (SAR) data, Landsat TM, airborne wide swath SAR, European Resource Satellite (ERS-1) SAR data; digital topography data (1: 250 000); and geological data including gravity, magnetics, geochemical and rock sample data. the claims holders of the

Manicouagan Properties contributed their exploration results including airborne and ground geophysical, geological and geochemical data. First Mark Technology Ltd contributed their expertise in processing the data. This information will be converted to a single geo-reference base and single map projection. The database will take the final form of a single integrated GIS using a software package which will run on a PC Windows-based platform.

The Manicouagan Database development effort was broken down into three phases. The Phase I focussed upon the collection, input and rationalization of the core "regional" datasets. These datasets included the topographical data, the geological and a subset of the remote sensing data. The volume of remote sensing datasets to be processed and input has been limited to the Radarsat and Landsat TM. Based upon an analysis of this data, and driven by the quality and coverage of that data, ERS-1 has been used to supplement the space-borne radar data. The Phase II will focus on the analysis of the Phase I products and identification of areas/features of interest. Based upon this analysis, Canada Centre for Remote Sensing (CCRS) airborne SAR data for the areas of interest has been input to create a series of "local" datasets. The volume of data associated with the airborne SAR, and its resolution (15 metres versus 30 meters for space-borne SAR), suggested that costs are optimized if data is input and analysed on an "as required" data basis. The Phase III will focus upon the production of a series of integrated products to support exploration plans for the Manicouagan impact site.

To date, 5 regional plots has been produced for analysis and a preliminary interpretation has been performed and will be revised based on the knowledge of local geology supplied by Richard Grieve, and Lauri Boivin. These products are regional plots of the Radarsat and Landsat data; regional plots of integrated Radarsat/geology, Radarsat/gravity and Radarsat/magnetics.

As a preliminary interpretation, an overlay was prepared by extracting faults and foliation from Murtaugh's published geology map. Additional information was added to the overlay by interpreting the lineament and textural information within both the Radarsat dat and integrated composite images. Lineament information supported the foliated measurements highlighting the continuity of regional structure. Textural information was used to infer lithological contacts and dissect the image.

Radarsat data was useful in defining the extent of the melt sheet Lineament information related to foliation was highlighted in units of gneissic lithology. North of the reservoir, the information in the Radarsat image is dominated by north-south fluted lineaments inferring the glacial deposition of till and fluvial deposits. This cover masks underlying bedrock structure. The composite of Radarsat and regional magnetics was invaluable for interpreting faulting and foliation as the subtle Radarsat lineaments are supported by contoured trends/patterns interpreted from the regional magnetics.

6.2 QUERTIER PROPERTY

REGIONAL PROSPECTING AND GEOLOGICAL MAPPING OF MANICOUAGAN CRATER

Prospecting and reconnaissance work in the Manicouagan Crater performed by Minéraux Manic Inc. discovered Cu-Ni-PGE showings on a group of small islands located near the shores of the René-Levasseur Island. The rocks on these islands are part of the brecciated mafic basement. Three grab samples were taken from one island part of the brecciated mafic basement and crosscut by a steeply dipping very fine grained ultramafic dyke with numerous tension fractures, and assayed for Au, Ag, Cu, Ni and PGE (Rh, Pt, Pd). The best values reported are 0.90% Cu, 0.27% Ni, 0.96 g/T Pt, 2.3 g/T Pd, 0.50 g/T Au and traces of Rh and Ag (L2-6-3). The following table summarizes assay values obtained on the original copper-nickel showing in 1990.

Table 7 Assay results on the original Cu-Ni-PGE showing - Quertier Property

SAMPLE NUMBER	Cu (PPM)	Ni (PPM)	Au (PPB)	Pt (PPB)	Pd (PPB)
L2-6-1	6660	2350	430	920	2300
L2-6-2	4030	1660	220	490	1300
L2-6-3	8990	2740	500	960	2300

This outcrop hosts the original nickel and copper showing, which precipitated the initial staking.

6.2.1 SUMMER EXPLORATION WORK 1991

GEOLOGICAL SURVEY 1991

In summer 1991, The initial property was mapped and prospected in an effort to locate favourable geology for nickel-copper mineralization by Kenwood (1991). The mapping and prospecting successfully located a large ridge (150 metres by 75 meters) of brecciated mafic gneiss which returned anomalous copper and nickel values similar to that which hosts the original showing. The following table summarizes the best assay values obtained during the mapping and prospecting work done in 1991.

Table 8 Assay results of prospecting and mapping work 1991- Quertier Property

SAMPLE NUMBER	Cu (PPM)	Ni (PPM)	Pt (PPB)	Pd (PPB)
MJ-05	1793	649	256	520
MJ-06	361	378	51	86
MJ-10A	180	718	69	137
MJ-10B	55	607	17	34

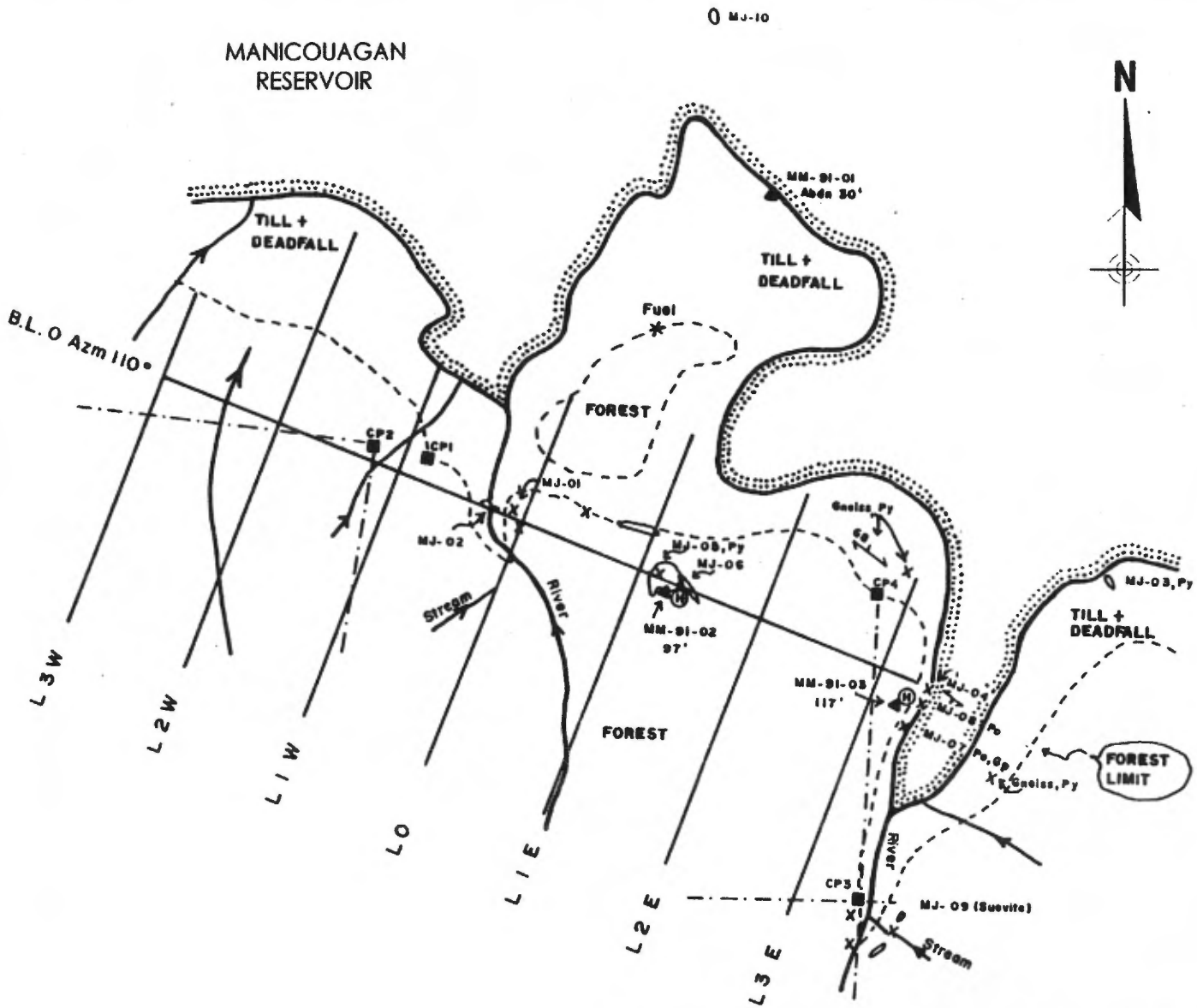
VLF-EM SURVEY

In conjunction with the mapping and prospecting program an electromagnetic survey, EM-VLF, using a Geonics EM-16, was performed. The Annapolis Maryland station (NSS, 21.4 kHz) was used for this survey. which covered 1125 m of survey line with readings every 25 m. The balance of the grid was planned for survey but instrument problems precluded this. The lines covered are presented below.

Table 9 Lines covered by VLF(NSS)-EM survey in 1990 - Quertier Property

LINES	STATIONS	DISTANCE (km)
L0+00E	2+00S-1+00N	0.3
L1+00E	2+00S-1+00N	0.3
L2+00E	2+00S-1+00N	0.3
L3+00E	2+00S-0+75N	0.275
	TOTAL	**1.175**

The survey data, as shown in Fig. 9, displays an erratic spikey pattern suggesting poor coupling with bedrock. It is likely that the choice of NSS as the survey station was inappropriate due to it being at an azimuth of approximately 190 degrees to the property, and the strike of the local geology is 310. A more effective station would have been NLK (Seattle, Washington), which was probably not working at the time.



LEGEND

GEOLOGY

Pyrrhotite	Po
Pyrite	Py
Graphite	Gp
Foliation	

OTHER SYMBOLS

Till + deadfall
Edge of forest _____
Claim line _____
Claim post
Helicopter pad Ⓗ
Outcrop No MJ-10

CLAIM POSTS

CP1	5046583-2
	586-3
	582-2
	586-4
	588-3
	581-1
	588-4
	587-4
	581-2
	582-1
	582-1
	583-1
	587-3
CP2	5046584-1
	585-4
CP3	5046184-1
	191-4
	592-3
	585-2
CP4	5046588-1
	589-4
	592-4
	590-4
	588-2
	589-3
	585-1
	591-3
	586-2
	587-2
	591-4
	590-3
	586-1

MINERAUX MANIC INC.
QUERTIER PROPERTY

COMPILATION MAP

MADE: R. MOAR

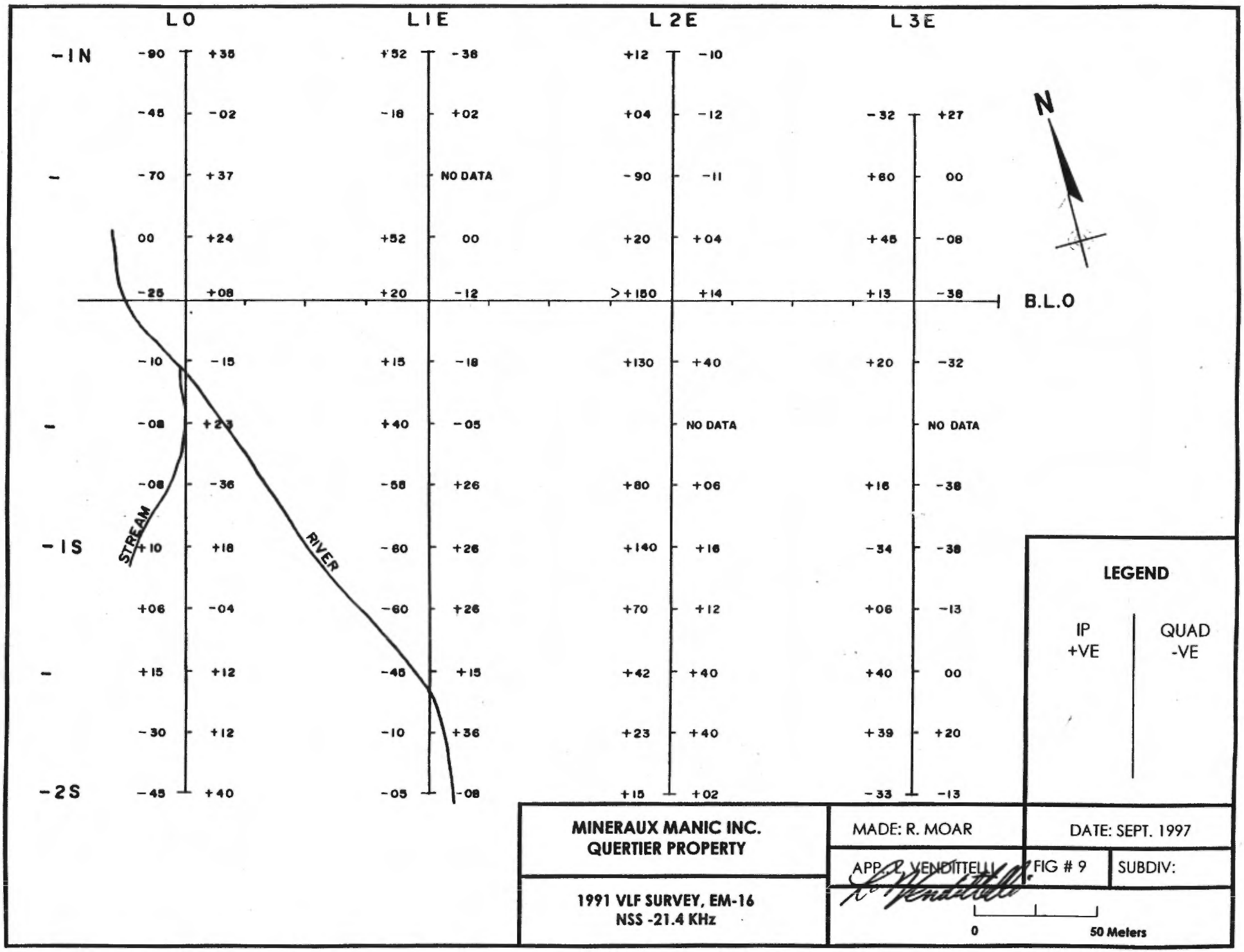
DATE: SEPT. 1997

APP: R. VENDITTELLI

FIG # 8

SUBDIV:

SCALE 1 : 5,000


L0
L1E
L2E
L3E
-1N
-1S
-2S
B.L.0
N
STREAM
RIVER
NO DATA
LEGEND
IP
+VE
QUAD
-VE
MINERAUX MANIC INC.
QUERTIER PROPERTY
1991 VLF SURVEY, EM-16
NSS -21.4 KHz
MADE: R. MOAR
DATE: SEPT. 1997
APP: L. VENDITTELLI
FIG # 9
SUBDIV:
0
50 Meters

6.2.2 AUTUMN EXPLORATION WORK 1991

In the fall of 1991, Minéraux Manic Inc. undertook a diamond drilling campaign for test holes, sampling surface mineralization and to provide information regarding the extent of mineralization on the property. A total of 74 m was drilled with 3 DDH.

DDH MM-91-01

The objective of DDH MM-91-01, drilled vertically on the shores of the Manicouagan Reservoir, was to determine the south extension of the original Cu-Ni showing. Drilling was abandoned at 9.14 m in overburden due to technical difficulties.

DDH MM-91-02

Hole MM-91-02 was collared at grid coordinates 1+25E / 0+08S at 60°N with a dip 65°. This was drilled to sample at greater depth the mineralized and brecciated mafic gneisses of outcrops MJ-05 and MJ-06. This hole intersected brecciated mafic gneisses at a depth of 1.8 m. These dark gray, fine-grained brecciated gneisses show little evidence of foliation and are enclosed in a black coloured magnetic matrix. The rock shows slight alteration to epidote, calcite and quartz as veinlets. One can observe an increase in brecciation and matrix material with depth. Pyrite forms up to 1% of the mineralization and occurs finely disseminated or as fracture filling. The hole was terminated at 29.6 m. The best intersection in this hole revealed values of 0.31% Cu, 0.07% Ni and 1.1 g/T Pt over 0.60 m (sample # MM-91-02-2).

DDH MM-91-03

Hole MM-91-03 was collared at grid coordinates 3+24 / 0+27S at 45°N dipping 53°. DDH MM-91-03 was drilled to determine the extension at depth of mineralization (Po and Py) occurring on outcrops MJ-07 and MJ-08. The hole intersects brecciated gneisses at 4.6 m. These rocks alternate with gneisses of quartzo-feldspathic composition and fine grained mafic gneisses with locally, sections of melt rock containing gneiss fragments. The hole had a total depth of 35.66 m with no significant mineralization.

6.2.3 AUTUMN EXPLORATION WORK 1996

LINE CUTTING, PROSPECTING AND SAMPLING

Prospecting and sampling work was undertaken on the property in the fall of 1996. This work did not reveal any new copper and nickel showings on the property. However, grab samples were collected from outcrops identified during Kenwood's work in 1991 for re-evaluation. This examination revealed values superior to those obtained from the 1991 prospecting and sampling

work. One grab sample assayed 0.58% Cu and 0.21% Ni and 1.87 g/T Pt (RM-97-11 / 52001) and was taken from the same outcrop mapped by Kenwood in 1991 (MJ-02).

Following this prospecting and sampling work, the lines grid was extended in order to extend ground geophysical surveys over the entire property. Lines were spaced at every 100 m and were picketed and chained at every 25 m. A total of 37.98 km of lines including the baseline were cut.

6.3 SOUTHWEST ISLAND PROPERTY

No exploration work has been done on this property other than the prospecting and sampling done by Minéraux Manic Inc. in 1990 and 1996.

The 1990 regional prospecting and evaluation work in the Manicouagan by Minéraux Manic Inc. revealed the presence of a second showing of Cu-Ni-PGE associated with a post-impact ultramafic dyke. The presence of an ultramafic dyke on the property that does not show any evidence of shock metamorphism indicates post-impact magmatic activity. The petrographic examination of a sample collected in 1990 from this ultramafic dyke reveals that the rock is a plagioclase bearing pyroxene hornblendite consisting of 90% amphiboles and pyroxenes and 5% plagioclase, 3% iron bearing biotite and 1-2% opaques (Chabot, 1990). This outcrop hosts the original nickel and copper showing, which precipitated the initial staking. Three grab samples were taken in 1990 from this outcrop and assayed for Cu, Ni and PGE (Pt, Pd). Assay result reported 0.17% Cu, 0.19% Ni and traces of Pt and Pd (5.1-MIN-B).

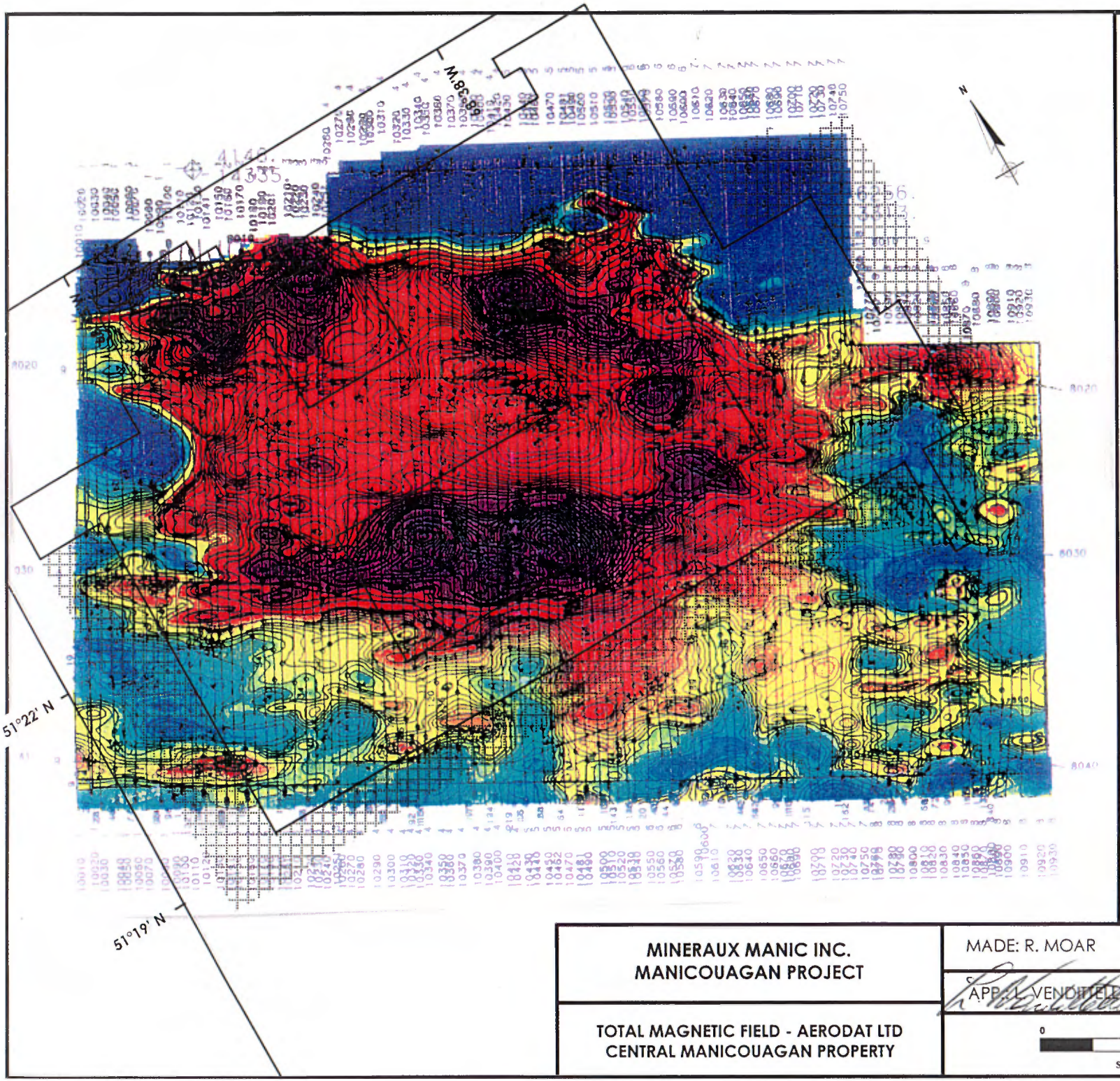
Prospecting conducted in the fall of 1996 revealed weakly disseminated pyrrhotite (Po), pyrite (Py) and malachite (Ma) on this outcrop. Geochemical analysis of samples taken from this site indicate values of 0.012% - 0.037% Cu and 0.029% - 0.133% Ni (RM-96-08/52002; RM-96-07/52003; RM-96-09/52004; RM-96-05/59006; RM-96-04/590070).

Table 10 Assay results of prospecting and mapping work 1990-1996- Southwest Island Property

SAMPLE NUMBER	Cu (PPM)	Ni (PPM)	Pt (PPB)	Pd (PPB)
5.1.MIN-A	348	128	10	18
5.1.MIN-B	1670	1900	10	14
M-5-1B-1	88.2	282	<10	<1
RM-96-04 (59007)	125	290	52	<10

Table 10 Assay results of prospecting and mapping work 1990-1996- Southwest Island Property

SAMPLE NUMBER	Cu (PPM)	Ni (PPM)	Pt (PPB)	Pd (PPB)
RM-96-05 (59006)	225	680	32	88
RM-96-07 (59003)	303	630	76	192
RM-96-08 (59002)	371	870	138	<10
RM-96-08 (59004)	125	290	52	<10



LEGEND

FLIGHT PATH

Navigation and recovery using a Global Positioning System (GPS). Average terrain clearance 60 m. Average line spacing 200 m.

MAGNETICS

Total Field Magnetic Intensity contours in nT. Cesium high sensitivity magnetometer. Sensor elevation 45 m

60300.
59140.
58850.
58700.
58580.
58490.
58410.
58300.
58170.
58060.
57950.
57840.
57740.
57670.
57610.
57550.
57500
57460
57410
57380
57340
57290
57240.
57170.
57050.
56860.
56620.
55650

MINERAUX MANIC INC.
MANICOUAGAN PROJECT

MADE: R. MOAR

DATE: SEPT. 1997

APP'D: L. VENDITTELLI

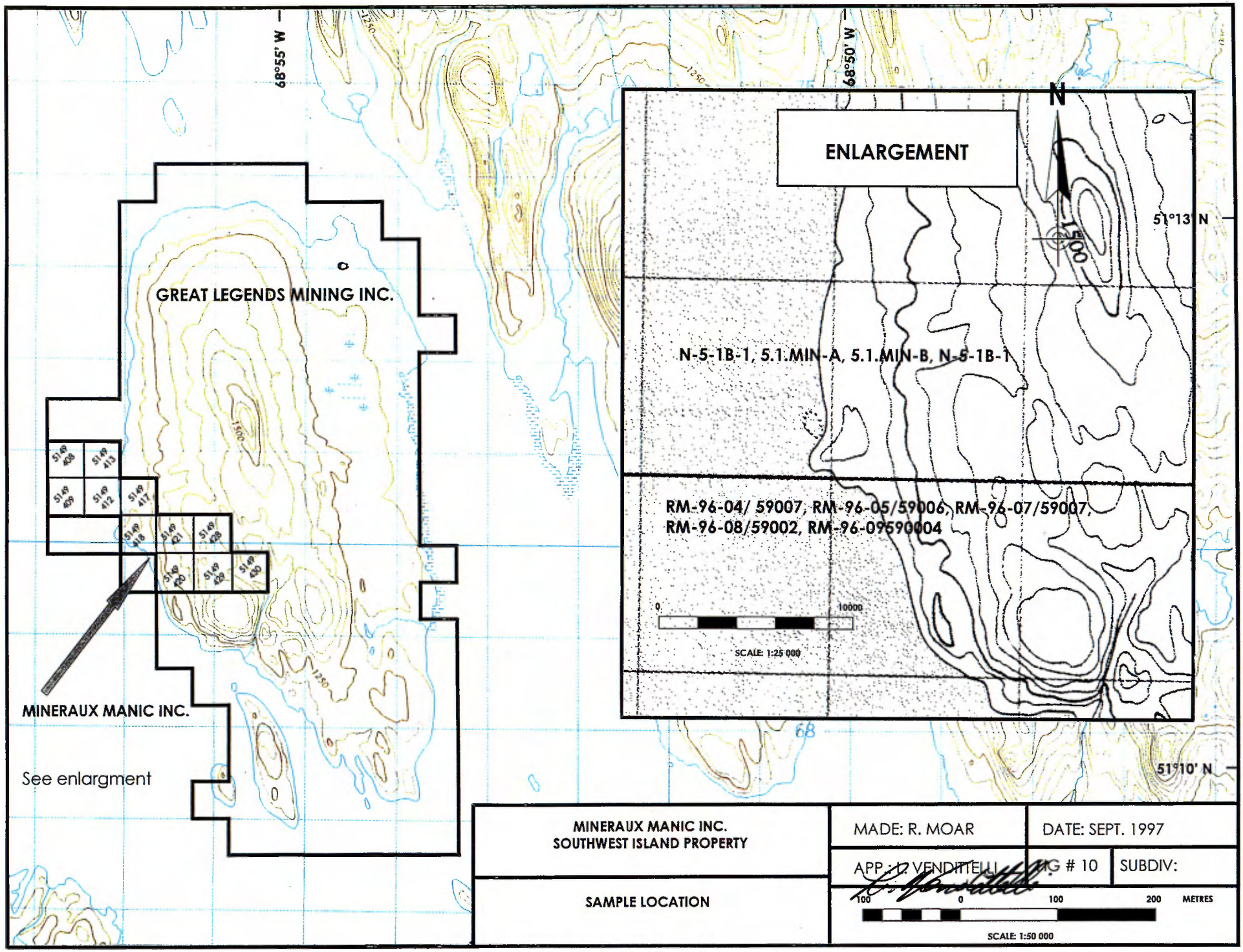
FIG # 7

SUBDIV:

TOTAL MAGNETIC FIELD - AERODAT LTD
CENTRAL MANICOUAGAN PROPERTY

0 5 km

SCALE 1: 1 000 000


68°55' W
68°50' W
51°13' N
51°10' N
GREAT LEGENDS MINING INC.
MINERAUX MANIC INC.
See enlargment
ENLARGEMENT
N
1500
N-5-1B-1, 5.1.MIN-A, 5.1.MIN-B, N-5-1B-1
RM-96-04/ 59007, RM-96-05/59006, RM-96-07/59007,
RM-96-08/59002, RM-96-09590004
0
10000
SCALE: 1:25 000
MINERAUX MANIC INC.
SOUTHWEST ISLAND PROPERTY
SAMPLE LOCATION
MADE: R. MOAR
DATE: SEPT. 1997
APP: D. VENDITELLI
MAP # 10
SUBDIV:
100
0
100
200
METRES
SCALE: 1:50 000

7.0 GENERAL DISCUSSION

7.1 GENERAL DISCUSSION OF THE MANICOUAGAN IMPACT

Several facts related to the age of the impact event conspire against a typical Sudbury model. At the moment of the Sudbury event 2.1 Ga (whether this event was an explosion from exterior or interior forces is moot), the crust at the time was thin and still hot, and the forces could provoke the ascension of mantle material into near surface conditions. The later mineralization was formed mainly due to gravitational differentiation and post-event magmatism.

In the case of the Manicouagan impact, the continental crust into which the meteorite fell was probably at least 100 km thick, and was cold and hardened, as the result of crustal differentiation and cooling over the long period of the planet's history. The impact site was located in the center of the single planetary continental craton. Therefore, while it may appear debatable that the force of the impact was sufficient to provoke the intrusion of mantle material, there is certainly sufficient field evidence to indicate that the force was sufficient to generate post-impact magmatism in the form of ultramafic sulfide mineralized dykes and breccia dykes and mineralized breccia zones. The activation of post-impact magmatic events and possible hydrothermal recirculation of fluids in the host rocks could certainly provoke the remobilization of ore elements which could be later concentrated in favorable environments such as faults, shear zones, breccia zones and dyke formations.

Certainly, a cursory review of meteorite impact data indicates that, economic resources occur in approximately 25% of known terrestrial impact structures. Of these, 12% are either currently being exploited or have been exploited in the recent past. The current worth of economic materials produced from impact structures is estimated at five billion dollars per year for North America alone. Grieve and Masaitis (1994) have classified the larger economic deposits as progenetic, syngenetic and epigenetic.

Syngenetic deposits include impact diamonds at several structures and Cu-Ni-PGE ores of the Sudbury Igneous Complex, interpreted as part of the impact melt system of the Sudbury Structure. Company field workers have certainly obtained evidence that similar Sudbury type structures and mineralization are present in the Manicouagan Basin.

Epigenetic deposits include post-impact hydrothermal and sedimentary related deposits as well as hydrocarbon deposits such as at Ames, U.S.A.

Progenetic deposits include iron and uranium ore exploitable due to central uplift structures at Ternovka, Russia (375+/-25 Ma) and Carswell, Canada (115 +/- 25 Ma) as well as gold and uranium deposits in the Vredefort impact structure, especially the Witwatersrand Basin gold fields.

7.2 MINERALIZATION MODELS FOR THE MANICOUAGAN IMPACT SITE

As discussed above, and elsewhere in this report, there is strong evidence that the Manicouagan Impact Structure can host mineralization of a type and nature similar or identical to the Sudbury Impact Structure, which is a famous world-class mining camp for base metals. However, in addition to a magmatic and/or hydrothermal model for mineralization which, despite the very high magnetism and the relatively deeper depths at which the magnetic body is suspected to be located in the central area of the crater, still remain distinct possibilities for the explanation of the very high magnetic anomaly, there is a third very probable explanation for the magnetic anomaly and for the potential discovery of economic mineralization. The third model would be that of the remnants of an iron-nickel meteoritic body which could generate the magnetic readings currently observed in the field. This model i.e. iron-nickel remnant, is the first explanation that came to the mind of Dr. Norman Paterson, (see references and Annexe V.C of the present report) in which his computer modeling of the anomaly indicated a magnetic susceptibility greater than 80% of the body that might cause this anomaly if the center of the body causing this anomaly was located at depths of about 1,000 meters. Since iron formation has a magnetic susceptibility ranging from 7-12% and since magnetite is the most magnetic mineral known to man on earth, it is obvious that a body buried at that depth would have to be many times more magnetic that of magnetite to account for such a anomaly. The two minerals present in iron-nickel meteorites, kamacite and taenite, possess magnetism substantially higher than magnetite (7 times higher).

It has been said that any object travelling at cosmic velocities and impacting over the hard rocks of the Grenville metamorphic province, would generate and release such an amount of energy that the would vaporize instantly. However, there is no proof or actual studies undertaken that would conclusively support this contention. There are scientists who claim to have found evidence of meteorites which, according to their theories, should not have survived an impact (Schultz, 1992).

Therefore, in summary, mineralization models involving magmatism and hydrothermal activity, as indicated by discoveries made on the Quertier and Southwest Island blocks deserve to be pursued in the future in exploration programs. In addition, special attention must be made in determining the cause of the high intensity magnetism emanating from the area surrounding the point of impact of the meteorite i.e. the center of the Manicouagan crater. The Company's best efforts, in fact, have been made in the past and will be made in the future on this promising central zone. The hydrothermal or magmatic models merit serious investigation in this area of the Property as well. However, the third model, - that of the potential discovery of an iron-nickel meteorite remnant is also one of the strongest scientific possibilities to explain the very strong (6-8,000 gammas above background central anomaly. The Company has dedicated efforts using totally conventional geological, geophysical and other approaches in its preliminary search for the cause of this magnetic body. In so doing and with the aid of recognized experts in their fields, the Company has arrived at the consideration of what appears, at this time, to be an unconventional model. However, it must be pointed out that this unconventional model fits geophysical data far better and far more aptly than any other presently known. Besides these three models above indicated, we can exclude the

possibility that the deposit is an iron formation, and field observation and other avenues of enquiry have eliminated for now the possibility that the anomaly is due to any topographical or known metamorphic phenomenon which could be responsible for the magnetism.

Before drawing any other theoretical conclusions, we should take a moment to discuss the topic of induced magnetization, a phenomenon that is not unfamiliar to meteorite impact sites around the world. Many large meteorite impact sites have magnetic features in their centre (personal communication Mark Pilklington - GSC), however, according to the experts who have catalogued such phenomenon, none resemble in strength and intensity the anomaly present in the centre of the Manicouagan crater. There is little doubt that the entire interior of the Manicouagan crater has been magnetized by shock metamorphism. Company workers have certified the presence of magnetite replacing all mafic minerals present in the impacted basement rocks. For this reason, the crater should normally possess a uniform magnetism over its entire magnetized area. Such is not the case. In fact, gneisses transformed to pure magnetite gneisses in areas of the Grenvillean basement inside the crater do not show-up in the regional magnetic maps, or they may be too small in aerial extent to do so. Some lunar basalts (personal communication Peter Schultz - 1997) demonstrate induced magnetization of several thousands gammas. The Manicouagan Central anomaly is 6-8,000 gammas above background, possibly a magnetization that if it were induced might exceed that of the admittedly little studied lunar basalts. Therefore, in the absence of further significance scientific developments in the understanding of magnetism we can reduce the possible models proposed to explain the positive body of the magnetic anomaly as below:

1) **Magnetization of a shallow ultra-mafic body** located originally in the Grenville basement rocks. This model is the least plausible. Field geology has proven to contradict some of the basic premises that this model is based on.

2) **A well-mineralized gabbroic or ultra-mafic shallow intrusion** having a magnetic susceptibility equivalent to about a third of that of iron formation. This is a popular theory and models like that described by Orphal and Schultz (1978) for Manicouagan, suggest the possibility of a ring dyke intrusion along steeply dipping faults that would have been the result of subsidence of the central uplift peak-ring along these faults subsequent to an intrusion -related uplift into the brecciated part of the crater floor. Problems with this model are firstly, even a shallow intrusion would have a root (there is no evidence of a deep root in the magnetic modelling) and secondly, a diapir-like magma emplacement at shallow depth as a result of magmatic differentiation of continental crust would be predictably felsic.

Ultra-mafic post-impact dyke intrusions mineralized with massive Cu-Ni rich sulfides occur outside the central magnetic highs mapped for the Manicouagan anomaly. These indicate the Sudbury Intrusion Model is a possibility and a strong economic incentive for exploration.

3) **Nickel-iron meteorite remnants**, buried at depth between 1,500 and 12,000 vertical feet. This metallic material is seven times more magnetic than magnetite and could clearly account for the gravity, magnetic and resistivity data accumulated to date.

The meteorite model could explain a number of observed properties such as the steep gradient , sharp contacts and uniform high-intensity across large widths of the magnetic anomaly as well as the absence of a magnetic 'root' and the location of the magnetic anomaly directly encircling the point of impact. This model also explains the coincidence of the gravity anomaly over the magnetic anomaly. The strongly magnetic nature of the dust matrix of the suevite and the unusually high ratios of ferric iron to ferrous iron in the whole rock lithochemistry of the impact melt rocks could also be explained.

The magnetic anomaly is different to any other known or similar structural feature, both in terms of size and intensity. The form of the magnetic anomaly is essentially an oval-shaped, northwest-southeast trending annulus open at the northwest end, and would conform to a geophysical response from a thick plate, slightly dish-shaped along its top surface. The upper surface of a large sharply-defined intrusive body would also create a similar response, but would require the intrusive to be much more magnetic at shallow, detectable depths..

Another very important premise on which the above models are based is that the magnetic anomaly was created and originated at the very moment of impact of the Manicouagan meteorite. This has been proven in paliomagnetic studies such as the one referenced to in this report. The age and cause of the magnetic anomaly is directly related to the age and timing of the meteorite impact event. This fact substantially reduces the number of potential causes for the magnetic anomaly. In addition, we must also consider the fact that three gravity peaks occur in the center of the crater. The two northernmost peaks are over anorthositic rocks of high elevation and the third is over a central low-lying plateau coincident with an extremely intense magnetic anomaly. The magnetic anomaly may be related to the related to the coincident gravity anomaly, which occurs over rocks different to what has generally been considered uplift rocks. Reliable in-situ rock samples in this area come from one deep drill hole which has intersected mostly leucocratic Grenville gneisses similar to those outcropping on the craton perimeter, with proportionally less massive anorthositic orthogneisses.

8.0 CONCLUSIONS AND RECOMMENDATIONS

I have collected all the available information on the Manicouagan structure and near regions from various sources, including several working sessions with personnel from the Company, a complete research of the GEOREF data system, the consultation of several papers on this and related subjects, and verbal communications from GSC staff and other scientific people. The geoscientific data base on the Manicouagan crater area is much more extensive than could ever be determined within the mandate of this report. Several universities, both here in North America and in Europe, possess extensive scientific data bases and samples suites from the Manicouagan crater. This crater is one of the most studied impact structures on the earth and for this reason there is an enormous amount of material in the scientific domain that has been generated by those attracted to its study because of its exceptionally well-preserved state and its almost text book similarity to the typical impact structures on the moon. fore, for the purposes of this report, although I have referred to the evolution and progress of scientific theory and to conversations I have had with Company staff including Lauri Boivin, the only geologist who has performed all of the regional geological as well as property geology and drill core logging from the Manicouagan Property, it has best behooved me to examine in some detail the results of the direct and conventional exploration and research work accumulated by the Company, in its study of the regional as well as the property characteristics of its claim holdings since 1990.

While there are many outcrops around the lakeshores bordering the interior crater area and there are many outcrops on the Quertier and Southwest Island Properties which have been detailed and described in this report and in the accompanying compilation maps, as far as concerns the Central Manicouagan Property, where very few outcrops occur and where none of these outcrops have contributed to finding a reasonable explanation for the cause of central magnetic anomaly, the main geological tools in this area have been:

- a broadly based geological knowledge of the crater as a whole;
- a knowledge of the relative thicknesses of strata that comprise its formational history;
- airborne geophysical data;
- ground geophysical surveys;
- filtration and subsequent manipulation of the airborne data (reduction to pole);
- the computer modelling thereof by several workers (Paterson 1992, Roest and Pilklington -GSC 1994);
- the study of drill core petrography, magnetic susceptibility and thin section analysis; and
- a regional Radarsat and remote sensing - based compilation of the entire area.

As a result of this work and analysis thereof, we would concur with Company management as to the determination of three possible models for potential economic mineralization.

Although the general region has been the subject of base metal exploration from such companies as Hudson Bay (1970's), during its prospecting and drilling campaign on the Manicouagan plateau some 60 km. to the east and in recent years by companies such as Falconbridge, Tiomin, Soquem, and other mining companies who are prospecting and continuing to explore the base metal showings within the Grenvillean gneisses, which is a very encouraging endorsement to the mineralization potential of the region. I could not be as optimistic as I am in recommending further exploration on these properties if it were not for the fact that all the mineralization discovered by the Company and that which it is still searching for were not directly associated, as it is, with the impact of a mega-meteorite such as that which caused the Sudbury mines to be emplaced and the Vredefort - Bushveld regions to host mineral wealth.

Although few would argue with the advisability or merits of exploration in the Grenvillean province per se, as is attested to by the list of companies above who are energetically pursuing such efforts, the fact is that until now the only producing mines located in the Grenvillean province are those of the Sudbury Basin and more is due to their meteorite impact origin then is due to their location in the Grenvillean province.

For this reason, I would suggest that the Manicouagan Properties may prove to be of higher merit then the properties being explored elsewhere in this region.

8.1 CENTRAL MANICOUAGAN PROPERTY

The basic recommendations I have to offer would be the continued indepth pursuit of the programs and strategies already underway by the Company. These include the immediate continuation of drill hole MC-1 and the drilling of four more vertical drill holes up to depths of 1,000 meters or more in order to determine the cause of magnetism on the Central Manicouagan Property. It is to be recommended, if at all possible, that the Company use either an IP probe or a magnetism probe down hole before continuing drilling on MC-1. The other four vertical drill holes should be positioned on target areas where both the total field magnetic anomalies and the Company's magnetic field reduced-to-pole anomalies coincide. These areas should indicate the sources of magnetism which are more likely to reflect the magnetism generated by the presence of a body without the interference of today's magnetic field, as well as the areas where this body may be closer to surface and easier to attain.

The samples obtained from these drill holes should be submitted to the same kind of study as the drill core already extracted from the property. As previous work performed by the GSC on the drill core has already indicated, metasomatic and hydrothermal aureoles tend to indicate stronger alteration with depth, which is an encouraging sign. The continued development of the Radarsat and remote sensing compilation will be most useful in obtaining a better estimate of the economic potential of the entire area. On a reconnaissance level, large scale geochemical studies may be recommended in the future for regional evaluation purposes. Proposed budgets are presented as follows in subsequent pages to best further the immediate objectives of the Company. For the Central Manicouagan

Property, the bulk of the budget should be dedicated to deep diamond drilling of the geophysical target areas. In the case of both Quertier and the Southwest Island Properties, where only initial reconnaissance and prospecting work has been done, these properties require standard Phase I type work such as: ground geophysical surveys, sampling, mapping, line cutting and test drilling of the mineralized zones and of the targets indicated by ground geophysical surveys. The Company should definitely pursue exploration on all three properties simultaneously so as to accrue a more detailed knowledge of the three different environments and enhance its chances of making discoveries of significant economic mineralization.

8.2 QUERTIER PROPERTY

Exploration work on the property to date has resulted in the identification of certain Cu-Ni showings associated with brecciated gneisses. Diamond drilling conducted in 1991 on the Cu-Ni showing from which samples MJ-05 and MJ-06 were taken reveals the extension of mineralization with depth.

The interesting geological and metallogenic context of the property fully justifies a systematic exploration program in order to evaluate the economic potential of cupro-nickeliferous mineralization in brecciated gneisses as well as in ultramafic intrusions crosscutting these gneisses. We recommend an exploration program for a total cost estimate of $181,220 aimed at studying and evaluating the ultramafic intrusions from which the mineralization seems to originate.

Exploration work will be aimed at locating magnetic and electromagnetic anomalies. Consequently, the initial phase of exploration will consist of airborne magnetic (total field and vertical gradient) and electromagnetic (5 frequency system) and VLF-EM (2 frequency system) surveys over the entire property. This airborne survey covers 485 km of lines nominally spaced at 200 m. The purpose of this survey is to detect interesting geophysical target zones requiring a more detailed ground study.

The property will be covered by a grid for detailed geological sampling and we recommend that the property be covered by appropriate ground geophysical survey to better identify and delimit ultramafic units and conductors. Property mapping will be done at the same time as the combined magnetic and electromagnetic surveys. Mapping will emphasize the evaluating of the volume of the most interesting mineralized unit, the mineralized breccia unit. This unit appears to have the potential for a large volume and has yielded the best Cu-Ni values. Work will also emphasize the structural relationships between the various lithologies, the identification of structures present as dykes or subvertical irregular cylinders, of more mafic units susceptible of being mineralized and of magnetic horizons that could be indicators of copper mineralization.

Finally, geological, magnetic and electromagnetic anomalies, concordant or not, will be examined by MaxMin II sections. At this stage, a budget of 30 km is enough to qualify these anomalies.

8.3 SOUTHWEST ISLAND PROPERTY

With respect to the mineral potential of the property, the authors recommend that surface exploration work be undertaken on the Southwest Island Property adjacent to the Manicouagan Crater. A two-phased exploration program is proposed. Exploration work will be aimed at determining the extent of the ultramafic dykes, their system of fractures and faults and associated sulfide mineralization.

The property will be covered by a line cutting grid with lines spaced every 100 m, picketed and chained at every 25m. This grid will total 15 km of cut lines, including the baseline and tie lines. Since sulphide mineralization is present, the property will be covered by a combined magnetic and electromagnetic (MAG /VLF-EM) survey in order to delimit the ultramafic dykes and to determine the conductive zones. Property mapping will be done at the same time as the combined magnetic and electromagnetic surveys. Mapping will emphasize the structural relationships between the various lithologies. Magnetic anomalies and conductors will be further studied by applying MaxiProbe surveys.

Geological, magnetic and electromagnetic anomalies, concordant or not, will be tested to provide both sampling and assaying by short diamond drilling holes. At this stage, a budget of 200 m of DDH is enough to qualify these anomalies.

9.0 RECOMMENDED WORK AND COSTS

9.1 CENTRAL MANICOUAGAN PROPERTY

PHASE I

PROPERTY FIELD WORK

Camp renovation, helicopter pads, construction core shack,office etc.	$ 40,000
Surveying - claims boundaries	$ 20,000
Work permits for 1997	$ 5,000
Total	$ 65,000

GEOPHYSICAL SURVEYS

MaxMin surveys along cut lines to test certain areas for the presence of shallow conductors	
50 km @ $300/km	$ 15,000
Deep penetrating EM resistivity survey to test the NW grid blocks using MaxiProbe or similar techonlogy	
10 km of lines @ $1,800/day	$ 25,000
Helicopter support	$ 10,000
Mob and demob	$ 4,000
2 field helpers , 14 days @ $125/day/man	$ 3,500
Total	$ 57,500

CAMP LOGISTICS

Monthly Cost - 30 days	
4 camp helpers @ $125/day	$ 15,000
2 geologists/supervisors @ $325/day	$ 19,500
Groceries for 12 men/day including 5 drillers, 1 pilot	$ 14,000
Fuel - cooking, heating	$ 2,000
Airplane support	$ 5,000
Material	$ 2,000
Total	$ 57,500
Total for 3 months:	**172,500**

DIAMOND DRILLING

Drilling for 4,525 m.		$ 325,700
Mob and demob		$ 7,500
Helicopter support		$145,000
Assays - 1,000 @ $22.50/sample		$ 22,000
Core splitter, generator, core racks		$ 15,000
	TOTAL: ($153,000/m.)	**$ 515,200**

DOWN-HOLE GEOPHYSICS

Pulse EM or IP or magnetic susceptibility approximately $3/m.		$ 13,575
	Total	$ 809,775
	Administration (15%)	$ 121,470
	Contigencies (10%)	$ 80,975
	TOTAL PHASE I:	**$ 1,012,220**

PHASE II

DIAMOND DRILLING

5 holes (near 5,000 m) @ $153 per m. Assays costs, helicopter, mob, demob, core-racks included	$ 765,000

DOWN-HOLE GEOPHYSICS

Magnetic and/or electromagnetic studies $3/m.	$ 15,000

CAMP LOGISTICS - 90 DAYS

2 senior geologists, 90 days @ $325/day	$58,500
1 junior geologist, 90 days @ 200/day	$ 18,000
1 helper, 90 days @ $125/day	$ 11,250

LOGISTICS - 90 days

Airplane support		$ 15,000
Fuel, material		$ 12,000
Groceries		$ 42,000
	Total ($187/m. all included)	$ 936,750

Administration (15%)	$ 140,510
Contigencies (10%)	$ 93,675
TOTAL PHASE II	**$ 1,170,935**

PHASE III

DIAMOND DRILLING - 3 months
5 holes (near 5,000 m)
Assay costs, overburden, fuel included.

Total ($187/m. all included)	$ 936,750
Administration (15%)	$ 140,510
Contigencies (10%)	$ 93,675
TOTAL PHASE III	**$ 1,170,935**

9.2 QUERTIER PROPERTY

LINE CUTTING		
60 km @ $250/km		$ 15,000
GEOLOGY: mapping - compilation - Reports - supervision		
1 senior geologist, 90 days @ $325/day		$ 29,250
1 junior geologist, 90 days @ $200/day		$ 18,000
AIRBORNE GEOPHYSICS		
485 line km @ $85/line km		$ 41,225
GROUND GEOPHYSICS		
MAXMIN II, 30 km @ $180/km		$5,400
GEOCHEMISTRY		
SAA assays, 50 samples @ $22/sample		$1,100
Logistics, field support, sir support, camp 1 month @ $25,000/month		$25,000
MOB / DEMOB		$10,000
	Total	$144,975
	Contingencies (10%)	$14,500
	Administration (15%)	$ 21,745
	TOTAL PHASE 1	**$181,220**

9.3 SOUTHWEST ISLAND PROPERTY

PHASE I

LINECUTTING		
15 km @ $250.00/km		$3,750.00
MAPPING AND PROSPECTING		
1 senior geologist, 5 days @ $325/day		$1,625.00
1 junior geologist, 5 days @ $200/day		$1,000.00
1 prospector, 5 days @ $125/day		$625.00
ASSAYS (SAA)		
50 samples @ $ 22.00/sample		$1,100.00
MAG/EM-TBF		
15 km @ $ 140.00/km		$2,100.00
MAXIPROBE		
5 km @ $ 3,500.00/km		$17,500.00
LOGISTICS		
Mob/ Demob		$5,000.00
Food in the field		$1,000.00
WORK REPORT		
1 geologist, 5 days @ $ 325.00/day		$1,625.00
	Total	$35,325.00
	Administration (15%)	$5,300.00
	Contingencies (10%)	$3,530.00
	TOTAL PHASE I	**$44,155.00**

PHASE II

DRILLING (WINKIE) (4 holes of 50 m)	
Drilling, 15 days @ 1,000/day	$15,000.00
Down the hole consumables, 200 m @ $16.50/m	3,300.00
Core boxes, 30 boxes @ 5.50/box	165.00
Core logging (Lac des Iles core shack facilities),	

1 geologist, 2 days @ $325/day	$650.00
Assays, 40 samples @ $22/sample	$880.00
LOGISTICS	
Food in the field	1, 500.00
Mob-Demob crew (Rouyn-Manic V)	4,800.00
Mob-Demob drill (Rouyn-Manic V)	6,400.00
Crew transportation (seaplane support)	
Lac Louise-Southwest Island Property, 2 flights @ $550/flight	$1,100.00
Drill and equipment transportation (helicopter support)	
Lac Louise-Southwest Island Property, 7.5 hours @ $750/hr	$5,625.00
Core transport (helicopter support)	
Quertier Property- Lac des Isles Camp, 3 hours @ $750/hr	$2,250.00
Total	$41,670.00
Administration (15%)	$6,250.00
Contingencies (10%)	$4,160.00
TOTAL PHASE II	**$52,080.00**
TOTAL ALL PHASES	**$96,235.00**

These budgets are considered essential for executing the recommendations. It is also considered as a minimum for evaluating the economic potential of these properties.

Respectfully submitted,

Luciano Vendittelli, B.Sc., APGGQ
Montreal, September 24, 1997

10.0 REFERENCES

Bassaget, J.P.,
1968 Géologie des Monts Manicouagan. Quebec Dept. Nat. Resources. DP 459, 44 p..

Berard, J.,
1962 Summary geological investigation of the area bordering Manicouagan-Mouchalagane Lakes, Saguenay County. Québec Dept. Nat. Resources, PR No. 489, 14 pp.

Bunch, T.E. *et Al,*
1967 Natural terrestrial maskelinite. Am. Mineralogist, Vol. 52, p. 244-253.

Coles, R.L. and Clark, J.F.,
1978 The Central Magnetic Anomaly, Manicouagan Structure, Québec. Journal of Geophysical Research, Vol.83, No. B6, pp. 2805-2809.

Currie, K.L.,
1972 Geology and petrology of the Manicouagan resurgent caldera. Geol. Surv. Can. Bull., 198, 153 pp.

Dence, M.R.,
1964 A comparative structural and petrographic study of probable Canadian meteorite craters. Meteoritics, Vol 2, p. 249-270.

1971 Impact melts. Journal of Geophysics Research, Vol.76, pp.5552-5565.

Dworak, ULF.
1969 Stosswellenmetamorphose des anorthosits von Manicouagan Krater, Qubec, Canada, Dokt. Dissert., Univ. Tubingen, 105 p.

Floran, R.J. *et Al.*
1978 Manicouagan impact melt, Québec, 1, Stratigraphy, petrology and chemistry. Journal of Geophysics Research, Vol. 83, No B6, pp. 2737-2759.

Geological Survey of Canada,
1996 Petrograghy and rock magnetic properties of drill core from the central magnetic anomaly, Manicouagan Impact Structure. IPP Project # 930022. Private Report. 61 pp.

Goodfellow, W.,
1992 Giant Impacts: Consequences for biological extinctions, global environments and ore formation. GEOS, Vol.21, No. 1, pp 10-11.

Grieve, R.A.F., and Floran, R.J.,
1978 Manicouagan impact melt, Québec 2. Chemical interrelations with basement and formational processes. In Journal of Geophysical Research, Vol. 83, No. B6, pp. 2761 - 2771.

1978 Manicouagan impact melt, Québec 2. Chemical interrelations with basement and formational processes. In Journal of Geophysical Research, Vol. 83, No. B6, pp. 2761 - 2771.

Grieve, R.A.F. and Masaitis, V.L.,
1994 The Economic Potential of terrestrial Impact Craters. In International Geology Review, Vol.36, pp. 105-151.

Hammond, D.W.,
1946 Geology of the Mouchalagan lake area, Saguenay County, New Quebec; M. Sc thesis; University Toronto.

Kish, L.,
1962 Preliminary report on the lower Hart-Jaune River area, Saguenay County. Quebec Dept. Nat, PR 486, 9 p..

1963 Geology of middle Hart-Jaune River area, Saguenay country. Quebec Dept. Nat. Resources, PR 507, 8 p..

1968 Hart-Jaune River area. Quebec Dept Nat. Resources, RG 132, 98 p..

Larochelle, A. and Currie, K.L.,
1967 Paleomagnetic study of igneous rocks from the Manicouagan structure, Québec. Journal of Geophysical Research, 72, p. 4163-4169.

Low, A.P.,
1897 Report on explorations in the Labrador Peninsula, along the East Main, Kohsoak, Hamilton, Manicouagan, and portions of other rivers in 1892-1895. Geol. Survey Canada Ann. Rept. No 8, pt. L.

Marcotte, D. and Fox, J.S.,
1989 Analyse multidimensionnelle de données geochimiques de sediments lacustres dans la region de Manicouagan Quebec Dept. Nat. Resources, MB 89-58, 62 p..

Murtaugh, J.G. and Currie, K.L.,
1969 Preliminary study of the Manicouagan Structure. Québec Department of Natural Resources, Mines Branch, PR 583, 9 p.

Murtaugh, J.G.,
1976 Manicouagan Impact Structure; Québec Department of Natural Resources Report DPV-432,180pp.

1976 Stream sediment geochemistry, Manicouagan area, Saguenay County. Quebec Dept. Nat. Resources. DP 443, 9 p..

Naldrett, A.J.,
1981 Nickel Sulphide Deposits: Classification, Composition, and Genesis; Economic Geology, 75th Anniversary Volume, p. 628-685.

Oronato, P.I.K. *et Al.*
1978 The thermal history of the Manicouagan impact melt sheet, Québec. Journal of Geophysical Research, pp. 2789-2712.

Orphal, D.L., and Shultz P.H.,
1978 Manicouagan, a Terrestrial analog of Lunar Floor-Fractured craters?. Meteoritics, Vol. 13, No. 4, pp. 591 - 593.

Plante, L.,
1985 Étude métallogénique des indices de Cu-Ni-Co du Haut Plateau de la Manicouagan.

Quebec Dept. Nat. Resources
1981 Carte de location des travaux géoscientifique 022N, 1 carte (1: 250 000), CL 022N.

Robertson, W.A.,
1967 Manicouagan, Québec, Paleomagnetic Results. Canadian Journal of Earth Sciences, pp. 641-649.

Roest, W.R. and Pilkington M.,
1994 Manicouagan Crater. Identifying remanent magnetization effects in magnetic data. Geophysics, Vol. 58, No. 5.

Rose, E.R.,
1955 Manicouagan-Mushalagan lakes area, Quebec. Geol. Survey Canada, Paper 59-2 (geol. map with marginal notes.

Shultz, P.H.,
1992 Private Communication.

Siriunas, J.M.,
1994 A Lithogeochemical Study of the Manicouagan Impact Site. Private Report. 31 p.

Vendittelli, L., Valls, R.A.,
1996, The Manicouagan Impact Structure: An evaluation of the project for Great Legends Mining Inc.; Report: 50 p.

ASSESSMENT WORK

CENTRAL MANICOUAGAN PROPERTY

GM 51166 EXPLORATION MINIERE LASARRE INC.; Report on a geological survey - Manic Project by Podolsky, T., Salamis, C., Boivin, L., 1990, 23 p..

GM 51168 SOCIETE EXPLORATION MINIERE LA SARRE INC.; Rapport d'un levé électromagnétique (MaxiProbe) - Projet Manicouagan, by Chabot, N. and Kenwood, J, 1991, 91 p..

GM 51170 SOCIETE EXPLORATION MINIERE LA SARRE INC.; Rapport de sondage au diamant avec 1 journal du trou MC-1, Projet Manicouagan, by Chabot, N. and Boivin, L., 1991, 18 p., 1 plan.

GM 51186 419947 ALBERTA LTD; Leve électromagnétique (MAXI-PROBE), Projet Manicouagan by Chabot, N, 1991, 24 p.. 2 plans.

GM 51188 419947 ALBERTA LTD; Report on a total field magnetic survey, Manicouagan Property by Kenwood, J., 1991. 7 p., 4 plans.

GM 51197 419947 ALBERTA LTD; A combined helicopter-borne magnetic (total field & vertical gradient) and electromagnetic (AERODAT 4-frequency, V L F-NLK & NSS) survey Manicouagan Reservoir Property by Podolsky, G., 1990, 39 p., 10 plans.

GM 51247 419947 ALBERTA LTD; Levé géologique Ile René-Levasseur - Propriété Manicouagan. By Chabot, N., 1990. 24 p., 2 plans.

QUERTIER PROPERTY

GM 51167 EXPLORATION MINIERE LASARRE INC.; Rapport pétrographique - Projet Manicouagan by Chabot, N., 1990. 22 p..

GM 51166 EXPLORATION MINIERE LASARRE INC.; Report on a geological survey - Manic Project by Podolsky, T., Salamis, C., Boivin, L., 1990, 23 p..

GM 51455 MINERAUX MANIC INC.; Quertier twp; Geological mapping, prospecting, electromagnetic (VLF-NSS and BEEP-MAT II) and diamond drilling program with 3 logs of holes MM-91-01 to 91-03 by Kenwood, J. 1991, 29 p..

SOUTWEST ISLAND PROPERTY

GM 51166 EXPLORATION MINIERE LASARRE INC.; Report on a geological survey - Manic Project by Podolsky, T., Salamis, C., Boivin, L., 1990, 23 p.

ANNEXE I

CERTIFICATE OF QUALIFICATION

CERTIFICATE OF QUALIFICATION

I, Luciano Vendittelli, do hereby certify that:

Canada.

2. I am a graduate of McGill University (1985), with a Bachelor of Science Degree in Geology.

3. I am a member in good standing of the A.P.G.G.Q. (#1035)

4. I am a member of The Prospectors and Developers Association of Canada;

5. I have not visited the actual property but have visited the nearby surrounding terrain on other assignements for other companies not associated with Minéraux Manic Inc. I have consulted with the Minéraux Manic Inc. geologists and have studied and used their reports and documents and maps provided by Minéraux Manic Inc. in my evaluation.

6. I have not directly or indirectly received or expect to receive any interest, direct or indirect, in the property of the issuer Minéraux Manic Inc. or any affiliate. I do not own directly or indirectly any securities of Minéraux Manic Inc. or any affiliate.

7. I consent to the use of this report, in whole or in part, to be included in the prospectus to be sent to a Canadian Securities Commission or any other regulatory body concerned.

Montreal, this 24th day of September 1997.

Luciano Vendittelli, B.Sc., APGGQ

ANNEXE II

CORE LOG

COMPANY: MINERAUX MANIC INC

PROPERTY: QUERTIER HOLE #: MM-91-01

Date started: 20 octobre 1991

Date finished: 22 octobre 1991

Grid co-ordinates 3+00N 0+85E

Range – Lot –

Direction – Dip -90

Depth of casing 30 feet 9.14 meters

Final depth of hole 30 feet 9.14 meters

Logged by:

Logging started:

Logging finished:

Reason Drilled: Vérifier l'extension sud du showing original de Ni, Cu

Comments: Abandonné dans le mort-terrain à 30 pieds

ACID TESTS:

Depth	Tube angle	Corrected dip

TROPARY TESTS:

Depth	Direction read	Corrected direction	Dip

COMPANY: MINERAUX MANIC INC

PROPERTY: QUERTIER HOLE #: MM-91-02

Date started: 26 octobre 91

Date finished: 27 octobre 91

Grid co-ordinates 0+08S 1+25E

Range _____ Lot _____

Direction 060° Dip -65

Depth of casing 6 feet 1.83 meters

Final depth of hole 97 feet 29.57 meters

Logged by: N. Chabot

Logging started: _____

Logging finished: _____

Reason Drilled: Vérifier l'extension en profondeur des gneiss mafiques bréchifiés et minéralisés (Py) des affleurements MS-05, MS-06

Comments: _____

ACID TESTS:

Depth	Tube angle	Corrected dip

TROPARY TESTS:

Depth	Direction read	Corrected direction	Dip

TROU NO:			MM-91-02		PAGE: 1 de 1									
					ECHANTILLONS				ANALYSES					
De (pi)	A (pi)	Code	DESCRIPTIONS	MINERALISATION	No	De (pi)	A (pi)	Long (pi)	Au ppb	Cu ppm	Ni/Zn ppm	Pd ppb	PT ppb	
0	6		Mort-Terrain											
6	97		Gneiss mafiques bréchifiés Gneiss gris foncé à grains fins avec très peu d'évidence de foliation Matrice aphanitique noirâtre et magnétique. Le degré de bréchification et le pourcentage de matrice augmente de 52 pi à la fin du trou. < 1% de veinules d'Epidote, Calcite, Quartz, Opale Trace à 1% minéralisation en pyrite fine dissiminée ou associée aux fractures											
97			FIN DU TROU	<1% Py diss	1	37,0	39,0	2,0 pi	110	1300	55 4/9	410	180	
				1% Py diss ou dans des fractures	2	53,5	55,5	2,0 pi	180	3140	665/15	270	1100	

COMPANY: MINERAUX MANIC INC

PROPERTY: QUERTIER HOLE #: MM-91-03

Date started: 28 octobre 1991

Date finished: 30 octobre 1991

Grid co-ordinates 0+27S 3+24E

Range _____ Lot _____

Direction 045° Dip -53

Depth of casing _____ feet _____ meters

Final depth of hole 117 feet 35.66 meters

Logged by: V. Chabot

Logging started: _____

Logging finished: _____

Reason Drilled: Intersecter en profondeur les gneisss follés et mineralisés (Po,Py) des affleurements mj-08, mj-07

Comments: Pas de minéralisation

ACID TESTS:

Depth	Tube angle	Corrected dip

TROPARY TESTS:

Depth	Direction read	Corrected direction	Dip

TROU NO: MM-91-03				PAGE: 1 de 1	ECHANTILLONS				ANALYSES				
De pi	A pi	Code	DESCRIPTIONS	MINERALISATION	No	De	A	Long					
0	15		Mort - Terrain										
15	112		Gneiss brechifiés Alternance de gneiss de composition quartzo- Feldspathique (qz-fd-grenat) et de gneiss mafique à grains fins. On trouve occasionnellement des sections où la roche est fondue et qui contiennent des fragments de gneiss. La matrice de cette roche possède un aspect fluidale. La roche est non magnétique Py disséminée associée avec une fractur										
112			Fin du trou										

COMPANY: MINERAUX MANIC INC

PROPERTY: MANICOUAGAN HOLE #: MC-1

Date started: 12 décembre 1990

Date finished: 11 janvier 1991

Grid co-ordinates L 14E 28+00N

Range _____ Lot _____

Direction 215° Dip -60

Depth of casing 97 feet 29,26 meters

Final depth of hole 1557 feet 471,53 meters

Logged by: N. Chabot / L. Boivin

Logging started: 14 décembre 1990

Logging finished: 15 octobre 1991

Reason Drilled: Tester une anomalie électromagnétique (Maxi-Probe) coincidente avec une anomalie magnétique aéroportée

Comments: le trou n'est pas complété

ACID TESTS:

Depth	Tube angle	Corrected dip
200 pi	-63.5°	-57° 00'
350 pi	-64°	-57° 45'
550 pi	-62°	-55° 30'
800 pi	-60°	-53° 15'
1000 pi	-62°	-55° 30'
1307 pi	-57°	-50° 00'

TROPARY TESTS:

Depth	Direction read	Corrected direction	Dip

TROU NO: MC-1				PAGE: 1 de 3	ECHANTILLONS				ANALYSES				
De	A	Code	DESCRIPTIONS	MINERALISATION	No	De	A	Long					
0	29,26		Mort-Terrain										
29.26	87,87		Gneiss felsique rose Prédominance de gneiss rose Très bien folié constitué de quartz, feldspath, amphibole et de quelques rares grenat. Le quartz et les feldspaths se présentent sous forme de lentilles étirées. Passages de gneiss mésocrate à mélanocrate. L'ensemble est recoupé par <1% de veines de Tachylite ? (vitreuse et rouge) de quelques mm ou centimètres. et de veines de pegmatite										
87,77	143.74		Gneiss gris Roche grisâtre à grains moyens composée de quartz - feldspath-biotite-amphibole. Foliation bien développée Moyennement magnétique · Présence de , de bandes plus foncée (mafique) <1% de veines rougâtres de Tachylite 126.8 → 134.05 Gneiss mésocrate à grains moyens 134.05 - 143.74 Orthodiorite à magnétite										

TROU NO:				PAGE: 2 de 3	ECHANTILLONS				ANALYSES				
De	A	Code	DESCRIPTIONS	MINERALISATION	No	De	A	Long					
143,74	194,00		Gneiss rose + Suevite "Veines" de suevite amydulaire (<10%) qui individualisent des grands blocs de gneiss rose et rose/gris. Un peu de magnétite.										
194,00	227,00		Gneiss mésocrate Folié, parfois hématitisé et recoupé par de la Tachylite rose, présence de bandes de suevite amygdulaires. La suevite est très magnétique ainsi que les petits lits mafiques dans le gneiss.										
227,00	247,00		Gneiss rose										
247,00	327.43		Gneiss gris Prédominance de roches dioritiques mésocrate à mélanocrate parfois recoupées par des pegmatites, petites veinules magnétiques, plus de veinules de suevite / Tachylite en descendant le trou. 307.41 - 327.30 Gneiss mésocrate peu folié.										

TROU NO:				PAGE: 3 de 3	ECHANTILLONS				ANALYSES				
De	A	Code	DESCRIPTIONS	MINERALISATION	No	De	A	Long					
327,73	424,33		Gneiss rose et sueuite Prédominance de gneiss rose. Veines de sueuite amygdulaire à texture fluidale de quelques centimètres a 1 ou 2 mètres. ex : 327.30 - 327.73, 329.49 - 330.59, 362.59 - 364.45, 367.38 - 369.30, 372.37 - 347.49, 374.89 - 375.50. Quelques passages de gneiss mésocrate peu folié (ressemble à un intrusif) concordant avec le gneiss rose. Quelques veines de pegmatite										
424,33	471.53		Gneiss mésocrate gris Prédominance de gneiss mésocrate gris. Avec veines de pegmatite d'une dizaine de mètres (428.23 - 438.47). Présence d'une zone de quelques mètres d'anorthosite ?										
471.53			Fin temporaire du trou										

ANNEXE III

CERTIFICATES OF ASSAYS

XRAL

LES LABORATOIRES XRAL
UNE DIVISION DES SERVICES DE SURVEILLANCE SGS INC.
150, 13e RUE • ROUYN-NORANDA • QUEBEC J9X 2H6
TEL: (819)764-9108 FAX: (819)764-4673

CERTIFICAT D'ANALYSE

RAPPORT No R 518

A: EXPLORATION MINIERE LA SARRE Inc.
ATTN: MRS. LAURI BOIVIN
15 GAMBLE RUE EST, NO. 102
ROUYN-NORANDA, QUEBEC
J9X 3B6

CLIENT No. 1988

DATE DE RECEPTION
1-Aug-90

REF. DOSSIER 436-J4

No de Pages 1

7 ROCHES

ELEMENTS	METHODE	LIMITE DE DETECTION
AU-1AT PPB	FADCP	1.
NI PPM	DCP	1.
CU PPM	DCP	0.5
RH PPB	FAPMS	1.
AG PPM	DCP	0.5
PT-1AT PPB	FADCP	10.
PD-1AT PPB	FADCP	1.

DATE 31-AUG-90

CERTIFIE PAR .....
Bernard Maurette, Directeur de Laboratoir

Numero	AU-1AT PPB	NI PPM	CU PPM	RH PPB	AG PPM	PT-1AT PPB	PD-1AT PPB
5.1.MIN-A	--	128	348.	<1	--	10	18
5.1.MIN-B	--	1900	1670.	<1	--	10	14
N-5-1B-1	--	282	88.2	<1	--	<10	<1
L2-6-1	430	2350	6660.	67	<0.5	920	2300
L2-6-2	220	1660	4030.	36	<0.5	490	1300
L2-6-3	500	2740	8990.	67	<0.5	960	2300
90-NC-10	<1	44	229.	<1	<0.5	<10	<1

AU-1AT PPB - ASSAY PERFORMED ON 30 GRAM ALIQUOT
PT-1AT PPB - ASSAY PERFORMED ON 30 GRAM ALIQUOT
PD-1AT PPB - ASSAY PERFORMED ON 30 GRAM ALIQUOT

LES LABORATOIRES XRAL 150, 13e RUE ROUYN-NORANDA QUEBEC J9X 2H6 TEL: (819)764-9108 FAX: (819)764-4673
Membre du Groupe SGS (Société Générale de Surveillance)

ASSAYERS
LABORATOIRES/LABORATORIES
DIVISION DE/OF ASSAYERS CORPORATION LTD.
780, AV. DU CUIVRE, C.P. 665, ROUYN-NORANDA (QUÉBEC) J9X 5C6 TÉL.: (819) 797-4653 FAX: (819) 797-4501

Certificat/Certificate

2R-0961-RG1

Comp: **MINERAUX MANIC**
Proj: QUERTIER
Attn: NATHALIE CHABOT

Date: JUIN/JUN-19-92

Nombre D'Echantillons/No. of Samples:
Soumis le/Submitted: MAI/MAY-28-92

No. D'Echantillon / Sample Number	AU PPB	AU CH'KS PPB	AU CH'KS PPB	CU PPM	NI PPM	ZN PPM	PD PPB	PT PPB
MM-91-02-1	110	100	120	1300	554	9	410	180
MM-91-02-2	180	180	180	3140	665	15	270	1100

Certifie par/Certified by

CTA

ABILAB INC.

1905, 3e Avenue, Val-d'Or (Québec) J9P 4N7
Tél.: (819) 874-4723 Fax: (819) 874-0625

CERTIFICAT D'ANALYSES N°: 38010 DATE: 16/12/96

Client: Great Legends Mining Échantillons: Roches Projet: Manicouagan

Reçu de: M.Roger Moar Nombre d'analyses: 16 Date reçu: 05/12/96

Éléments: Pd,Pt Limite de détection: Méthode: F.A. A.A.

Echantillions	Pd ppb	Pt ppb
52001	832	1870
52002	138	<10
52003	76	192
52004	52	<10
52005	52	<10
52006	32	58
52007	64	28
52008	30	<10
Check		
52001	718	1704

LF-3356

ANALYSTE:

CHIMISTE
Lyne Bizier
92-005
QUÉBEC

ABILAB INC.

1905, 3e Avenue, Val-d'Or (Québec) J9P 4N7
Tél.: (819) 874-4723 Fax: (819) 874-0625

CERTIFICAT D'ANALYSES N°: 37969 DATE: 12/12/96

Client: Great Legends Mining Échantillons: Roches Projet: Manicouagan

Reçu de: M Roger Moar Nombre d'analyses: 24 Date reçu: 09/12/96

Éléments: Cu,Zn,Ni Limite de détection: Cu,Zn,Ni 1ppm Méthode: pyro,A.A.

Echantillons	Cu ppm	Zn ppm	Ni ppm
52001	5760	29	2050
52002	371	52	870
52003	303	27	630
52004	125	22	290
52005	46	47	910
52006	225	42	680
52007	259	41	660
52008	26	46	1330
Check			
52007	261	43	670
Blanc	<1	<1	<1

LF-3356

ANALYSTE:

CHIMISTE (81) Lyne Bizier 92-005 QUÉBEC

ABILAB INC.

1905, 3e Avenue, Val-d'Or (Québec) J9P 4N7
Tél.: (819) 874-4723 Fax: (819) 874-0625

CERTIFICAT D'ANALYSES N°: 38186 DATE: 06/01/97

Client: Great Legends Mining inc. Échantillons: Roches Projet: Manicouagan

Reçu de: M.Roger Moar Nombre d'analyses: 17 Date reçu: 09/12/96

Éléments: Whole-Rock Limite de détection: Méthode: ICP

Echantillons	SiO2 %	Al2O3 %	Fe2O3 %	MnO %	MgO %	CaO %
52008	36.80	1.15	15.96	0.22	39.56	0.90

Echantillons	Na2O %	K2O %	TiO2 %	P2O5 %	Loi %	Total %
52008	0.15	0.02	0.03	0.02	5.42	100.23

Echantillons	Ba ppm	Sr ppm	Y ppm	Sc ppm	Zr ppm	Be ppm
52008	33	36	1	6	5	<1

Echantillons	V ppm
52008	21

LF-3356

ANALYSTE:

CHIMISTE
Lyne Binet
82-005
QUÉBEC

ANNEXE IV.A

Goodfellow, W., 1992. Giant Impacts : consequences for biological extinctions, global environments and ore formation; GEOS, Vol. 21, No. 1

GEOS

Energy, Mines and Resources Canada | Énergie, Mines et Ressources Canada

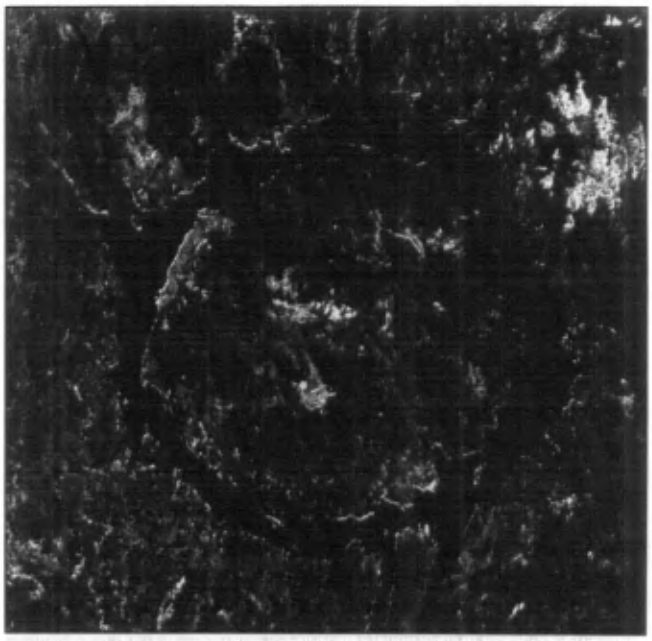
GIANT IMPACTS: CONSEQUENCES FOR BIOLOGICAL EXTINCTIONS, GLOBAL ENVIRONMENTS AND ORE FORMATION

by Wayne Goodfellow

For more than 4.5 billion years, the earth has been bombarded by extraterrestrial objects of variable size, composition and frequency of arrival. A multidisciplinary effort involving geophysicists, paleontologists, sedimentologists, analytical chemists and geochemists has made the GSC a world leader in studying the effects of meteorite impacts on terrestrial processes.

Over the past 600 million years, scientists estimate that bodies of 5-km-diameter or more hit Earth about once every 10 000 years. They estimate that the energy released from a 10-km-diameter asteroid, travelling at high speed, that lands in an ocean 5 km deep, is more powerful than any terrestrial process, such as volcanism, glaciation, sea level changes, earthquake activity or seafloor spreading. Because of the massive amount of energy released, a major impact would have catastrophic global consequences for the atmosphere, hydrosphere and biosphere. A large, heated mass of low-density air with peak temperatures of 20 000 Kelvin would form adjacent to Earth's surface and cause wildfires. Tsunamis as high as the ocean is deep would scour the seafloor, rework sediment, form tsunami deposits and destroy the habitat of organisms, particularly those in shallow-water shelf environments.

Earthquakes measuring 12.4 on the Richter scale would produce enough



LANDSAT image of the Manicouagan meteorite impact structure, northern Quebec. Impact structures are characterized by circular depressions with an uplifted outer rim and central core. Melt-rock formed from the cooling of melt generated by impact is commonly exposed in the outer rim. Image: Canada Centre for Remote Sensing

CONSÉQUENCES DES IMPACTS GIGANTESQUES : EXTINCTIONS BIOLOGIQUES, CHANGEMENT DANS L'ENVIRONNEMENT MONDIAL ET FORMATION DE MINERAIS

par Wayne Goodfellow

Pendant plus de 4,5 milliards d'années, la Terre a été bombardée d'objets extra-terrestres de dimensions et de compositions variables dont la fréquence d'arrivée était également variable. Un effort pluridisciplinaire de la part de géophysiciens, de paléontologues, de sédimentologistes, de chimistes spécialisés en analyse et de géochimistes a fait de la CGC un organisme de premier plan au niveau mondial dans l'étude des effets des impacts météoritiques sur les processus terrestres.

Image LANDSAT de la structure d'impact météoritique de Manicouagan au Québec septentrional. Les structures d'impacts sont caractérisées par des dépressions circulaires avec une bordure extérieure et une partie centrale soulevées. Des roches formées après refroidissement de produits fondus lors de l'impact sont couramment mises à nu dans l'anneau extérieur. Photo: Centre canadien de télédétection.

Les scientifiques estiment qu'au cours des dernières 600 millions d'années des corps d'un diamètre supérieur à 5km ont frappé la Terre environ à tous les 10 000 ans. Ils estiment également que l'énergie libérée lors de la chute d'un astéroïde d'un diamètre de 10km se déplaçant à haute vitesse dans un océan par une profondeur de 5km est supérieure à l'énergie libérée par tout processus terrestre, comme le volcanisme, les glaciations, les variations du niveau des mers, l'activité sismique ou l'expansion des fonds marins.

En raison des quantités énormes d'énergie libérées, un impact majeur aurait des conséquences catastrophiques à l'échelle du globe pour l'atmosphère, l'hydrosphère et la biosphère. Une grande masse d'air chauffé de faible densité, dont les températures de pointe seraient de l'ordre de 20000 degrés Kelvin, se formerait près de la surface de la Terre pour engendrer des tempêtes de feu. Dans le cas des impacts dans les océans, des tsunamis d'une hauteur égale à la profondeur des océans affouilleraient le fond marin, remanieraient les sédiments, formeraient des dépôts de tsunamis et détruiraient l'habitat des organismes, en particulier les milieux à faible profondeur sur les plates-formes continentales.

Des séismes mesurant 12,4 à l'échelle de Richter dégageraient suffisamment d'énergie pour mettre en mouvement des biseaux sédimentaires le long des marges continentales, déclenchant ainsi ou accélérant l'activité volcanique et

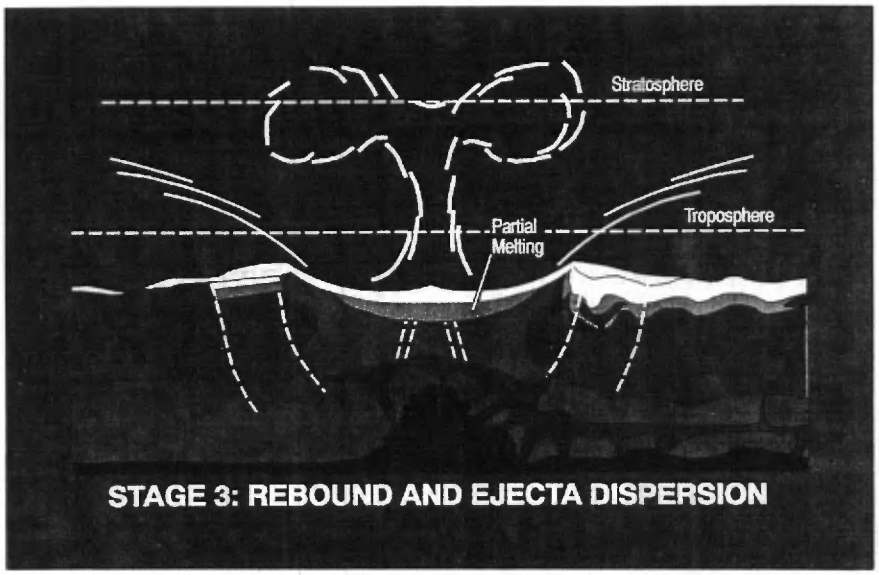
energy to release sedimentary prisms along continental margins and initiate or accelerate volcanism and hydrothermal activity. Shock heating of the atmosphere would form nitrogen compounds that cause acid rain, inhibit photosynthesis and deplete the ozone layer.

Because many of these effects are similar to the effects of man-made pollution, scientists study meteorite impacts to attempt to understand the influence of ozone depletion or acid rain on life-sustaining ecosystems over periods of thousands of years. This helps determine the capacity of the natural system to withstand the effects of human activity and pollution, and the rate of recovery from major environmental damage.

Up to 80 per cent of all life would die off as a result of a meteorite impact. This is because 10 to 20 per cent of ejecta dust and vaporized asteroid from the impact would remain suspended in the atmosphere long enough to circle the globe, block out sunlight, cool Earth's surface and disrupt the food chain. Many researchers believe that a major meteorite impact 65 million years ago wiped out the dinosaurs and killed off about 80 per cent of all living organisms. The biological record is punctuated with mass extinctions after each major bombardment. Rapid evolution of new life forms filled ecological niches after each extinction.

Meteorite impacts have also led to the formation of economically important mineral deposits. Magmas formed by crustal melting during impact cause volcanism, hydrothermal activity and the formation of magmatic, hydrothermal and sedimentary mineral deposits. The large nickel-copper-platinum and zinc-copper-silver deposits at Sudbury, Ontario, are examples of magmatic and hydrothermal deposits that appear to be generated by meteorite impacts. The Late Devonian NICK platinoid element deposit in the Yukon probably formed from the disintegration of a meteorite during impact and the raining of chondritic material to the seafloor.

Because of recent work at the GSC and elsewhere, geologists are beginning to look to the cosmos for answers to questions of earth evolution. The effect of impacts on Earth history is only beginning to be appreciated, initially in isolation with respect to the local effects of impacts, and more recently as they affect biological evolution and extinction, global climates and ore formation.



Schematic cross-section of an impact structure showing the excavated crater, outer rim and distribution of ejecta lofted to heights up to 100 km above Earth's surface.

Coupe schématique d'une structure d'impact montrant le cratère creusé, l'anneau extérieur et la répartition des projections souvent soulevées à des altitudes atteignant jusqu'à cent kilomètres au-dessus de la surface de la Terre.

hydrothermale. Le réchauffement instantané de l'atmosphère entraînerait la formation de composés azotés qui produiraient des pluies acides, inhiberaient la photosynthèse et épuiseraient la couche d'ozone.

Puisqu'un grand nombre des effets seraient similaires à ceux causés par la pollution d'origine anthropique, les scientifiques étudiant les impacts météoritiques tentent de comprendre l'influence de l'épuisement de la couche d'ozone ou des pluies acides sur les écosystèmes supportant la vie après des intervalles de milliers d'années. Ces travaux aident à déterminer l'aptitude des sytèmes naturels à résister aux effets de l'activité humaine et de la pollution ainsi que les taux de récupération après des dommages majeurs causés à l'environnement.

Jusqu'à 80% de toute vie pourrait être supprimée suite à un impact météoritique. Il en est ainsi parce que de 10 à 20% des poussières éjectées et de l'astéroïde vaporisé à l'impact resteraient en suspension dans l'atmosphère assez longtemps pour faire le tour du globe et bloquer la lumière solaire, ce qui refroidirait la surface de la Terre et perturberait la chaîne alimentaire. Un grand nombre de chercheurs pensent qu'un impact météoritique majeur a causé la disparition des dinosaures et d'environ 80 % de tous les organismes vivants il y a 65 millions d'années. L'enregistrement biologique est ponctué d'extinctions massives à la suite de chaque bombardement majeur. Une évolution rapide de nouvelles formes de vie vient combler les niches écologiques à la suite de chaque extinction.

Les impacts météoritiques ont également entraîné la formation de gisements de minéraux importants sur le plan économique. Les magmas formés par la fonte de la croûte terrestre lors des impacts engendrent une activité volcanique et hydrothermale ainsi que la formation de gisements minéraux magmatiques, hydrothermaux et sédimentaires. Les grands gisements de nickel, cuivre et platine ainsi que de zinc, cuivre et argent de Sudbury (Ontario) sont des exemples de gisements magmatiques et hydrothermaux qui semblent avoir été engendrés par des impacts météoritiques. Le gisement NICK d'éléments platinoïdes du Dévonien tardif au Yukon s'est probablement formé suite à la désintégration d'une météorite à l'impact et à une pluie de matériaux chondritiques sur le fond marin.

En raison de travaux récents menés à la CGC et ailleurs, les géologues commencent à se tourner vers le cosmos à la recherche de réponses à des énigmes de l'évolution de la Terre. L'on commence à peine à apprécier l'effet des impacts météoritiques dans l'histoire du globe, ce qui s'est effectué initialement de manière isolée par l'étude d'effets locaux d'impacts puis, plus récemment, de manière plus globale par l'examen de leur influence sur l'évolution et les extinctions biologiques, sur le climat de la planète et sur la formation des minerais.

ANNEXE IV.B

Roest, W.R. and Pilkington, M., 1993. Identifying remanent magnetization effects in magnetic data; Geophysics, Vol. 58, No. 5

GEOPHYSICS, VOL. 58, NO. 5 (MAY 1993): P. 653–659, 7 FIGS.

Identifying remanent magnetization effects in magnetic data

Walter R. Roest* and Mark Pilkington*

ABSTRACT

Remanent magnetization can have a significant influence on the shape of magnetic anomalies in areas that are generally characterized by induced magnetization. Since modeling of magnetic anomalies is nonunique, additional constraints on the direction of magnetization are useful. A method is proposed here to study the possible contribution of remanent magnetization to a particular anomaly, by comparing two functions that are calculated directly from the observations: (1) the amplitude of the analytic signal, and (2) the horizontal gradient of pseudogravity. From the amplitude and relative position of maxima in these derived quantities, we infer the deviation of the magnetization direction from that of the ambient field. The approach is applied to the magnetic anomaly in the center of the Manicouagan impact structure (Canada). Our results, based only on the magnetic anomaly observations, are in close agreement with constraints on the direction of remanent magnetization from rock samples.

INTRODUCTION

The utility of aeromagnetic data for geologic interpretation is complicated by the fact that, unlike gravity anomalies, magnetic anomalies are usually not located directly above their sources. The lateral displacement—phase shift or skewness—results from the fact that the direction of the geomagnetic field and the direction of source magnetization are nonvertical in regions away from the magnetic poles. The mathematical operation to reposition the magnetic anomalies directly over their respective sources is called reduction to the pole or RTP (Baranov, 1957). RTP requires knowledge of both the ambient field and source body magnetization directions. When magnetic anomalies over continental regions are reduced to the pole, the assumption is usually made that the magnetization of their sources is induced, i.e., parallel to the direction of the ambient field. In oceanic regions, on the other hand, the magnetization is largely assumed to be remanent, i.e., in the direction of the earth's field at the time that the oceanic crust was formed along a midocean ridge (Harrison, 1976). However, many examples exist of anomalous magnetization directions, both in continental and in oceanic areas. Here, we will discuss a continental example, namely the central anomaly in the Manicouagan Impact Structure, where the presence of remanent magnetization has been confirmed through rock sample measurements (Coles and Clark, 1978).

The problematic effects of remanent magnetization in magnetic interpretation have been elaborated upon extensively (e.g., Green, 1960; Books, 1962; Zietz and Andreasen, 1966). If remanent effects can be identified, several approaches can be used to determine the magnetization parameters (Hall, 1959; Bhattacharyya, 1966; Bott et al., 1966; Cordell and Taylor, 1971; Emilia and Massey, 1975; Shurbet et al., 1976; Schnetzler and Taylor, 1984; Muniruzzaman and Banks, 1989), many of which require restrictive assumptions about the geometry or the gravity field of the sources. Most often, forward modeling is the only way, absenting extensive sampling, to obtain an estimate of magnetization parameters which are, however, not unique.

We have developed an analytic method that helps determine whether or not remanent magnetization plays a significant role in a given region, before forward modeling is employed. This approach is a generalization to three dimensions of the method presented in Roest et al. (1992a) for the automated removal of skewness in marine magnetic anomaly profiles. The procedure is independent of assumptions about the directions of magnetization. As discussed in Roest et al. (1992a) this method is mathematically sound for near vertical contacts that are separated horizontally by distances at least as large as the depth to the top of the magnetic source bodies. Although this is a limitation, in practice the method yields useful results, and the advantage of being able to identify a priori areas of remanent magnetization is considerable.

Manuscript received by the Editor April 6, 1992; revised manuscript received December 4, 1992.
*Geophysics Division, Geological Survey of Canada, 1 Observatory Crescent, Ottawa, Ontario, Canada K1A 0Y3.
© 1993 Society of Exploration Geophysicists. All rights reserved.

METHOD

To evaluate remanent magnetization effects in magnetic data we compare two functions that are calculated directly from magnetic anomaly grids: the amplitude of the analytic signal (Nabighian, 1984; Roest et al., 1992b) and the horizontal derivative of the pseudogravity (Cordell and Grauch, 1985). Both these particular functions exhibit maxima over lateral contrasts in magnetization. The pseudogravity technique has been used extensively as a tool in magnetic interpretation. As shown by Roest et al. (1992b), the shape of the analytic signal over two-dimensional (2-D) features is independent of the direction of magnetization of the source bodies. However, the pseudogravity transformation implicitly requires that the magnetic field be reduced to the pole first. Consequently, the horizontal derivative of the pseudogravity, and more importantly, the locations and relative amplitudes of its maxima, depend on the parameters used in the reduction to the pole.

The procedure is schematically outlined in Figure 1. First, the observed magnetic field is reduced to the pole assuming induced magnetization. This step is done explicitly since, although its shape is independent of the direction of magnetization, the amplitude of the analytic signal is sensitive to the angle between the trend of the structure and the magnetic vector. Two functions are then derived from the RTP magnetic field. The discrepancies between them are due to either a significant remanent component in the observed anomalies or to deviations from the basic assumption that the magnetic contacts are nearly vertical and well separated. By adjusting the reduction to the pole parameters to include remanent magnetization, we can optimize the correlation between the two functions and thus estimate the direction of remanent magnetization.

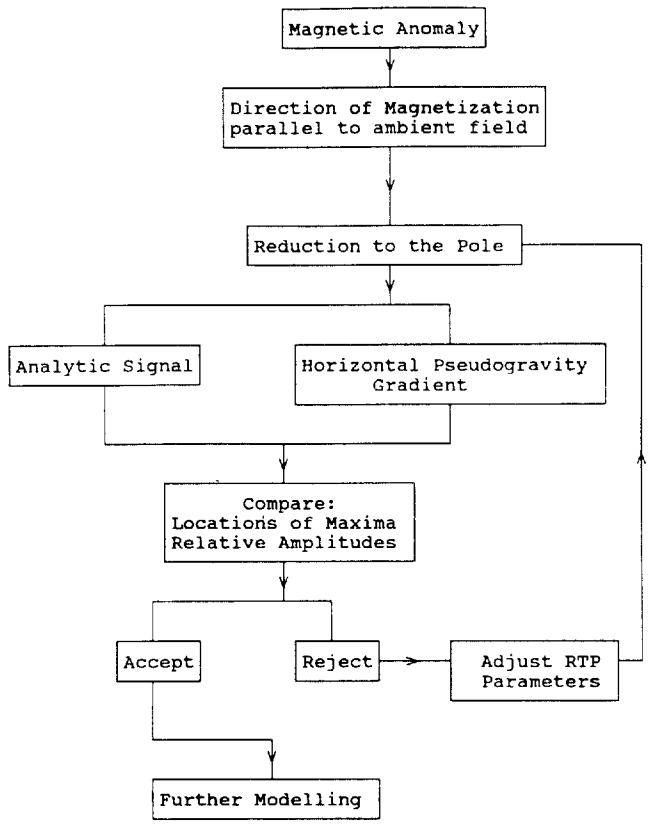


FIG. 1. Flow diagram of method outlined in this paper. The analytic signal and the horizontal derivative of the pseudogravity are calculated from the reduced to the pole magnetic field assuming induced magnetization, and then visually inspected. The reduction to the pole parameters for the direction of source magnetization are then adjusted until a satisfactory agreement between the two functions is reached.

Analytic signal

The analytic signal of the magnetic field is a complex function whose real and imaginary parts form a Hilbert transform pair. Since the horizontal and vertical derivatives of a magnetic anomaly are Hilbert transforms of one another (Nabighian, 1972), they can be used to construct the absolute value, or envelope of the analytic signal, $|A(x, y)|$, of a given magnetic anomaly $F(x, y)$:

$$|A(x, y)| = [(\partial/\partial x F(x, y))^2 + (\partial/\partial y F(x, y))^2 + (\partial/\partial z F(x, y))^2]^{1/2}. \quad (1)$$

As demonstrated by Roest et al. (1992b), the analytic signal is effective in mapping the edges of three-dimensional (3-D) magnetic sources by treating those edges as two-dimensional features, i.e., contacts. Consequently, we only consider the behavior of the analytic signal and the pseudogravity function over 2-D structures. In the following we will assume that the x-axis is perpendicular to the strike of the structure. The absolute value of the analytic signal over a vertical contact in a magnetic layer between depth z_1 and z_2 is then (Roest et al., 1992b)

$$|A(x)| \propto [(z_1 - z_2)^2/(z_1^2 + x^2)(z_2^2 + x^2)]^{1/2}, \quad (2)$$

which is independent of the direction of the source body magnetization (cf., Nabighian, 1972; 1974). The amplitude function is bell shaped, with the maximum located directly over the contact (at $x = 0$). The half-width of the maximum depends on both the thickness of and the depth to the source layer. Figure 2 shows the absolute value of the analytic signal (continuous lines) over the magnetic layer model for several ratios of depth and thickness.

For a very thin magnetic layer, with a magnetization inversely proportional to the layer thickness, i.e., $m(x) = \text{sign}(x)/(z_2 - z_1)$, equation (2) simplifies to:

$$\lim_{z_2 \to z_1} |A(x)| \propto 1/(z_1^2 + x^2). \quad (3)$$

Horizontal derivative of pseudogravity

The pseudogravity denotes the gravity anomaly that would be observed over a density distribution equivalent to the magnetization distribution that resulted in the magnetic anomaly. The horizontal derivative of the pseudogravity has been used for the detection and delineation of magnetic contacts (Cordell and Grauch, 1985; Blakely and Simpson, 1986) and can be derived from magnetic data using a simple

transformation. The (pseudo) gravity over a vertical contact at $x = 0$ in a layer between depths z_1 and z_2 is (Telford et al., 1976, p. 75):

$$G(x) \propto \rho\{z_2 \tan^{-1}(z_2/x) - z_1 \tan^{-1}(z_1/x) - x/2 \ln[1 + (z_2/x)^2] + x/2 \ln[1 + (z_1/x)^2]\}, \quad (4)$$

where ρ is the density contrast.

The absolute value of the horizontal derivative of the gravity is then

$$|H(x)| = |\partial/\partial x G(x)| \propto \rho|\ln[(x^2 + z_1^2)/(x^2 + z_2^2)]^{1/2}|. \quad (5)$$

Included in Figure 2 are examples of horizontal derivative curves, for different z_2/z_1 -ratios (dotted lines), calculated from expression (5). For a very thin layer, i.e., when z_2 approaches z_1, and $\rho = \rho'/(z_2 - z_1)$, equation (5) reduces to

$$\lim_{z_2 \to z_1} |H(x)| \propto z_1/(z_1^2 + x^2). \quad (6)$$

A comparison of equations (3) and (6) shows that for a single contact in a very thin layer, the absolute value of the analytic signal of the magnetic anomaly is proportional to the absolute value of the horizontal derivative of the pseudogravity anomaly. Figure 2 shows a comparison of the amplitude of the analytic signal (continuous lines) and the absolute value of the horizontal derivative of the gravity anomaly (dashed lines) over such a contact. For thin layers the two functions are indistinguishable, but even for thicker layers they are similar. Figure 3 shows the magnetic anomaly over a tabular body, observed at the magnetic pole, but with nonvertical magnetization (Figure 3a). As shown above, $|A(x)|$ is independent of the direction of source magnetization and thus the skewness of the magnetic profile it is based on. However, the shape of $|H(x)|$ depends on the skewness, and is only similar to $|A(x)|$ when the magnetization is vertical (Figure 3b).

The ability to determine the direction of magnetization from the anomaly over a single magnetic contact between depths z_1 and z_2 is demonstrated in Figure 4a, where the crosscorrelation of $|A(x)|$ with $|H(x)|$ is shown as a function of the direction of magnetization. A maximum correlation is

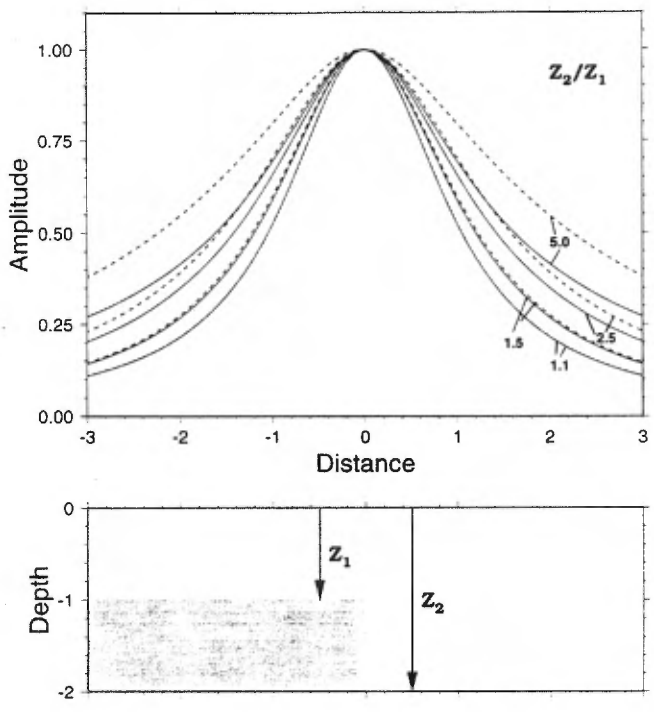


FIG. 2. Absolute value of the analytic signal (continuous lines) and of the horizontal derivative of the pseudogravity (dotted lines) over a single magnetic contact at location $x = 0$ in a magnetic layer between depths z_1 and z_2 for different values of the ratio z_2/z_1. For ratios close to 1, the functions are indistinguishable; for larger ratios, differences occur.

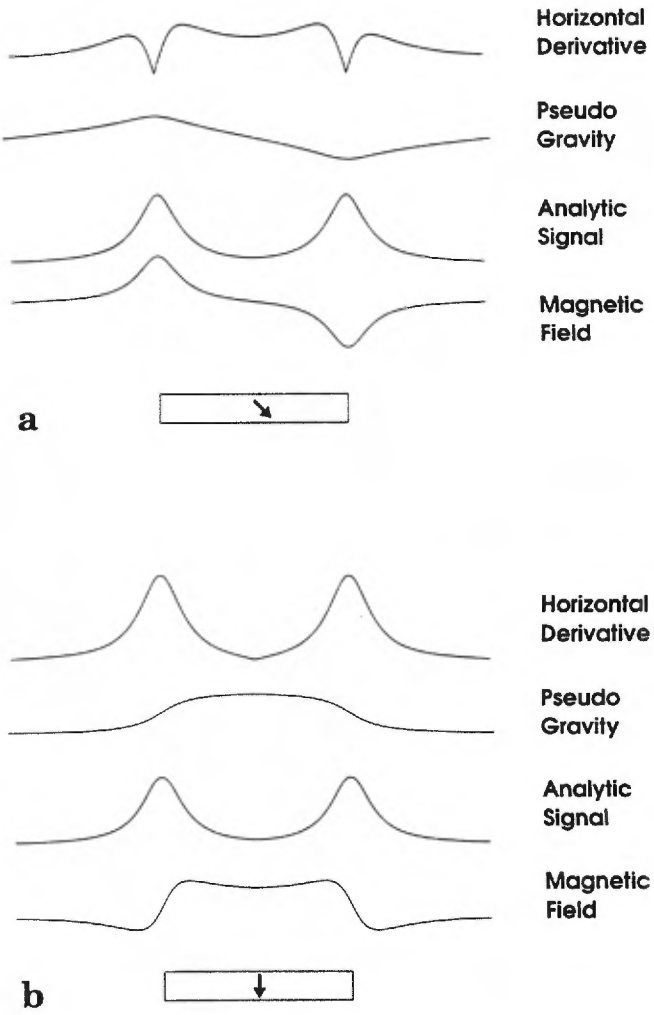


FIG. 3. (a) Magnetic anomaly profile over a 2-D body, with the absolute values of the analytic signal $|A(x)|$, the pseudogravity $G(x)$, and the horizontal derivative of the pseudogravity $|H(x)|$. When the direction of magnetization is not vertical, $|A(x)|$ displays maxima over the source body edges but $|H(x)|$ has a different shape and displaced maxima. (b) Reduction to the pole corrects the direction of magnetization to become vertical, in which case the anomaly becomes symmetrical, and the maxima of both $|A(x)|$ and $|H(x)|$ are located directly over the contacts.

reached for vertical magnetization. The correlation decreases significantly when the inclination of the source magnetization is shallower. Another way of determining the difference between the analytic signal and the horizontal gradient function is by looking at the actual locations of their peaks. As can be seen in Figure 3, the observed peaks of $|A(x)|$ and $|H(x)|$ are displaced with respect to one another. However, after reduction to the pole, both signals show maxima directly above the magnetization contacts. Figure 4b shows the maximum distance between the peaks, as a function of the direction of magnetization, for different source layer thicknesses. The distance is minimized for vertical magnetization.

MANICOUAGAN STRUCTURE ANOMALY

The study area for the application of the method is located over the central uplift of the Manicouagan impact structure, Quebec, Canada, and is centered on 51°23'N, 68°42'W. The aeromagnetic data in this area were collected at an altitude of 300 m along north/south oriented flightlines with a spacing of 812 m. Figure 5a shows the magnetic field intensity data over a 26 × 23 km area based on data with a grid interval of 200 m. The region is dominated by the intense (>2000 nT) anomaly that occurs in the center of the impact crater (Coles and Clark, 1978). The region within the boundary of the impact structure, which has a diameter of 100 km, is characterized by subdued magnetic relief with anomalies generally less than 500 nT. The exact origin of the central magnetic anomaly is unclear although the acquisition of a strong remanent magnetization component (D = 10°E, I = 40°N as compared to D = 23°W, I = 75°N for the ambient field) appears to be contemporaneous with the impact event (Larochelle and Currie, 1967). Sampling of Precambrian country rocks in the vicinity of the anomaly indicated susceptibilities of $<10^{-2}$ SI although ultramafic units sampled at greater distances revealed values up to $3.5\ 10^{-2}$ SI and remanent intensities of up to 200 A/m (Coles and Clark, 1978). On the basis of the high magnetic gradients and subsequent modeling, Coles and Clark postulated a shallow outcropping source for the anomaly with a depth extent ~3 km.

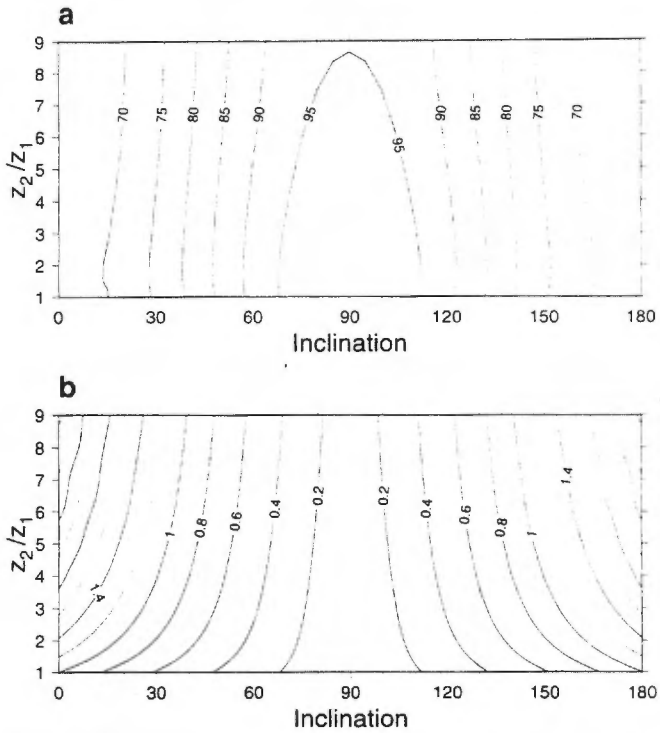


FIG. 4. (a) Crosscorrelation coefficient (in percent) and (b) displacement (relative to z_1) between the maxima in absolute values of both the analytic signal and the horizontal derivative of the pseudogravity over a single contact, for different values of z_2/z_1 as a function of the direction of remanent magnetization.

We proceed in evaluating the significance of the remanent component of magnetization in the area by calculating the analytic signal (Figure 5b) and the horizontal gradient of the pseudogravity (Figure 5c) from the data in Figure 5a. Figure 5b shows the maxima in the analytic signal, which coincide with the edges of the postulated source body. The continuity of these maxima reflects the form of the magnetic field data and shows the highest values in the northwest corner which coincides with the shallowest part of the modeled body (Coles and Clark, 1978). The horizontal gradient maxima also approximate the body edges but display a significant difference in amplitude between the northern and southern edges, which is not present in the analytic signal. Also, in comparison with Figure 5b, the southern edge maximum in Figure 5c is displaced ~1 km south of the corresponding analytic signal maxima indicated by the white line. This difference in gradient amplitude and the displacement of the maxima are both indicative of a significant remanent component in the anomaly.

The optimum direction of magnetization was determined by varying the reduction to the pole parameters and visually inspecting the resulting functions. The criteria used in this particular case were the balance between the northern and southern edge amplitudes and a minimal distance between the maxima of the two different functions. We found it was not possible to satisfy both criteria simultaneously for the northern edge. A compromise was found for inclination 45 degrees and declination 10 degrees (Figure 5d), which are close to the values determined from rock magnetic measurements. As indicated by the white lines in Figure 5d, the southern boundary maxima of $|H(x)|$ and $|A(x)|$ are coincident but the northern maxima of $|H(x)|$ are still displaced northward relative to the analytic signal. This shift is most likely the result of a nonvertical northern edge of the source body, consistent with results obtained by Coles and Clark (1978). For sloping interfaces, we expect the analytic signal maxima located over the top edge and the horizontal gradient shifted down dip (Grauch and Cordell, 1987; Hansen et al., 1987). Figure 6 shows an observed and reduced to the pole magnetic field profile across the structure (see Figure 5a for location). The difference in slope between the northern and southern edges of the source body is exemplified by the different gradients in the reduced to the pole magnetic field over them.

Using the optimal direction of remanent magnetization, a simple forward model for the Manicouagan central anomaly was constructed. The depth to source was estimated from

the half-widths of the analytic signal and the horizontal gradient function using equations (3) and (6) (see Roest et al., 1992b). Both methods yield similar results, but the horizontal gradient is much more continuous and allows us to determine the outline of the source body more accurately (compare Figures 5b and d). The depth estimates obtained from the horizontal gradient function are shown in Figure 7 (bottom), where the size of the circles is proportional to the depth to source. It clearly illustrates the shallowing of the structure towards the northwest, whereas the eastern and western edges seem to be less well resolved and probably more deeply buried. The topography of the surface of the body was estimated by fitting a minimum curvature surface through the estimated depth values at the body edges (Figure 7, middle). The bottom was held fixed at 3 km, in agreement with the estimate of Coles and Clark (1978). The anomaly calculated over this model body is shown in the top panel of Figure 7. It shows that with this very simple model we are able to match the observed anomaly quite well (compare with Figure 5a), further substantiating the calculated remanent magnetization direction. The model in Figure 7 is only a starting model that can be further refined. It has the necessary characteristics, however, and is mainly based on analysis of the magnetic field.

CONCLUSION

The method presented for the analysis of magnetic anomalies is a significant help in determining a possible remanent component. For theoretical models it is possible to minimize the crosscorrelation function and derive the correct direction of magnetization. However, the magnetization declination is the more difficult parameter to determine, especially for high inclination values. The application of such a fully automated procedure to real data is complicated by variable data quality, especially short wavelength noise, and interference of multiple anomalies. However, visual inspection of analytic signal and horizontal derivatives provides a good way of optimizing the remanent magnetization parameters. A simple forward model has illustrated the use of the approach.

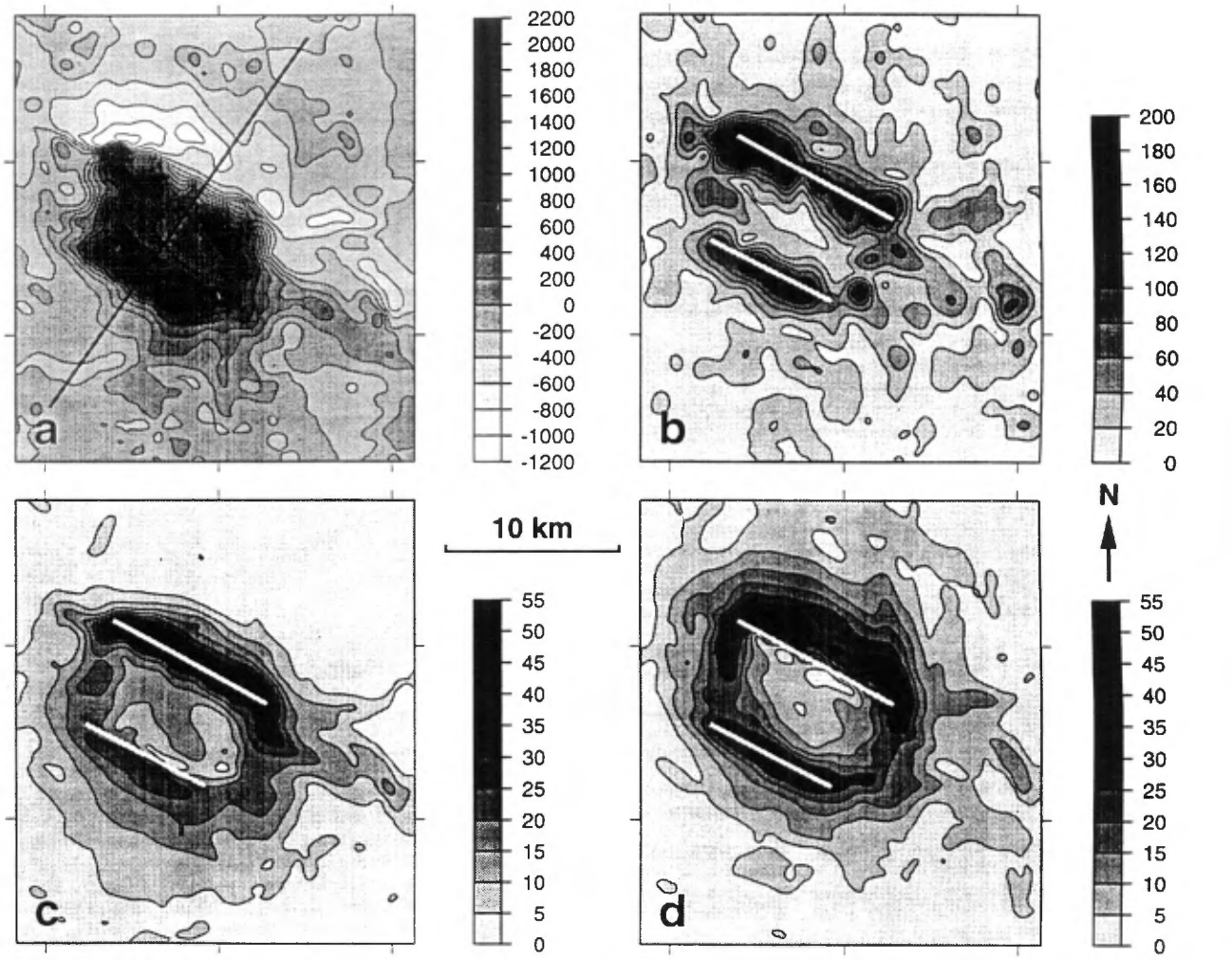


FIG. 5. (a) Magnetic field intensity of the central area of the Manicouagan impact structure, Quebec, Canada (51°23'N, 68°42'W). Line indicates location of profile in Figure 6. (b) Analytic signal, (c) Horizontal derivative of pseudogravity, (d) horizontal derivative of pseudogravity, after reduction to the pole, using a magnetization direction with inclination 45 degrees and declination 10 degrees. White lines indicate the locations of the source body edges inferred from the analytic signal.

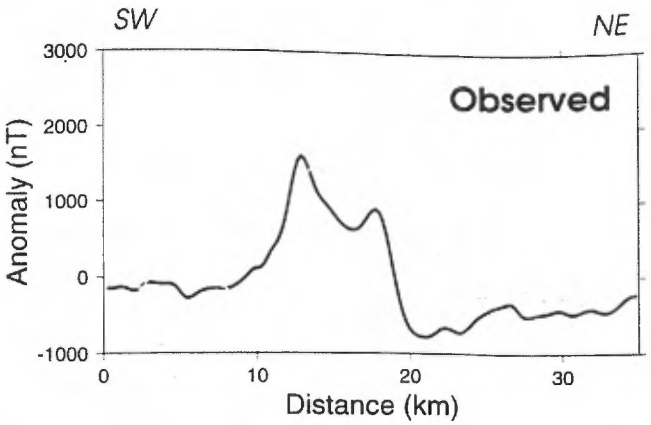


FIG. 6. Magnetic field profile across the Manicouagan central anomaly (see Figure 5a for location). The observed magnetic anomaly is asymmetric, with a pronounced negative to the northeast of the structure. After reduction to the pole, the northern gradient of the anomaly is less steep than the southern gradient, indicating a sloping contact.

ACKNOWLEDGMENTS

The comments of Peter McGrath, Pierre Keating, and Lindrith Cordell on this paper are gratefully acknowledged. We thank Walter Smith and Paul Wessel for their release of GMT graphics software used to computer generate the illustrations. This is Geological Survey of Canada Contribution, No. 10892.

REFERENCES

Baranov, V., 1957, A new method for interpretation of aeromagnetic anomalies: Pseudogravimetric anomalies: Geophysics, **22**, 359–383.

Bhattacharyya, B. K., 1966, A method for computing the total magnetization vector and the dimensions of a rectangular block-shaped body from magnetic anomalies: Geophysics, **31**, 74–96.

Blakely, R. J., and Simpson, R. W., 1986, Approximating edges of source bodies from magnetic or gravity anomalies: Geophysics, **51**, 1494–1498.

Books, K. G., 1962, Remanent magnetization as a contributor to some aeromagnetic anomalies: Geophysics, **27**, 359–375.

Bott, M. H. P., Smith, R. A., and Stacey, R. A., 1966, Estimation of the direction of magnetization of a body causing a magnetic anomaly using a pseudogravity transformation: Geophysics, **31**, 803–811.

Coles, R. L., and Clark, J. F., 1978, The central magnetic anomaly, Manicouagan structure, Quebec: J. Geophys. Res., **83**, 2805–2808.

Cordell, L., and Taylor, P. T., 1971, Investigation of magnetization and density of a North Atlantic seamount using Poisson's Theorem: Geophysics, **36**, 919–937.

Cordell, L., and Grauch, V. J. S., 1985, Mapping basement magnetization zones from aeromagnetic data in the San Juan Basin, New Mexico, *in* Hinze, W. J., Ed., The utility of regional gravity and magnetic anomaly maps: Soc. Expl. Geophys., 181–197.

Emilia, D. A., and Massey, R. L., 1975, Magnetization-inclination estimation from prism-like anomaly profiles: Geophysics, **40**, 443–450.

Grauch, V. J. S., and Cordell, L., 1987, Limitations of determining density or magnetic boundaries from the horizontal gradient of gravity or pseudogravity data: Geophysics, **52**, 118–121.

Green, R., 1960, Remanent magnetization and the interpretation of magnetic anomalies: Geophys. Prosp., **8**, 98–110.

Harrison, C. G. A., 1976, Magnetization of the oceanic crust: Geophys. J. Roy. Astr. Soc., **47**, 257–283.

Hall, D. H., 1959, Direction of polarization determined from magnetic anomalies: J. Geophys. Res., **64**, 1945–1959.

Hansen, R. O., Pawlowski, R. S., and Wang, X., 1987, Joint use of analytic signal and amplitude of horizontal gradient maxima for

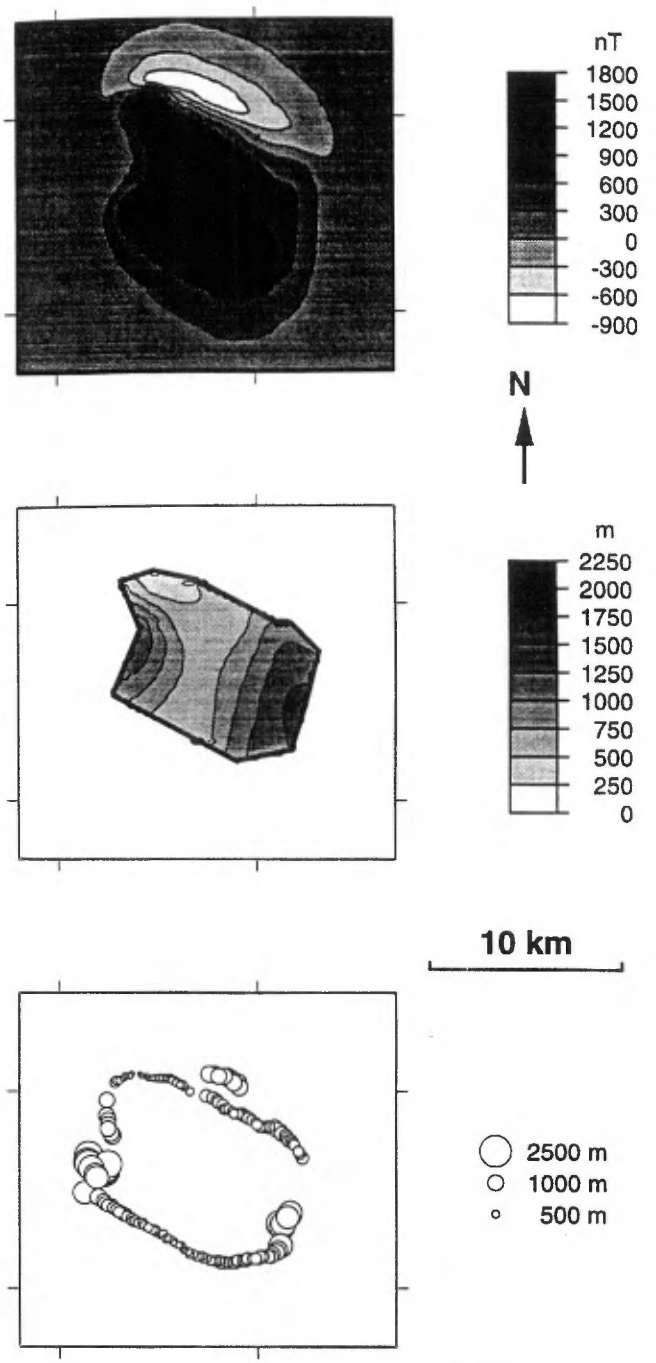


FIG. 7. Simple forward model for the Manicouagan central anomaly; projection as in Figure 5, but slightly smaller area. Bottom: depth estimates of body edges, based on half-width horizontal gradient function. Only maxima in the gradient with values exceeding 20 were used (see Figure 5d). Center: model body with the outline determined from locations of depth estimates, the topography of the surface estimated from the depth estimates around its edges. Top: modeled anomaly, showing several of the characteristics of the observed anomaly (Figure 5a).

three-dimensional gravity data interpretation: 57th Ann. Internat. Mtg., Soc. Expl. Geophys., Expanded Abstracts, 100–102.
Larochelle, A., and Currie, K. L., 1967, Paleomagnetic study of igneous rocks from the Manicouagan structure, Quebec: J. Geophys. Res., **72**, 4163–4169.
Muniruzzaman, M., and Banks, R. J., 1989, Basement magnetization estimates by wavenumber domain analysis of magnetic and gravity maps: Geophys. J. Int., **97**, 103–117.
Nabighian, M. N., 1972, The analytic signal of two-dimensional magnetic bodies with polygonal cross-section: Its properties and use for automated anomaly interpretation: Geophysics, **37**, 507–517.
——— 1974, Additional comments on the analytic signal of two-dimensional magnetic bodies with polygonal cross-section: Geophysics, **39**, 85–92.
——— 1984, Toward a three-dimensional automatic interpretation of potential field data via generalized Hilbert transforms: Fundamental relations: Geophysics, **49**, 780–786.
Roest, W. R., Arkani-Hamed, J., and Verhoef, J., 1992a, The seafloor spreading rate dependence of the anomalous skewness of marine magnetic anomalies: Geophys. J. Int., **109**, 653–669.
Roest, W. R., Verhoef, J., and Pilkington, M., 1992b, Magnetic interpretation using the 3-D analytic signal: Geophysics, **57**, 116–125.
Schnetzler, C. C., and Taylor, P. T., 1984, Evaluation of an observational method for estimation of remanent magnetization: Geophysics, **49**, 282–290.
Shurbet, D. H., Keller, G. R., and Friess, J. P., 1976, Remanent magnetization from comparison of gravity and magnetic anomalies: Geophysics, **41**, 56–61.
Telford, W. M., Geldart, L. P., Sheriff, R. E., and Keys, D. A., 1976, Applied Geophysics: Cambridge Univ. Press.
Zietz, I., and Andreasen, G. E., 1966, Remanent magnetization and aeromagnetic interpretation, *in* Mining Geophysics: Soc. Expl. Geophys., Vol. 2, 569–590.

ANNEXE IV.C

Information on iron meteorites

8

The Iron Meteorites and Pallasites

We owe the largest meteorite in captivity to a man who is far better known as the first to reach the North Pole. In 1894, on the second of several expeditions to explore Greenland, Lieutenant—later Admiral—Robert E. Peary fell under a spell that had beguiled polar explorers since 1818, when Captain John Ross of the Royal Navy found Eskimos using weapons and tools tipped with nickel-iron and heard stories of the "iron mountain" from whence the metal had come. Led to the site on the coast of West Greenland by a hunter, Peary discovered that the "mountain" was really three huge chunks of meteoritic iron: a 59-ton, almost wholly buried mass that the Eskimos called *Ahnighito* or "the Tent," and two smaller masses called "the Woman" and "the Dog."

With the determination that would take him to the North Pole 15 years later, Peary set out to bring the three Cape York irons back to New York City. The job, which his grandson has described in vivid detail (Stafford, 1980), entailed four summers of backbreaking work punctuated by winters of lecturing and lobbying for funds—no small task in those pre-NASA years. But Peary persevered, and in October 1897, *Ahnighito* reached New York (Figure 8.1).

I got to know the first three Cape York irons (several more pieces were found more recently) when they were in the foyer of the Hayden Planetarium at New York City's American Museum of Natural History. Like most other school children who visited the museum, I was awed by the immensity of "the Tent" and fascinated by the ablation pits that dot its dark bronze surface like giant thumbprints. Visitors can see the Cape York irons to still better advantage today in the

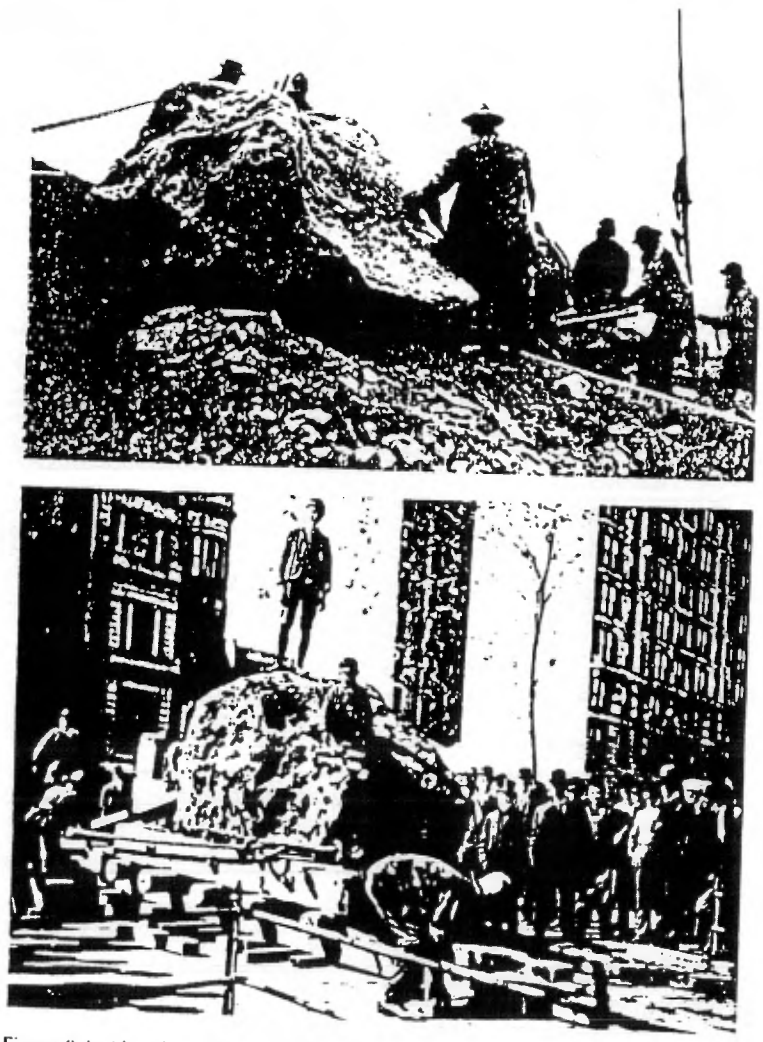


Figure 8.1 *Ahnighito* ("the Tent"), biggest of the Cape York iron meteorites. (*top*) Members of Peary's party struggle to take the 59-ton meteorite to the coast of Greenland. (Photograph by Lt. Robert E. Peary, negative no. 329141.) (*bottom*) *Ahnighito* arrives at the American Museum of Natural History. (Photograph by Orchard, negative no. 45086; both photographs courtesy of the Department of Library Services, American Museum of Natural History.)

museum's new Arthur Ross Hall of Meteorites. As a long-time fan of *Ahnighito*, I was disappointed to learn that although it is the biggest meteorite ever displayed in a museum, it is not the biggest ever found. That distinction belongs to the Hoba meteorite, which was discovered on a farm in South West Africa in 1920. Hoba measures 9 × 9 × 3¼ feet and weighs about 66 tons. Far too big to move, it still lies where it was found, though pieces of it have found their way to many museums.

Iron meteorites command our attention for several reasons, one of which is their majestic size. Though we know of no other chunks of metal as big as Hoba and *Ahnighito*, one of Western Australia's Mundrabilla meteorites weighs 10 to 12 tons, and the Willamette, Oregon, iron—also in residence at the American Museum of Natural History—weighs 13.5 tons. In contrast, the biggest single piece of a stony meteorite—the Norton County enstatite achondrite, which fell in Kansas in 1948—weighs barely a ton.

Iron meteorites also intrigue us because our forebears used them in their early efforts at metallurgy. The Eskimos' use of the Cape York irons illustrates this, as does the scarcity of iron meteorites in much of the Middle East. As our need for some of the rarer metals that occur in such meteorites outruns terrestrial supplies, we may well turn to the irons again or, more likely, to the asteroids from which they come.

But iron meteorites and the closely related pallasites fascinate us most because they take us to the deep interiors of their parent bodies and bear clues to processes that took place in the Earth billions of years ago and gave our planet its metal core and magnetic field. Irons and pallasites also give us some of the strongest evidence we have for the number and sizes of meteorite parent bodies.

The Widmanstätten Structure

Museum curators and meteorite researchers often get calls from people who think they have found a meteorite. Most of these discoveries prove to be something else—one curator built a large collection of such objects, which he whimsically called "meteor-wrongs"—but exceptions are common enough so that most of us greet such calls with courtesy or even warmth. How can we tell whether a rusty chunk of metal that surfaces in someone's garden is an iron meteorite or a piece of an old plow? A simple test is to shave off a bit of the sample and test it for nickel, which is present in all meteoritic metal. A more elegant test, which works for all but a few iron meteorites, is based on

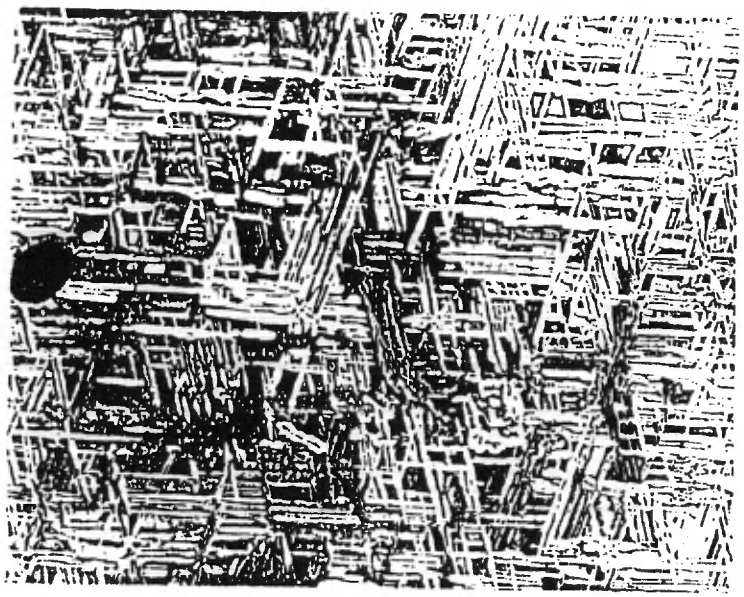


Figure 8.2 Polished, etched slab of the Carbo iron meteorite (medium octahedrite), showing bright kamacite plates separated by darker taenite to form the Widmannstätten structure observed in most irons. The field viewed is 4¾ inches wide. (Smithsonian Institution photograph, reproduced with permission.)

the fact that their metal has a highly characteristic texture: it consists of two nickel-iron alloys arranged in a geometrical pattern (Figure 8.2). This pattern, discovered in 1804 by Count Alois von Widmannstätten in Vienna and William Thomsen in Naples, appears when an iron meteorite is sliced, polished, and etched lightly with a dilute solution of nitric acid in alcohol.

The Widmannstätten pattern both positively identifies most iron meteorites (a few, which contain either a great deal of nickel or very little, lack an obvious pattern) and tells us a lot about their history. To see how this pattern formed and why it is important to our story, we have to take a short detour into another branch of science: metallurgy.

Like the carbon, silica, and olivine discussed earlier in the book, nickel-iron alloys occur in more than one crystalline form. At high temperatures and for high nickel contents, the atoms in such alloys arrange themselves in the pattern shown in Figure 8.3a: they lie at the

corners of cubes and in the centers of cube faces. A natural nickel-iron alloy with this "face-centered cubic" structure is called *taenite*. At lower temperatures and for low nickel contents, nickel-iron alloys adopt a second structure, in which each cube of atoms surrounds a central atom (Figure 8.3b). This arrangement is called "body-centered cubic," and the corresponding natural alloy is known as *kamacite*.

By slowly cooling nickel-iron alloys in the laboratory, metallurgists have determined which polymorph occurs at what combinations of temperature and composition. Figure 8.4 summarizes the results of this research. Like the diagram for water-salt mixtures shown in the previous chapter (Figure 7.1), this figure is a map in which composition and temperature substitute for the more familiar coordinates of latitude and longitude. Unlike the salt-water diagram, this one shows only what happens to nickel-iron alloys at temperatures well below melting.

To see how the Widmannstatten pattern developed in iron meteorites, let us follow an alloy of typical meteoritic composition (about one part nickel to nine parts iron) as it cools. Figure 8.4 tells us that at high temperatures, such an alloy (composition a) has the structure and form of taenite. As the temperature falls, the alloy enters the

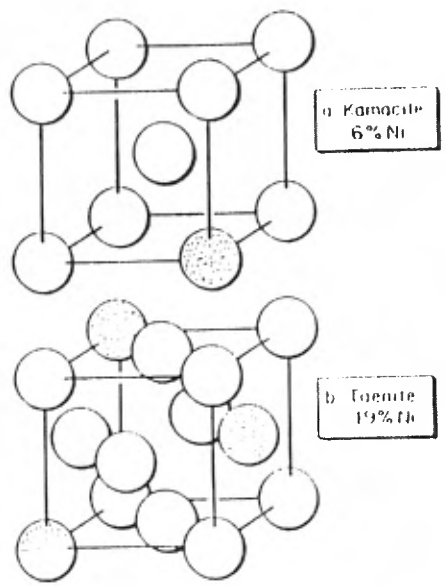


Figure 8.3 Structures of common nickel-iron polymorphs, with atoms spread apart to show their geometrical relationships. Nickel atoms are stippled, iron atoms clear. (*a*) Body-centered cubic structure of nickel-poor kamacite. (*b*) Face-centered cubic structure of nickel-rich taenite.

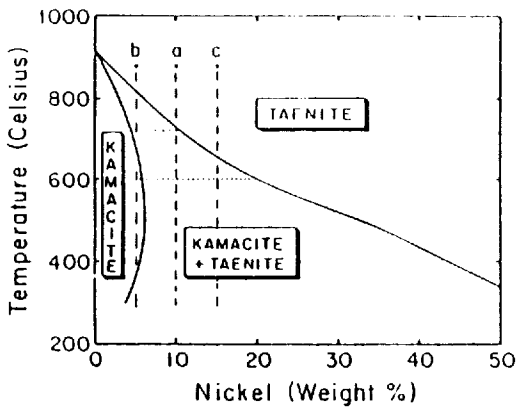


Figure 8.4 Distribution of kamacite and taenite in iron-nickel alloys at various temperatures, based on experimental studies by Romig and Goldstein (1979). Horizontal dotted lines connect the compositions of the two forms of metal at different temperatures. Compositions a, b, and c are appropriate to octahedrites, hexahedrites, and ataxites, respectively.

region marked "taenite + kamacite." When it does so, the taenite structure can no longer hold all of the iron present, and nickel-poor kamacite begins to form within it. At this point, the taenite has the same composition as the bulk alloy (10 percent nickel), the kamacite a more iron-rich composition (slightly more than 4 percent nickel). As the temperature continues to fall, kamacite grows at the expense of taenite, and both minerals become more nickel-rich. For example, at 600° C, taenite contains about 20 percent nickel and kamacite about 6 percent.

Figure 8.4 shows why iron meteorites that contain about 10 percent nickel consist of two nickel-iron alloys, but why do these minerals form the distinctive crisscross pattern that we see in such meteorites? This structure arises because kamacite does not appear at random in the taenite but grows on planes that are oriented like the faces of a regular octahedron (Figure 8.5). This octahedral arrangement of kamacite plates gives us our name for those iron meteorites that have an obvious Widmanstätten pattern: *octahedrites*. Most iron meteorites are octahedrites, because most contain between 6 and 13 percent nickel.

Iron-nickel alloys that contain much less than 10 percent nickel (for example, composition b in Figure 8.4) evolve in much the same way as they cool, but they arrive at a different destination. Because such alloys are iron-rich, the kamacite plates become very thick—so thick that they replace almost all of the taenite. The structure that results consists almost wholly of cubic crystals of kamacite. Since a cube is hexahedral (six-sided), we call nickel-poor iron meteorites that have this structure *hexahedrites*.

It is easy to see why nickel-poor iron meteorites lack the Widmanstätten structure, but why is it absent from nickel-rich meteorites as well? To understand this, we need to look more closely at what happens when metal cools. For kamacite to form and grow in taenite, nickel and iron atoms have to move through the metal, a process called *diffusion*. Atoms diffuse rapidly at high temperatures; hence kamacite plates grow swiftly at first. However, as the temperature falls, diffusion becomes more and more sluggish, causing the growth of kamacite to slow down and, eventually, stop altogether. Figure 8.4 shows that as their bulk nickel content increases, alloys enter the

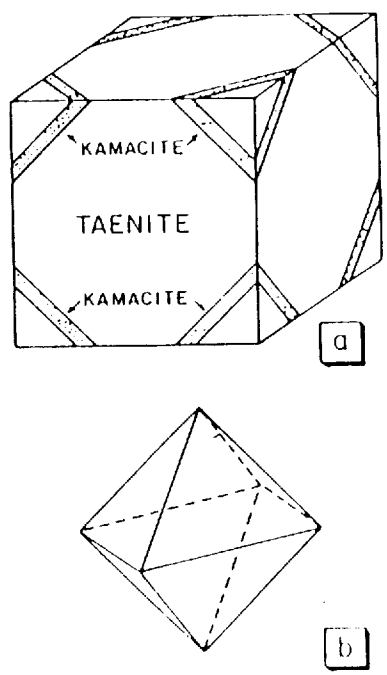


Figure 8.5 Geometrical distribution of kamacite plates in a crystal of taenite (a). These plates parallel the faces of a regular octahedron (b).

kamacite + taenite region at lower and lower temperatures. Thus alloy b starts to form kamacite at about 800° C, but alloy c does so at 660°. Kamacite appears in the latter alloy at such a low temperature that it has very little time to grow before diffusion stops. Hence the kamacite-taenite intergrowth in a meteorite of composition c is extremely fine-grained—so fine-grained that the meteorite appears structureless to the naked eye. Our name for nickel-rich iron meteorites, *ataxites*, refers to this apparent lack of structure.

Thus all three textural varieties of iron meteorites—the abundant octahedrites and the less common hexahedrites and ataxites—reflect slow cooling of metal with different nickel contents. This conclusion may not seem worth the long discussion that led to it, but it is very important. As we shall see later in this chapter, careful analysis of the Widmannstätten pattern has told us a great deal about the structures and sizes of iron meteorite parent bodies.

Classification of Iron Meteorites

Students of iron meteorites divide them into eight types on the basis of texture: hexahedrites, ataxites, and six kinds of octahedrites with different thicknesses of kamacite plates. This structural classification is of very long standing, and it remains useful for describing newly discovered iron meteorites. But just what do the chemical and structural differences among iron meteorites mean? Did these meteorites form in one parent body or in many bodies? Do they come from centrally located cores or from small pockets of metal that are scattered through the parent bodies like the fruit in raisin bread?

When I examined the question of the number of chondrite parent bodies, I based my answer on three pieces of evidence: first, small but sharp compositional differences among the eight or nine chondrite groups; second, the prevalence of one-group breccias; and third and most compelling, differences of oxygen isotopic composition from one group to the next. These three arguments will be used again in Chapter 9 when I discusss the various kinds of achondrites, and I shall add a fourth criterion, age, that is particularly useful for working out the genealogy of those igneous meteorites.

Most of the criteria that we use to work out associations of silicate-bearing meteorites are of little or no use for the irons. Though many iron meteorites bear the scars of shock events, few are breccias whose components might tell us which kinds of irons formed close together and which formed far apart. Fewer contain minerals that we can use to detect oxygen isotopic differences or to establish different times of

formation. Even traditional chemical analyses tell us little about relationships among iron meteorites, for they report just a handful of the more abundant elements: iron, nickel, cobalt, sulfur, and small amounts of carbon and phosphorus.

To subdivide and interpret the iron meteorites, we rely principally on *trace elements*, which can be defined for our purposes as those chemical constituents whose abundances are so low—commonly a few atoms per million or billion iron atoms—that they do not appear in traditional chemical analyses. To study these elements, chemists irradiate samples with neutrons to convert the trace elements to radioisotopes; they then use the decay of these isotopes to tell which elements are present and in what abundances.

To understand how trace elements help us interpret the iron meteorites, we need to know something about the way in which a nickel-iron liquid crystallizes. When molten nickel-iron cools, the metal that forms at each stage of crystallization contains less nickel than the associated liquid. Hence fractional crystallization produces a mass of solid metal that is iron-rich at its base and progressively enriched in nickel upward (Figure 8.6). John Lovering showed in

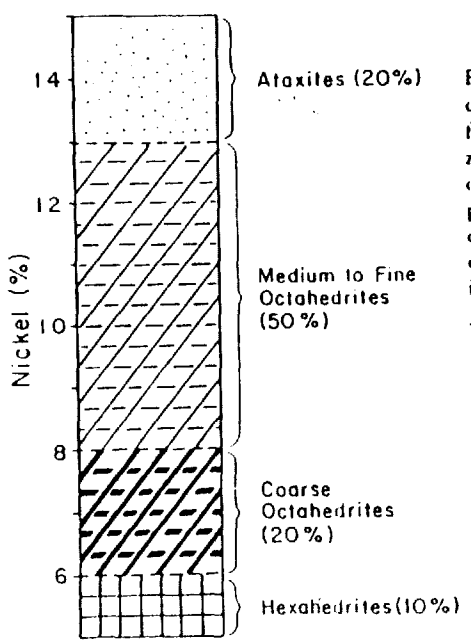


Figure 8.6 Cross-section of a differentiated nickel-iron core formed by fractional crystallization of a liquid composed of 11 percent nickel and 89 percent iron by weight. The distribution of various kinds of iron meteorites in this core is based on calculations by John Lovering (1957).

1957 that fractional crystallization of a liquid with the composition of an average iron meteorite (about 11 percent nickel) can produce solids that span the observed range of iron meteorite compositions. This simple process can even account for the observation that octahedrites are far more abundant than nickel-poor hexahedrites and nickel-rich ataxites.

How would trace elements be distributed in a differentiated metal core? As we saw in the discussion of layered igneous intrusions, the trace elements in a magma distribute themselves among crystallizing minerals in accordance with Pauling's rules. Those ions that fit comfortably in the structure of olivine, oxidized nickel for example, enter that mineral and follow it to the bottom of the intrusion. Other elements that fit in feldspar, for example strontium, follow that mineral. Still others, including some that are commercially important, find no homes in the major igneous minerals and accumulate in the remaining liquid, from which they may eventually crystallize to form ore deposits. As a result of this process of sorting trace elements according to their affinity for various minerals, samples taken from various levels in a layered intrusion describe distinctive trends of abundance for different trace elements. Thus nickel is abundant near the bottom of such an intrusion and decreases more or less regularly upward; strontium shows the opposite tendency. By studying trends for these and other trace elements, geologists can work out the crystallization history of an intrusion in considerable detail.

The rules that govern trace element distribution in a crystallizing magma work just as well in a crystallizing nickel-iron liquid. In fact, trace element trends in a metallic core are simpler than those observed in igneous rocks, since there are fewer kinds of crystals to compete for trace elements. Thus we would expect elements that prefer solid nickel-iron to liquid to be carried down by settling crystals and concentrated near the center of the core. Elements with the opposite preference should remain in the liquid, to be concentrated upward in the core.

Figure 8.7 shows some simple relationships between iridium and nickel that might result from fractional crystallization of iron-nickel liquids with various starting compositions and histories. The first point to note in this diagram is that different scales are used for nickel (percent) and iridium (parts per million); the second is that iridium varies far more widely than nickel. Much of the value of trace elements lies in the fact that fractional crystallization affects them much more strongly than it affects the major elements.

The data points in Figure 8.7 are not scattered across it but are

gathered together in elongate fields or trends. Trend A is what one would expect to find in random samples of the differentiated core shown in Figure 8.6. Because iridium prefers solid metal to liquid, it is most abundant in the nickel-poor cumulates that lie deep in the core; its abundance decreases upward as the nickel content increases. Fields B, C, and D in Figure 8.7 show different trends of iridium abundance that might result from fractional crystallization of liquids with different initial compositions—for example, richer (B, C) or poorer (D) in nickel. They also show that iridium-nickel diagrams and other trace-element diagrams can tell us a lot about crystallization history. Trend A shows the wide chemical variation that results from very efficient separation of crystals and liquid. In contrast, the modest variation evident in B indicates very slight fractional crystallization.

For our present purposes, the important question is whether the iron meteorites lie on one trend in trace-element diagrams or on many trends, that is, whether they formed from one liquid or from many liquids. Early studies of trace elements in iron meteorites were inconclusive on this point. When Lovering and his co-workers analyzed 88

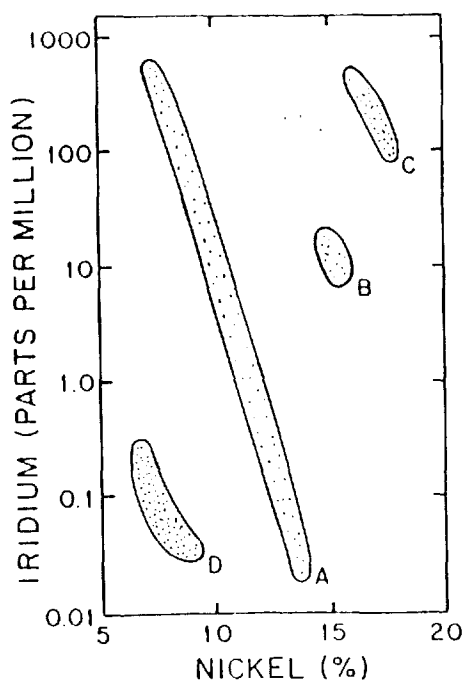


Figure 8.7 Hypothetical distributions of iridium and nickel in the core shown in Figure 8.6 (A) and in cores that are, on average, richer (B, C) or poorer (D) in nickel.

irons for gallium and germanium in 1957, they found that most of them fell into four groups on a diagram that compared these two elements, but that the four groups appeared to lie on one line. Lovering and his colleagues regarded the groups as important enough to label (I to IV), but they were more impressed by their alignment, which suggested that they all came from one differentiated core.

The simple picture that emerged from this early trace-element study vanished when other researchers examined more elements in more iron meteorites. Between 1967 and 1978, John Wasson and his colleagues at UCLA analyzed more than 500 irons for gallium, germanium, and iridium. Figure 8.8 summarizes their data for iridium and nickel. This figure and analogous diagrams for germanium and gallium make it clear that the iron meteorites do not fall on one trend but constitute at least 12 chemical groups. Some of these groups overlap in Figure 8.8, but they are distinct in diagrams for other elements. In naming these iron groups, Wasson and his co-workers used the Roman numerals that Lovering had devised, adding letters to subdivide the four original groups. In cases where two groups appeared to be related, they showed this by using two letters. Thus groups IIIA and IIIB, which are similar in many respects and appear to intergrade, appear as the field IIIAB in Figure 8.8.

Because there is no obvious way for crystal-liquid differentiation to shift meteorites from one chemical group to another, Wasson and his colleagues concluded that the 12 to 16 groups defined by trace elements sample at least a dozen parent bodies. As startling as this conclusion is, it tells only part of the story: the UCLA researchers also found that about 14 percent of the iron meteorites they analyzed fell in *none* of the known iron groups but were scattered wildly on trace-element diagrams. These unclassified irons may represent perhaps 50 more groups, samples of which seldom reach the Earth.

The groups that Wasson defined on the basis of trace-element data differ in other respects as well. For example, Figure 8.8 shows that some groups consist almost wholly of nickel-poor (IIA and IIB) or nickel-rich (IVB) meteorites, that is, hexahedrites or ataxites. Others, for example IIIA and IIIB, include only octahedrites. There are also mineralogical differences: most iron meteorites contain more or less iron sulfide (troilite) and iron-nickel phosphide (schreibersite), but members of some groups contain other minerals as well. For example, two groups of irons contain olivine, pyroxenes, and other silicates, which have yielded most of the meager data we have on the ages of iron meteorites. Other groups contain minerals—for example the chromium nitride carlsbergite—that are known from nowhere else.

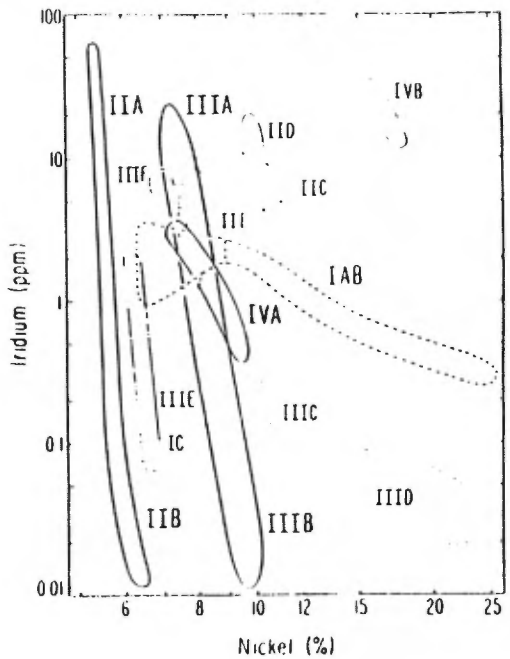


Figure 8.8 Distribution of nickel and iridium in various chemical groups of iron meteorites. (After Scott and Wasson, 1975, reproduced by permission of the authors and the American Geophysical Union.)

Thus detailed chemical study of the iron meteorites has produced a picture that is even more complex than the one we saw for chondrites. And as we shall see, cooling rates complicate that picture still further.

Cores or Raisins?

A question that trace-element distributions do not answer is whether the iron meteorites formed in centrally located cores or in small pods of metal that were scattered through their parent bodies. The answer to this question lies in the rates at which iron meteorites cooled. Irons that formed at about the same depth in a parent body—in its core, for example—should have cooled at very similar rates. Irons that formed at various depths, and hence were insulated by different amounts of overlying rock, should have cooled at very different rates.

But how can we tell how fast an iron meteorite cooled? The answer lies in the phenomenon that explains the very fine grained Widmannstätten structure found in nickel-rich ataxites: sluggish diffusion of iron and nickel at low temperatures. If diffusion were rapid at all temperatures, an octahedrite would consist of homogeneous, nickel-

rich taenite and homogeneous, nickel-poor kamacite; we would expect a series of microprobe analyses across the two minerals to show a nickel distribution like that in Figure 8.9b. In fact, the microprobe sees a very different pattern of nickel variation as it makes its way across an octahedrite (Figure 8.9c): the edge of each taenite region is nickel-rich as expected, but the nickel content drops inward, passes through a minimum value near the center of the taenite, and then rises toward the opposite edge. The reason for this M-shaped nickel profile is that during the last stages of kamacite growth, diffusion was too sluggish to carry nickel into the centers of taenite regions.

In the early 1960s, shortly after the microprobe became available for use by meteoriticists, two young scientists, Joseph Goldstein and John Wood, independently suggested that the shape of the M profile in taenite reflects the rate at which the metal cooled and can be used to estimate that rate. A very flat M, similar to the ideal nickel distribution shown in Figure 8.9b, testifies to extremely slow cooling—slow enough for diffusion to produce nearly homogeneous taenite. The sharp, deep M profile in the left-hand taenite plate shown in Figure 8.9c reflects very rapid cooling, while the shallower M in the right-hand plate of part c reflects an intermediate cooling rate. By calculating the shapes of nickel profiles that should result for various

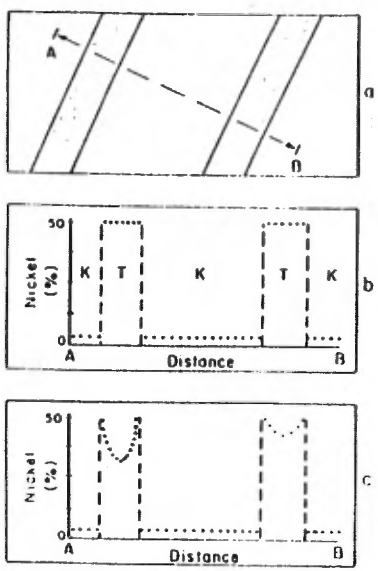


Figure 8.9 Growth of the Widmanstätten structure at various rates of cooling. (*a*) Kamacite plates (clear) and taenite (stippled) in a hypothetical octahedrite, showing the path traversed by the microprobe in parts b and c. (*b*) Distribution of nickel anticipated for infinitely slow cooling or perfectly efficient diffusion. (*c*) Nickel distributions expected for a high (left-hand plate) or a moderate cooling rate (right-hand plate).

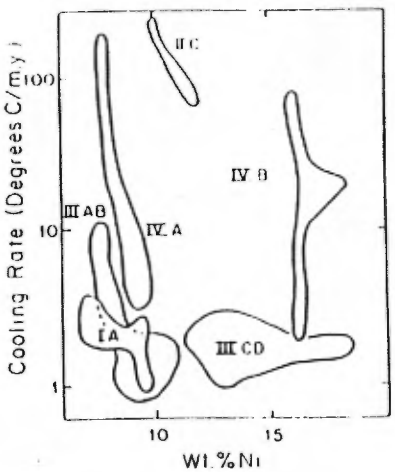


Figure 8.10 Cooling rates and nickel contents of various iron meteorite groups. (From Dodd, 1981.)

bulk meteorite compositions and cooling rates, Goldstein and Wood were able to translate the microprobe's observations into cooling rates for various kinds of octahedrites. Their method, subsequently simplified and modified by themselves and by others, has been applied to a great many iron meteorites and to other metal-bearing meteorites as well.

Figure 8.10, which compares the nickel contents and cooling rates of several groups of iron meteorites, shows very clearly that the irons had varied thermal histories. Some groups, notably IIIA, IIICD, and IIC, show little variation of cooling rate, suggesting that each group formed in one mass of metal—perhaps, though not necessarily, a central core. Other groups, in particular IVA and IVB, have widely varied thermal histories, which suggest that they formed in smaller masses—raisins—scattered throughout their parent bodies.

Twenty years ago meteoriticists argued almost as vehemently about whether iron meteorites formed in cores or raisins as they did about the number and sizes of parent bodies. This issue has now faded into history. As is often true in science, the answer to this "either/or" question has proved to be "both."

Pallasites

Although there are only 35 pallasites, all but two of them finds, these olivine stony-irons are important as a bridge between the iron and stony meteorites. They are also among the handsomest of rocks, with

beautifully formed, golden crystals of olivine set in gleaming metal like topaz in a fine ring. Evidently earlier residents of the Americas also appreciated the pallasites, for one of them—Hopewell Mounds—was discovered at a prehistoric burial site, and pieces of others were found so far apart that we believe primitive man transported them over long distances.

The Thiel Mountains pallasite, an Antarctic meteorite shown earlier (Figure 3.3), is typical of the class in that it consists of about two-thirds magnesian olivine, one-third metal, a bit of troilite and schreibersite (iron-nickel phosphide), and little else. Readers with unusually sharp eyes may see two kinds of metal in Figure 3.3, for Thiel Mountains, like other pallasites, contains kamacite and taenite arranged in a Widmannstätten pattern. This pattern is much more obvious in Figure 8.11, which shows a metal-rich portion of Brenham, an unusually inhomogeneous pallasite.

Long before meteoriticists had access to the microprobe and neutron-activation analysis, the textural similarity between the metal in pallasites and that in iron meteorites led them to suspect that the two kinds of meteorites are very closely related. These modern tools have confirmed that suspicion: most of the pallasites have trace-element distributions and cooling rates that closely resemble those observed

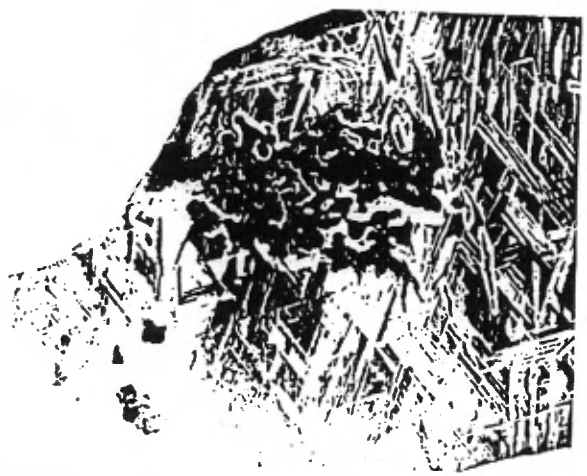


Figure 8.11 The Brenham, Kansas, pallasite, showing an unusually metal-rich region with a well-developed Widmannstätten structure. (Smithsonian Institution photograph, reproduced with permission.)

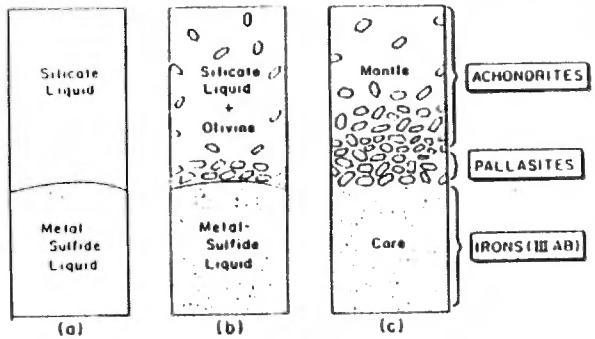


Figure 8.12 Development of pallasites and related iron meteorites from a chondritic liquid. (*a*) Metal-sulfide and silicate liquids separate, with the former sinking because of its high specific gravity. (*b*) Fractional crystallization of the silicate liquid produces a cumulate of settled olivine crystals just above the metal-silicate boundary. (*c*) As the metal-sulfide liquid solidifies, the nickel-rich residual liquid is drawn upward into the olivine cumulate to produce pallasites.

for one of the largest iron groups, IIIAB (see Figures 8.8 and 8.10). The few exceptions suggest that pallasites, like iron meteorites, sample more than one parent body.

There is still some debate about just how pallasites formed, but we have little doubt that they sample one or more boundary regions between masses of metal and silicates—environments analogous to the Earth's core-mantle boundary. One plausible process for the formation of pallasites is shown in Figure 8.12. Molten chondritic material separated into two liquids: a metal-sulfide core and a silicate mantle (Figure 8.12a). As the mantle cooled, olivine crystallized early and settled out to form a cumulate just above the core-mantle boundary (Figure 8.12b). How liquid metal from the core moved into the olivine cumulate is less clear (Figure 8.12c). One possibility is that silicate liquid between the olivine crystals moved upward as basaltic magma, and molten metal simply replaced that liquid, just as soda replaces air when you suck on a straw. Another is that the mantle shrank as it cooled, squeezing molten metal out of the core and into the olivine-rich layer.

We conclude, then, that most of the pallasites are samples of the core-mantle boundary of the body that housed group IIIAB iron

meteorites. The few pallasites that have unusual compositions may have formed in similar environments, but in different parent bodies.

Clearly, the IIIAB parent body has sent us generous samples of its core and lower mantle. Has it sent us bits of its upper mantle and crust as well? We shall return to that question when we examine the igneous achondrites in Chapter 9.

History: Theme and Variations

Twenty years ago it seemed possible to describe the history of iron meteorites quite simply: (1) a chondritic parent body started to melt; (2) the resulting iron-nickel-sulfur liquid trickled inward to form a molten core; (3) that core solidified, with iron-rich crystals sinking to the center through a more nickel-rich liquid; (4) at a late stage in crystallization, nickel-rich liquid from the core invaded the parent body's lower mantle to produce those rocks that we call pallasites.

At least one group of iron meteorites—that labeled IIIAB in Figures 8.8 and 8.10—played this theme more or less as written, but many other groups played quite elaborate variations on it. The fact that some groups have varied cooling rates suggests that they formed as dispersed pockets of metal rather than central cores. One group, the IAB irons, has a peculiar iridium distribution (see Figure 8.8) and other properties that lead us to think these meteorites were never entirely molten. Evidently these peculiar, silicate-bearing irons sounded just the first notes of the iron meteorite theme before they froze in a form that they have maintained for 4.5 billion years.

A glance at Figures 8.8 and 8.10 shows us that the various iron groups differ in average composition as well as history: Some consist entirely of iron-rich and some of nickel-rich meteorites, hexahedrites and ataxites respectively. Clearly, these groups formed from liquids with different compositions. How can we explain these differences? As we saw in Chapter 7, differences in the availability of oxygen could produce nickel-rich and nickel-poor liquids from one type of chondritic parent material. If that material melted under oxygen-rich (oxidizing) conditions, it would produce a nickel-rich liquid and a solid residue of iron-rich silicates (Figure 7.9b). If it melted under oxygen-poor (reducing) conditions, the liquid would be much more abundant and richer in iron, and the solid residue would consist of iron-poor silicates (Figure 7.9c).

No doubt some of the chemical differences among iron meteorite groups are due to different degrees of oxidation or reduction. Indeed, the reason for our suspicion that some nickel-poor irons, specifically

those of group IIAB (Figure 8.8), are related to the enstatite chondrites and achondrites is that all three kinds of meteorites record strongly reducing conditions. However, some chemical differences among the iron meteorites—for example, the high iridium contents of some and the low iridium contents of others—cannot be explained in this way. It is clear that iron meteorites formed from several different kinds of chondritic material.

Before moving on to consider other differentiated meteorites, I shall conclude this chapter on the irons and pallasites with a brief look at what we know—and still do not know—about two important aspects of these meteorites: when they formed and what kinds of parent bodies they came from.

Few iron meteorites contain minerals that can be dated by conventional means. In fact, we have radiometric ages for only two groups, and we are not sure just what those ages mean. The most reliable ages now in hand come from a small group of irons (IIE) that contain feldspar and can thus be dated by the very precise rubidium-strontium method. Some of these meteorites have ages that are similar to those of chondrites—about 4.55 billion years. Others have younger ages, down to a minimum of 3.8 billion years for the Kodaikanal meteorite. Taken at face value, these dates suggest that the parent body of IIE meteorites started to melt very shortly after the sun formed and was still molten, at least in part, 700 million years later.

We are no longer surprised by evidence that the meteorite parent bodies became very hot very early, but it is hard to understand how any of them could have stayed hot for as long as 700 million years. This is particularly puzzling in the case of irons, whose parent bodies were, it seems, very tiny indeed. It is unfortunate that IIE is a very small group, for its peculiar history invites further study.

The other group of silicate-bearing irons (IAB) lacks feldspar, but iodine-xenon ages of other silicates and troilite in these meteorites are very high—close to those obtained for chondrites. It appears that these meteorites, like some of the IIE irons, formed very early in the history of the solar system.

We know nothing about the formation ages of the other iron meteorites, most of which lack silicates altogether. Fortunately, this problem has attracted the attention of nuclear chemists, who are exploring isotopic systems based on elements—such as palladium and silver—that occur in meteoritic metal. If this work is successful, it will strengthen what is now a very weak link in our knowledge of iron meteorites.

The final question that must be asked about the varied objects that produced iron meteorites and pallasites is how big they were. We saw in Chapter 6 that we can use both pressure-sensitive minerals and cooling rates to determine how deeply a meteorite was buried in its parent body. If that meteorite formed at the center of the parent body, its depth of burial equals the body's radius; if not, it gives us only a minimum radius for its parent body. Laboratory experiments tell us that the Widmannstätten pattern cannot form at pressures greater than about 12,000 atmospheres. Therefore, no octahedrite comes from the center of a body with a radius greater than about 500 miles. This fact alone rules out parent bodies as big as the moon. Unfortunately, it is impossible to use pressure arguments to narrow further the range of permissible body sizes, because few irons contain pressure-indicative minerals.

However, most irons do contain kamacite and taenite, and we can use the nickel distributions in these minerals to calculate cooling rates. These cooling rates, in turn, can be used to estimate depths of formation. When I made such calculations a few years ago (Dodd, 1981), I concluded that those iron groups that sample cores formed in bodies with radii between 120 and 170 miles—the size of moderately large asteroids. Calculations for other groups yielded similar sizes, which are, of course, minima.

As noted in Chapter 6, recent laboratory experiments on iron-nickel alloys have changed this picture dramatically. When we take into account the minor elements in iron meteorites, the calculated cooling rates increase sharply and the sizes we infer for parent bodies drop just as sharply. It now appears that almost all iron meteorites cooled at rates of at least 100° C per million years. These revised cooling rates are startling and a bit unsettling, for they imply parent bodies less than 12 miles in diameter for those iron meteorites that sample central cores. Larger bodies are possible for iron groups that sample "raisins," but even these meteorites appear to have formed in rather small asteroids. Thus parent bodies that we once pictured as at least as big as the moon have shrunk, in just 20 years, to objects about as big across as Manhattan Island is long.

The iron meteorite parent bodies are unlikely to "shrink" further, for the new cooling-rate calculations have eliminated the principal causes of uncertainty in the old ones. In fact, I suspect that the tiny parent bodies now in view will prove to be too small: it is very hard to see how such gravity-driven processes as fractional crystallization and core formation could take place in tiny bodies with insignificant gravitational fields. Perhaps our assumption that similar cooling rates for a group of irons indicate that if formed in a central core is incorrect, since all this really tells us is that a group of meteorites formed at about the same depth.

Once thought to be the simplest of meteorites, the irons have proved on careful study to be surprisingly complex. Just how many parent bodies they represent is a fascinating question. Taken at face value, the many irons that do not fit in our present trace-element classifications—about 14 percent of those studied to date—suggest that the Earth has sampled bits of perhaps 50 more bodies during the last few hundred years. Do these unclassified irons come from objects that are just beginning to favor us with samples, or from parent bodies that made most of their contributions long ago?

The ancient iron meteorites from Antarctica may answer this question. It will be interesting to see whether some of the orphan irons will find their families among meteorites that fell thousands, even millions, of years ago.

ANNEXE IV.D

Grieve, R.A., and Masatitis, v.l., 1994. The Economic Potential of Terrestrial Impact Craters; International Geology Review, Vol. 36

International Geology Review, Vol. 36, 1994, pp. 105–151
Copyright © 1994 by V. H. Winston & Son, Inc. All rights reserved

The Economic Potential of Terrestrial Impact Craters

R. A. F. GRIEVE

Geological Survey of Canada, Ottawa, Ontario, Canada

AND V. L. MASAITIS

Karpinskiy Geological Institute, St. Petersburg, Russia

Abstract

Like concentrations of economic resources, terrestrial impact structures are the result of relatively rare geologic events. Economic resources occur in a number of terrestrial impact structures. After providing a context by briefly summarizing the salient points of the terrestrial impact record and the characteristics of impact craters, the relationship between impact craters and economic resources is explored. Approximately 25% of the known terrestrial impact craters are associated with some form of economic resources and ~ 12% currently are exploited or have been exploited in the recent past. The resources range from world-class ore deposits to relatively localized occurrences of materials. The larger economic deposits are discussed under the genetic classification of progenetic, syngenetic, and epigenetic. The progenetic deposits include the iron and uranium ore exposed at Ternovka, Russia, and Carswell (Saskatchewan), Canada, which are exploitable because of uplift in the center of complex impact structures. Progenetic deposits also include most of the gold and uranium deposits in the Witwatersrand Basin, South Africa, which have been protected from erosion by structures associated with the Vredefort impact structure. Syngenetic deposits include the occurrence of impact diamonds at several impact structures and the Cu-Ni-PGM ores of the Sudbury Igneous Complex, which is interpreted as part of the impact melt system of the Sudbury Structure, Ontario, Canada. Epigenetic deposits include various deposits resulting from post-impact hydrothermal and sedimentary activity. They also include hydrocarbon deposits. One of several examples is at Ames (Oklahoma), USA, where hydrocarbons are recovered from several lithologies, including crystalline basement. At Ames, the impact structure not only provided the necessary structural trap but also was instrumental in localizing the source rock, which was local post-impact oil shales.

The current worth of economic materials produced from impact structures worldwide is unknown, but is estimated at $5 billion per year for North America. As the known record of terrestrial impact cratering is far from complete, there remain many impact structures (and, therefore, potentially economic deposits) to be found. As such deposits are highly varied in type and impact structures are random in both geologic time and terrestrial location, it is difficult to develop an overall exploration strategy, although some generalized guidelines can be provided. Once an economic deposit has been located, however, the relatively fixed morphology and structure of impact structures of a given diameter can considerably simplify further exploration and exploitation.

Introduction

AS THE RESULT of the planetary exploration programs of the former USSR and the United States, impact craters now are recognized as a common and important landform on planetary surfaces. In parallel with this recognition, there has been considerable progress in understanding the nature of the cratering process and its effects on planetary evolution, particularly early planetary evolution. Prior to planetary exploration, the earth science community was slow to recognize the occurrence of terrestrial impact craters and some individuals opposed vigorously the origin of specific terrestrial structures by impact. Today, however, the occurrence of terrestrial impact craters is accepted more generally, largely through the weight of self-consistent evidence with regard to their structure, the range and distribution of impact lithologies (showing so-called shock metamorphic features), and the current understanding of the physics of impact. A historical discussion of the acceptance of terrestrial impact structures by the general earth science

0020-6814/94/43/105-47 $10.00

community can be found in Marvin (1990). The current awareness of the nature and occurrence of terrestrial impact structures is such that new discoveries are being made by members of the general geoscience community just as often as by specialists in their study.

The terrestrial impact record has served as a proverbial "gold mine" of ground-truth data for constraining the results of experiments and calculations on the nature of the cratering process (Grieve, 1991). Impact is an extraordinary geologic process involving vast amounts of energy, resulting in near instantaneous rises in temperature and pressure, and in the structural redistribution of target materials. By the same token, economic deposits, in general, are the result of extraordinary geologic circumstances. There are a number of instances in which terrestrial impact structures have economic resources—in some cases, with considerable commercial value. Indeed, the exploration of the first known terrestrial impact crater, Barringer or Meteor Crater, Arizona, was based on its economic potential (Barringer, 1906). The principals believed that several million tons of iron, nickel, and platinum-group metals contained in the iron meteorite were buried beneath the crater floor. As a commercial enterprise, however, it was a failure. For, as is now known, extraterrestrial bodies over ca. 10^7 kg impact with undiminished cosmic velocities. These velocities result in shock pressures sufficient largely to vaporize the impacting body, and thus result in the effective physical removal of much of this material from the immediate area of the impact structure.

More recently, it has been recognized that some well-known economic deposits are located within impact structures. Of the over 140 known terrestrial impact structures (Grieve and Shoemaker, 1994), approximately 35 have some form of potentially economic deposits (Masaitis, 1989, 1992). The number currently (or in the relatively recent past) producing some form of economic resources is 17. In this contribution, we examine the nature of some of these deposits and their relation to the formation of the impact structure. We do not consider those structures that have been or are exploited for building materials (e.g., Ries, Germany; Rochechouart, France), as well as cement production (Ries), or for hydroelectric power (e.g., Puchezh-Katunki, Russia; Manicouagan, Quebec, Canada). These types of economic potential, however, can be considerable. For example, the hydroelectric power produced from the reservoir inside the Manicouagan structure is on the order of 4000 gigawatt hours annually. Similarly, the production of cement and lime products from the Ries crater is worth more than of $70 million per year.

This paper considers examples where the economic deposits are related directly to the impact structure through structural disturbance of the target rocks, shock heating and/or hydrothermal activity, and the formation of a structural or topographic trap—that is, from the point of view of progenetic, syngenetic, and epigenetic deposits. As readers may be relatively unfamilar with the subject, we provide a context by describing some of the salient characteristics of known terrestrial impact craters, before discussing some examples of these types of deposits. The intention is not to review in detail the considerable literature on impact cratering, shock metamorphism, and the geological and geophysical character of terrestrial impact craters. The interested reader is referred to such compendia and reviews as French and Short (1968), Roddy et al. (1977), Masaitis et al. (1980), Melosh (1989), Grieve (1991), Pilkington and Grieve (1992), and references therein, for further details.

Basic Characteristics of Terrestrial Impact Craters

In many cases, terrestrial impact craters are highly degraded or modified by other terrestrial geologic processes, such as erosion, sedimentation, and, to a lesser extent, tectonism. Nevertheless, the known sample of the terrestrial impact crater population illustrates the basic morphological progression with size observed on other planets (Wood and Head, 1976). The two basic forms are so-called simple and complex impact craters. The range of final rim diameters (D) over which a particular form occurs on the terrestrial planets is primarily a function of the size of the impact event and planetary gravity, with target rock properties and possibly impact velocity having a secondary influence (Pike, 1980). On earth, simple craters occur at diameters of up to ca. 2 km if the



...material outside the rim is the remains of



FIG. 2. Vertical aerial photograph of the simple Brent Crater, Canada. The crater is 450 ± 3 Ma old and has a present diameter of ~3 km. The original rim has been removed by erosion and the interior filled with post-impact sediments. In contrast to Barringer (Fig. 1), Brent is not immediately recognizable as a crater form because of terrestrial geologic processes.

target rocks are sedimentary and up to around 4 km if the target rocks are crystalline (Dence, 1972). Above these respective diameters, terrestrial impact craters have a complex form.

Simple craters

Simple craters consist of a bowl-shaped depression with a structurally uplifted and locally overturned rim area. The classic

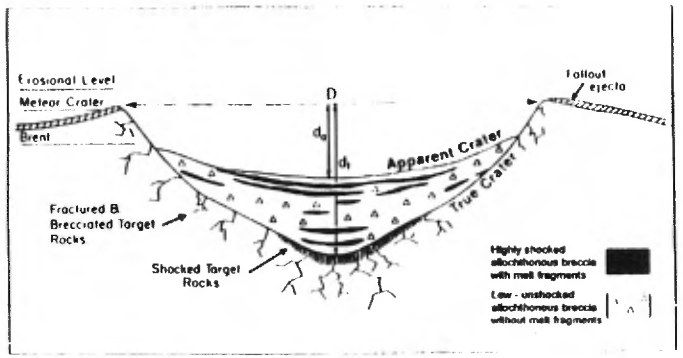


FIG. 3. Cross-section of a simple crater based on drillhole information mainly from Brent and Meteor Crater. Note presence of a lens consisting of breccias with a range of shock levels. The bulk of the breccia is relatively unshocked, and shocked autochthonous target rocks are restricted to the base of the crater in the center. The current erosional levels of Brent and Meteor Crater are indicated.

terrestrial simple crater is the 1.2-km-diameter Barringer or Meteor Crater, Arizona, USA (Fig. 1). Meteor Crater was formed ca. 50,000 years ago (Sutton, 1985) by the impact of an iron meteorite (Buchwald, 1975), estimated to be in the size range of around 50 m (Schmidt, 1980). For an impact velocity of 25 km s^{-1}, this corresponds to the release of ca. 10^{16}J of kinetic energy, which is equivalent to around 60 megatons TNT. Most other terrestrial simple craters (e.g., Brent, Canada, Fig. 2) are not as well preserved as Meteor Crater, which still retains its overturned flap of bedrock on the rim and a large portion of its exterior ejecta blanket.

Drilling at Meteor Crater, Brent, and other simple craters indicates that the apparent floor of simple craters is underlain by a breccia lens, which is approximately parabolic in cross-section (Fig. 3). This lens consists of brecciated target material and is contained in the fractured, but essentially autochthonous, target rocks of the floor and wall of the so-called true crater. Although the breccia lens does contain some highly shocked materials, including melted target rock, the bulk (ca. 90%) shows no diagnostic evidence of shock. Shock metamorphic effects in the autochthonous target rocks are restricted to the floor of the true crater (Fig. 3), where maximum shock pressures on the order of 25 GPa (250 kilobars) are recorded and attenuate rapidly with depth (Robertson and Grieve, 1977).

Peak shock pressures occur at the point of impact and are a function of impact velocity and the physical properties of the impacting body and the target rocks. For example, the impact of an iron body into silicate materials at 30 km s^{-1} results in a peak shock pressure of ca. 1600 GPa (16 Megabars) (Ahrens and O'Keefe, 1977; Melosh, 1989). In simple craters, however, the largely unshocked breccia lens materials lie stratigraphically closer to the impact point than the shocked target rocks of the true crater floor. This apparent reversal of "shock stratigraphy" indicates that the breccia lens materials are allochthonous in nature and has led to the concept of the so-called "transient cavity" in the formation of simple craters.

The transient cavity is the initial cavity produced on impact by the cratering flow field. The transient cavity results from the movement of target materials by particle velocities imparted to the target rocks by the shock and the following release or rarefaction waves. It grows by a combination of the upward and outward excavation of relatively near-surface materials and the downward and outward displacement of relatively deeper materials (Fig. 4A). Various levels of detail on the mechanics of simple crater formation can be found in Gault et al. (1968), Stöffler et al. (1975), Dence et al. (1977), Croft (1980), Grieve and Garvin (1984), Melosh (1989), and others. At its maximum growth, the transient cavity is parabolic in cross section and

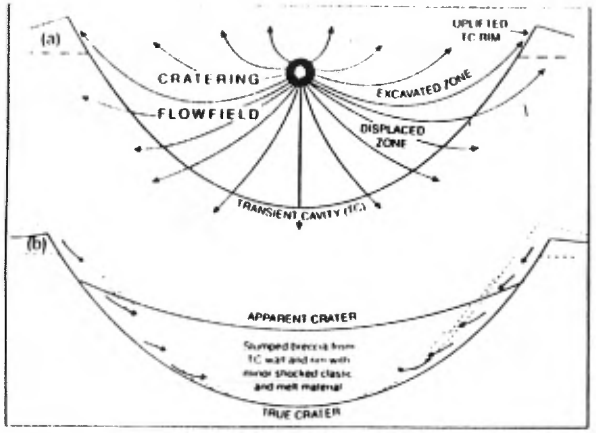


FIG. 4. A. Formation of parabolic transient cavity by excavation and displacement along the flow lines of the cratering flow field (see text for more details). B. Collapse of transient cavity walls to form interior allochthonous breccia lens, resulting in the formation of the so-called apparent and true craters (see text for more details).

reaches a depth roughly one-third its diameter (Fig. 4A). The time for the transient cavity to reach its maxium dimension at kilometer-sized craters is on the order of 10 seconds (Melosh, 1989). The walls and floor of this cavity are, in part, lined with melted and shocked materials set in motion and driven down into the expanding cavity. The transient cavity is, however, highly unstable during its late-stage growth, and its walls collapse inwards. This collapse enlarges the final diameter slightly compared to the transient cavity diameter and partially fills the final crater with brecciated, but largely unshocked, material from the transient cavity wall, resulting in the observed breccia lens (Fig. 4B).

Models of the relative geometries of the transient cavity and final crater have been tested successfully with observational data from terrestrial simple craters. Unfortunately, only 20% of the ca. 35 known simple craters have sufficient morphometric data on crater depths, breccia lens volumes, and other morphometric parameters to test the model and, in some of these cases, dimensions, such as depth to the base of the breccia lens, are based on the interpretation of gravity data. The morphometry of the simple craters with the best available data (Grieve et al., 1989) define the relationships:

$$d_a = 0.13D^{1.06} \text{ and}$$

$$d_t = 0.28D^{1.02},$$

where D is final rim diameter, and d_a and d_t are apparent and true depth (Figs. 3 and 4) and are defined as the maximum depth from the original ground surface to the top and bottom of the breccia lens, respectively, and units are in kilometers. The sample used to define these morphometric relationships includes craters in both crystalline and sedimentary targets. Target rock type, therefore, does not appear to have a major effect on d:D relationships for simple craters.

Complex craters

Complex impact craters are characterized by an uplifted central area, occurring as a central topographic peak and/or ring (Fig. 5). This is surrounded by an annular depression and a normally faulted structural rim area. Although differential erosion modifies, in some cases severely, the original morphology of terrestrial complex craters (e.g., Fig. 5B), examples of the morphological subgroups of complex craters, which are more clearly observed on other planetary bodies (Wood and Head, 1976), can be found in the terrestrial record. With increasing

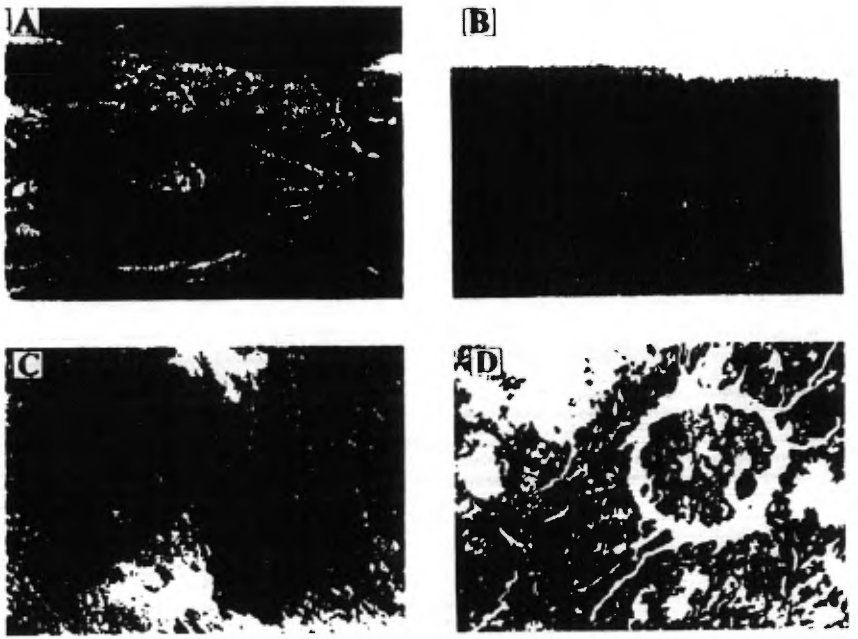


FIG. 5. Some examples of terrestrial complex impact craters. A. Oblique aerial photograph of Steinheim, Germany (3.8 km, 15.1 ± 1.0 Ma) with a central peak and flat floor. B. Oblique aerial photograph of Gosses Bluff, Australia (22 km, 142.5 ± 0.5 Ma), which has been heavily modified by erosion. The prominent ring of hills is 5 km in diameter and is an erosional remnant of a central peak within a much larger structure (see text for details). C. Shuttle photograph of the twin craters in Clearwater Lake, Canada (22 km and 32 km, respectively, 290 ± 20 Ma). A central peak is submerged in the East crater and a small central peak occurs within the ring of islands at the West crater. D. LANDSAT image of Manicouagan, Canada (100 km, 214 ± 1 Ma). The original rim lay outside the annular lake, which is 65 km in diameter.

diameter these are: central peak craters (e.g., Steinheim, Germany), central peak basins with both a central peak and a surrounding ring (e.g., Red Wing Creek, USA; West Clearwater, Canada (Fig. 5C)), peak ring basins with only a ring (e.g., Puchezh-Katunki, Russia), and possibly multi-ring basins with several rings (e.g., Popigay, Russia).

Geologic observations at complex craters indicate that the central structures consist of shocked target rocks stratigraphically uplifted to their present position. The surrounding annular depression is partially filled by allochthonous target material, in the form of polymict breccia and/or impact melt rocks (Fig. 6). The volume of impact melt rocks can be significant. For example, the present thickness of the annular impact melt sheet at Manicouagan (Fig. 5D) reaches ca. 250 m over an area of 2000 km^2, with an estimated original volume of approximately 1000 km^3 (Phinney and Simonds, 1977). In the case of Sudbury, recent analyses suggest that the so-called Igneous Complex is part of a massive impact melt sheet (Faggart et al., 1985; Stöffler et al., 1989; Lakomy, 1990) with an original volume of at least 8000 km^3 (Grieve et al., 1991). This allochthonous material—breccia or melt rock or a mixture—overlies the target rocks of the true crater floor, which rises through a series of faults to form the structurally complex rim area (Fig. 6).

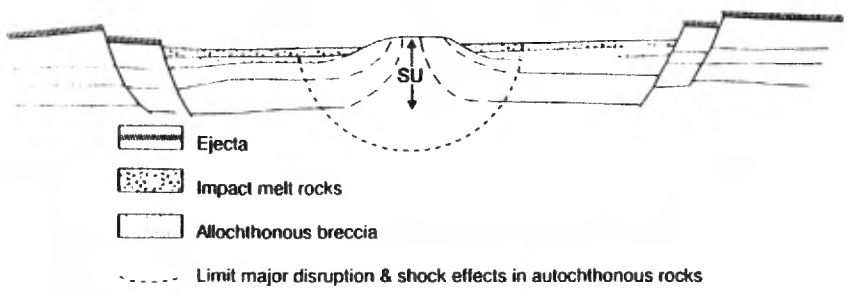


FIG. 6. Schematic cross-section of a complex impact crater with a central uplift. Note the limitation of major disruption to the central area and the structural uplift (SU) of originally deeper target lithologies to the surface in the central uplift. See text for more details.

Observations at terrestrial complex craters, particularly those in sedimentary targets, on such parameters as the pre- and post-impact position of various units indicate that the transient cavity has approximately the same relative dimensions as at simple craters (Fig. 7) (Grieve et al., 1981). The modification or collapse of the transient cavity, however, is considerably more severe in complex craters, resulting in much shallower d:D ratios for the final crater. While transient cavity collapse at simple craters involves only the cavity walls, transient cavity modification at complex craters involves a volume of target material beyond the limit of the transient cavity diameter. It represents a volume of target material that, during the cratering process, has a range of material strengths from essentially zero in the center and increasing outward. A volume outside the transient cavity collapses to form an annular depression and, at the point where the stresses in this volume no longer exceed the dynamic tensile strength of the target rocks, an outer rim (Fig. 7). The differences in the transition diameters of complex forms between crystalline and weaker sedimentary targets indicate that the intrinsic strength of the target rock plays a role in the final form. This effect of material strength is reflected in the final morphology of complex craters. For example, complex craters are shallower in sedimentary (weaker) targets than in crystalline (stronger) targets. The relationships for apparent depth are:

$$d_a = 0.12D^{0.30} \text{ and}$$

$$d_a = 0.15D^{0.43},$$

for sedimentary and crystalline targets, respectively. These relationships are based on data from relatively few complex craters and are subject to considerable uncertainty, particularly as erosion affects d:D ratios more severely at the relatively shallower complex craters than at simple craters. We do, however, have some confidence in the general form of the relationships, as $d \propto D^{0.3}$ is the form of d:D ratios for complex craters on the moon (Pike, 1977).

Stratigraphic observations and determinations of the level of shock (ca. 30–40 GPa) (Robertson and Grieve, 1977; Stöffler et al., 1988) in the target rocks of the central structures at complex craters indicate that they correspond to the uplifted floor of the transient cavity. The current consensus is that uplift occurs initially under highly dynamic conditions, when the target rocks of the central area are behaving hydrodynamically with essentially no strength (Fig. 7). Some indication of the status of knowledge of cratering mechanics at complex impact craters can be found in papers in Schultz and Merrill (1981) and in Melosh (1989), although many of the details are the subject of current study (e.g., Ivanov, 1994).

In some cases, differential erosion has removed essentially all topographic expression of complex craters except for a residual central positive structure. For example, geological and geophysical data indicate that the ca. 140 Ma Gosses Bluff crater, Australia, is 22 km in diameter. The present surface topographic expression of the crater, however, is restricted to a central annular ridge 5–6 km in diameter rising roughly 200 m above the surrounding plain (Fig. 5B). This annular ridge represents the remnant core of erosionally resistant Devonian sandstone in the original central uplift. Thus, the present form of Gosses Bluff owes as much to erosion and lithology as to the original complex crater morphology. The fact that eroded terrestrial complex impact craters can appear ultimately as positive topographic features with uplifted lithologies has contributed historically to the reluctance of some workers to accept the impact origin of certain structures.

The amount of structural uplift (SU) in the central structures at complex craters can be measured, where the subsurface stratigraphy is known. The relationship is:

$$SU = 0.06D^{1.1},$$

where SU is the amount of stratigraphic uplift undergone by the deepest lithology now uplifted and exposed at the surface in the center (Grieve et al., 1981). Therefore, for the larger complex craters, this uplift may involve a good portion of the upper crust. Drilling and geophysical data indicate, however, that complex impact craters are inherently near-surface features, with residual structural disturbance associated with the crater dying out at depths of ~ 1.5–2.0 SU (Fig. 6).

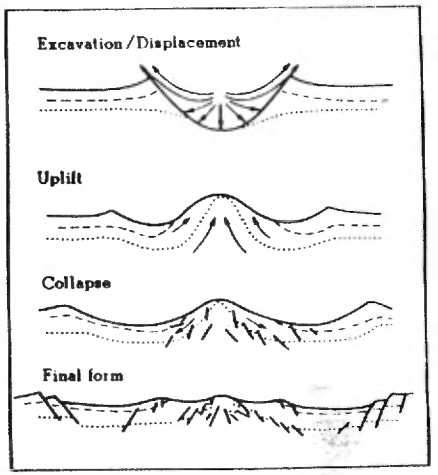


FIG. 7. Schematic diagram (simplified) of the formation of a complex impact crater. An initial transient cavity is formed in much the same manner as at simple craters. However, the downward displacements are not locked in and the central area rebounds upwards, only to collapse, forming central uplifted structure(s), surrounded by an annular trough and a structurally complex rim area.

Geology

In contrast to planetary impact craters, which are recognized by their morphology, terrestrial impact craters are recognized primarily by the geologic effects of impact. Although an obvious crater form with the appropriate morphometric relations is an excellent indicator of an impact origin, a near pristine form is restricted in the terrestrial environment to impact craters that are either very young or were buried and protected from erosion very soon after formation. In addition to the modifying effects of erosion on morphology, the highly active terrestrial geologic environment results in a number of processes that can produce circular or quasi-circular geologic features. Thus, the principal criterion for the recognition of terrestrial impact craters is the occurrence of shock metamorphic effects in the target rocks.

Shock metamorphism is the progressive breakdown in the structural order of minerals and rocks due to the passage of a high-pressure shock wave (French and Short, 1968). The physical conditions are a function of the initial impact parameters: projectile and target rock type and impact velocity, which determine peak pressures at impact, and projectile size, which determines the absolute radial distance at which particular shock metamorphic effects occur. Minimum shock pressures required for the onset of diagnostic shock effects in silicates are $\geq$ 5–10 GPa and maximum shock pressures reach $>$ 1000 GPa in impact events. Post-shock temperatures accompanying pressures $\geq$ 60 GPa and $\geq$ 120 GPa reach above the melting and vaporization points, respectively, of silicate rocks (Fig. 8) (Ahrens and O'Keefe, 1977; Melosh, 1989).

Sub-solidus shock metamorphic effects

The only known diagnostic megascopic indicator of shock metamorphism is the occurrence of shatter cones (Dietz, 1968). These conical striated fracture surfaces are best developed in fine-grained, structurally isotropic lithologies, such as carbonates and quartzites (Fig. 9A).

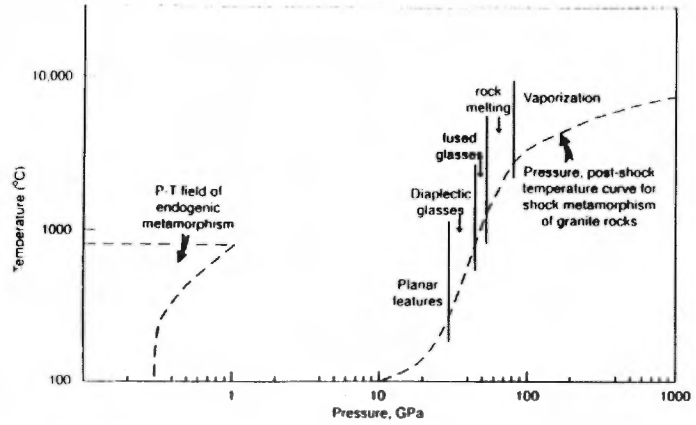


FIG. 8. Log pressure–log temperature plot of fields of shock metamorphism and endogenic metamorphism. The onset pressures and associated temperatures for various shock metamorphic effects in quartzo-feldspathic crystalline rocks are indicated.

They have, however, been noted in coarser-grained crystalline rocks, such as granites, but are less common and generally poorly developed (Dietz, 1972). Shatter cones develop at relatively low shock pressures (Roddy and Davis, 1977), but also have been found in rocks subjected to up to ca. 25 GPa (Milton, 1977). As a result, they are generally developed in the autochthonous rocks of the crater floor and are most often exposed in eroded central uplift structures of complex craters. Several studies (e.g., Manton, 1965; Milton, 1977) have indicated that when the beds containing shatter cones at such craters are rotated back to their pre-impact position, the majority of the apices of the shatter cones point to a central location, representing the point of impact or origin of the shock wave.

The most common shock metamorphic effect is the occurrence of microscopic so-called planar deformation features in tectosilicates, most commonly in quartz (Hörz, 1968). When fresh, the majority of these microscopic features in quartz are filled with glass (Engelhardt and Bertsch, 1969). At older impact structures, they are more commonly annealed and are manifest as linear chains of microscopic inclusions (Fig. 9B). Such features are called decorated planar deformation features (Robertson et al., 1968). Most studies of planar deformation features have focused on quartz, because of its resistance to alteration, its relatively simple crystal structure, and its widespread occurrence in terrestrial rocks. A recent, comprehensive review of shock metamorphism in quartz is given in Stöffler and Langehorst (1994). Planar deformation features, however, do occur in other minerals. Specific crystallographic orientations of planar deformation features are characteristic of successive grades of shock metamorphism (Robertson et al., 1968). Studies of the crystallographic orientation of planar deformation features in quartz from terrestrial impact structures and shock recovery experiments have established a classification scheme, whereby the number of sets of features, with specific and well-characterized orientations, has been related to threshold values of shock pressures in the range 7.5–16 GPa (Fig. 8) (Hörz, 1968; Robertson and Grieve, 1977; Stöffler and Langehorst, 1994).

Accompanying progressive planar-deformation-feature development with increasing shock pressure are parallel changes in optical properties, such as birefringence, refractive index, optical axial angle, etc. (Stöffler, 1972, 1974; Stöffler and Langehorst, 1994). With the progressive breakdown in mineral order, changes occur in X-ray properties, apparent as asterism and line broadening (Chao, 1968; Hörz and

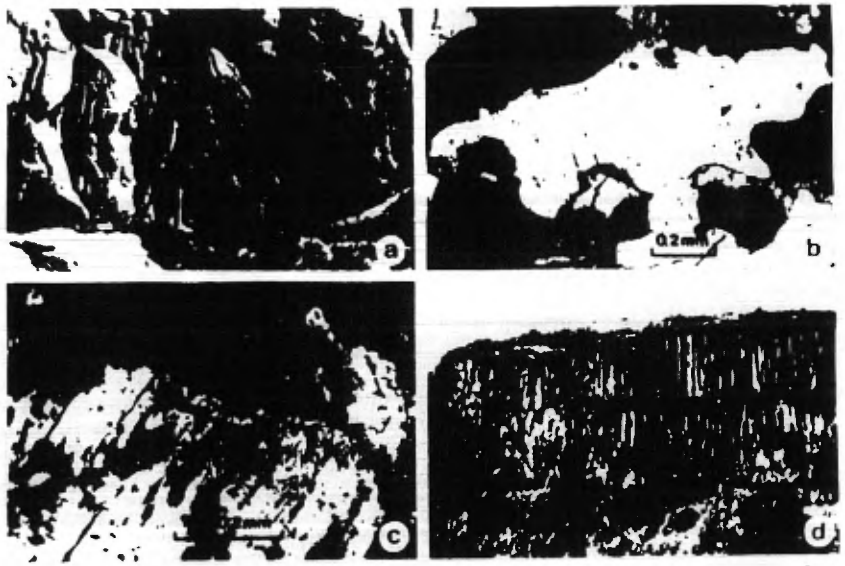


FIG. 9. Various shock metamorphic effects. A. Shatter cones in quartzite, Sudbury, Canada. B. Planar deformation features in quartz, Charlevoix, Canada. C. Partial development of diaplectic feldspar glass known as maskelynite (isotropic area), St. Martin, Canada. D. Erosional remnant of impact melt rocks lining the crater floor, Mistastin, Canada. Outcrop is roughly 80 m high.

Quaide, 1973); in infrared absorption spectra, apparent as bond-length stretching (Stöffler and Hornemann, 1972); and in density, apparent as reduced density (von Engelhardt and Bertsch, 1969).

At pressures in excess of ca. 30 GPa and ca. 40 GPa, shock-induced disorder is sufficient to render feldspar and quartz, respectively, to a glass (Fig. 9C). These are solid-state glasses with properties distinct from fusion glasses (Stöffler and Hornemann, 1972). They are referred to as diaplectic or thetomorphic glasses to distinguish them from fusion glasses. The term "maskelynite" is reserved for shock-induced solid state plagioclase glass (Bunch et al., 1967), which was first observed in the meteorite Shergotty (Tschermak, 1872). In addition to progressive structural disorder, shock also can generate metastable high pressure mineral polymorphs, e.g., stishovite and coesite from quartz (Chao, 1968) and diamond from graphite (Masaitis et al., 1972) have been documented at terrestrial craters.

Shock melting

Upon release from shock pressures above ca. 50 GPa, individual minerals begin to thermally decompose or melt (Stöffler, 1972, 1984), leading to the production of mixed mineral melts. Melting occurs because of the fact that not all the pressure-volume work done during shock compression is recovered on pressure release, which occurs adiabatically. This excess work is manifest as irreversible waste heat. Above ca. 60 GPa, the waste heat generated on shock decompression is sufficient to result in whole rock melting. The resulting impact melts have compositions characteristic of the target rocks and occur as glass bombs in crater ejecta (von Engelhardt, 1990), as glassy to crystalline lenses within the breccia fill, or as coherent annular sheets lining the floor of complex craters (Fig. 9D) (Grieve et al., 1977). When crystallized, the rocks of impact melt sheets have igneous textures but tend to be heavily charged with clastic debris towards their lower

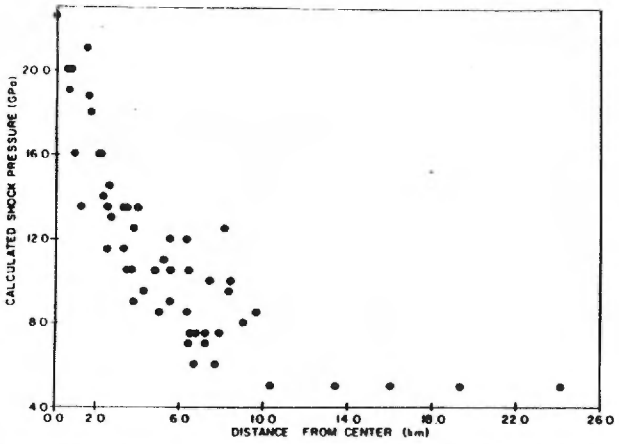


FIG. 10. Plot of recorded shock pressure, determined from the orientation of planar deformation features in quartz, with radial distance from the center of the Charlevoix crater, Canada (estimated original diameter of 55 km).

and upper contacts. They may, therefore, have a textural resemblance to endogenic igneous rocks. This is not surprising, as both represent crystallized silicate melts. In some cases, impact melt rocks were identified initially as volcanic lithologies by earlier workers. Impact melt rocks, however, can have an unusual chemistry as compared to endogenic volcanic rocks. Their chemistry is governed by melting of some mix of target rocks, as opposed to partial melting and/or fractional crystallization relationships in the case of endogenic igneous rocks. Isotopic analyses also indicate that such parameters as $^{87}Sr/^{86}Sr$ and $^{143}Nd/^{144}Nd$ ratios reflect the pre-existing target rocks, while isochron dating methods indicate much younger crystallization ages related to the impact event (e.g., Jahn et al., 1978; Faggart et al., 1985).

Enrichments above target rock levels in trace siderophile and platinum group elements, and sometimes Cr, have been identified in some impact melt rocks (Palme, 1982). These are due to an admixture of up to a few percent of meteoritic projectile material. In some cases, the relative abundances of the various trace elements in impact melt rocks have constrained the projectile responsible to the level of meteorite class. In other cases, no geochemical anomaly has been identified. This may be due to the inhomogeneous distribution of meteoritic material within the impact melt rocks and sampling variations (Palme et al., 1981) or to differentiated, non-siderophile-enriched projectiles, such as basaltic achondrites (Wolf et al., 1980), which have compositions essentially indistinguishable from terrestrial rocks.

Shock attenuation

Because of attenuation, diagnostic shock metamorphic effects in autochthonous rocks are not observed in the rim area of simple craters and are limited in complex craters to radial distances of ≤ 0.3 the final diameter (Robertson and Grieve, 1977). That is, they occur only in the central area of the true crater floor, i.e., at the base of the breccia lens in simple craters and in the central uplifted structure and immediately surrounding area at complex craters. They diminish in intensity with radial distance from the center of the crater (Fig. 10) and with depth. They also occur, of course, in allochthonous lithologies, such as breccias and melt rocks. Not all terrestrial craters have preserved the full spectrum of shock metamorphic effects. Deeply eroded craters have a reduced spectrum of effects, limited in autochthonous rocks to the lower grades of shock metamorphism.

Brecciation

Brecciation is ubiquitous at impact craters. A wide variety of breccias—from polymict breccias containing a wide range of shock metamorphosed clasts including impact melt (known as suevites) to monomict breccias—occur as allochthonous bodies within craters and as exterior ejecta, as dikes within the target rocks, and as parautochthonous bodies in the target rocks of the crater floor. There is evidence for multi-generations, with some breccias being formed during cavity excavation and others during cavity modification (Lambert, 1981; Müller-Mohr, 1992). Pseudotachylite also occurs at large impact structures in crystalline targets and was first described at the Vredefort structure, South Africa (Shand, 1916). Pseudotachylite and other types of breccias, however, also can occur as the result of endogenic geologic processes. They are, therefore, characteristic but not diagnostic of impact. The identification of shock metamorphic effects in the clasts in breccias is required before they can be categorically ascribed to impact.

Distribution in Space and Time

At present, there are over 140 known terrestrial impact craters (Grieve and Shoemaker, 1994). This number does not include the numerous small (<10 m) impact pits that appear to be associated with recent meteor showers. New discoveries are made at the rate of 3–5 impact craters per year, with major increases in the number of discoveries having taken place in the last 20 years in Australia and the former USSR. There also are a number of probable impact craters, which have several of the characteristics of known impact craters but lack definitive evidence such as the occurrence of shock metamorphic features. As more information becomes available on these structures, it is likely that some will acquire a confirmed status. The impact origin of all these stuctures, however, is not universally accepted and there are still a few geologists who have difficulty accepting the occurrence of terrestrial impact craters, preferring to ascribe their origin to various tectonic-cryptovolcanic processes (Nicolaysen and Ferguson, 1990).

Spatial distribution

The active terrestrial geologic environment serves to remove the evidence of impact cratering through erosion, burial, or tectonism. Thus, the known record is only a small sample of an originally larger population. This record is further biased as a result of these terrestrial processes and non-systematic search efforts. Concentrations of known craters occur on the cratonic areas of North America, Australia, Europe, and the western portion of the former USSR (Fig. 11). These are geologically stable areas with relatively low levels of erosion and tectonic activity. They also are areas where there have been active programs to search for and to study impact craters. The apparent deficit of known craters on other major cratonic blocks, such as Africa and South America (Fig. 11), reflects recognition difficulties resulting from the generally lower level of knowledge of the geology and geophysics of these areas. Remotely sensed data, such as orbital imagery, have helped identify possible impact craters in these areas, but ultimate confirmation of an impact origin requires ground-based geologic observations. Approximately 30% of the known terrestrial impact structures are buried. They were discovered initially as geophysical anomalies and later drilled for commercial or scientific purposes.

The incompleteness of the known record is exemplified by considering the marine record of impact. Only one confirmed impact crater is currently known in the world's oceans. This is the 45-km-diameter, 50-m.y. Montagnais structure on the continental shelf off Nova Scotia, Canada (Fig. 11) (Jansa et al., 1989). Montagnais was discovered and drilled in the course of hydrocarbon exploration. Another structure, Mjølnir (39 km in diameter), has been defined in seismic data in the Barents Sea (Gudlaugsson, 1993). It has not been drilled to date and has not been confirmed as an impact structure. No impact craters are known in the true oceanic crust of the ocean basins. This reflects lack of knowledge of the detailed topography and geology of the world's ocean basins.

Temporal distribution

There is a clear bias in the ages of terrestrial impact craters. Over 50% of the known craters



FIG. 11. Spatial distribution of currently known terrestrial impact craters (see text for details regarding its significance).

were formed more recently than 200 Ma. As surface features, this reflects the ability of erosion to remove the topographic and geologic expression of impact craters. Some of the recognized craters, however, are exhumed structures, having been buried by post-impact sediments and only relatively recently re-exposed at the surface. If observations are restricted to large, young craters on the well-searched cratons, then the terrestrial record indicates a cratering rate of $5.4 \pm 2.7 \times 10^{-15}$ km^2 a^{-1} for $D \geq 20$ km (Grieve, 1984). The large uncertainties attached to this estimate reflect concerns over completeness of search and crater recognition. This rate is very similar to that calculated from astronomical observations by Shoemaker et al. (1990) for the present rate of impact by asteroids and comets and is equivalent to 4 ± 2 impact structures with $D \geq 20$ km being formed on the land surface of the earth every 5 million years.

General Character of Economic Deposits

The location and origin of economic deposits in impact structures are controlled by several factors related to the impact process and the specific nature of the target. As impact structures can occur on any type of target rock and in any paleoenvironment, the resultant economic deposits are highly varied (Tables 1 and 2). In the simplest terms, the types of deposits can be classified according to their time of formation and are discussed below under the classification: progenetic, syngenetic, and epigenetic (Table 1). Progenetic economic deposits are those that originated prior to the impact event by purely terrestrial concentration mechanisms. The effect of the impact event has been to spatially redistribute, with respect to the surrounding area, the lithologies containing these deposits and, in some cases, bring them to a surface or near-surface position, where they can be exploited. Syngenetic deposits are those that originated during the impact event, or immediately afterwards. They owe their origin to the energy deposition of the impact event in the local environment, resulting in phase changes and melting. Epigenetic deposits result from hydrothermal alteration, the formation of an enclosed topographic basin with restricted sedimentation, or the long-term flow of fluids into the structural trap formed by the impact structure.

There have been suggestions that deep-seated faults associated with ancient large impact structures have acted as controls for the endogenic deposition of various metals from depth

TABLE 1. Genetic Groups of Economic Deposits

Genetic group	Principal mode of origin	Types of known deposits
Progenetic	Brecciation	Earth silica
	Structural displacement	Iron, uranium, gold
Syngenetic	Phase transitions	Impact diamond
	Crustal melting	Cu, Ni, PGM[1], glass
Epigenetic	Hydrothermal activity	Lead, zinc, uranium, pyrite, zeolite, agate
	Sedimentation	Placer diamond and tektites
	Chemical and biochemical sedimentation	Zeolite, bentonite, evaporites, oil shale, diatomite, lignite, amber, calcium phosphate
	Underground flow	Oil, natural gas, fresh and mineralized water

[1]PGM = platinum-group metals.

(Zeylick and Seytmuratova, 1974; Saul, 1978) and that massive basin-forming impact events, which must have occurred early in earth history, affected subsequent magmatic and hydrothermal activity to produce distinct metallogenic provinces in areas of the earth's crust (Zeylick and Seytmuratova, 1974; Saul, 1978; Witschard, 1984). These suggestions presently are speculative. As no critical evidence for the occurrence of impact, beyond general statements regarding "circular structures," has been presented, they are beyond the scope of this paper.

Progenetic Deposits

Progenetic economic deposits in impact craters include iron, uranium, gold, and other minerals (Tables 1 and 2). In many cases, the deposits are relatively small. Here, we consider only the larger and more active deposits.

Iron at Ternovka

Iron and uranium ores occur in the basement rocks of the crater floor and in impact breccias at the Ternovka structure, Ukraine (Nikolsky et al., 1981, 1982). The structure is 375 ± 25 m.y. (Nikolskiy, 1991) and was formed in the Lower Proterozoic fold belt of the Krivoy Rog iron ore basin. It is a highly eroded complex crater. The parautochthonous rocks of the crater floor are exposed and there is a central uplift and annular trough (Fig. 12). The central uplift is, in part, brecciated and injected by dikes of impact melt rock up to 20 m wide. The annular trough contains remnants of allochthonous breccia with patches and lenses of suevite. The present diameter of the structure is roughly 10–11 km (Val'ter, 1988) and its original diameter may have been 15–18 km.

The iron ores at Ternovka have been exploited for over 50 years. Originally, the ores were the result of hydrothermal and metasomatic action, which occurred during the Lower Proterozoic, on ferruginous quartzites (jaspilites) and some other lithologies, producing zones of albitites, aegirinites, and amphibole-magnetite and carbonate-hematite rocks (along with uranium mineralization), which now are exposed in the crater floor. Post-impact hydrothermal alteration led to the remobilization of some of the uranium mineralization and the formation of veins of pitchblende. The production of uranium ceased in 1967, but iron ore is still extracted from two main open pits—Annovskiy and Pervomaysk. The total reserves at the Pervomaysk open pit are estimated at 74 million metric tons, with additional reserves of lower-grade deposits estimated at approximately 675 million tons. As a result of brecciation and displacement, blocks of iron ore are mixed with barren blocks. These blocks are up to hundreds of meters in diameter and are "rootless," having been rotated and displaced from their pre-impact positions by hundreds of meters. This displacement and mixing of lithologies causes difficulties in operation and evaluating the reserves. On the other hand, impact-induced fracturing aids in extraction and processing.

TABLE 2. Deposits and/or Indications of Economic Resources in Impact Structures

Structure	Location (Lat., Long)	Diameter, km	Economic material	Genetic type of economic deposit
[1]Ames, USA	36°15′ N; 98°10′ W	16	Oil, natural gas	Epigenetic
[1]Avak, USA	71°15′ N; 156°38′ W	12	Natural gas	Epigenetic
[1]Barringer, USA	35°02′ N; 111°01′ W	1.2	Earth silica	Progenetic
Beyenchime-Salaatin, Russia	71°50′ N; 123°30′ W	8	Pyrite	Epigenetic
Boltysh, Ukraine	48°45′ N; 32°10′ W	24	Oil shale	Epigenetic
[1]Carswell, Canada	58°27′ N; 109°30′ W	39	Uranium	Progenetic
[1]Charlevoix, Canada	47°32′ N; 70°18′ W	54	Ilmenite	Progenetic
[1]Crooked Creek, USA	37°50′ N; 91°23′ W	7	Lead, zinc	Epigenetic
Decaturville, USA	37°54′ N; 92°43′ W	6	Lead, zinc	Epigenetic
Ilyinets, Ukraine	49°06′ N; 29°12′ E	4.5	Agate	Epigenetic
Kaluga, Russia	54°30′ N; 36°15′ W	15	Mineral water	Epigenetic
Kara, Russia	69°05′ N; 64°18′ E	65	Diamond, zinc	Syngenetic, epigenetic
Logoisk, Belarus	54°12′ N; 27°48′ E	17	Amber, calcium phosphate	Epigenetic
[1]Lonar, India	19°59′ N; 76°31′ E	1.8	Various salts	Epigenetic
[1]Marquez, USA	31°17′ N; 96°18′ W	22	Oil, natural gas	Epigenetic
Obolon, Ukraine	49°30′ N; 32°55′ E	15	Oil shale	Epigenetic
Popigay, Russia	71°30′ N; 111°00′ E	100	Diamond	Syngenetic
Puchezh-Katunki, Russia	57°00′ N; 43°35′ E	80	Diamond, zeolite	Syngenetic, epigenetic
Ragozinka, Russia	58°18′ N; 62°00′ E	9	Diatomite	Epigenetic
[1]Red Wing, USA	47°36′ N; 103°33′ W	9	Oil, natural gas	Epigenetic
[1]Ries, Germany	48°53′ N; 10°37′ E	24	Lignite, bentonite, moldavites	Epigenetic, syngenetic
[1]Rotmistrovka, Ukraine	49°00′ N; 32°00′ E	2.7	Oil shale	Epigenetic
[1]Saint Martin, Canada	51°47′ N; 98°32′ W	40	Gypsum, anhydrite	Epigenetic
[1]Saltpan, South Africa	25°24′ S; 28°50′ E	1.1	Various salts	Epigenetic
Serpent Mound, USA	39°02′ N; 83°24′ W	8	Lead, zinc	Epigenetic
[1]Siljan, Sweden	61°02′ N; 14°52′ E	55	Lead, zinc, oil	Epigenetic
Slate Islands, Canada	48°40′ N; 87°00′ W	30	Gold	Progenetic
[1]Steen River, Canada	59°31′ N; 117°37′ W	25	Oil	Epigenetic
[1]Sudbury, Canada	46°36′ N; 81°11′ W	250	Copper, nickel, PGM	Syngenetic
[1]Ternovka, Ukraine	48°01′ N; 33°05′ E	12	Iron, uranium	Progenetic
Tookoonooka, Australia	27°00′ S; 143°00′ E	55	Oil	Epigenetic
Ust'-Kara, Russia	69°18′ N; 65°18′ E	25	Diamond	Syngenetic
Vredefort, South Africa	27°00′ S; 27°30′ E	300	Gold, uranium	Progenetic
Zapadnaya, Ukraine	49°44′ N; 29°00′ E	4	Diamond	Syngenetic
[1]Zhamanshin, Kazakhstan	48°24′ N; 60°58′ E	13.5	Bauxite, impact glass	Progenetic, syngenetic

[1]Resources exploited currently or in the past. Above listing does not include structures that are a source of fresh water or various building materials, or are used as hydroelectric reservoirs.

FIG. 12. Geological sketch map of the floor of the Ternovka crater. Open pits, from which iron ore is extracted, are indicated.

Uranium at Carswell

Uranium ores also occur at the Carswell structure, which is located in northern Saskatchewan, Canada, approximately 120 km south of Uranium City. Carswell is barely visible in LANDSAT imagery as a vague circular feature, corresponding to the outcrop of ridges of the dolomites of the Carswell Formation. This ring is ~ 39 km in outer diameter and generally is quoted as the diameter of the structure. There is an annular trough, which is about 5 km wide and rises to a core, roughly 20 km in diameter, of metamorphic basement (Fig. 13). Essentially no crater-filling materials remain, beyond allochthonous dike-like and other bodies of breccia and impact melt rock. The Carswell impact structure has been eroded to the floor of the original crater, although the impact structure is only 115 ± 10 m.y. (Bottomley et al., 1990). The original form cannot be determined beyond classifying it as a complex structure. Similarly, the original diameter is poorly constrained. By analogy with other complex structures—e.g., Charlevoix (Rondot, 1972), Manicouagan (Grieve and Head, 1983), Siljan, Sweden (Rondot, 1975; Grieve, 1988) with preserved inliers forming a ring of down dropped lithologies, the original diameter of the

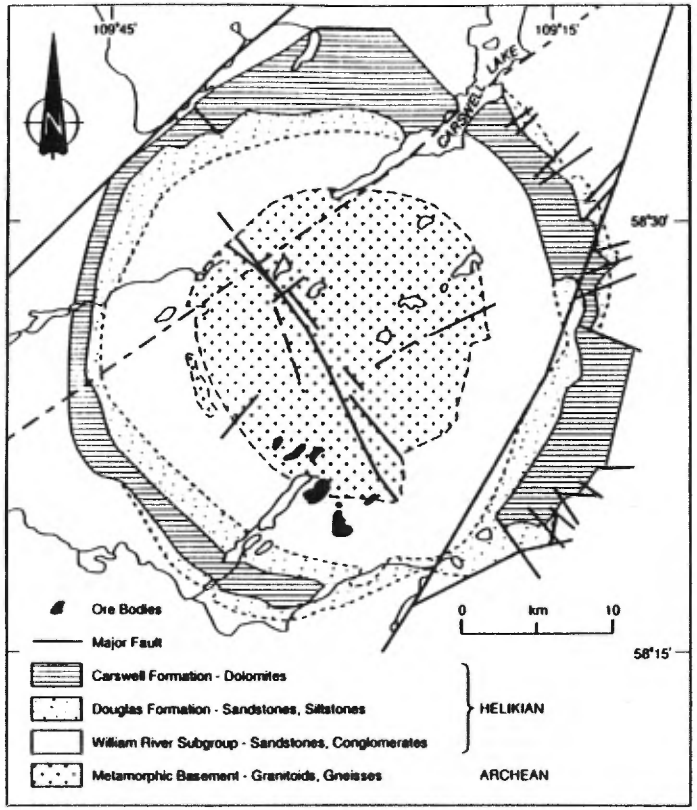


FIG. 13. Geological sketch map of the Carswell crater. Locations of known uranium orebodies are indicated.

Carswell structure may have been in the 50–55 km range.

The basement core consists of mixed feldspathic and mafic gneisses of the Earl River Complex, overlain by the more aluminous Peter River gneiss. Details of their mineralogy and chemistry can be found in Herring (1976), Harper (1982), Bell et al. (1985), and Pagel and Svab (1985). The basement core is believed to have been uplifted at least 2 km (Harper, 1982). Surrounding the core are units of the unmetamorphosed Athabasca Group: sandstones and conglomerates of the William River Subgroup, sandstones and siltstones of the Douglas Formation, and dolomites of the Carswell Formation. The inner contact with the basement core is, in places, faulted and truncated and offset by radial faults. The outer contact of the Carswell Formation also is characterized by arcuate faulting, drag folding, and local overturning of beds, as well as offsets by radial faults (Fig. 13). There also are a number of regional faults unrelated to the structure. The Carswell and Douglas formations are the uppermost units of the Athabasca Group. Their outcrop is unique to the area and they owe their preservation to having been downfaulted at least 1 km to their present position (Harper, 1982; Tona et al., 1985).

Uranium mineralization is concentrated along the south to southwest contact between the basement core and the Williams River Subgroup, with an estimated 46,500 metric tons of uranium originally being present in the currently known ore deposits (Harper, 1982; written communication, 1994). Mineralization occurs in both the basement core and the Williams River Subgroup (Fig. 13). The original mineralization is believed to reflect regolith development under tropical lateritic weathering of the basement prior to deposition of the Athabasca Group. The main exploited mineralization resulted from a hydrothermal event at ~ 1100 ± 50 Ma, which produced a uraninite-polymetallic sulfide assemblage. Variations in the mineralogy of the ores are related to the type of host rock. Additional periods of remobilization also occurred, producing pitchblende and a number of separate parageneses for the ores. Details of the ore deposits and their origin can be found in papers in Lainé et al. (1985). Like Ternovka, the relationship between the ores and the Carswell impact structure is not a genetic one; rather, it was the physical uplift of the basement core by at least 2 km, during the formation of a complex crater, that brought the ores to their present high levels, where they could be recognized and exploited. In addition to mechanical mixing due to brecciation, minor remobilization of ores occurred, following the impact with the production of a coffinite-sulfide mineralization in the breccias (Ruhlmann, 1985).

Gold and Uranium of Vredefort

Gold has been mined intermittently in the collar rocks surrounding the so-called Vredefort Dome, with the main mining occurring in an area known as the Venterskroon or Rooderand Goldfield (Holland et al., 1990). The origin of Vredefort has been controversial (e.g., see Nicolaysen and Reimold, 1990), with several workers in S. Africa attributing a cryptoexplosion origin to the structure. The structure is generally taken to consist of an uplifted central core of predominantly Archean granites roughly 44 km in diameter, a collar of steeply dipping to overturned Proterozoic sedimentary and volcanic rocks of the Witwatersrand and Ventersdorp supergroups approximately 18 km wide, and an outer broad synclinorium of gently dipping Proterozoic sedimentary and volcanic rocks of the Transvaal sequence ~ 28 km wide. The southeastern portion is covered by younger sandstones and shales of the Karoo sequence (Fig. 14). The general circular form with an uplifted central core, the occurrence of stishovite and coesite, and planar deformation features in quartz and shatter cones all have been presented as evidence that the Vredefort structure is the eroded remnant of a very large, complex impact structure (e.g., Dietz, 1961; Hargraves, 1961; Carter, 1965, 1968; Manton, 1965; Martini, 1978, 1991). The impact interpretation has been challenged (Hart et al., 1981; Schreyer, 1983; Winter, 1986) and even the existence of bona fide shock metamorphic features has been questioned (Lilly, 1981; Simpson, 1981; Reimold, 1990). The problem at Vredefort is that, as the center of the structure is approached, the planar deformation features in quartz die out (as opposed to increasing in number and occurring in differing orientations—representing increasing levels of recorded shock pressure—as at other large complex impact structures) (e.g., Fig. 10). This unusual behavior is attributed to increasing levels of recrystallization of quartz as the center is approached (Grieve et al., 1990). Another unusual feature is that the planar deformation features are dominated by so-called basal features, which are the planar deformation features produced at the lowest pressures (>7 GPa) (Robertson and Grieve, 1977; Stöffler and Langehorst, 1994).

Recent work on planar deformation features in quartz using a transmission electron microscope (TEM) has indicated that there is a fundamental difference in the nature of basal planar deformation features and other orientations; namely, the basal features are the result of mechanical Brazil twins, whereas the others, when fresh, are lamellae of a mixture of silica glass and crystallites (Goltrant et al., 1992; Stöffler and Langehorst, 1994). This fundamental difference results in quite different responses to thermal annealing. In the case of Vredefort, TEM investigations have confirmed the presence of basal planar deformation features, coesite, stishovite, and evidence for high temperature annealing (White, 1993; Leroux et al., 1994). These recent developments, plus other ongoing work at Vredefort, have been sufficient to convince some of the previous antagonists that Vredefort is the site of a major impact event that occurred ~ 2 Ga (e.g., Hart et al., 1991; Gibson et al., 1994). The metamor-

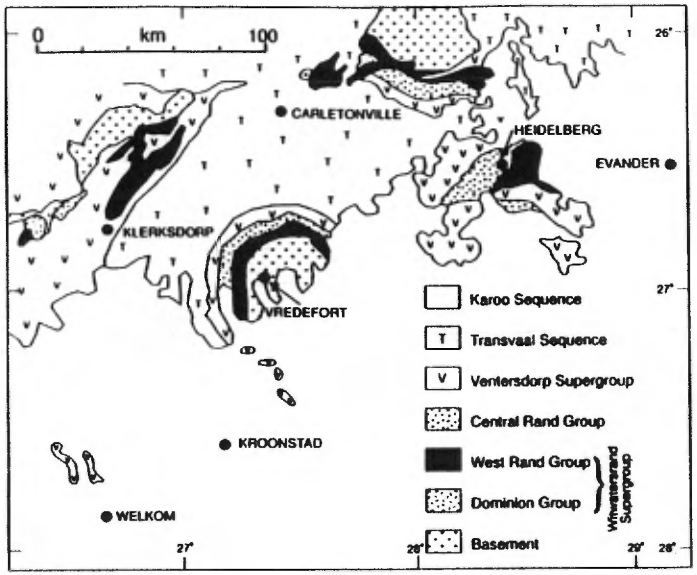


FIG. 14. Geological sketch map of the area including the Vredefort structure.

phism is the result of the intrinsic heat of the rocks of the core at their original depth plus some post-shock heating (Grieve et al., 1990; Hart et al., 1991; Martini, 1992; Gibson et al., 1994). Recent work also has confirmed that a roughly 36-km section of the crust is exposed at Vredefort and that the entire structure has been tilted to the northwest by post-impact tectonic forces (Hart et al., 1991). In addition, Re-Os isotopics on the so-called bronzite granophyre, which occurs in dike-like bodies at Vredefort and has been interpreted as the remnants of the impact melt rocks at Vredefort (French and Nielsen, 1990), indicate an admixture of meteoritic material (Koeberl, oral communication, 1994).

With a greater understanding of Vredefort, and its somewhat complex geologic history, has come a reassessment of its original size. Previous estimates for the original diameter were on the order of approximately 140 km (Grieve, 1991). They were based on the thickness of the uplifted section exposed in the collar rocks and did not take account of the ~ 22 km crustal section exposed in the central core (Hart et al., 1991). If the entire crustal section exposed to the center is roughly 36 km, then the relationship for the amount of structural uplift in the center of complex impact craters given earlier would indicate that the original diameter of the Vredefort impact crater was on the order of 335 km. Using arguments involving the relative spatial distribution of shock metamorphic features and downfaulted outliers in the annulus surrounding the central core, developed originally to reconstruct the dimensions of the Sudbury Structure, Therriault et al. (1993) estimated that the rim of the transient cavity at Vredefort was ~ 100 km in diameter, at the present level of erosion. When the amount of erosion (~ 8 km) is taken into account (Therriault et al., 1993) and the transient cavity is scaled to final crater rim, the original rim diameter may have been on the order of 300 km. If the center of the surrounding Potchefstroom synclinorium is taken as the beginning of the central uplifted area, the central uplift area has a diameter of ca. 75 km (Fig. 15). From the relationship of diameter of central uplifted area to crater diameter illustrated in Grieve (1991), the original rim diameter at Vredefort is again estimated to be ca. 300 km, although the relationship shows considerable scatter.

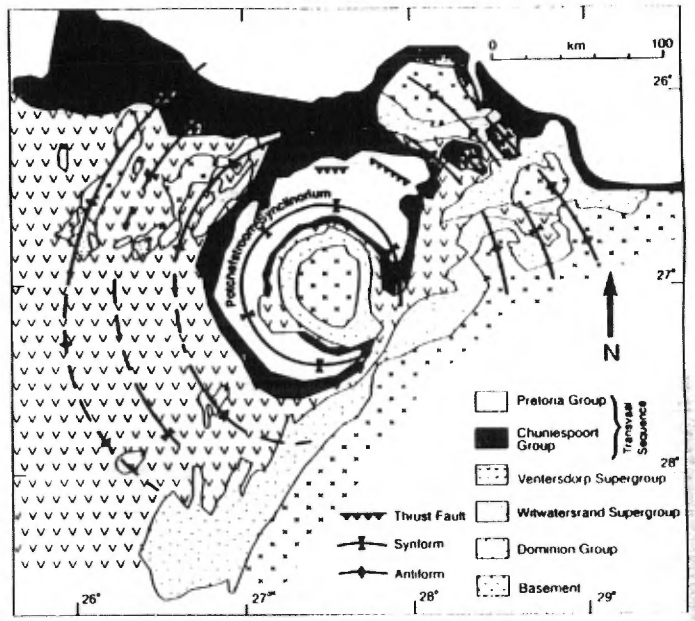


FIG. 15. Geological sketch map of the Vredefort structure, with the partially overlying Karoo Sequence removed. Indicated are the series of concentric antiform and synform structures surrounding and related to Vredefort. Source: After McCarthy et al. (1990).

With an estimated original diameter of roughly 300 km and an age of about 2.0 Ga (Walraven et al., 1990; Spray et al., 1994), the Vredefort structure encompasses a series of post-Transvaal anticlinal and synclinal structures surrounding the central core, identified by Simpson (1977) and McCarthy et al. (1990) as being related to Vredefort (Fig. 15). More importantly, McCarthy et al. (1990) also note that if it were not for the preservation effects of these structures concentric to the core of the Vredefort structure, much of the Central Rand Group would have been eroded from the area (Fig. 16). The major gold deposits of Witwatersrand Basin occur in an ~ 180° arc at the outer edge of the outcrop of the Central Rand Group (Fig. 17). The situation differs from that at, for example, Carswell, where the ores are exposed because of uplift in the center. At Vredefort, the ores are preserved because they have been downdropped within the annular trough exterior to the central uplifted core of a very large, probably originally multi-ringed, impact structure.

The gold fields of the Witwatersrand Basin are a geologic wonder, having produced over half the gold ever mined! They have been mined for over 100 years, with total production, as of 1985, being over 40,500 metric tons and a value on the order of $50 billion (Pretorius, 1986a). Associated with the gold is uranium, with total production, as of 1985, of over 130,500 metric tons, with a value on the order of $4 billion (Pretorius, 1986a). Current revenues from mining of gold and uranium are of the order of $7 billion p.a. There is a massive literature on the ores of the Witwatersrand Basin and it is not our intention to review it here (e.g., see Pretorius, 1976, 1986b and references therein). The uranium is in the form of uranite and is detrital in origin, with times of formation of ~ 3 Ga compared to ~ 2.8 Ga for the lowest section

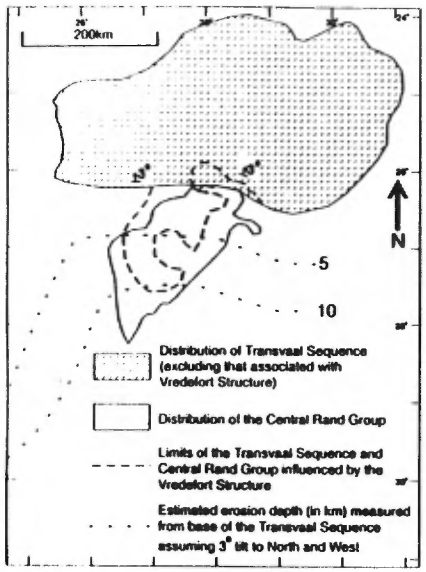


FIG. 16. Distribution of Transvaal Sequence and Central Rand Group in the area of Vredefort. Shown is the area of the Central Rand influenced and protected from erosion by Vredefort-associated structures. Also shown are estimated depths of erosion of Central Rand, in the absence of Vredefort. Source: After McCarthy et al. (1990).

of the Witwatersrand sequence. Its source is Archean granites, which intruded nearby granite-greenstone terrane of the southern Kaapval craton (Robb et al., 1990). There are indications of lead loss and redistribution of uranium at ~ 2 Ga, indicating a thermal event (Rundle and Snelling, 1977; Giusti et al., 1986), which may be related to the Vredefort event (Frimmel et al., 1993). Alternatively, it may be the result of hydrothermal activity related to magmatic activity associated with the emplacement of the Bushveld Igneous Complex, which also occurred ~ 2 Ga. It has been suggested that the Bushveld Igneous Complex results from a number of major impacts in close spatial and temporal association by some workers (e.g., Hamilton, 1970; Rhodes, 1975; Elston and Twist, 1986; Elston, 1992) but, at present, there is no documented evidence of the occurrence of shock metamorphic effects at the Bushveld (French, 1990).

The primary source of the gold is generally believed to be the mafic igneous rocks associated with the same granite-greenstone terrane (Pretorius, 1976). It also has been suggested, however, that the gold is primarily related to the introduction of hydrothermal fluids (Graton, 1930) or magmatic fluids (Davidson, 1955). Recent analyses of the role of fluids in the Witwatersrand Basin do not support these hypotheses (Phillips et al., 1990), although partial remobilization may have occurred and may be related to hydrothermal activity as a result of the Vredefort event (Reimold, 1994). The main gold deposits occur in what are considered to be arenaceous fluvial fans or fan deltas formed at the interface of a relatively short fluvial system and a shallow-water inland sea. The fans formed on the edge of the basin, which was bounded largely by strike faults in the north and west (Stanistreet et al., 1986). McCarthy et al. (1986) note a series of faults that postdate these structures, causing considerable structural complexity. Foremost of these faults is the Master Bedding Plane Fault, which is extensively developed in the mines of Carletonville area (Fig. 17). The fault appears to have two phases of movement: an initial movement that is outward with respect to the Vredefort core, followed by subsequent retraction. It is tempting to relate such movements to the initial outward and later inward movements associated with the formation of a complex crater.

With an original diameter of 300 km, all the pseudotachylite occurrences within the Witwatersrand Basin, which are widespread but are concentrated in the collar rocks surrounding the core and the northern and northwestern portions of the Basin, especially in the Carletonville and Klerksdorp gold fields (Fig. 17) (Killick and Reimold, 1990), now lie within the original crater rim. These pseudotachylites in the northern and northwestern portions are associated with normal and bedding plane faults and would have been, in fact, in the area of the original rim area. Field relations indicate that there are multiple generations of pseudotachylite but similar relations occur at Sudbury, with the so-called Sudbury breccias and with dike breccias in other impact structures (Lambert, 1981). These relations merely indicate generation during different phases of the cratering event. Claims that $^{40}Ar/^{39}Ar$ dating

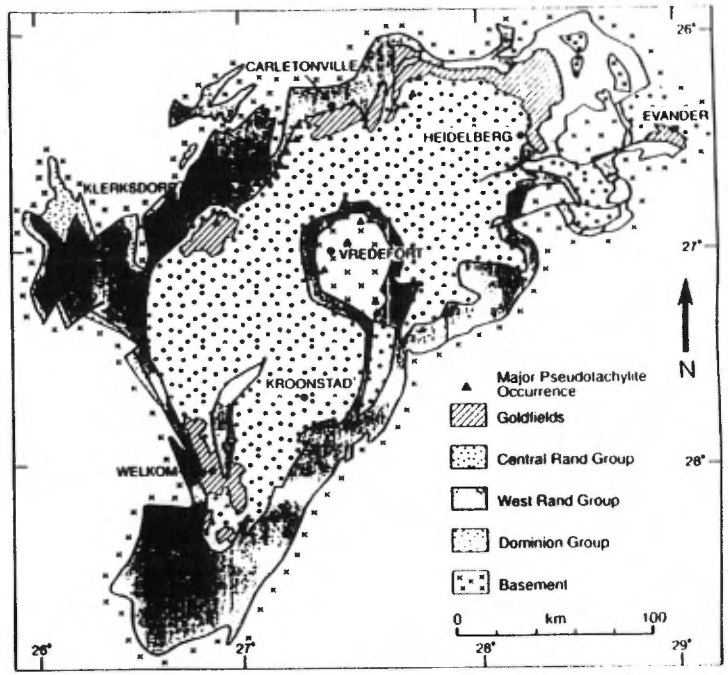


FIG. 17. Location of major gold fields of the Witwatersrand Basin. Note the majority of the gold fields occur within the area protected from erosion by Vredefort-related structures (Fig. 16). Also shown are the major pseudotachylite occurrences related to Vredefort. Source: Modified from Myers et al. (1990).

shows a range of ages for pseudotachylites from the core and collar rocks at Vredefort from ~ 2.0 Ga to ~ 1.1 Ga (Reimold et al., 1992) have been disproved by recent laser $^{40}Ar/^{39}Ar$ dating, which indicates some resetting on the edges but ~ 2.0 Ga ages in the center of the pseudotachylite veins (Spray et al., 1994). This latter age is that of the dikes of granophyre in the basement core (Walraven et al., 1990), which as the vestigal roots of the impact melt sheet is taken as the age of the Vredefort impact. The pseudotachylites from the north of the Witwatersrand basin around Johannesburg also have $^{40}Ar/^{39}Ar$ ages indistinguishable from 2.0 Ga (Trieloff et al., 1992), further strengthening their genetic link to the Vredefort structure with original dimensions on the order of 300 km.

Syngenetic Deposits

Syngenetic economic minerals at impact structures include impact diamonds, Cu-Ni and PGMs in sulfides, and other metals (Tables 1 and 2).

Impact diamonds

The first indication of impact diamonds was the discovery in the 1960s of diamond with lonsdaleite, another high-pressure polymorph of (hexagonal) carbon in placer deposits, e.g., in Ukraine, but their source was unknown (Cymbal and Polkanov, 1975). In the 1970s, diamond with lonsdaleite was discovered in the impact lithologies at the Popigay impact structure. Since then, they have been discovered at a number of other impact structures, e.g., Kara, Puchezh-Katunki, Ries, Ternovka, Zapadnaya, and others (Masaitis, 1993a)

Impact diamonds originate from phase transitions from graphite or crystallization from coal, which originally has been shocked to a liquid or, possibly, gaseous state. They occur when their precursor carbonaceous lithologies were subjected to shock pressures $\gtrsim$ 30 GPa (Masaitis, 1993a). The diamonds from graphite in crystalline targets usually occur as paramorphs, with inherited crystallographic features (Masaitis et al., 1990; Val'ter et al., 1992). They occur generally as microcrystalline aggregates, which can reach 10 mm in size, consisting of cubic diamond and lonsdaleite, with individual microcrystals of 10^{-4} cm. The diamonds from coal, or from other carbon in sediments, generally are porous, colored, and may have a palimpsest biogenic texture, i.e., they have some of the structural properties of the original biologic matter.

Diamonds occur in a variety of allochthonous lithologies at impact craters. They are most common as inclusions in impact melt rocks and in impact melt clasts in suevite breccias. For example, at Zapadnaya, Ukraine, they occur in impact melt dikes in the central uplift and in suevite breccias in the peripheral trough. Zapadnaya, ~ 3.8 km in diameter and 115 ± 10 m.y., is formed in Proterozoic granite containing graphite (Gurov et al., 1985). At Popigay, Russia, the allochthonous breccia filling the peripheral trough is capped by diamond-bearing suevites and coherent bodies of impact melt rocks (Figs. 18, 19). The largest of these melt-rock bodies can be traced for 10–15 km along strike and is 500 m thick (Masaitis et al., 1980). In the case of Popigay, 100 km in diameter and 35 ± 5 m.y., the original source of the carbon is Archean gneisses with graphite, which are overlain by up to 1.5 km of Proterozoic, Cambrian, Permian, and Cretaceous terrigenous and carbonate sediments. The diamonds at Kara, Russia also occur in impact melt rocks. Kara, 65 km in diameter and 67 ± 6 m.y., is located in a Paleozoic fold belt, in which Permian terrigenous sediments contain coal (Ezerskii, 1982).

In impact melt rocks at structures with carbon-bearing lithologies, diamonds can occur in very minor amounts, with provisional average estimates on the order of 10 ppb. When the melt matrix has cooled relatively slowly, the diamonds show evidence of reversion to graphite and oxidation. The distribution of diamonds with an individual impact structure and within individual impact melt and suevite bodies can be irregular. They tend to be concentrated in rays or zones emanating from areas where the original carbon-bearing lithologies are most abundant (Masaitis, 1993a). They also tend to be radially restricted. Closer to the center of the structure, high post-shock temperatures cause more rapid oxidation of the diamonds. On the other hand, at some critical distance from the center, the shock pressures are too low to result in the phase transformation to diamond. Chilling of the impact melt aids preservation. Although diamonds associated with known impact structures are not currently exploited commercially, those produced by shock transformation of graphite have some technical advantages over normal diamonds in that they tend to be harder and more resistant to breaking.

Carbonados are irregular polycrystalline diamond aggregates that occur in placers and in low-grade metamorphic rocks. They occur in Brazil, Russia, South Africa, Ukraine, Venezuela, and the Central African Republic, where they are the main export for industrial diamond applications (Treub and de Wys, 1971; Kaminsky et al., 1978). Carbonados are associated with crustal parageneses and are not related to kimberlites. They have a range of $\delta^{13}C$ values that overlap those of the diamond-lonsdaleite aggregates in the Ukrainian placers (-15.8‰ to -20.5‰) (Kaminskiy et al., 1977) and the diamond-lonsdaleite-graphite aggregates in the suevite breccias at Popigay (-12.3‰ to -17.6‰) (Galimov et al., 1980). In some cases, lonsdaleite also is present in carbonados and they generally are believed to be Precambrian in age (Kaminskiy et al., 1978). The origin of carbonados is debatable but the isotopically light character, noble gas contents indicating trapped atmosphere (Ozima et al., 1991), rare earth abundance patterns (Shibata et al., 1993), and associated parageneses indicate a crustal source.

The wide variety of parageneses between carbonado deposits suggests a variety of progenitors. This range of sources and the presence of lonsdaleite led Smith and Dawson (1985) to suggest that carbonados were formed by Precambrian-aged impacts into carbon-bearing lithologies. The associated breccias long since have been eroded away, but the carbonados survived the subsequent physical and chemical activity and became incorporated in later sediments and low-grade metamorphic rocks, in some cases, passing through the sedimentary cycle several times. Apart from the lonsdaleite, there is little other evidence of shock in associated minerals, but this could be a result of the age of the carbonados, the effects of annealing, and repeated recycling through the sedimentary cycle. At the present time, however, impact must be considered as only one of several competing hypotheses for the origin of carbonados (e.g., Kaminskiy, 1987; Kagi et al., 1994).

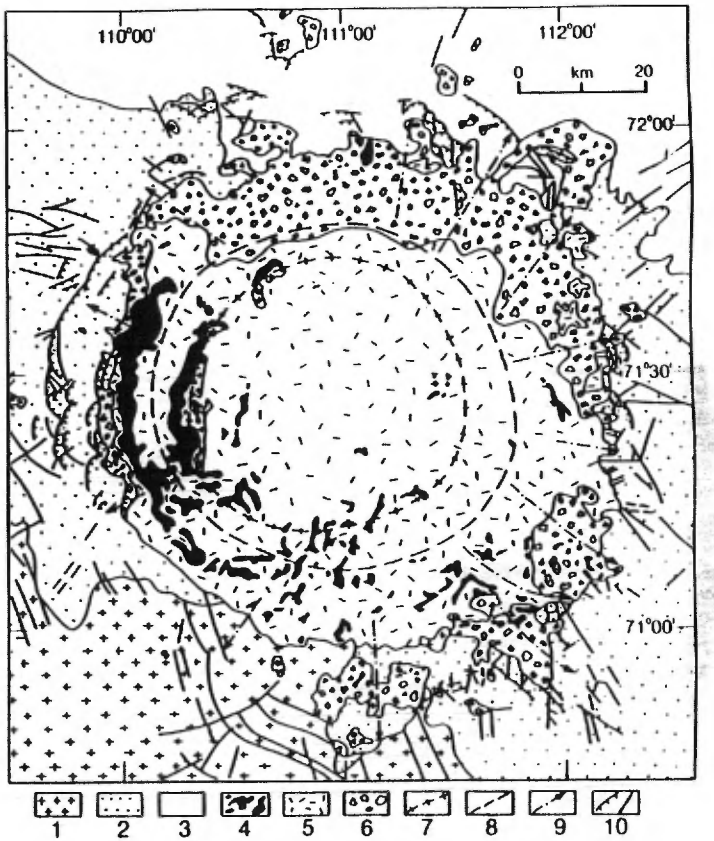


FIG. 18. Geological sketch map of the Popigay crater. Legend: 1 = Archean schists and gneisses; 2 = Upper Proterozoic and Cambrian quartzites, dolomites, and limestones; 3 = Permian sandstones; 4 = impact melt rocks; 5 = suevites with lenses of clastic allochthonous breccia, 6 = allochthonous breccia, 7 = uplifted area, 8 = axis of annular trough; 9 = radial troughs; 10 = faults, thrusts.

Cu-Ni sulfides at Sudbury

The Cu-Ni and PGM ores at Sudbury are world class, with an estimated 1.65×10^9 metric tons of 1.2% Ni and 1.05% Cu; they are related to the Sudbury Igneous Complex (SIC). Over the last five years, the extraction of these ores has had an average value of ~ $2 billion per annum. The origin of the SIC has been controversial and a considerable literature exist-

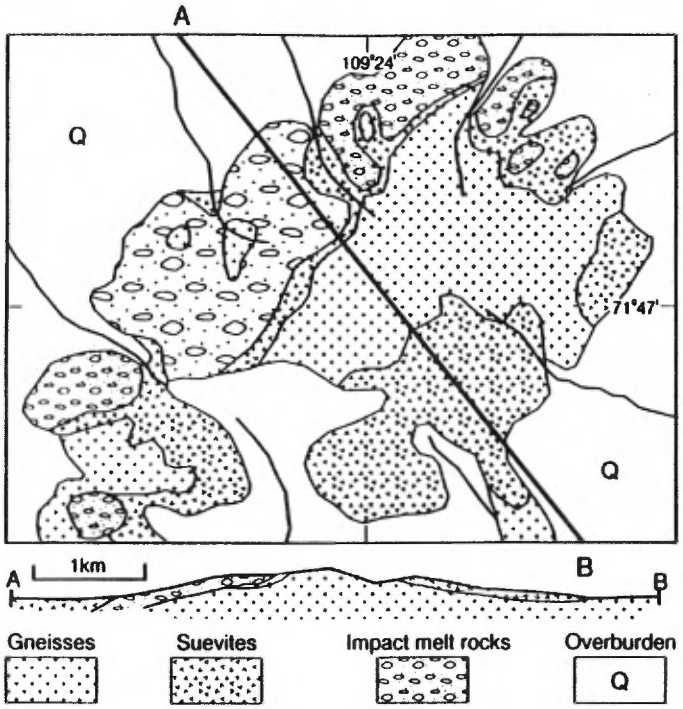


FIG. 19. Geological sketch map of Udarone impact diamond deposit at Popigay. Diamonds occur in the melt rocks and melt glasses of the suevite. No vertical exaggeration in the cross-section.

concerning aspects of Sudbury geology (e.g., papers in Pye et al., 1984; Lightfoot and Naldrett, 1994; and references therein). Sudbury was considered the site of explosive volcanism combined with intrusive igneous activity, until Dietz (1964) suggested that Sudbury was the site of a major impact, based on the occurrence of shatter cones. Since then, other physical evidence of impact in the form of other shock metamorphic effects has been described in the basement of the so-called Footwall rocks, in the Onaping suevitic breccias overlying the SIC, and the so-called Sudbury breccias in the Footwall rocks (e.g., French, 1968; Peredery, 1972). The major stumbling block in understanding Sudbury as an impact structure has been the presence of the SIC and the elliptic nature of its outcrop (Fig. 20). Although impact melting was recognized early as an integral part of the impact process, the voluminous nature of the SIC and the fact that it was differentiated into lower noritic-gabbroic and upper granophyric units posed problems for a simple impact origin. As a result, even proponents of the impact origin suggested some combined impact and magmatic models (e.g., French, 1970; Dressler et al., 1987).

Recent advances, however, in understanding the relative amount of impact melting at large impact structures (Grieve and Cintala, 1992), as well as geologic, geophysical, and geochemical studies at Sudbury (e.g., Faggart et al., 1985; Deutsch et al., 1989; Lakomy, 1990; Shanks and Schwerdtner, 1991a, 1991b; Walker et al., 1991; Dickin et al., 1992; Milkereit et al., 1992; Hirt et al., 1993; Avermann, 1994; Cowan and Schwerdtner, 1994; Deutsch, 1994; and others) point to a relatively consistent picture for the origin of the Sudbury Structure and the SIC

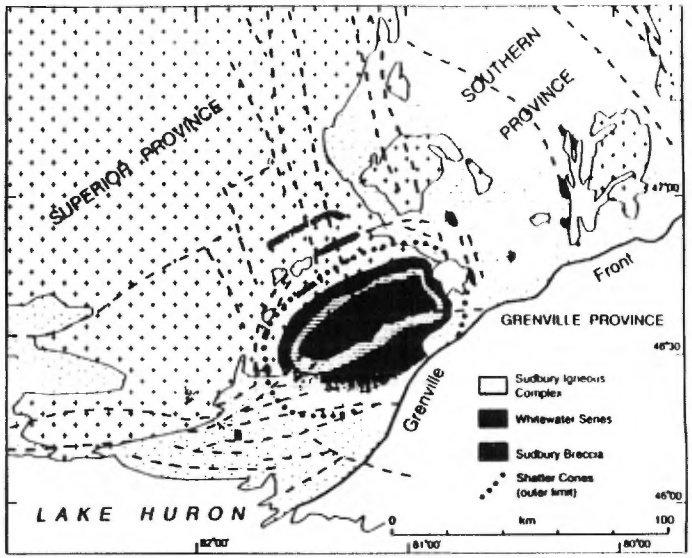


FIG. 20. Geological sketch map of the Sudbury Structure and its environs. Note occurrence of Sudbury Breccia at considerable distances from the Sudbury Igneous Complex (SIC) and the distribution of shatter cones outside the SIC, indicating that the Sudbury impact structure is much larger than the outcrop of the SIC. Source: After Peredery and Morrison (1984).

and its ores by impact, followed almost immediately by extensive deformation due to the Penokean orogeny. It is not our intent to review this recent literature here, except to point out some salient conclusions. For a more complete development of the more recent arguments and conclusions regarding the impact model, the reader is referred to Grieve et al. (1991), Deutsch and Grieve (1994), Grieve (1994), and Stöffler et al. (1994). This is not to say that there is complete consensus and understanding of all aspects and details of the impact origin of the Sudbury Structure and the SIC (e.g., Chai and Eckstrand, 1993; Chai et al., 1993; Masaitis, 1993b).

Despite the voluminous literature on the geology of the Sudbury region there is often, and still, a basic misunderstanding as to what constitutes the Sudbury Structure. The Sudbury Structure is a collective term for: the brecciated country rocks of the Superior and Southern provinces of the Canadian Shield surrounding the Sudbury Igneous Complex, the SIC itself with its associated ores, and the interior Sudbury Basin (Giblin, 1984). The Sudbury Structure covers currently an area of >15,000 km² (Fig. 20). The outcrop of the SIC is not synonymous with the Sudbury Structure. The SIC is only a part of the Sudbury Structure. The Sudbury Structure is superimposed on a Proterozoic supracrustal sequence (Huronian Supergroup), overlying Archean basement rocks (Abitibi Subprovince of the Superior Province). The Proterozoic metasediments and metavolcanics are exposed mainly in the south and east, whereas the basement rocks to the north and west are Archean Levack gneisses bordered by granite-greenstone lithologies. To the north, erosional remnants of the Huronian Supergroup also are found as outliers in a ring-like graben zone parallel to the boundary of the SIC at a distance of 20 to 25 km (Fig. 20).

Formations related directly to the Sudbury Structure occur up to 80 km away from the outer margin of the SIC (Fig. 20). The following formations, proceeding inwards and stratigraphically upwards through the Sudbury Structure, can be identified: (1) dike breccias

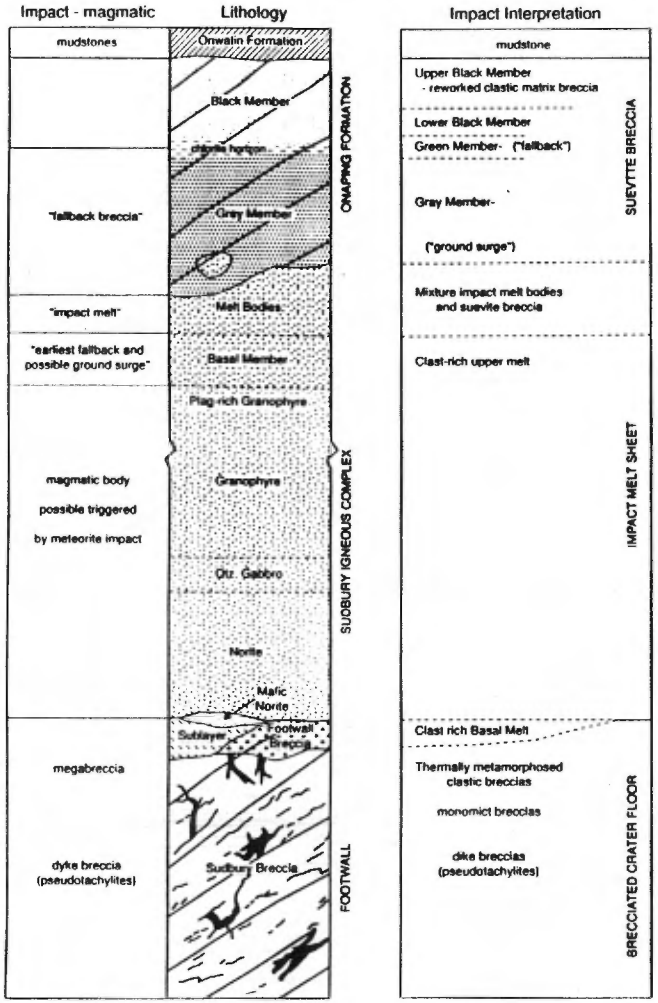


FIG. 21. Stratigraphic column at the Sudbury Structure with previous and current impact genetic interpretation.

and pseudotachylite (collectively named Sudbury Breccia), (2) shocked footwall rocks, (3) Footwall Breccia, (4) Contact Sublayer and Sublayer-Offset dikes of the SIC, (5) Main Mass of the SIC, (6) Basal Member, Onaping Formation (OF), (7) Gray Member, OF, (8) Green Member, OF, (9) Black Member, OF, and (10) Onwatin and Chelmsford formations.

The interpretation of this stratigraphic succession in terms of current understanding of the formation of a large complex impact crater differs from previous views that considered an endogenic or mixed endogenic-exogenic origin and is presented in Figure 21. Details of the basic geologic, petrographic, geochemical, and isotopic studies that have led to this general

impact interpretation are contained in the previously cited references. The major conclusions of these studies can be synthesized as: (1) all "polymict" formations (breccia and melt lithologies) can be explained by impact-induced brecciation or melting, mixing, and transport of Precambrian basement rocks, which now are exposed at the Sudbury Structure; (2) there is no chemical or physical requirement for additional "volcanic-magmatic" components derived from the mantle 1.85 Ga during the Sudbury event in any of the formations of the Sudbury Structure, in particular for the Sudbury melt system (the SIC, the Basal Member of the OF, and melt particles in various other breccia units) and the ore deposits.

The interpretation of recent seismic reflection data indicates clearly that the SIC has been highly tectonized in the south and subjected to NW–SE shortening as a result of the Penokean orogeny (Milkereit et al., 1992; Wu et al., 1994). This picture of northwestward thrusting is consistent with recent structural observations that indicate ductile deformation was followed by thrusting (Shanks and Schwerdtner, 1991a, 1991b; Cowan and Schwerdtner, 1994). Thus, the present configuration of the SIC is the result of tectonic modification. In acknowledgement of the role of tectonism for the present geological and geophysical character of the Sudbury Structure, Roest and Pilkington (1994) reconstructed the original spatial relations of the potential field data by removing the effects of a simple NW–SE stress field. Their conclusion is that the anomaly pattern of the present SIC could well have been originally circular.

Stöffler et al. (1989), Lakomy (1990), and Grieve et al. (1991) presented estimates of the dimensions of the original Sudbury Structure. These estimates were derived by analogy with empirical relations at other large impact structures between the observed radial extent of various levels of shock effects, breccia layers, dike breccias, and specific morphological and structural elements of impact structures. These estimates of the diameter for the original final crater and the transient cavity depend strongly on the original diameter of the SIC at the present erosional level. The "destraining" of the pattern of potential field anomalies related to the SIC (Roest and Pilkington, 1994) suggests that the original diameter of the present exposure of the SIC could have been at least 65 km and, perhaps, as much as 75–80 km in its pre-erosional form. A similar conclusion is reached by Hirt et al. (1993), who removed the strain in the Onaping and Chelmsford Formation, based largely on magnetic anisotropy fabrics. Using the same empirical relations as previously (Grieve et al., 1991), this would extend the maximum diameter of the final crater rim to some 250 km (Deutsch and Grieve, 1994). Regardless of the detailed determination of the original size, the basic conclusion is that the Sudbury Structure represents an eroded and heavily tectonized remnant of an originally 200- to 250-km-diameter peak-ring, or possibly a multi-ring, impact basin. The amount of erosion at the Sudbury Structure is generally unknown. It generally is estimated at a few kilometers (Naldrett and Hewins, 1984; Lowman, 1992), certainly less than at the similarly aged and sized Vredefort Structure. U-Pb ages of new zircons from the SIC, the immediate Footwall Levack Gneisses, as well as shocked zircons from the Onaping, all indicate an age of 1.85 Ga for the Sudbury event (Krogh et al., 1984).

In general, many of the orebodies at Sudbury are located in what are termed locally as "embayments," which may be related to terraces in the original impact crater (Morrison, 1984; Morrison et al., 1994). In detail, the ore deposits at Sudbury occur in a variety of associations. Naldrett (1984) recognizes five major associations: (i) South Range, where the ores occur largely as massive sulfide deposits at the base of the Sublayer; (ii) North Range, where the ores occur largely as concentrations of sulfides (up to 60%) in the Footwall Breccia and as stringers in the Footwall; (iii) offset dikes, where the ores occur largely as concentrations of sulfides in breaks and constrictions in the dikes; (iv) faults, where the ores occur as remobilized masses; and (v) other associations. The association of the ores is complex, varied, and, in some cases, exceptional. This variability reflects complications resulting from thermal metamorphism, including partial melting of the Footwall, and hydrothermal activity that occurred because of the extremely hot SIC and elevated post-impact temperatures in the Footwall because of shock and uplift. More impor-

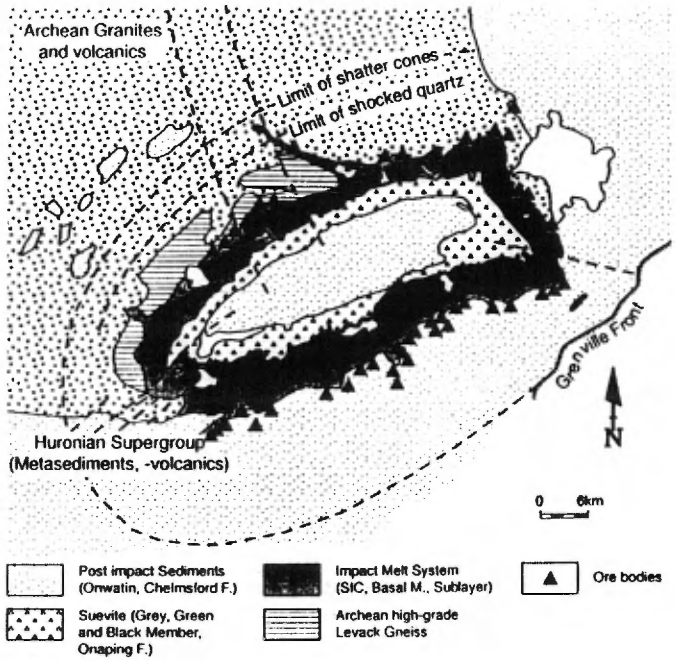


FIG. 22. Location of main orebodies at Sudbury. Note their spatial relation to the base of the impact melt system (SIC) (see text for other details).

tantly, the formation of the Sudbury Structure and its almost immediate deformation by Penokean folding and, later, thrusting (Cowan and Schwerdtner, 1994; Deutsch and Grieve, 1994) gave rise to complex post-impact movements and mobilization.

The overall commonality to all the ore deposits is that they lie at the base or just beneath the SIC (Fig. 22). In previous magmatic models of the origin of ores at Sudbury, it was suggested that they resulted from the segregation of sulfides as an immiscible liquid, due to the assimilation of siliceous rocks by a basaltic magma, followed by gravitational settling and, later, fractional crystallization and, in some cases, remobilization (Naldrett et al., 1982; Morrison et al., 1994). In the impact model, the situation is essentially the same, except that the original source of the metals is crustal and sulfide immiscibility reflects the fact that the combination of lithologies melted to form the impact melt (SIC) resulted in a liquid with an initial composition that already was enriched in SiO_2 (~64%) compared to endogenic magmatic compositions. Additional assimilation of clastic debris may have abetted this unusual compositional character and, indeed, assimilation of local clastic debris may account for some of the compositional differences between the North and South ranges of the SIC (Naldrett et al., 1984).

The key difference, therefore, between endogenic magma with assimilation and the impact models is that a "disequilibrium" composition (with respect to the expected equilibrium crystallization of endogenic silicate melts) was an original property of the SIC. That the metals in the ores, as well as the associated silicates, have an original crustal source is indicated by the Re-Os isotopic composition of the ores and the Nd-Sm composition of the silicates (Fig. 23) (Dickin et al., 1992). While we acknowledge that many details still are to be determined, recent work at Sudbury generally can be fitted within the general framework of the formation of a 200- to 250-km impact basin 1.85 Ga, with accompanying massive crustal melting producing a melt of an unusual composition that gave rise to immiscible sulfides and ultimately the present ore deposits. A complicating but essential component of the evolutionary history is the almost immediate deformation by the penecontemporaneous Penokean orogeny. Although explanations involving massive crustal assimilation by magma (e.g., Walker et al., 1991) or "unique igneous activity" (e.g., Chai and Eckstrand, 1993) still are forthcoming, it should be noted that even in these cases an impact event is required to trigger the activity. Thus, impact still remains an essential component for the genesis of the Sudbury ores.

Epigenetic Deposits

Epigenetic deposits generally reflect the fact that impact structures can result in isolated topographic basins or locally disrupt underground flow. They can originate almost immediately or over an extended period after the impact event. Examples include various hydrothermal deposits, liquid and gaseous hydrocarbons, oil shales, various organic and chemical sediments, as well as flows of fresh and mineralized waters (Tables 1 and 2).

Hydrothermal ores

Hydrothermal ore deposits occur at Siljan, Sweden (55 km, 368 ± 1 Ma). Here, Pb, Zn, and Ag sulfides occur in veins in the contact zone between sandstone and limestone blocks in the annular trough outside the central uplift. The amount of ore is estimated at 300,000 metric tons with 3% Pb, 1.5% Zn, and 70 ppm Ag. Isotopic studies indicate that ore formation is related to the impact event (Johansson, 1984). Some of these deposits, e.g., at Boda, were exploited commercially until the last century. Other small deposits of Pb, Zn sulfides, and other minerals are known at Crooked Creek, USA (7 km, 320 ± 80 Ma), where both galena and barite were mined in the past (Kilsgaard et al., 1962). Pb and Zn sulfides occur at Serpent Mound, Ohio, USA (8 km, < 320 Ma) (Heyl and Brock, 1962) and at Decaturville, USA (6 km, < 300 Ma) (Zimmermann and Amstutz, 1972).

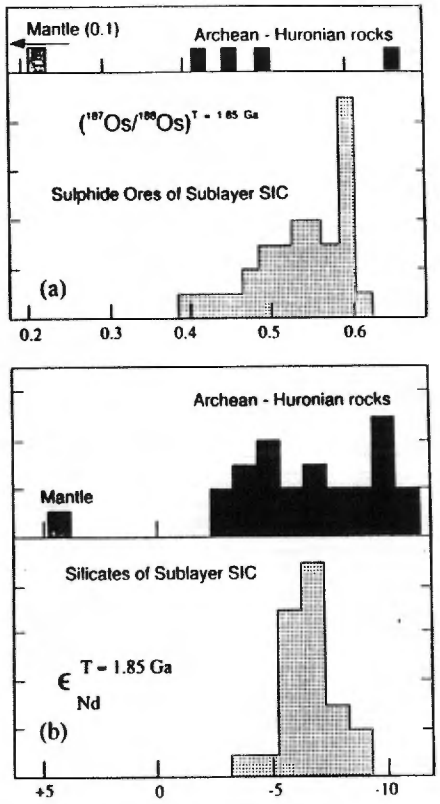


FIG. 23. Histograms of calculated osmium isotopic data for sulfide ores and country rocks at 1.85 Ga (A) and calculated neodymium isotopic data for silicates from Sublayer ores and country rocks at 1.85 Ga (B) at Sudbury. Source: After Dickin et al. (1992).

These types of deposits are related to hydrothermal activity in the brecciated carbonates of the central uplifts. Although individual fragments of rock are estimated to contain 5–20% Zn at, for example, Serpent Mound, the known sulfides are not abundant enough to form a current commercial-grade deposit.

In large impact structures, the circulation of hot solutions can continue for considerable time after the impact event and result in sedimentary exhalative mineralization. This is believed to be the origin of the Zn, Pb, Cu, As, and Au mineralization in the Vermillion

member at the base of the Onwatin formation at Sudbury (Rousell, 1984; Davies et al., 1990). These deposits contain over 6 million tons of 4.4% Zn, 1.4% Cu, and 1.2% Pb, and have been mined in the past (Gibson et al., 1994). The fine-grained nature of the ore, however, has caused problems in recovery and the ores currently are not exploited (Rousell, 1984). At Puchezh-Katunki, Russia (80 km, 175 ± 5 Ma), the post-impact sediments contain gritstone and clays. There is a basin formed over a central pit in the central uplift of the structure, and here the gritstone has been altered to up to 30% zeolite (Masaitis et al., 1980). These deposits currently are not exploited. Hydrothermal mineralization of post-impact sediments is to some degree transitional between syngenetic and epigenetic, as it requires a thermal component that is directly related to the impact event.

Hydrocarbons

Hydrocarbons occur at a number of impact structures. Only the major deposits—at the Ames, Red Wing Creek, and Avak structures—are discussed here.

Ames. The Ames structure is located in Oklahoma, USA, and contains the town of Ames within its boundaries. It is a complex structure, roughly 14 km in diameter, with a central uplift, an annular trough, and slightly uplifted rim. It is buried by up to 3 km of Ordovician to Recent sediments (Carpenter and Carlson, 1992). The structure is a recent discovery, having been identified during the course of oil exploration (Roberts and Sandridge, 1992).

A local structure known as the Hunton graben, in which the Ordovician-Silurian Hunton Formation thickens from ca. 70 m to ca. 145 m and lies roughly 60 m below its regional level, has been known for some time. During recent oil exploration, it was recognized that this was part of a much larger structure and that this graben corresponds to thickened post-impact deposits in the annular trough of a complex impact structure (Fig. 24). The rim of the structure is defined by the structurally high Lower Ordovician Arbuckle dolomite, and > 600 m of Cambrian-Ordovician strata and some underlying basement are missing in the center of the structure as a result of excavation. The entire structure is covered by Middle Ordovician Oil Creek shale, which forms a seal for structural traps for hydrocarbons. The (~ 60 m) post-impact Oil Creek shale within the Ames structure also is the source of the hydrocarbons (Kuykendall et al., 1994). The general form of the structure is visible in the variations in depth of the overlying sediments (Fig. 24).

The first oil and gas discoveries were in 1990 from an approximately 500-m-thick section of Lower Ordovician Arbuckle dolomite in the rim. Locally, the Arbuckle does not have much matrix porosity, but as a result of impact-induced fracturing and karsting, the Arbuckle in the rim of Ames has considerable economic potential. For example the 27-4 Cecil well, drilled in 1991, had drill stem rates of 3440 million cubic feet of gas and 300 barrels of oil per day (Roberts and Sandridge, 1992). Wells drilled in this center failed to encounter the Arbuckle dolomite and bottomed in granite breccia of the central uplift or, closer to the rim, granite-dolomite breccia. These wells include the famous Gregory 1-20, which is reported to be the most productive oil well from a single pay zone in Oklahoma. It encountered a roughly 80-m section of granite breccia below the Oil Creek shale with very effective porosity. A drill stem test of the zone flowed at approximately 1300 barrels of oil per day, with a conservative estimate of primary recovery of in excess of 10 million barrels from this single well (Carpenter, pers. comm., 1994; Kuykendall et al., 1994). Approximately 100 wells have been drilled, 52 of which are producing oil, 1 of which produces gas. Based on the initial two years of production, conservative estimates of reserves at Ames suggest they will exceed 50 million barrels of oil and 60 billion cubic feet of gas, which is energetically equivalent to an additional 40 million barrels of oil (Isaac and Stewart, 1993; Carpenter, pers. comm., 1994).

The age of the structure is Lower Ordovician, ca. 450 ± 10 Ma, based on the absence of the Arbuckle dolomite within the structure and the presence of the Oil Creek shale over the entire structure. It is believed that the impact was sufficient to result in emergent topography in the rim area and central uplift, the latter having been uplifted a minimum of 600 m. This resulted in granite wash around the central uplift and karst topography in the rim (Roberts and Sandridge, 1992). This has further enhanced the porosity of the reservoir rocks.

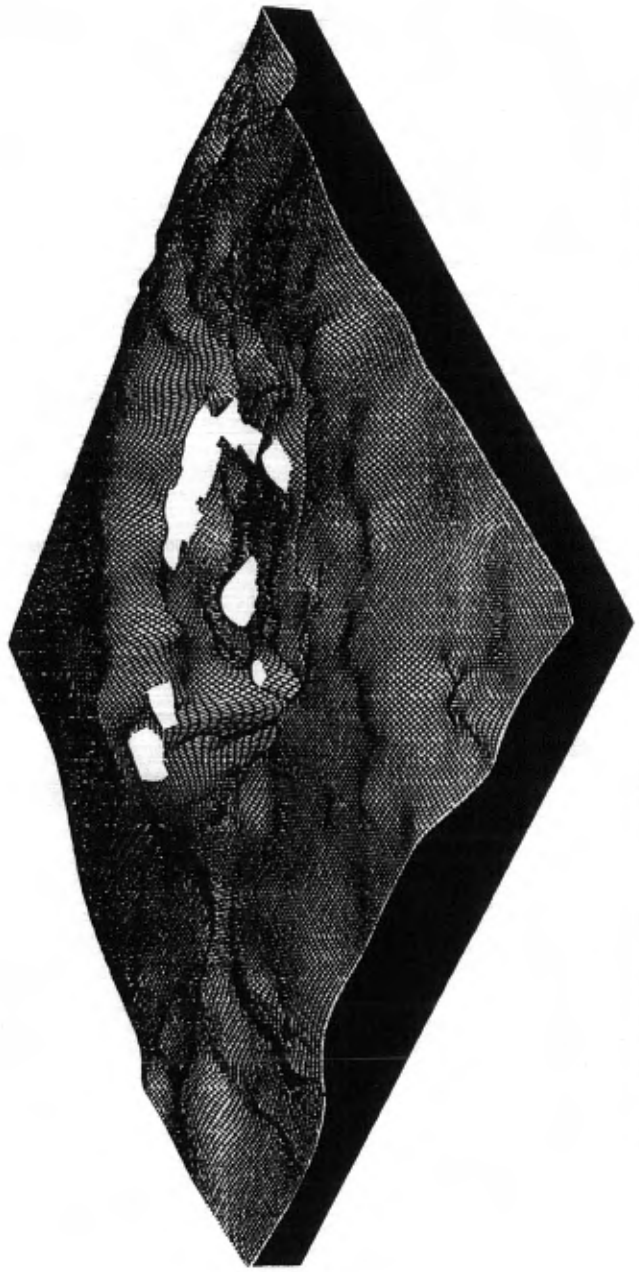


FIG. 24. Residual structure on the Upper Ordovician Sylvan shale, which lies ca. 240 m above the Arbuckle at the Ames crater, reflecting the rim, inner ring, and floor of the crater. The vertical exaggeration is 20×, perspective is elevated 25° and looking to the northwest. The areas of hydrocarbon are shown in white, with the original DLB Cecil discovery well on the western rim. Original diagram supplied by J. H. Stark, Continental Resources.

Hydrocarbon production is from the Arbuckle dolomite, the brecciated granite, and granite-dolomite breccia, and largely is due to impact-induced fracturing and brecciation, which has resulted in significant porosity and, more importantly, permeability. The source of the Ames oil is the lower section of post-impact Oil Creek shale, which has not been recognized outside the feature (Castaño et al., 1994). In the case of Ames, the impact produced not only the required structural traps but also the paleo-environment for the deposition of post-impact shales that upon subsequent burial and maturation provided oil and gas. There are similarities between the Ames crater shale and a locally developed Ordovician shale in the Newporte (North Dakota) structure, an oil-producing suspected impact crater (~ 120,000 barrels per year) in Precambrian basement rocks of the Williston Basin (Castaño et al., 1994). The Ames discovery has important implications for oil and gas exploration in crystalline rock underlying petroleum basins. Donofrio (1981) proposed the existence of such hydrocarbon-bearing impact craters and that major oil and gas deposits may occur in brecciated basement rocks. If these structures also generate conditions favorable for source rock development, such as at Ames, their potential could be considerable.

Red Wing Creek. A slightly different situation occurs at the Red Wing Creek structure in North Dakota, USA, where hydrocarbons also are recovered from the brecciated rocks of the central uplift. In this case, the impact structure provides the structural trap but, unlike Ames, is not responsible for the source of the oil. Red Wing Creek is a complex structure, approximately 9 km in diameter, with seismic records and drill-core data indicating a central peak in which strata have been uplifted up to 1 km, an annular trough containing crater-fill products, and a partially eroded structural rim (Fig. 25) (Brenan et al., 1975; Sawatsky, 1977). The structure is formed in Silurian to Triassic carbonates with minor sandstones and evaporites and is buried by ~ 1.5 km of Jurassic to Neogene post-impact sediments. On this basis, the structure is assigned an age of 200 ± 25 Ma (Gerhard et al., 1982).

As the result of a pronounced anomaly in seismic data, the structure was drilled in 1965 by Shell Oil, which drilled the NW flank of the central uplift. The drillhole indicated a structurally high and thickened Mississippian and Pennsylvanian section, compared to drillholes outside the structure. The well, however, was a dry hole. In 1968, Shell drilled another hole to the NW in the annular trough. Here, the Mississippian was found to be structurally low compared to exterior. It also was a dry hole and the structure, as a whole, was assumed to be dry. However, True Oil redrilled what was later recognized as the central uplift in 1972 and discovered ca. 820 m of Mississippian oil column, with considerable high-angle structural complexity and brecciation and a net pay of ca. 490 m. This is in contrast to the surrounding area, with gentle dips and roughly 30-m oil columns.

The large oil column is the result of the structural repetition of what apparently is the Mississippian Mission Canyon Formation in the central uplift (Brenan et al., 1975). The addition of impact-induced porosity and permeability results in relatively high flow rates of over 1000 barrels per day, with cumulative production since discovery in excess of 12.7 million barrels of oil and 16.2 billion cubic feet of natural gas (Pickard, 1994). Current production is restricted to ~ 300,000 barrels per year, to preserve unexploited reserves of natural gas. It is estimated that the brecciated central uplift contains over 130 million barrels of oil, and primary and secondary recoverable reserves may exceed 70 million barrels (Donofrio, 1981; Pickard, 1994). The natural gas reserves are estimated at 100 billion cubic feet. Virtually all the oil has been discovered within a diameter of ~ 3 km, corresponding to the central uplift. Based on net pay and its limited aerial extent, Red Wing is probably the most prolific oil field in the United States, with the wells in the central uplift having the highest cumulative productivity of all the wells in North Dakota.

Avak. The Avak structure is located on the Arctic coastal plain of Alaska. The structure has been known for some time as a "disturbed zone" in seismic data (Lantz, 1981) and only recently was evidence of shock metamorphism forthcoming in the form of shatter cones and planar deformation features in quartz (Kirschner et al., 1992). Avak is buried by late Pleistocene and Quaternary deposits and affects Ordovician-Silurian to Cretaceous rocks. Thus, its age is only constrained to some-

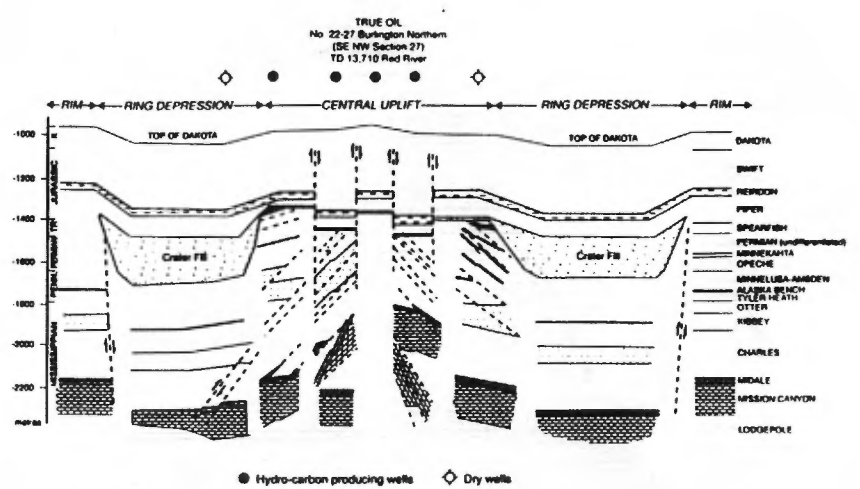


FIG. 25. Geological cross-section across the Red Wing Creek crater. Hydrocarbons are produced from the central uplift area. Source: After Gerhard et al. (1982).

time between 95 and 3 Ma. Kirschner et al. (1992) suggest that the formation of Avak may have triggered submarine landslide deposits in the Aptian and Albian Formation 200 km to the east. If this is the case, its age is 100 ± 5 Ma.

The structure itself has the form of a complex impact structure ca. 12 km in diameter (Fig. 26). It is bounded by listric faults, which define a rim area, and has an annular trough and central uplift. In the central uplift, the Lower-Middle Jurassic Kingak Shale and Barrow Sand are uplifted more than 500 m from their regional levels. The central uplift has been drilled by the Avak 1 well, which penetrated to a depth of 1225 m. The well penetrated the general succession of the area: Lower Cretaceous pebble shale, Jurassic Kingak Shale, Lower Jurassic Barrow Sand and (Ordovician) Frankilian argillite. In addition to structural uplift and the occurrence of shock metamorphic features, repetition of beds and out-of-sequence beds were encountered (Collins, 1961; Kirschner et al., 1992). For example, the pebble shale, which has a regional thickness of 140 m, has an aggregate thickness of 320 m in the Avak well, caused by steep dips and repetition by faulting. Breccia containing argillite clasts in a matrix of Jurassic and Cretaceous rocks also was encountered. Included as clasts in some breccias are Triassic and Permian strata, which occur *in situ* south and southeast of Avak 1. This breccia provides evidence for centripetal transport toward the center of ~ 3 km in the formation of the central uplift (Kirschner et al., 1992).

Oil shows occur in Avak 1, but the well is not a commercial producer. Indeed, Kirschner et al. (1992) suggest that pre-Avak hydrocarbon accumulations may have been disrupted and lost due to the formation of the Avak structure. There are, however, the South Barrow, East Barrow, and Sikulik gas fields (Fig. 26), which are post-impact and are related to the Avak structure. They occur outside the structure and are due to listric faults of the crater rim, which have truncated the Lower Jurassic Barrow Sand and placed Lower Cretaceous Torok shales against the sand, creating an effective up-dip gas seal. The South and East Barrow fields currently are in production and primary recoverable gas is estimated at ~ 37 billion cubic feet (Lantz, 1981). The Sikulik gas field is not currently exploited.

Other structures. Other impact structures also produce hydrocarbons. For example, the 25-km-diameter Steen River structure, Canada, produces a respectable 600 barrels of oil per day from two wells on the northern rim. Gas is also produced at the 22-km-diameter Marquez structure, USA. There may be a zone of potential

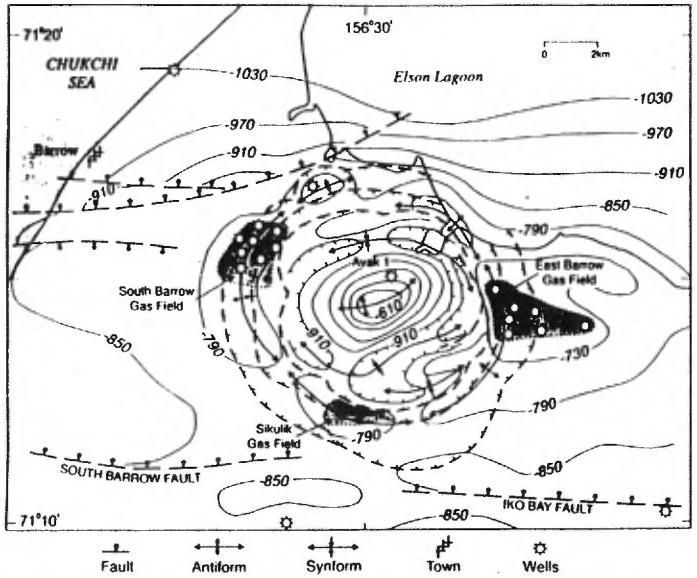


FIG. 26. Structure contour map on top of Franklinian argillite (Ordovician-Silurian) at Avak. Contour interval 60 m. Source: After Kirschner et al. (1992). Gas fields are indicated.

stratigraphic trapping within the 55-km-diameter Tookoonooka structure, Australia. More importantly for hydrocarbon exploration, however, the Tookoonooka structure has created a shadow zone to hydrocarbon migration from the Eromanga Basin depocenter since the early Cretaceous (Gorter et al., 1989). A number of other impact structures have been drilled in the course of hydrocarbon exploration—e.g., Gosses Bluff, Australia—and generally before they were recognized as impact structures. On the other hand, Siljan represents a case where hydrocarbon exploration was undertaken, in part, because it was an impact structure. In this case, exploration, which was highly controversial, was aimed at what were believed to be abiogenic hydrocarbons from the mantle that were channelled to the Siljan area because of impact-induced fracturing of the crust (Gold, 1988).

Oil from Jurassic rocks is recovered from the Lomas Triste breccia deposit at the Cretaceous-Tertiary boundary in the Campeche oil field in the Gulf of Mexico (Camargo Zanoguera and Quezada Muñeton, 1992). Shocked quartz has been reported in the upper portion of these breccias and their genesis has been linked to the 180-km Chicxulub crater in nearby Yucatan, Mexico (Limon et al., 1994), which is at the center of the debate as to whether its formation was or was not the cause of the Cretaceous-Tertiary mass extinction event (Hildebrand et al., 1991). There also are a number of structures that may be of impact origin, such as Newporte, USA, which was noted earlier (Clement and Mayhew, 1979), and Viewfield, Canada (Sawatsky, 1977), that produce hydrocarbons. In these two cases, the impact interpretation suggests they are simple bowl-shaped craters. In neither case have shock metamorphic effects been identified. The recoverable reserves associated with Viewfield are estimated to be 20 million barrels of oil (Isaac and Stewart, 1993). Over 500,000 barrels of oil have been produced since 1978 from the Calvin structure, USA, which most likely is an 8.5-km-diameter complex impact structure (Milstein, 1988). In addition, a number of seismic targets with the characteristics of impact structures, which have hydrocarbon potential, also have been

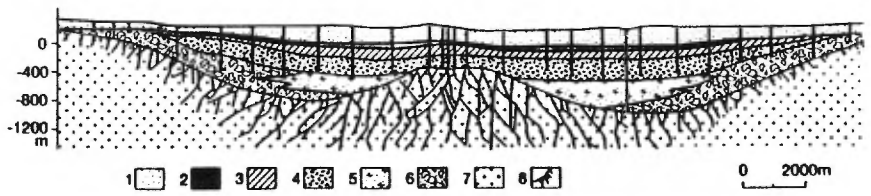


FIG. 27. Geological cross-section of the Boltysh. Legend: 1 = Quarternary clays, sands; 2 = Eocene to Paleocene clays, siltstones; 3 = Paleocene–Upper Cretaceous oil shales, siltstones; 4 = Lower Cretaceous sandstones and carbonates; 5 = impact melt rocks; 6 = allochthonous breccia; 7 = Proterozoic granites, gneisses; 8 = fractured and brecciated gneisses.

noted (e.g., Gudlaugsson, 1993; Isaac and Stewart, 1993; Tooth and Stewart, 1994).

Oil shales

Oil shales are known at Boltysh (25 km, 88 ± 3 Ma), Obolon (15 km, 215 ± 25 Ma), and Rotmistrovka (2.7 km, 140 ± 20 Ma) in Ukraine (Masaitis et al., 1980; Gurov and Gurova, 1991). They represent the unmatured equivalent of the hydrocarbon reserves at Ames. The most significant reserves are at Boltysh, where there is an estimated 4.5 billion metric tons. The Boltysh was formed in Archean and Lower Proterozoic granites and is completely buried by Upper Mesozoic and Cenozoic sediments (Fig. 27). It was recognized initially as a geophysical anomaly and has been drilled extensively. Surrounding the central uplift is an annular trough partially filled by a coherent impact melt sheet, suevites, and allochthonous breccia. They are capped by various shales, including oil shales, and siltstones (Fig. 28). The total productive sequence is ca. 400–500 m and consists of five sections containing 25–40 beds of oil shale with thicknesses up to 4.5 m (Bass et al., 1967). The oil shales are the result of biological activity involving algae in this isolated basin. They currently are not exploited.

Placers

Placer deposits fall into the category of epigenetic deposits. These result from terrestrial erosion of impact lithologies and include placer diamonds related to Popigay, found up to distances of 150 km from the structure, and other occurrences of what are believed to be impact-related diamonds in Ukraine, Kazakhstan, and the Urals of Russia (Masaitis, 1993a). The occurrence of impact-related diamonds at considerable distances from their source crater suggests that they originated from the erosion of ejecta deposits and later reworking. A similar situation occurs with respect to the moldavite tektite placers in Bohemia, which have Ries as their original source (Bouska et al., 1973). The moldavites are used as stones in the production of jewelry (Turnovec, 1987; Turnovec and Sevcik, 1987). Jewelry also is produced locally from the tektite-like glasses, known as irghizites, found within the Zhamanshin structure (13.5 km 0.9 ± 0.1 Ma), Kazaksthan (Schnetzler, pers. comm., 1994).

Other deposits

The post-impact sedimentary fill at the Ries crater, Germany (24 km, 15.1 ± 1.0 Ma), contains beds of lignite and bentonite; deposits of diatomite occur at Ragozinka, Russia (9 km, 55 ± 5 Ma); and phosphorite at Logoisk, Belarus (17 km, 40 ± 5 Ma). Gypsum and anhydrite from the Jurassic-aged post-impact sediments have been quarried since 1901 at Saint Martin, Canada (40 km, 219.5 ± 32 Ma). Other local concentrations of gypsum, anhydrite, and other chemical sediments are known at other impact structures and owe their origin to post-impact chemical sedimentation from saline lakes. At present, various carbonates, bicarbonates, and chlorides are exploited at Lonar, India (1.8 km, 0.05 ± 0.01 Ma) and Saltpan, South Africa (1.1 km, 0.22 ± 0.05 Ma), both from saline lakes, resulting from a local closed catchment basin and a warm climate.

Concluding Remarks

In this review, we have attempted to illustrate the known scope of potential economic deposits in impact structures. They vary from minor

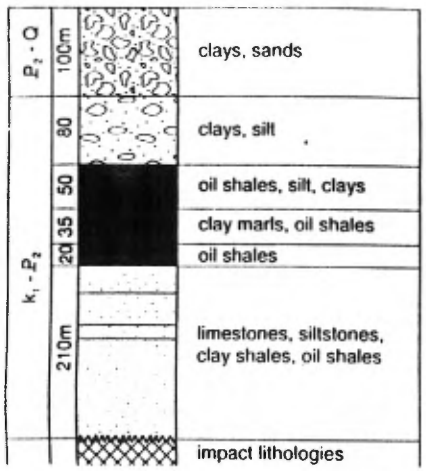


FIG. 28. Stratigraphic column of post-impact sediments, containing oil shales, at Boltysh.

deposits of little commercial value to world-class orebodies and significant hydrocarbon producers. Given the relatively small number of known impact structures, it would seem that, as a class of geologic features, impact structures have considerable economic potential overall. For example, the total gross direct worth of materials extracted from impact structures in North America is estimated at $5-6 billion per year. As noted in the introduction, this type of accounting does not include other economic considerations, such as impact structures as current sources for drinking or mineralized water (e.g., Manson, USA; Kaluga, Russia), as lakes for the generation of hydroelectric power (Manicouagan, Canada; Puchezh-Katunki, Russia), as sources of building materials (Ries, Rouchechouart), and the direct and indirect benefits that accrue from the establishment of an infrastructure to exploit these resources.

From an exploration point of view, the occurrence of impact structures has the disadvantage of being random in both space and time. On the other hand, there are areas of the world where the numbers of known impact structures are well below those expected from the known cratering rate, indicating that there are many impact structures yet to be found. For example, the estimated number of impact structures in the size range of Sudbury that formed on the land surface in the last 2 Ga is approximately 10. At present 3 are known: Chicxulub, Sudbury, and Vredefort. Chicxulub is buried beneath roughly one kilometer of post-impact sediments and is unlikely, therefore, to have economically viable mineral deposits, although it has exerted considerable control over the local hydrology (Pope et al., 1991) and may be the cause of the hydrocarbon-bearing Lomas Triste breccia deposit. Both Sudbury and Vredefort are associated with major mining camps with world-class syngenetic and progenetic ore deposits, respectively. It would appear that the largest impact structures have the higher probability of having significant economic resources. This is not surprising, as they are the most energetic events, affect the largest volumes of target rocks, have the largest post-impact hydrothermal systems, and form the largest topographic basins.

Impact structures do have a general property that is an advantage in exploitation. At a large scale, they tend to have fixed morphometric and structural relationships for a given diameter. The advantage is that once a structure is known to be of impact origin and its diameter is known, it is possible to make considerable predictions as to the structural and lithological character of the feature as a whole. This is generally not possible for most endogenic geologic features. The development of an exploitation strategy based on these relationships, once a particular structure is recognized as being of impact origin, is most notably illustrated by the drilling for hydrocarbons at Ames. One can only wonder how Sudbury would have been explored and exploited had our current state of knowledge of its impact origin and tectonic evolution been known soon after it had been discovered. For the case of Sudbury, the level of current knowledge on its origin and evolution undoubtedly will be used in future exploration.

Epigenetic economic deposits currently are the most common (Table 2), but all three types of economic deposits at terrestrial impact craters are roughly similar in cumulative value. It would appear that, for progenetic types of deposits, the central uplift area of complex impact structures is the most promising target. It provides an environment where deeply buried deposits can be brought close to the surface. Syngenetic deposits are more closely associated with impact lithologies involving phase changes and are, thus, more likely to be concentrated in and around such lithologies as impact melt sheets and suevitic breccias. Secondary epigenetic associations also are to be expected as a result of hydrothermal processes in areas above and below such lithologies. The brecciated and fractured rocks of the central uplift also provide an environment for the structural repetition of beds and increased porosity and permeability and would appear to be targets for hydrocarbon exploration. Other epigenetic deposits are most closely linked with the crater form itself, generally as an isolated basin with localized sedimentary and geochemical activity not present in the area as a whole or as a barrier to the migration of external fluids. The fact that these isolated basins within impact craters not only can provide the structural traps but also can produce the source rocks for hydrocarbons, such as at Ames, enhances considerably their exploration prospects, for they need not occur in known hydrocarbon-producing areas to have hydrocarbon potential.

Acknowledgments

This work was initiated while RAFG was an Alexander von Humboldt-Stiftung Forschungspreisträger at the Institut für Planetologie, Münster, receipt of which is gratefully acknowledged. D. Donofrio and A. Therriault read an earlier version of the manuscript and their comments have helped greatly, as has a formal review by R. Hargraves. J. H. Stark, Continental Resources, kindly supplied the original version of Figure 24, depicting the Ames structure.

REFERENCES

Ahrens, T. J., and O'Keefe, J. D., 1977, Equations of state and impact-induced shock-wave attenuation on the moon, *in* Roddy, D. J., Pepin, R. O., and Merrill, R. B., eds., Impact and explosion cratering: New York, Pergamon Press, p. 639-656.

Avermann, M. E., 1994, Origin of the polymict, allochthonous breccias of the Onaping Formation, Sudbury Structure, Ontario, Canada: Geol. Soc. Amer. Spec. Paper (in press).

Barringer, D. M., 1906, Coon Mountain and its crater: Philadelphia Acad. Nat. Sci. Proc., v. 57, p. 861-886.

Bass, Yu. B., Galaka, A. I., and Grabovskiy, V. I., 1967, The Boltysh oil shales, *in* Exploration and conservation of minerals: p. 11-15 (in Russian).

Bell, K., Cacciotti, A. D., and Schnessl, J. H., 1985, Petrography and geochemistry of the Earl River Complex, Carswell structure, Saskatchewan—a possible Proterozoic Komatiitic succession: Geol. Assoc. Canada, Spec. Paper 29, p. 71-80.

Bottomley, R. J., York, D., and Grieve, R. A. F., 1990, 40 Argon-39 Argon dating of impact craters [abs.]: Proc. 20th Lunar Planet. Sci. Conf., p. 421-431.

Bouska, V., Benada, J., Randa, Z., and Kuncir, J., 1973, Geochemical evidence for the origin of moldavites: Geochim. et Cosmochim. Acta, v. 37, p. 121-132.

Brenan, R. L., Peterson, B. L., and Smith, H. J., 1975, The origin of Red Wing Creek Structure: McKenzie County, North Dakota: Wyoming Geol. Assoc. Earth Sci. Bull., no. 8, p. 1-41.

Buchwald, V. F., 1975, Handbook of iron meteorites: Berkeley, Univ. California Press, p. 937-942.

Bunch, T. E., Dence, M. R., and Cohen, A. J., 1967, Natural terrestrial maskelynite: Amer. Mineral., v. 52, p. 244-253.

Camargo Zanoguera, A., and Quezada Muñeton, J., 1992, Analysis of economic geology of areas of the Gulf of Mexico with hydrocarbon potential: Boletín Asociación Géologos Petroleros, v. XLI, p. 1-32 (in Spanish).

Carpenter, B. N., and Carlson, R., 1992, The Ames impact crater: Oklahoma Geol. Survey, v. 52, p. 208-223.

Carter, N. L., 1965, Basal quartz deformation lamellae—a criterion for recognition of impactites: Amer. Jour. Sci., v. 263, p. 786-806.

———, 1968, Dynamic deformation of quartz, *in* French, B. M., and Short, N. M., eds., Shock metamorphism of natural materials: Baltimore, Mono Book Corp., p. 453-474.

Castaño, J. R., Clement, J. H., Kuykendall, M. D., and Sharpton, V. L., 1994, Source rock potential of impact craters [abs.]: AAPG Ann. Convention, p. 118.

Chai, G., and Eckstrand, O. R., 1993, Origin of the Sudbury Igneous Complex, Ontario—differentiate of two separate magmas: Canada Geol. Survey Spec. Paper 93-1E, p. 219-230.

Chai, G., Eckstrand, O. R., and Gregoire, C., 1993, Platinum group element concentrations in the Sudbury rocks, Ontario—an indication of petrogenesis: Canada Geol. Survey Spec. Paper 93-1C, p. 287-293.

Chao, E. C. T., 1968, Pressure and temperature histories of impact metamorphosed rocks—based on petrographic observations, *in* French, B. M., and Short, N. M., eds., Shock metamorphism of natural materials: Baltimore, Mono Book Corp., p. 135-158.

Clement, J. H., and Mayhew, T. E., 1979, Newporte discovery opens new pay: Oil and Gas Jour., v. 77, p. 165-172.

Collins, F. R., 1961, Core test and test wells, Barrow area, Alaska: U. S. Geol. Survey Prof. Paper 305-K, p. 569-644.

Cowan, E. J., and Schwerdtner, W. M., 1994, Fold origin of the Sudbury Basin, *in* Lightfoot, P. C., and Naldrett, A. J., eds., Proceedings of the Sudbury-Noril'sk Symposium, Ontario Geol. Survey Spec. Vol. 5: Toronto, Ministry of Northern Development and Mines, p. 45-55.

Croft, S. K., 1980, Cratering flow fields: Implications for the excavation and transient expansion stages of crater formation: Proc. 11th Lunar Planet. Sci. Conf., p. 2347-2378.

Cymbal, S. N., and Polkanov, Yu. A., 1975, Mineralogy of titanium-zirconium placers of Ukraine: Kiev, Nauka Press, 247 p. (in Russian)

Davidson, C. F., 1955, The mineralization of the Witwatersrand: Mineralog. Mag., v. 92, p. 152-156.

Davies, J. F., Leroux, M. V., Whitehead, R. E., and Goodfellow, W. D., 1990, Oxygen-isotope composition and temperature of fluids involved in deposition of Proterozoic sedex deposits, Sudbury Basin, Ontario: Can. Jour. Earth Sci., v. 27, p. 1299-1303.

Dence, M. R., 1972, The nature and significance of terrestrial impact structures: 24th Internat. Geol. Congr., Montreal, 1972, p. 77-89.

Dence, M. R., Grieve, R. A. F., and Robertson, P. B., 1977, Terrestrial impact structures: Principal characteristics and energy considerations, *in* Roddy, D. J., Pepin, R. O., and Merrill, R. B., eds., Impact and explosion cratering: New York, Pergamon Press, p. 247-275.

Deutsch, A., 1994, Isotope systematics support the impact origin of the Sudbury Structure: Geol. Soc. Amer. Spec. Paper (in press).

Deutsch, A., and Grieve, R. A. F., 1994, The Sudbury Structure: Constraints on its genesis from the probe results: Geophys. Res. Letters, v. 21, p. 963-966.

Deutsch, A., Lakomy, R., and Buhl, D., 1989, Strontium- and neodymium-isotopic characteristics of a heterolitic breccia in the basement of the Sudbury impact structure, Canada: Earth Planet. Sci. Lett., v. 93, p. 359-370.

Dickin, A. P., Richardson, J. M., Crocket, J. H., McNutt, R. H., and Peredery, W. V., 1992, Osmium isotope evidence for a crustal origin of platinum group elements in the Sudbury nickel ore, Ontario, Canada: Geochim. et Cosmochim. Acta, v. 56, p. 3531-3537.

Dietz, R. S., 1961, Vredefort ring structure: Meteorite impact scar?: Jour. Geology, v. 69, p. 499-516.

———, 1964, Sudbury Structure as an astrobleme: Jour. Geology, v. 72, p. 412-434.

———, 1968, Shatter cones in cryptoexplosion structures, *in* French, B. M., and Short, N. M., eds., Shock metamorphism of natural materials: Baltimore, Mono Book Corp., p. 267-285.

———, 1972, Shatter cones (shock fractures) in astroblemes: 24th Internat. Geol. Cong., Montreal, 1972, p. 112-118.

Donofrio, R. R., 1981, Impact craters: Implications for basement hydrocarbon production: Jour. Petrol. Geol., v. 3, p. 279-302.

Dressler, B. O., Morrison, G. G., Peredery, W. V., and Rao, B. V., 1987, The Sudbury Structure, Ontario, Canada—a review, *in* Pohl, J., ed., Research in Terrestrial Impact Structures: Braunschweig/Wiesbad, Friedrich Vieweg und Sohn, p. 39-68.

Elston, W. E., 1992, Does the Bushveld-Vredefort system (South Africa) record the largest known terrestrial impact catastrophe? [abs.]: Inter. Conf. Large Meteorite Impacts Planetary Evolution, LPI Contrib. No. 790, p. 23-24.

Elston, W. E., and Twist, D., 1986, Bushveld Complex, South Africa: Is the Rooiberg Felsite an impactite? [abs.]: Lunar Planet. Sci., v. XVII, p. 204-205.

Ezerskii, V. A., 1982, Impact-metamorphosed carbonaceous matter in impactites: Meteoritika, v. 41, p. 134-140 (in Russian).

Faggart, B. E., Jr., Basu, A. R., and Tatsumoto, M., 1985, Origin of the Sudbury complex by meteoritic impact: Neodymium isotopic evidence: Science, v. 230, p. 436-439.

Frimmel, H. E., Le Roex, A. P., Knight, J., and Minter, W. E. L., 1993, A case study of the post depositional alteration of the Witwatersrand basal reef gold placer: Econ. Geol., v. 88, p. 249-265.

French, B. M., 1968, Sudbury Structure, Ontario: Some petrographic evidence for an origin by meteorite impact, *in* French, B. M., and Short, N. M., eds., Shock metamorphism of natural materials: Baltimore, Mono Book Corp., p. 383-412.

———, 1970, Possible relations between meteorite impact and igneous petrogenesis, as indicated by the Sudbury Structure, Ontario, Canada: Bull. Volcanologique, v. XXXIV-2, p. 466-517.

———, 1990, Absence of shock-metamorphic effects in the Bushveld complex, South Africa: Results of an intensive search: Tectonophysics, v. 171, p. 287-301.

French, B. M., and Nielsen, R. L., 1990, Vredefort bronzite granophyre: Chemical evidence for origin as a meteorite impact melt: Tectonophysics, v. 171, p. 119-138.

French, B. M., and Short, N. M., eds., 1968, Shock metamorphism of natural materials: Baltimore, Mono Book Corp., 644 p.

Galimov, E. M., Ivanovskaya, I. N., Klyuyev, Yu. A., Nepsha, V. I., Yepishina, N. I., Plotnikova, S. P., Galyulina, O. I., Poberezhskiy, V. A., Gritsik, V. V., and Koptil, V. A., 1980, Isotopic composition and peculiarities of crystalline structure of natural diamond polycrystals with lonsdaleite: Geokhimiya, no. 4, p. 533-539 (in Russian).

Gault, D. E., Quaide, W. L., and Oberbeck, V. R., 1968, Impact cratering mechanics and structures, *in* French, B. M., and Short, N. M., eds., Shock metamorphism of natural materials: Baltimore, Mono Book Corp., p. 87-99.

Gerhard, L. C., Anderson, S. B., Lefever, J. A., and Carlson, C. G., 1982, Geological development, origin, and energy mineral resources of Williston Basin, North Dakota: Amer. Assoc. Petrol. Geol. Bull. v. 66, p. 989-1020.

Giblin, P. E., 1984, Glossary, *in* Pye, E. G., Naldrett, A. J., and Giblin, P. E., eds., The geology and ore deposits of the Sudbury Structure, Ontario Geol. Survey Spec. Vol. 1: Toronto, Ministry Nat. Res., p. 571-574.

Gibson, R. L., Reimold, W. U., Wallmach, Th., and Colliston, W. P., 1994, A reappraisal of metamorphism in the Vredefort Dome, South Africa and its implications for the origin and evolution of the dome [abs.]: 25th Lunar Planet. Sci. Conf., p. 423-424.

Giusti, L., Hallbauer, D. K., Allsopp, H. L., Evans, L. B., and Welke, H. J., 1986, Dating and isotopic characterization of components of Witwatersrand conglomerates and possible source rocks [ext. abs.]: Geocongress '86, Johannesburg, South Africa, Trans. Geol. Soc., p. 123-128.

Gold, T., 1988, The deep earth gas theory with respect to the results from the Gravberg-1 well, *in* Bodén, A., and Eriksson, K. G., eds., Deep drilling in crystalline bedrock: Berlin, Springer-Verlag, v. 1, p. 18-27.

Goltrant, O., Leroux, H., Doukhan, J.-C., and Cordier, P., 1992, Formation mechanisms of planar deformation features in naturally shocked quartz: Physics Earth Planet. Interiors, v. 74, p. 219-240.

Gorter, J. D., Gostin, V. A., and Plummer, P. S., 1989, The enigmatic sub-surface Tookoonooka complex in south-west Queensland: Its impact origin and implications for hydrocarbon accumulations, *in* O'Neil, B. J., ed., The Cooper and Eromanga basins, Australia: Adelaide, Petrol. Explor. Soc. Australia, Soc. Petrol. Eng., Australian Soc. Explor. Geophysicists, p. 441-456.

Graton, L. C., 1930, Hydrothermal origin of the Rand gold deposits, part 1: Econ. Geol., v. 25, supp., no. 3, 185 p.

Grieve, R. A. F., 1984, The impact cratering rate in recent time: Jour. Geophys. Res., supp., v. 89, p. B403-B408.

———, 1988, The formation of large impact structures and constraints on the nature of Siljan, *in* Bodén, A., and Eriksson, K. G., eds., Deep drilling in crystalline bedrock: Berlin, Springer-Verlag, v. 1, p. 328-348.

———, 1991, Terrestrial impact: The record in the rocks: Meteoritics, v. 26, p. 175-194.

———, 1994, An impact model of the Sudbury Structure, Ontario, *in* Lightfoot, P. C., and Naldrett, A. J., eds., Proceedings of the Sudbury-Noril'sk Symposium, Ontario Geol. Survey Spec. Vol. 5: Toronto, Ministry Northern Development and Mines, p. 119-132.

Grieve, R. A. F., and Garvin, J. B., 1984, A geometric model for excavation and modification at terrestrial simple impact craters: Jour. Geophys. Res., v. 89, p. 11,561-11,572.

Grieve, R. A. F., and Head, J. W., 1983, The Manicouagan impact structure: An analysis of its original dimensions and form: Jour. Geophys. Res., supp., v. 88, p. A807-A818.

Grieve, R. A. F., Dence, M. R., and Robertson, P. B., 1977, Cratering processes: As interpreted from the occurrence of impact melts, *in* Roddy, D. J., Pepin, R. O., and Merrill, R. B., eds., Impact and explosion cratering: New York, Pergamon Press, p. 791-814.

Grieve, R. A. F., Robertson, P. B., and Dence, M. R., 1981, Constraints on the formation of ring impact structures, based on terrestrial data, *in* Schultz, P. H., and Merrill, R. B., eds., Multi-ring basins: New York, Pergamon Press, p. 37-57.

Grieve, R. A. F., Garvin, J. B., Coderre, J. M., and Rupert, J., 1989, Test of a geometric model for the modification stage of simple impact crater development: Meteoritics, v. 24, p. 83-88.

Grieve, R. A. F., Coderre, J. M., Robertson, P. B., and Alexopoulos, J. S., 1990, Microscopic planar deformation features in quartz of the Vredefort structure: Anomalous but still suggestive of an impact origin: Tectonophysics, v. 171, p. 185-200.

Grieve, R. A. F., Stöffler, D., and Deutsch, A., 1991, The Sudbury Structure: Controversial or misunderstood?: Jour. Geophys. Res., v. 96, p. 22,753-22,764.

Grieve, R. A. F., and Cintala, M. J., 1992, An analysis of differential impact melt-crater scaling and implications for the terrestrial impact record: Meteoritics, v. 27, p. 526-538.

Grieve, R. A. F., and Shoemaker, E. M., 1994, The record of past impacts on Earth, *in* Gehrels, T., ed., Hazards due to comets and asteroids: Tucson, AZ, University of Arizona Press (in press).

Gudlaugsson, S. T., 1993, Large impact crater in the Barents Sea: Geology, v. 21, p. 291-294.

Gurov, E. P., and Gurova, E. P., 1991, Geological structure and composition of rocks in impact craters: Kiev, Nauka Press, 160 p. (in Russian).

Gurov, E. P., Melnychuk, E. V., Metalidi, S. V., Ryabenko, V. A., and Gurova, E. P., 1985, The characteristics of the geological structure of the eroded astrobleme in the western part of the Ukrainian Shield: Dopovidi Akad. Nauk Ukrainskoi Radyanskoi Sotsialisychnoi Respubliky, Seriya B, p. 8-11 (in Ukrainian).

Hamilton, W., 1970, Bushveld Complex—product of impacts?: Spec. Publ. Geol. Soc. S. Africa., v. 1, p. 367-379.

Hargraves, R. B., 1961, Shatter cones in the rocks of the Vredefort Ring: Trans. Proc. Geol. Soc. S. Africa, v. 64, p. 147-154.

Harper, C. T., 1982, Geology of the Carswell structure, central part: Saskatchewan Geol. Survey, Rept. 214, p. 1-6.

Hart, R. J., Welke, H. J., and Nicolaysen, L. O., 1981, Geochronology of the deep profile through Archean basement at Vredefort, with implication for early crustal evolution: Jour. Geophys. Res., v. 86, p. 10,663-10,680.

Hart, R. J., Andreoli, M. A. G., Reimold, W. U., and Tredoux, M., 1991, Aspects of the dynamic and thermal metamorphic history of the Vredefort cryptoexplosion structure: Implications for its origin: Tectonophysics, v. 192, p. 313-331.

Herring, B. G., 1976, The metamorphism and alteration of the basement rocks in the Carswell circular structure, Saskatchewan: M. Sc. thesis, Univ. British Columbia, unpub., 134 p.

Heyl, A. V., and Brock, M. R., 1962, Zinc occurrence in the Serpent Mound structure of Southern Ohio: U. S. Geol. Survey Prof. Paper 450-D, p. D95-D97.

Hildebrand, A. R., Penfield, G. T., Kring, D. A., Pilkington, M., Camargo, A. Z., Jacobsen, S. B., and Boynton, W. V., 1991, Chicxulub Crater: A possible Cretaceous/Tertiary boundary impact crater on the Yucatan Peninsula, Mexico: Geology, v. 19, p. 867-871.

Hirt, A. M., Lowrie, W., Clendenen, W. S., and Kligfield, R., 1993, Correlation of strain and the anisotropy of magnetic susceptibility in the Onaping Formation: Evidence for a near-circular origin of the Sudbury Basin: Tectonophysics, v. 225, p. 231-254.

Holland, M. J., Stanistreet, I. G., and McCarthy, T. S., 1990, Tectonic control on the deposition of the Turffontein Subgroup around the Vredefort Dome: South African Jour. Geol., v. 93, p. 158-168.

Hörz, F., 1968, Statistical measurements of deformation structures and refractive indices in experimentally shock loaded quartz, *in* French, B. M., and Short, N. M., eds., Shock metamorphism of natural materials: Baltimore, Mono Book Corp., p. 243-253.

Hörz, F., and Quaide, W. L., 1973, Debye-Scherrer investigations of experimentally shocked silicates: The Moon, v. 6, p. 45-82.

Isaac, J. H., and Stewart, R. R., 1993, 3D seismic characterization of possible meteorite impact structure [abs.]: Canadian Geophys. Union, Program and Abstracts, p. 28.

Ivanov, B. A., 1994, Geochemical models of impact cratering: Geol. Soc. America Spec. Paper (in press).

Jahn, B., Floran, R. J., and Simonds, C. H., 1978, Rb-Sr isochron age of the Manicouagan melt sheet, Quebec, Canada: Jour. Geophys. Res., v. 83, p. 2799-2803.

Jansa, L. F., Pe-Piper, G., Robertson, P. B., and Freidenreich, O., 1989, Montagnais: A submarine impact structure on the Scotian Shelf, eastern Canada: Geol. Soc. Amer. Bull., v. 101, p. 450-463.

Johansson, A., 1984, Geochemical studies on the Boda Pb-Zn deposit in the Siljan astrobleme, central Sweden: Geol. Fören. I Stockholm Förh., v. 106, p. 15-25.

Kagi, H., Takahashi, K., Hidaka, H., and Masuda, A., 1994, Chemical properties of Central African carbonado and its genetic implications: Geochim. Cosmochim. Acta, v. 58, p. 2629-2638.

Kaminskiy, F. V., 1987, Genesis of carbonado; polycrystalline aggregate of diamond: Doklady Akad. Nauk SSSR, v. 291, p. 439-440 (in Russian).

Kaminskiy, F. V., Galimov, E. M., Ivanovskaya, I. N., Kirilitsa, S. I., and Polkanov, Yu. A., 1977, Isotopic distribution in carbon of small diamonds from Ukraine: Doklady Akad. Nauk SSSR, Earth Sciences Sec., v. 236, p. 174-175 (in Russian).

Kaminskiy, F. V., Klyuyev, Yu. A., Prokopchuk, B. I., Shckeka, S. A., Smirnov, V. I., and Ivanovskaya, I. N., 1978, First carbonado and new ballas find in the Soviet Union: Doklady Akad. Nauk SSSR, Earth Sciences Sec., v. 242, p. 152-155 (in Russian).

Killick, A. M., and Reimold, W. U., 1990, Review of the pseudotachylites in and around the Vredefort 'dome,' South Africa: South African Jour Geol., v. 93, p. 350-365.

Kilsgaard, T. H., Heyl, A. V., and Brock, M. R., 1962, The Crooked Creek disturbance, southeast Missouri: U. S. Geol. Survey Prof. Paper 450-E, p. E14-E19.

Kirschner, C. E., Grantz, A., and Mullen, M. W., 1992, Impact origin of the Avak structure, Arctic Alaska, and genesis of the Barrow gas fields: Amer. Assoc. Petrol. Geol. Bull., v. 76, p. 651-679.

Krogh, T. E., Davis, D. W., and Corfu, F., 1984, Precise U-Pb zircon and baddeleyite ages for the Sudbury area, *in* Pye, E. G., Naldrett, A. J., and Giblin, P. E., eds., The geology and ore deposits of the Sudbury Structure, Ontario Geol. Surv. Spec. Vol. 1: Toronto, Ministry of Natural Resources, p. 431-446.

Krogh, T. W., McNutt, R. H., and Davis, G. L., 1982, Two high-precision U-Pb zircon ages for the Sudbury nickel irruptive: Can. Jour. Earth Sci., v. 19, p. 723-728.

Kuykendall, M. D., Johnson, C. L., and Carlson, R. A., 1994, Reservoir characterization of a complex impact crater: "Ames Crater," Northern Shelf, Anadarko Basin [abs.]: AAPG Ann. Convention, p. 191.

Lainé, R., Alonso, D., and Svab, M., eds., 1985, The Carswell Structure uranium deposits, Saskatchewan: Geol. Assoc. of Canada Spec. Paper 29: Toronto, Geological Assoc. Canada, 230 p.

Lakomy, R., 1990, Implications of cratering mechanics from a study of the Footwall Breccia at the Sudbury impact structure, Canada: Meteoritics, v. 25, p. 195-200.

Lambert, P., 1981, Breccia dikes: Geological constraints on the formation of complex craters, *in* Schultz, P. H., and Merrill, R. B., eds., Multi-ring basins: New York, Pergamon Press, p. 59-78.

Lantz, R., 1981, Barrow gas fields—N. Slope, Alaska: Oil and Gas Jour., v. 79, p. 197-200.

Leroux, H., Reimold, W. U., and Doukhan, J.-C., 1994, A TEM investigation of shock metamorphism in quartz from the Vredefort Dome, South Africa: Tectonophysics, v. 230, p. 223-239.

Lightfoot, P. C., and Naldrett, A. J., eds., 1994, Proceedings of the Sudbury-Noril'sk Symposium, Ontario Geological Survey Spec. Vol. 5: Toronto, Ministry Northern Development and Mines, 423 p.

Lilly, P. A., 1981, Shock metamorphism in the Vredefort collar: Evidence for internal shock sources: Jour. Geophys. Res., v. 86, p. 10,689-10,700.

Limon, M., Cedillo, E., Quezada, J. M., Grajales, J. M., Alvarez, W., Hildebrand, A. R., Sanchez, M. A., Rosales, C., and Gonzalez, V., 1994, Cretaceous-Tertiary boundary sedimentary breccias from southern Mexico: Normal sedimentary deposits or impact-related breccias? [abs.]: AAPG Ann. Convention, p. 199.

Lowman, P. D., 1992, The Sudbury structure as a terrestrial mare basin: Rev. Geophys., v. 30, p. 227-243.

McCarthy, T. S., Charlesworth, E. G., and Stanistreet, I. G., 1986, Post-Transvaal structural features of the northern portion of the Witwatersrand Basin: South Africa Trans. Geol. Soc., v. 89, p. 311-324.

McCarthy, T. S., Stanistreet, I. G., and Robb, L. J., 1990, Geological studies related to the origin of the Witwatersrand Basin and its mineralization—an introduction and a strategy for research and exploration: South African Jour. Geol., v. 93, p. 1-4.

Manton, W. I., 1965, The orientation and origin of shatter cones in the Vredefort Ring: New York Acad. Sci. Annals, v. 123, p. 1017-1049.

Martini, J. E. J., 1978, Coesite and stishovite in the Vredefort Dome, South Africa: Nature, v. 272, p. 715-717.

———, 1991, The nature, distribution and genesis of the coesite and stishovite associated with the pseudotachylite of the Vredefort Dome, South Africa: Earth Planet. Sci. Lett., v. 103, p. 285-300.

———, 1992, The metamorphic history of the Vredefort Dome at approximately 2 Ga as revealed by coesite-stishovite-bearing pseudotachylites: Jour. Metamorphic Geol., v. 10, p. 517-527.

Marvin, U. B., 1990, Impact and its revolutionary implications for geology: Geol. Soc. America, Spec. Paper 247, p. 147-154.

Masaitis, V. L., 1989, The economic geology of impact craters: Int. Geol. Rev., v. 31, p. 922-933.

———, 1992, Impact craters: Are they useful?: Meteoritics, v. 27, p. 21-27.

———, 1993a, Diamantiferous impactites, their distribution and petrogenesis: Regional Geology and Metallogeny, v. 1, p. 121-134 (in Russian).

———, 1993b, Origin of the Sudbury Structure in the light of new petrographic, mineralogical and geochemical data: Zapiski Vserossiyskogo Mineralogicheskogo Obshchestva, v. 122, p. 1-17 (in Russian).

Masaitis, V. L., Futergendler, S. I., and Gnevushev, M. A., 1972, Diamonds in impactites of the Popigay meteorite crater: Zapiski Vsesoyuznogo Mineralogicheskogo Obshchestva, v. 101, p. 108-112 (in Russian).

Masaitis, V. L., Danilin, A. I., Mashchak, M. S., Raikhlin, A. I., Selivanovskaya, T. V., and Shadenkov, E. M., 1980, The geology of astroblemes: Leningrad, Nedra Press, 231 p. (in Russian).

Masaitis, V. L., Shafranovsky, G. I., Ezersky, V. A., and Reshetnyak, N. B., 1990, Impact diamonds from ureilites and impactites: Meteoritika, v. 49, p. 180-195 (in Russian).

Melosh, H. J., 1989, Impact cratering: A geologic process: New York, Oxford Univ. Press, 245 p.

Milkereit, B., Green, A., and Sudbury Working Group, 1992, Deep geometry of the Sudbury Structure from seismic reflection profiling: Geology, v. 20, p. 807-811.

Milstein, R. L., 1988, The Calvin 28 structure: Evidence for impact origin: Can. Jour. Earth Sci., v. 25, p. 1524-1530.

Milton, D. J., 1977, Shatter cones—an outstanding problem in shock mechanics, *in* Roddy, D. J., Pepin, R. O., and Merrill, R. B., eds., Impact and explosion cratering: New York, Pergamon Press, p. 703-714.

Morrison, G. G., 1984, Morphological features of the Sudbury Structure in relation to an impact origin, *in* Pye, E. G., Naldrett, A. J., and Giblin, P. E., eds., The geology and ore deposits of the Sudbury Structure, Ontario Geol. Survey Spec. Vol. 1: Toronto, Ministry of Natural Resources, p. 513-520.

Morrison, G. G., Jago, B. C., and White, T. L., 1994, *in* Lightfoot, P. C., and Naldrett, A. J., eds., Footwall

mineralization of the Sudbury Igneous Complex: Proceedings of the Sudbury-Noril'sk Symposium, Ontario Geol. Survey Spec. Vol. 5: Toronto, Ministry of Northern Development and Mines, p. 57–64.

Müller-Mohr, V., 1992, Breccias in the basement of a deeply eroded impact structure, Sudbury, Canada: Tectonophysics, v. 216, p. 219–226.

Myers, R. E., McCarthy, T. S., and Stanistreet, I. G., 1990, A tectono-sedimentary reconstruction of the development and evolution of the Witwatersrand Basin, with particular emphasis on the Central Rand Group: South African Jour. Geol., v. 93, p. 180–201.

Naldrett, A. J., 1984, Mineralogy and composition of the Sudbury ores, *in* Pye, E. G., Naldrett, A. J., and Giblin, P. E., eds., The geology and ore deposits of the Sudbury Structure, Ontario Geol. Survey Spec. Vol. 1: Toronto, Ministry of Natural Resources, p. 309–325.

Naldrett, A. J., and Hewins, R. H., 1984, The main mass of the Sudbury Igneous Complex, *in* Naldrett, A. J., Hewins, R. H., and Giblin, P. E., eds., The geology and ore deposits of the Sudbury Structure, Ontario Geol. Survey Spec. Vol. 1: Toronto, Ministry of Natural Resources, p. 235–251.

Naldrett, A. J., Innes, D. G., Sowa, J., and Gorton, M., 1982, Compositional variation within and between five Sudbury ore deposits: Econ. Geol., v. 77, p. 1519–1534.

Naldrett, A. J., Hewins, R. H., Dressler, B. O., and Rao, B. V., 1984, The contact sublayer of the Sudbury Igneous Complex, *in* Pye, E. G., Naldrett, A. J., and Giblin, P. E., eds., The geology and ore deposits of the Sudbury Structure, Ontario Geol. Survey Spec. Vol. 1: Toronto, Ministry of Natural Resources, p. 253–274.

Nicolaysen, L. O., and Ferguson, J., 1990, Cryptoexplosion structures, shock deformation and siderophile concentration related to explosive venting of fluids associated with alkaline ultramafic magmas: Tectonophysics, v. 171, p. 303–335.

Nicolaysen, L. O., and Reimold, W. U., eds., 1990, Cryptoexplosions and catastrophes in the geological record, with a special focus on the Vredefort structure: Tectonophysics, v. 171, 422 p.

Nikolskiy, A. P., 1991, Geology of Pervomaysk iron-ore deposit and transformation of its structure by meteoritic impact: Moscow, Nedra Press, 71 p. (in Russian).

Nikolskiy, A. P., Naumov, V. P., and Korobko, N. I., 1981, Pervomaysk iron deposit, Krivoy Rog, and its transformations by shock metamorphism: Geologia rudnykh mestorozhdeniy, v. 5, p. 92–105 (in Russian).

Nikolskiy, A. P., Naumov, V. P., Mashchak, M. S., and Masaitis, V. L., 1982, Shock metamorphosed rocks and impactites of Ternovka astrobleme: Trans. VSEGEI, v. 238, p. 132–142 (in Russian).

Ozima, M., Zashu, S., Tomura, K., and Matsuhisa, Y., 1991, Constraints from noble-gas contents on the origin of carbonado diamonds: Nature, v. 351, p. 472–474.

Pagel, M., and Svab, M., 1985, Petrographic and geochemical variations within the Carswell structure metamorphic core and their implications with respect to uranium mineralization: Geol. Assoc. Canada, Spec. Paper 29, p. 55–70.

Palme, H., 1982, Identification of projectiles of large terrestrial impact craters and some implications for the interpretation of Ir-rich Cretaceous/Tertiary boundary layers: Geol. Soc. Amer. Spec. Paper 190, p. 223–233.

Palme, H., Grieve, R. A. F., and Wolf, R., 1981, Identification of the projectile at Brent crater, and further considerations of projectile types at terrestrial craters: Geochim. et Cosmochim. Acta, v. 45, p. 2417–2424.

Peredery, W. V., 1972, Chemistry of fluidal glasses and melt bodies in the Onaping Formation: Geol. Assoc. Canada, Spec. Paper 10, p. 49–59.

Peredery, W. V., and Morrison, G. G., 1984, Discussion of the origin of the Sudbury Structure, *in* Pye, E. G., Naldrett, A. J., and Giblin, P. E., eds., The geology and ore deposits of the Sudbury Structure, Ontario Survey Spec. Vol. 1: Toronto, Ministry of Natural Resources, p. 491–511.

Phillips, G. N., Law, J. D. M., and Meyers, R. E., 1990, The role of fluids in the evolution of the Witwatersrand Basin: South African Jour. Geol., v. 93, p. 54–69.

Phinney, W. C., and Simonds, C. H., 1977, Dynamical implications of the petrology and distribution of impact melt rocks, *in* Roddy, D. J., Pepin, R. O., and Merrill, R. B., eds., Impact and explosion cratering: New York, Pergamon Press, p. 771–790.

Pickard, C. F., 1994, Twenty years of production from an impact structure, Red Wing Creek field, McKenzie County, North Dakota [abs.]: AAPG Ann. Convention, p. 234.

Pike, R. J., 1977, Size-dependence in the shape of fresh impact craters on the moon, *in* Roddy, D. J., Pepin, R. O., and Merrill, R. B., eds., Impact and explosion cratering: New York, Pergamon Press, p. 489–509.

———, 1980, Control of crater morphology by gravity and target type: Mars, earth, moon: Proc. 11th Lunar Planetary Sci. Conf., p. 2159–2189.

Pilkington, M., and Grieve, R. A. F., 1992, The geophysical signature of terrestrial impact craters: Rev. Geophys., v. 30, p. 161–181.

Pope, K. O., Ocampo, A. C., and Dullen, C. E., 1991, Hydrological evidence for a possible 200 km diameter K/T impact crater in Yucatan, Mexico [abs.]: Proc. 22nd Lunar Planet. Sci. Conf., p. 1083–1084.

Pretorius, D. A., 1976, The nature of the Witwatersrand gold-uranium deposits, *in* Wolf, K. H., ed., Handbook of strata-bound and stratiform ore deposits: New York, Elsevier, p. 29–88.

———, 1986a, The gold fields of the Witwatersrand Basin, *in* Anhaeusser, C. R., and Maske, S., eds., Mineral deposits of southern Africa, v. 1: Johannesburg, Geol. Soc. South Africa, p. 489–493.

———, 1986b, Witwatersrand gold: The men, the money, the mineralization [ext. abs.]: Geocongress '86, Johannesburg, South Africa Trans. Geol. Soc., p. 1–4.

Pye, E. G., Naldrett, A. J., and Giblin, P. E., eds., 1984, The geology and ore deposits of the Sudbury Structure, Ontario Geol. Survey Spec. Vol. 1: Toronto, Ministry of Natural Resources, 604 p.

Reimold, W. U., 1990, The controversial microdeformations in quartz from the Vredefort Structure, South Africa—a discussion: South Africa, Jour. Geol., v. 93, p. 645–663.

———, 1994, Hydrothermal Witwatersrand gold mineralisation caused by the Vredefort mega-impact event [abs.]: New developments regrading the KT event and other catastrophes in earth history, LPI Contrib. 825, p. 92–93.

Reimold, W. U., Stephan, T., and Jessburger, E. K., 1992, Testing younger than 2 Ga ^{40}Ar-^{39}Ar ages for pseudotachylite from the Vredefort structure: South African Jour. Sci., v. 88, p. 563–573.

Rhodes, R. C., 1975, New evidence for impact origin of the Bushveld Complex, South Africa: Geology, v. 3, p. 549–554.

Robb, L. J., Meyer, F. M., Ferraz, M. F., and Drennan, G. R., 1990, The distribution of radioelements in Archean granites of the Kaapvaal Craton, with implications for the source of uranium in the Witwatersrand Basin: South African Jour. Geology, v. 93, p. 5–40.

Roberts, C., and Sandridge, B., 1992, The Ames hole: Shale Shaker, v. 42, p. 118–121.

Robertson, P. B., Dence, M. R., and Vos, M. A., 1968, Deformation in rock-forming minerals from Canadian craters, *in* French, B. M., and Short, N. M., eds., Shock metamorphism of natural materials: Baltimore, Mono Book Corp., p. 433–452.

Robertson, P. B., and Grieve, R. A. F., 1977, Shock attenuation at terrestrial impact structures, *in* Roddy, D. J., Pepin, R. O., and Merrill, R. B., eds., Impact and explosion cratering: New York, Pergamon Press, p. 687–702.

Roddy, D. J., and Davis, L. K., 1977, Shatter cones formed in large-scale experimental explosion craters, *in* Roddy, D. J., Pepin, R. O., and Merrill, R. B., eds., Impact and explosion cratering: New York, Pergamon Press, p. 715–750.

Roddy, D. J., Pepin, R. O., and Merrill, R. B., eds., 1977, Impact and explosion cratering: New York, Pergamon Press, 1301 p.

Roest, W. R., and Pilkington, M., 1994, Restoring post-impact deformation at Sudbury: A circular argument: Geophys. Res. Lett., v. 21, p. 959–962.

Rondot, J., 1972, Geology of the Charlevoix structure: 24th Internat. Geol. Cong., Montreal, p. 140–147 (in French).

———, 1975, Comparison of the astroblemes of Siljan, Sweden, and Charlevoix, Quebec: Bull. Geol. Instit. Univ. Uppsala v. 6, p. 85–92 (in French).

Rousell, D. H., 1984, Mineralization in the Whitewater group, *in* Pye, E. G., Naldrett, A. J., and Giblin, P. E., eds., The geology and ore deposits of the Sudbury Structure, Ontario Geol. Survey Spec. Vol. 1: Toronto, Ministry of Natural Resources, p. 219–232.

Ruhlmann, F., 1985, Mineralogy and metallogeny of uraniferous occurrences in the Carswell structure: Geol. Assoc. Canada Spec. Paper 29, p. 105–120.

Rundle, C. C., and Snelling, N. J., 1977, The geochronology of uraniferous minerals in the Witwatersrand Triad: An interpretation of new and existing U-Pb age data on rocks and minerals of the Dominion Reef: Royal Soc. [London] Philos. Trans., A286, p. 567–583.

Saul, J. M., 1978, Circular structures of large scale and great age on the Earth's surface: Nature, v. 271, p. 345–349.

Sawatzky, H. B., 1977, Buried impact craters in the Williston Basin and adjacent area, *in* Roddy, D. J., Pepin, R. O., and Merrill, R. B., eds., Impact and explosion cratering: New York, Pergamon Press, p. 461–480.

———, 1974, Astroblemes in the Williston Basin: Jour. Can. Soc. Explorat. Geophys., v. 10, p. 23–38.

Schmidt, R. M., 1980, Meteor Crater: Energy of formation-implications of centrifuge scaling [abs]: Proc. 11th Lunar Planet. Sci. Conf., p. 2099–2128.

Schreyer, W., 1983, Metamorphism and fluid inclusions in the basement of the Vredefort Dome, S. Africa: Guidelines to the origin of the structure: Jour. Petrol., v. 24, p. 26–47.

Schultz, P. H., and Merrill, R. B., eds., 1981, Multi-ring basins: New York, Pergamon Press, 295 p.

Shand, S. J., 1916, The pseudotachylite of Parijs (Orange Free State), and its relation to "trap-shotten gneiss" and "flinty crush rock": Geol. Soc. London Quart. Jour., v. 72, p. 198–221.

Shanks, W. S., and Schwerdtner, W. M., 1991a, Crude quantitative estimates of the original northwest-southeast dimension of the Sudbury Structure, south-central Canadian Shield: Can. Jour. Earth Sci., v. 28, p. 1677–1686.

———, 1991b, Structural analysis of the central and southwestern Sudbury Structure, Southern

Province, Canadian Shield: Can. Jour. Earth Sci., v. 28, p. 411–430.

Shibata, K., Kamioka, H., Kaminsky, K. F., Koptil, V., and Svisero, D., 1993, Rare earth patterns of carbonado and yakutite: Evidence for their crustal origin: Mineral. Mag., v. 57, p. 607–611.

Shoemaker, E. M., Wolfe, R. F., and Shoemaker, C. S., 1990, Asteroid and comet flux in the neighborhood of earth: Geol. Soc. America Spec. Paper 247, p. 150–170.

Simpson, C., 1977, A structural analysis of the rim synclinorium of the Vredefort Dome: M. Sc. Thesis, University of Witwatersrand, 257 p.

————, 1981, Occurrence and orientation of shatter cones in Pretoria Group quartzites in the collar of the Vredefort Dome: Impact origin precluded: Jour. Geophys. Res., v. 86, p. 10701–10706.

Smith, J. V., and Dawson, J. B., 1985, Carbonado: Diamond aggregates from early impacts of crustal rocks?: Geology, v. 13, p. 342–343.

Spray, J. G., Kelley, S. P., and Reimold, W. U., 1994, Laser-probe ^{40}Ar-^{39}Ar dating of stishovite- and coesite-bearing pseudotachylytes and the age of the Vredefort impact event: Meteoritics (in press).

Stanistreet, I. G., McCarthy, T. S., Charlesworth, E. G., Myers, R. E., and Armstrong, R. A., 1986, Pre-Transvaal wrench tectonics along the northern margin of the Witwatersrand Basin, South Africa: Tectonophysics, v. 131, p. 53–74.

Stöffler, D., 1972, Deformation and transformation of rock-forming minerals by natural and experimental shock processes. I. Behavior of minerals under shock compression: Fortschr. der Mineralogie, v. 49, p. 50–113.

————, 1974, Deformation and transformation of rock-forming minerals by natural and experimental shock processes. II. Physical properties of shocked minerals: Fortschr. der Mineralogie, v. 51, p. 256–289.

Stöffler, D., and Hornemann, U., 1972, Quartz and feldspar glasses produced by natural and experimental shock: Meteoritics, v. 7, p. 371–394.

Stöffler, D., and Langehorst, F., 1994, Shock metamorphism of quartz in nature and experiment: I. Basic observation and theory: Meteoritics, v. 29, p. 155–181.

Stöffler, D., Gault, D. E., Wedekind, F. J., and Polkowski, G., 1975, Experimental hypervelocity impact into quartz sand: Distribution and shock metamorphism of ejecta: Jour. Geophys. Res., v. 80, p. 4062–4077.

Stöffler, D., Bischoff, L., Oskierski, W., and Weist, B., 1988, Structural deformation, breccia formation, and shock metamorphism in the basement of complex terrestrial impact craters: Implications for the cratering process, *in* Bodén, A., and Eriksson, K. G., eds., Deep drilling in crystalline bedrock: Berlin, Springer-Verlag, v. 1, p. 277–297.

Stöffler, D., Avermann, M., Bischoff, L., Brockmeyer, P., Deutsch, A., Dressler, B. O., Lakomy, R., and Müller-Mohr, V., 1989, Sudbury, Canada: Remnant of the only multi-ring (?) impact basin on Earth [abs.]: Meteoritics, v. 24, p. 328.

Stöffler, D., Deutsch, A., Avermann, M., Bischoff, L., Brockmeyer, P., Buhl, D., Lakomy, R., and Müller-Mohr, V., 1994, The formation of the Sudbury Structure, Canada: Towards a unified impact model: Geol. Soc. Amer. Spec. Paper (in press).

Sutton, S. R., 1985, Thermoluminescence measurements on shock-metamorphosed sandstone and dolomite from Meteor Crater, Arizona. 2. Thermoluminescence age of Meteor crater: Jour. Geophys. Res., v. 90, p. 3690–3700.

Therriault, A. M., Reid, A. M., and Reimold, W. U., 1993, Original size of the Vredefort Structure, South Africa [abs.]: Proc. 24th Lunar and Planetary Sci. Conf., p. 1419–1420.

Tona, F., Alonso, D., and Svab, M., 1985, Geology and mineralization in the Carswell structure—a general approach: Geol. Assoc. Canada, Spec. Paper 29, p. 1–18.

Tooth, J., and Stewart, R. R., 1994, The Steen River structure, Alberta: Geology and oil production [abs.]: AAPG Annual Convention, p. 272.

Trieloff, M., Kunz, J., Jessbburger, E. K., Reimold, W. U., Boer, R. H., and Jackson, E. K., 1992, ^{40}Ar-^{39}Ar dating of pseudotachylites from the Witwatersrand Basin, South Africa, with implications for the formation of the Vredefort Dome [abs.]: Inter. Conf. Large Meteorite Impacts Planetary Evolution, LPI Contrib. No. 790, p. 75–77.

Trueb, L. F., and de Wys, E. C., 1971, Carbon from Ubangi-A microstructural study: Am. Mineralogists, v. 56, p. 1252–1268.

Tschermak, G., 1872, The Shergotty and Gopalpur meteorites: Akad. Wiss. Wien. Math.-Naturwiss. Kl., v. 165, p. 122–145 (in German).

Turnovec, I., 1987, Use of moldavites in jewel production, *in* Konta, J., ed., Second International Conference in Natural Glasses: Prague, Charles Univ., p. 323–330.

Turnovec, I., and Seveik, J., 1987, Exploitation of moldavites, *in* Konta, J., ed., Second International Conference on Natural Glasses: Prague, Charles Univ., p. 313–318.

Val'ter, A. A., 1988, Geochemical features of the meteoritic material in the impactites of the Terny astrobleme, *in* The composition and origin of meterorites: p. 85–92 (in Russian).

Val'ter, A. A., Yeremenko, G. K., Kwasnitsa, V. N., and Polkanov, Yu. A., 1992, Shock metamorphosed carbon minerals: Kiev, Nauka Press, 171 p. (in Russian).

Val'ter, A. A., Rysbenko, V. A., and Kotlovskaya, F. I., 1981, The Ternovka Astrobleme: New and most deeply eroded meteorite crater on the Ukrainian shield: Doklady Akad. Nauk SSSR, v. 2, p. 3–7 (in Russian).

von Engelhardt, W., 1990, Distribution, petrography and shock metamorphism of the ejecta of the Ries crater in Germany—a review: Tectonophysics, v. 171, p. 259–273.

von Engelhardt, W., and Bertsch W., 1969, Shock induced planar deformation structures in quartz from the Ries Crater, Germany: Contrib. Mineral. Petrol., v. 20, p. 203–234.

Walker, R. J., Morgan, J. W., Naldrett, A. J., Li, C., and Fassett, J. D., 1991, Re-Os isotope systematics of Ni-Cr sulfide ores, Sudbury Igneous Complex, Ontario: Evidence for a major crustal component: Earth Planet. Sci. Lett., v. 105, p. 416–429.

Walraven, F., Armstrong, R. A., and Kruger, F. J., 1990, A chronostratigraphic framework for the north-central Kaapvaal craton, the Bushveld Complex, and the Vredefort structure: Tectonophysics, v. 171, p. 23–48.

White, J. C., 1993, Shock induced melting and silica polymorph formation, Vredefort Structure, South Africa, *in* Boland, J. A., and Fitz Gerald, J. D., eds., Defects and processes in solid state: Geoscience applications: New York, Elsevier, p. 69–84.

Winter, H. de la R., 1986, Cratonic foreland model for Witwatersrand Basin development in a continental back arc plate tectonic setting [ext. abs.]: Geocongress '86, Johannesburg, South Africa Trans. Geol. Soc., p. 75–80.

Witschard, F., 1984, Large-magnitude ring structures on the Baltic shield–metallogenic significance: Econ. Geol., v. 79, p. 1400–1405.

Wolf, R., Woodrow, A. B., and Grieve, R. A. F., 1980, Meteoritic material at four Canadian impact craters: Geochim. et Cosmochim. Acta, v. 44, p. 1015–1022.

Wood, C. A., and Head, J. W., 1976, Comparison of impact basins on Mercury, Mars and the moon: Proc. 7th Lunar Sci. Conf., p. 3629–3651.

Wu, J., Milkereit, B., and Boerner, D., 1994, Timing constraints on deformation history of the Sudbury impact structure: Can. Jour. Earth Sci. (in press).

Zeylik, B. S., and Seytmuratova, E. Yu., 1974, Giant meteorite-impact structure in central Kazakhstan and its magma- and ore-controlling significance: Doklady Akad. Nauk SSSR, v. 218, p. 167–170 (in Russian).

Zimmermann, R. A., and Amstutz, G. C., 1972, The Decaturville sulfide breccia—a Cambro-Ordovician mud volcano: Chemie der Erde, v. 17, p. 253–273.

ANNEXE V.A.

Boivin, L., 1990. Press Release: Manicouagan Crater - Ni/Cu Property

EXPLORATION
MINIÈRE
LA SARRE INC.

P R E S S R E L E A S E

MANICOUAGAN CRATER - NI/CU PROPERTY

December 11, 1990
Rouyn Noranda

Exploration Miniere LaSarre Inc. has mobilised a diamond drill onto the Manicouagan nickel-copper property situated at the center of a very large meteoritic impact site north of Baie Comeau.

The diamond drill program is designed to test a very strong elliptical magnetic anomaly of unknown source that is located in the dead center of the crater. Drill holes will also test the very strong and wide conductors located for the most part under the magnetic anomalies at relatively shallow depths of about 500 vertical feet. These conductors can be vertical or horizontal in nature, and their causes are also unknown.

The company has retained several geological models in its exploration strategy. Among these models is the well-known "Sudbury" model of mafic granitoid intrusions hosting basemetals that distinguishes the world class mining camp of Sudbury, the only other known site of meteoritic impact of similar proportions in the Western world. The company has designed other models to account for the geophysical signature witnessed on the property, and many of them are equally encouraging for economic metal mineralization.

The fact is that although much is conjectured about the nature of the phenomenom that Exploration Miniere LaSarre is about to drill, very little is known. The company will be the first to drill a hole in the center of a meteorite impact. For this reason, both the scientific community at large and explorationists in general are focusing on this project.

/2

15, rue Gamble Est
Bureau 102
Rouyn-Noranda
Quebec J9X 3B6
Tel.: 819 762-4364
Fax: 819 762-9090

Exploration Results to Date

The company completed linecutting in early summer. A helicopter-borne geophysical survey was carried out prior to field work, and geological prospecting and mapping on the property and surrounding ground was finished in August 1990.

A high-resolution magnetic map was produced, and no EMH conductors were found from the air survey. This was considered to be encouraging since the company did not expect to find any conductors above the survey-penetration level of 400 vertical feet. A second and third ground geophysical survey was carried out more recently using the GEOPROBE method to penetrate the crater's horizontal layers and locate conductors.

Results from this method are highly encouraging. The location of strong, wide conductors coincides with the conclusions of the field geologists who mapped and inspected the crater's geology during the summer. These conductors tend to begin at about 500 vertical feet under the surface, the same thickness estimated by the company geologists to cover the vertical basement rocks. The company predicts that mineralization of either intrusive, hydrothermal, or other origin will be found near this interface.

In accordance with the Sudbury model theory, company geologists wanted to determine whether, as in the case of Sudbury, the area was already a Ni/Cu metallogenic province before the meteorite impact, and also to determine whether younger mafic intrusions of sills or dykes apt to host these metals were present.

In both cases, company geologists confirmed the prescence of significant nickel/copper/platinoid mineralization in older pre-impact mafic rocks in the crater, and similar mineralization was also discovered in very young ultra-mafic dykes crosscutting older rocks in the crater. Owing to the lack of outcrops available on the LaSarre claims group, these encouraging results were discovered elsewhere in the crater during the course of the field work, but **Exploration Miniere LaSarre** believes that these results are promising and vindicate their interest in this project.

Some of the values obtained are as follows:

	Cu	Ni	Pd	Pt
Sample A:	0.67%	0.24%	2.3 gm/t	0.92 gm/t
Sample B:	0.90%	0.27%	2.3 gm/t	0.96 gm/t

Drill Program

About 10,000 feet of drilling have been planned in a total of 7 drill holes. Targets are mostly geophysical in nature, and the company expects to intersect the unexpected, i.e. new lithological units and environments.

Results from the first drill hole(s) are not expected to be available before January 1991. The drill will function until Dec. 19th, and will close down for the Christmas holidays until January 6th.

Lauri Boivin
Vice President Exploration
EXPLORATION MINIERE LASARRE INC.

ANNEXE V.B

Boivin, L., 1994. Information Letter on the Manicouagan Project

July 17, 1994

Let's start the scientific discussion of the exploration merits of my project by first stating that, statistically speaking, there is probably no more favorable geological context for finding mineral deposits than meteorite impacts. And the statistics would probably be better if more people explored them for this reason alone. Of the 140 or so known terrestrial impact sites, ranging in size from small to 300 km. in diameter, 35 of them have economic deposits (more than 20%), and 17 of them were in production at a a recent date. That's a better than 10% ratio in a geological environment that is not really sought after. It is really hard to figure out why not.

In North America alone, 5 - 6 billion dollars a year are produced in natural resources from impact sites. Given the relatively small number of impact sites, these geologic features have extremely high odds for finding economic potential.

Of all the structures known, absolutely none of them have the outstanding magnetic drill targets of Manicouagan, and the only other sites of a size analogous to Manicouagan have very rich mineral deposits, of often world- class status i.e., Sudbury (ni-Cu-PGE), Vredefort (gold, uranium, bentonite), Kara, Russia (diamond, zinc), Popigai, Russia (diamond), Tookoonooka, Australia (oil).

As a function of risk, these sites are the least risky for exploration. Add to that the fact that impact geology can be rather easily and rapidly predicted, with known structural and stratigraphic and geophysical constraints, and the challenge is even less. It is a bit like arriving at Sudbury 150 years ago with our present state of knowledge.

As far as regards the scientific background, etc. the most convincing evidence to date is the accumulated magnetic studies, as well as the field observations.

To summarize the work performed:

Geomagnetic Studies:

Various academic articles and research performed since 1970's, some of which is included with the enclosed bibliography of reproduced articles, most notably:

The Central Magnetic Anomaly - Manicouagan Structure, by Coles and Clark 1978, which concludes that there are highly magnetic rocks close to the surface over an area of about 8 X 12 km., and that the depth to the base of the body is not more than 3 km. They suggest that magnetization of a mafic body, subsequently up-lifted, to be the cause of the anomaly.

Their systematic sampling and measuring of the magnetic susceptibility of the country and melt rocks concluded that none of the samples, with the exception of two shocked ultra-mafic rocks is sufficiently magnetic to form any significant portion of the causative body of the central anomaly.

Coles and Clark discuss the cause of the magnetization of the proposed mafic or ultra-mafic body perhaps underlying the central anomaly. There is no chance that an anomaly the size of the one we see here can be caused by magnetization of anything other than an ultra-mafic body. The possiblility that the country rock in the area could have been magnetized to the necessary degree is very difficult to imagine, and science has yet to witness or observe such an occurence.

They think it unlikely that thermal magnetization could have caused the magnetization as there is little evidence that the temperature below the melt rocks would be as high as the Curie temperature over a large enough volume.

They believe that a shock pressure - induced magnetization is totally adequate to produce the magnetization of mafic minerals, as such an impact can produce an order of magnitude of 20 - 30 GPa, which decreases rapidly downward and outward. They believe the steep vertical gradient of the central mag anomaly can be explained by the rapid decrease in pressure downward and outward and further delineated by rapid uplift of the affected area. If this is the case made to explain the shape and intensity of the mag anomaly then, in my opinion, two rather unlikely events may have had to occur:

i) mafic minerals at any appreciable distances from the mag anomaly would not have undergone magnetization, which is not the case, and

ii) The area directly under the mag anomaly would have to be a sharp vertically-bounded graben, representing one of several central uplifts. Although I am not aware of the existence of more than one central uplift within an impact crater, it is true that vertical structural constraints seem most reasonable, but in such a case, I would expect clear erosional boundaries to exist, with the graben either occupying a topographic low, or a high, as in the case of the anorthositic uplifted areas to the north. The topography does not delineate the mag highs in any way.

Conclusions of our field work:

a) the mafic body which would have been magnetized would have had to be the only large plug-like mafic geological unit in a rather large region. The rocks would have had to be ultra-mafic in order to produce 100% magnetite equivalent; there are no ultra-mafic units of that size in the region that I am aware of, although there are occurences of mafic gabbroic gneisses, some of them in the NE region of the crater.

b) These latter units do not demonstrate the high magnetization gradient of the central rocks, despite the fact that virtually all mafic minerals within the confines of the crater have been

transformed to magnetite, resulting in the case just mentioned, in wide bands of almost pure magnetite. Of course, these mafic gneisses do not have an areal extent (at surface at least) comparable to the central area of the mag anomaly, and even if they did, buried as they would be under about several hundred feet of overlying magnetic suevite and other unknown material such as impact melt and gravel overburden, the overall magnetic signature is very considerably attenuated, in no way similar to the steep central gradient, which is itself buried.

The central rocks could not have produced a higher magnetization than other rocks of similar composition, i.e. some magnetite cannot be more magnetic than other magnetite, especially when created by the same event at the same geological time. Also, it is pretty definite that there is at least several hundred feet of overlying cover on top of the magnetic body creating the central anomaly, a circumstance which in no way appears to have attenuated in this case the steepness of the vertical magnetic gradient nor the uniformly high intensity across its entire width.

More recent magnetic work includes:

1. 1990 Aerodat survey of anomalous region, flown at 200 m. spacings, confirming and enhancing all previous measurements of the area.

2. Subsequent ground work in 1992 which verified and confirmed the airborne data.

3. Comparison work performed in 1993 by Peter Schultz of Rhode Island with our data to compare this magnetic signature with other known terrestrial impacts of like size, e.g. the Vredefort and the Sudbury structures. Schultz supports the possibilities of our models. You have a copy of one of his letters to us.

4. Work performed for us in 1992-93 by the Geological Survey of Canada, in measuring and re-aligning the remanent magnetization to magnetic north, thereby seperating and distinguishing the observed total field magnetics from the magnetic field reduced to pole, the latter which reflects more accurately the "real" magnetic intensity and dimensions of the central anomaly. A copy of a recently published article on this work is included herewith. The most important part of this work concluded beyond a shadow of a doubt that the anomaly was definitely caused by the impact, was not present beforehand, and did not happen after the impact. So, the magnetic anomaly cannot be a huge chunk of displaced iron formation, or the topographic

expression of shallow basement rocks, as has been speculated from time to time by various geologists in the past.

Subsequent work has located the exact boundaries and relative intensities of this induced anomaly and changed the location of the most highly magnetic or shallow locations of the body with respect to the observed total field. The results are no less impressive, if confidential.

I will provide you with the phone numbers of Peter Schultz and of Mark Pilkington of the GSC who performed a lot of the magnetic work. Both are experts in meteorite impacts, Mark from a geophysical viewpoint, and they can confirm the unique nature of the Manic anomly with respect to the width of high-intensity, which is extremely unusual.

Coles and Clark's conclusions also support the relative shallowness of the body (bottom of body not deeper than 3 km) producing the magnetization, as do most recent tests performed by the University of California in lab tests (1991-92). These replicated the Manicouagan impact, using a metal projectile. These latter experiments determined that an iron/nickel meteorite slamming at cosmic velocity into anorthositic rocks at Manicouagan would not have penetrated more than about 3 km. deep.

5. Computer modelling of our magnetic data was performed by Dr. Paterson in Toronto with conclusions outlined in the letter you already have. His modelling papers are included herewith, and coincide pretty well with everyone else's., i.e. we are not looking at a tectonic feature, but a drill target.

As the most experienced guy in the group with relating magnetic signatures to actual geology, his strong belief that the anomaly is not an intrusion, and his statement to me that he had never in his entire life seen such an anomaly, should be given weight.

6. Our field observations indicate that:

1) all mafic minerals in pre-existing basement rocks are transformed to magnetite within the confines of the crater as delineated by the water reservoir. Post-impact ultra-mafic dykes are not transformed, of course, which is how come we assume they are post-impact occurences. These

dykes are totally fresh, large-grained peridotite-pyroxenites, unmetamorphosed and unaltered. Dating these will be difficult, owing to their ultra-mafic composition and rarity of zircons.

2) the suevite (fall-back breccia) is uniformly highly magnetic, covering scattered regions around the periphery of the crater-zone, and nowhere reflects the high magnetic signature found in the centre. It is a strong possiblility that the oxidation of an iron-nickel meteorite could have created the highly magnetic microcrystalline dust of the suevite matrix.

3) A hill-sized blasted fragment of mafic basement rocks has been injected and cross-cut with tachylytic stockwerk of highly magnetic microcrystalline black material (magnetite dust?) and veins of transparent silica glass melt. I postulate that the impact blast blew this mega-fragment into the air, thus limiting to a minimum the usual impact magnetization of the mafic minerals typically found in the in-situ basement rocks, and in the smaller gneissic fragments caught up in the impact melt and in the suevite. The (stockwerk) could be either an impact tachylite of oxidized meteoritic composition (or a derivative thereof) or the result of a chimney of magnetic hydrothermal fluids, such as might be found in a vent near a caldera.

At any rate, one would expect a significant magnetic anomly over this feature, however, the signature . on a regional scale, is insignificant when compared with the central anomaly. More work needs to be done here, obviously.

Other geophysical work includes:

The airborne EM Aerodat surveys, indicating no conductors above 400 vertical feet depth, make the Manicouagan crater region a naked area in a Grenvillean area where airborne INPUT anomalies are as thick as ants at a picnic, and probably underline the difference in age, homogeneity, and nature of the 200 m.y. old Manicouagan impact rocks from the surrounding area. However, a larger area than that which we covered over the central anomaly would have to be surveyed in order to make more credible generalizations about this.

Ground EM resistivity surveys using high-penetration (2000 feet) surveys which yield very unusual profiles of extremely wide areas of low resistivity with a strong horizontal component,

usually under the observed intense magnetic fields. At first analysis, and with no petrography or other geological info to go on, conductivities of these anomalies could be compared to values one might expect from native nickel or iron oxide minerals, not necessarily typical copper or iron sulphides. Nobody has ever seen anomalies like these, using this instrument elsewhere in Archaean or Continental-type rocks.

Gravity surveys have been done in the past on a regional scale (see Gravity Study of Great Impact by Sweeney, 1978 which I have included in the accompanying biblio), and the gravity highs in the region are located dead center over the central part of the crater, which is to be expected in an impact crater, as it is modeled by uplift of more dense, less fractured or porous rocks from beneath the transient cavity. The reports concludes that the central gravity high swells gently to a high of 0 mGal over the central uplift of anorthositic gneisses.

In fact, this central high is composed of three peaks, the center lowermost one covering the magnetic anomaly to the south of the uplifted anorthositic hills, which is the point of impact of the meteorite, and where no anorthositic material outcrops, in fact where just about nothing outcrops.

The model postulated by Sweeney uses a uniform thickness of impact melt over the entire interior region of the plateau, but, in fact it is usual in an impact like Manicouagan that the impact melt is splashed out of the center to one side, and basement rocks may predominate, i.e. shocked, suevite-injected Grenvillean gneisses, which in fact is what we have intersected in our only drill hole to date, near the point of impact and under the magnetic anomaly.

The conclusions of the gravity study, which employed comet-impact and meteorite-impact models and seismic velocity data hypothesizing transient cavity depths and associated seismic horizons, would indicate that the comet model does not work, as it would require high-density surface target rocks (mafic to ultra-mafic rocks) which would be entirely too "fortuitous", to use Sweeney's term, given the relatively lower-density of the rocks in the immediate environs. (see my comments in Conclusions starting on page one of this letter).

Conclusions would also indicate that there is no way that the transient impact cavity could have been excavated to 9 km. or greater, unless the target rocks were considerably less dense than can reasonably be expected. Instead, a cavity depth of between 2 - 3 km. is most reasonable,

given observed rock densities and allowing for a density horizon which could be hard to detect due to the closing of minute cracks at the transient cavity boundary. Such a boundary within the topmost few kilometers of the crust is the most reasonable conclusion of the gravity study.

This liklihood has been independantly arrived at in unconnected and more recent tests using totally different means (firing bullets in lab tests) at the University of California. The results were presented at a symposium in Sudbury in 1992.

Since, at the time of Sweeney's work, his conclusions did not really jive with accepted current theory, he examined closely the only other alternative model to explain the findings of the study, i.e. the theory that a mass of denser material, rose from below a 9 - 12 km. density horizon, to a maximum elevation of 8 km. below surface. (which would not, in my opinion, ever produce a magnetic anomaly like we have at Manic).

But, given that the indications run contrary to a cavity depth of 9 km. or greater, and given of course the mag data, Sweeney plays around a little bit with the density parameters, significantly increasing the density contrast of the rising material by eliminating a seismic parameter, and comes to the conclusion that this kind of model could work with increased density contrast in a cavity of about 5 km. deep, and with the denser material moving upward a couple of km, having been magnetized by the impact, conforming to the possible explanation presented by Coles and Clark, 1978 - The Central Magnetic Anomaly-Manicouagan. These postulations of magnetization were briefly discussed in earlier pages.

If it is considered unlikely that highly dense material would be so conveniently located on surface target area by Sweeney, then how likely is it that such material would be present directly underneath the target at relatively shallow depth?

Also, in literature modelling the kinetic effects of a Manicouagan-type impact, it is postulated that the central uplift rises almost instantaneously after the impact like a piston of rock, bounded by steep faults, from depths exceeding 10 km. This is a reasonable explanation of the fact that the central uplift has a rather unique composition for the Manicougan area, composed almost entirely of massive moderately foliated, leucocratic anorthositic orthogneisses. This likely represents what underlies this immediate region at depth. Further work on our drill core may establish the precise depth extent of the uplift.

We do not have such anorthositic gneisses outcropping near the mag anomaly, nor does this area have the typical topography of the Mont Babel central uplift to the north, and while there has been some controversary regarding whether or not a smaller satellite mountain of anorthosite situated to the SW of Mont Babel is an in-situ part of the central uplift, (which it is not) nobody has yet described the lower plateau region under the mag anomaly as part of the central uplift. A hump-shaped uplift with three different gravity peaks might not produce the vertical fault boundaries postulated by Coles and Clark to explain the steep mag gradient over one of these humped peaks.

My understanding of the mechanics of the uplift would be different from what might produce an associated uplifted annular "shelf" at elevations some several hundred meters lower than the central uplift mountainous region. Of the three gravity peaks in the center of the crater, two of them (the northernmost) are over anorthositic rocks of high elevation, and the third is over a low-lying plateau with a coincident, extremely intense magnetic anomaly.

It's about time we imagined for a moment that the mag anomaly might have something to do with the coincident gravity anomaly, which occurs over rocks with considerable differences to what has generally been considered uplift rocks. This should not be a stretch for any thinker.

The only reliable in-situ rock samples in this latter area come from one deep drill hole which has intersected mostly leucocratic Grenvillean gneisses, similar in most respects to those outcropping on the perimeters of the crater, with proportionately much much less material that can be interpreted as the massive anorthositic orthogneisses seen continually over the up-lifted expanses of Mont Babel.

The indications that the area underlying the mag anomaly has been substantially uplifted is moot, in my opinion, at this early stage in the field work, and is not really a necessary event to postulate the probabilities of a magnetized ultra-mafic rock occuring less than 3 km. under the direct point of impact or the debatably enhanced probablities of one occurring slightly deeper, and then being uplifted.

Conclusion

So here are the models we can reasonably consider to explain the causative body:

1) Magnetization of a shallow ultra-mafic body located originally in Grenvillean basement rocks. This is the hardest model to buy for many of the above reasons already discussed. But, we would have a hell of an iron deposit, maybe.

2) A well-mineralized gabbroic or ultra-mafic shallow intrusion having a magnetic susceptibilty equivalent to about a third of that of iron formation. (see Paterson in business plan).

This theory is popular, and models like that described by Orphal and Schultz (1978) for Manicouagan, suggest the possibility of a ring dyke intrusion along steeply dipping faults that would have been the result of subsiding of the central uplift peak-ring along these faults subsequent to an intrusion-related uplift into the brecciated part of the crater floor.

It is a little difficult to imagine an ultra-mafic or mineralized gabbroic magmatic source as shallow as 5 km., but it is undeniable that we do have ultra-mafic post-impact dyke intrusions outside of the central magnetic highs, and that they are mineralized with massive sulphide Cu-Ni rich mineralization.

These do not have 2000 nT magnetic relief, like the mag anomaly does, but the "Sudbury" intrusion model is definitely a possibility, and a strong economic incentive for exploration.

3) Nickel-iron meteorite remnants, buried at depths between 1500 vertical feet and 12,000 vertical feet. This metallic material is seven times more magnetic than magnetite and could clearly account for all the gravity,magnetic, and resistivity data accumulated to date.

Since large fragments of iron-nickel meteorites have been found and mined in South Africa, and elsewhere in areas absent of evident cratering, it may not be such a revolutionary idea to look for remnants where there is evidence of cratering and sufficient fallen object mass to have perhaps left something significant behind.

If you talk to Shoemaker, for instance, about this possibility, he will dismiss it out of hand, because as far as he is concerned only comets can create large impact zones the size of Manicouagan. The fact nobody has ever looked for meteoritic material in big craters is not an

important point. All I can say is it is will be interesting what explanations will account for the total lack of H20 in the preliminary spectrometer readings coming from the impacts on Jupiter of the "comet" that is currently creating pretty humongous black eyes on that planet right now.

Peter Schultz, on the other hand, has a more open mind, and has told me he has found meteorite pieces in places where theoretically the survival of this matter was impossible.

4) The only other possible model I have come up with is the "Olympic Dam" kind of bullseye mag anomalies located over that very richly mineralized area in Australia. The anomalies are similar to those situated in your AMerican Midwest where in both cases, the mag anomalies are associated with volatile-rich hydrothermal solutions of magnetite, closely associated with rich basemetal and gold deposits, REE and other things indicative of extensive caldera activity (Olympic Dam) or crustal rifting (Midwest ?)

Western of Australia is not talking about the cause of their very intense mag anomaly,(coincident with gravity high) because its high intensity is still not sufficiently explained, or at least, they are not talking.

Kennecott and other companies are very hot on the trail of such models. I suggest you talk to Gary Sidder of the USGS for more background. (303-236-5607)

Discussion

Well, I have tried to present a synopsis of some of the scientific findings and the evolution of study over the last 25 years, as objectively as possible. I reject the first model because although the technical aspects of the geophysical study is demonstrably excellent, acute ignorance of the field geology which contradicts some of the basic premises that the model is based on, as well as a rather complicated scenario relating to timing, precise faulting, the far too fortuitous prescence of perfect material which is absent elsewhere, as well as a hoped-for intrusive event to explain some of the fore-going, is quite a hike for lab research geophysicists to make. More of a hike than I make with the other models.

The intrusive model is perfectably acceptable due to excellent field evidence of post-impact intrusives, which nonetheless occurs some distance from the central anomaly, and does not possess the mag profile of the center anomaly. Using an intrusive explanation to explain the center anomaly gives me several problems, nonetheless. Even a shallow intrusion would likely have a root, and there is no evidence of a deep root in the magnetic modelling, a diapir-like magma emplaced into a shallow locale as a result of magmatic differentiation of continental crust might be predictably felsic, far less predictably mafic.

As for magmatic segregation or layering of the impact melt, forget it, because the impact melt is extremely homogenous compositionally-wise, and demonstrates no zoning not accountable for by a slightly more higher level of integration of anorthositic material into the melt in the northeastern half of the central impact melt plateaus. Nonetheless, we can't get around the fact that there does appear to have been some post-impact ultramafic magmatism, although no evidence of large volumes of it, and it is mineralized with the things we are looking for. Repeated hydrothermal activity along fractures under the impact from deeper sources might reasonably be expected to have caused some fluctuation somewhere in Trace element values throughout the large area sampled in lithogeochemistry studies, but there are none. So, it could be a shallow mafic, highly magnetic intrusion. But, the mag profile over the body does not cry "intrusive body" to either me or Mr. Paterson. I have a lot of field experience mapping intrusives in Archaean terrain. Of course, I've never seen a very large ring dyke complex, either, and would be quite delighted to find one here.

The Sept-Iles mafic layered intrusive located not far away to the SE, has the same dimensions as the Manicouagan crater. Both the mag and gravity data suggest a deep root, and field evidence is abundant for layering. The mag anomaly looks just like what an intrusion would normally give, and the vertical gradient clearly outlines a suspected thin, ring- dyke structure. Manic lacks anything resembling these magnetic profiles.

If you read Podalsky's report, he is certain that the impact melt is an intrusive, but I think he was basing this opinion on very outdated and subsequently well-refuted work done by the first workers in the region, and in the field I saw nothing that would confirm in my opinion that the impact melt could be anything else.

Of course, the meteorite model could explain a lot of things, such as:

1. The steep gradient, sharp contacts. and uniform high-intensity across large widths of the mag anomaly.

2. The abscence of a magnetic "root".

3. The location of the mag anomaly directly encircling the point of impact and the ring structure would reflect the break-up and equidistant distribution of the big fragments.

4. The strongly magnetic nature of the dust matrix of the suevite. Geochemical analyses of the black stockwerk material might reveal the prescence of nickel. Meteoritic iron/nickel splash remnants have been found elsewhere in the world around impact sites.

5. The coincident gravity anomaly over the mag anomaly and the area which very well might not be part of the central uplift ridge. In fact, were it not for this anomaly, no one would ever have speculated that this high gravity area formed part of it.

6. The unusually high ratios of ferric iron to ferrous iron in the whole rock lithogeochemistry of the impact melt rocks which can not be explained when compared to values in the surrounding country rock. No feasible source of this almost unique discrepancy with expected results has been advanced. We must try to determine if there is any discrepency with trace elemental nickel values. Previous workers did not notice the magnetic nature of the suevite matrix, nor possibly the ubiquitous magnetization of mafic minerals in shocked basement rocks at radii of 30 km. away from the point of impact.

(Iron-nickel meteorites are composed of between 20 -50 % nickel)

I think I should decide to stop this letter. I am also sending you some info on the composition of iron meteorites, and very shortly you will receive an as yet unpublished work outlining the billions of dollars of worth already derived from the few major impacts that mankind has so far bothered to drill.

PLease call me to continue the discussion, and I hope you will decide to invest soon in this fantastic project. The management philosophy outlined in the business plan is sincere, and an

association with perspicacious people like yourself can add to the diminishment of controllable risks.

Sincerely yours.

Lauri Boivin

office in Mtl. 514-845-0393
at ungodly hours, you are welcome to call 849-7692 , DAYS - 514 - 447-6473
Weekends and Mondays - 819-346-6290

ANNEXE V.C

Paterson, N.R., 1992. Communication on Modeling of the Magnetic Anomaly

Paterson, Grant
& Watson Limited

Consulting
Geophysicists

FACSIMILE MESSAGE

DATE: June 18/92 # of Pages (including cover): 13

TO: Ms. Lauri Boivin
Minéraux Manic

FAX NO. 1-819-764-9944

File Ref: 9257

FROM: Dr. N. R. Paterson
Paterson, Grant & Watson Limited
Toronto, Canada
TELEFAX NO: (416) 971-7520, Phone: (416) 971-7343

Re: Manicouagan Prospect

1. I have not received the package yet with the helicopter data and drilling location.

2. Magnetic modelling of central anomaly produces the attached results.

   a) The causative body could be as deep as 1000 m, with a susceptibility of 0.21 emu (roughly 80% Fe_3O_4 or less), or as shallow as 560 m with a susceptibility of 0.01 emu (roughly 4% Fe_3O_4 or less).

   b) The width of the body could be a minimum of 660 m but is more likely to be close to 1800 m. Depth extent is unknown but we could determine this if we could pin down its depth.

3. The in-phase component of the EM response will be very useful in determining depth and magnetic susceptibility.

I will get back to you when I see the rest of your data.

Regards,

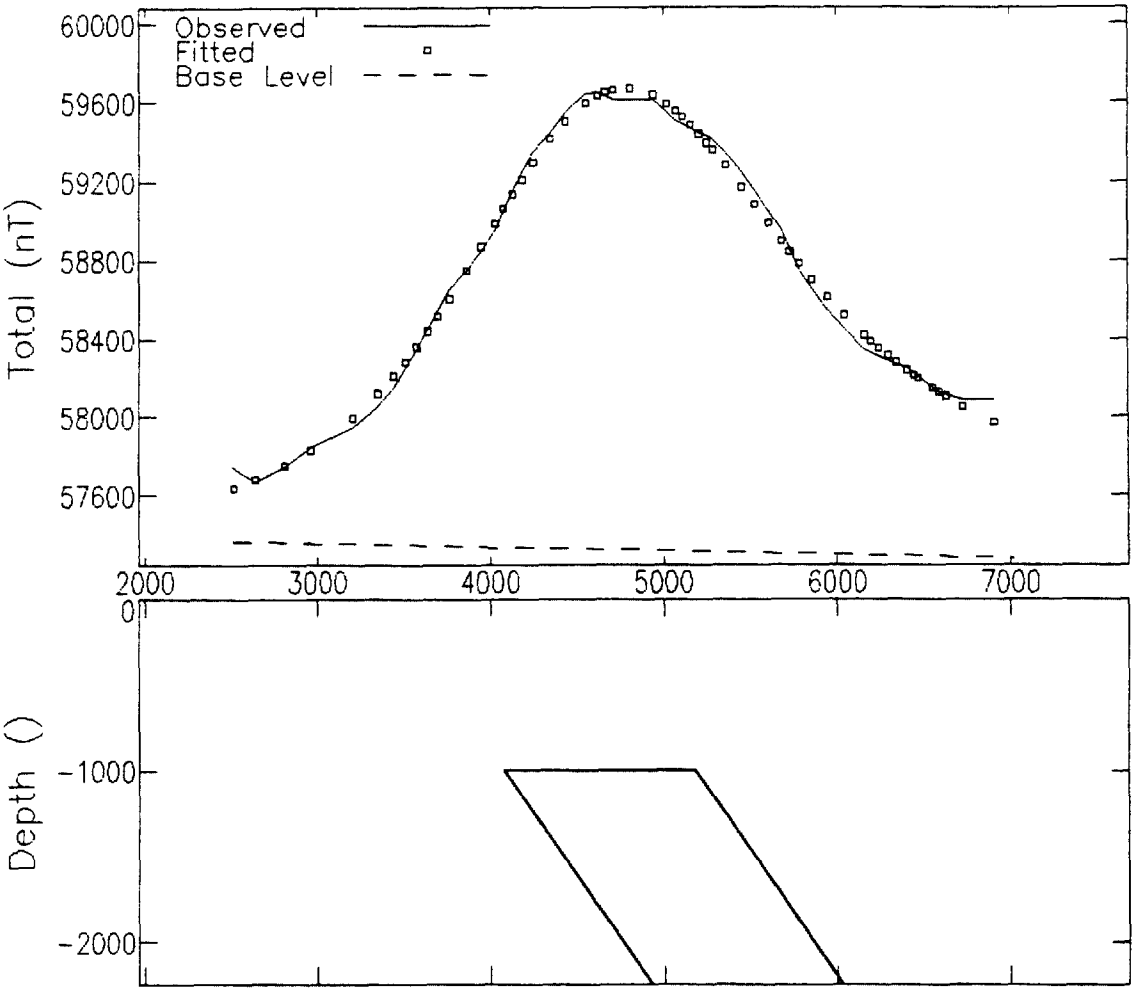
PATERSON, GRANT & WATSON LIMITED

Norman R. Paterson

7000
6000
5000
4000
3000
2500

Tabular model

Depth fixed at 1000m



MODEL PARAMETERS:

Model Type		Tabular
Depth	X	1000
Half Width	F	549
Dip	F	56 deg
Susceptibility	F	0.0272 emu
Remnance Ratio	X	0
Remnance Incl	X	0 deg
Remnance Decl	X	0 deg
Main Position	F	4625.197
Cross Position	X	10470
Base Level	F	57329.86 nT
Base Slope	F	-.0190578 nT/

(F-fitted, X-fixed, L-limit)

GEOMAGNETIC FIELD:

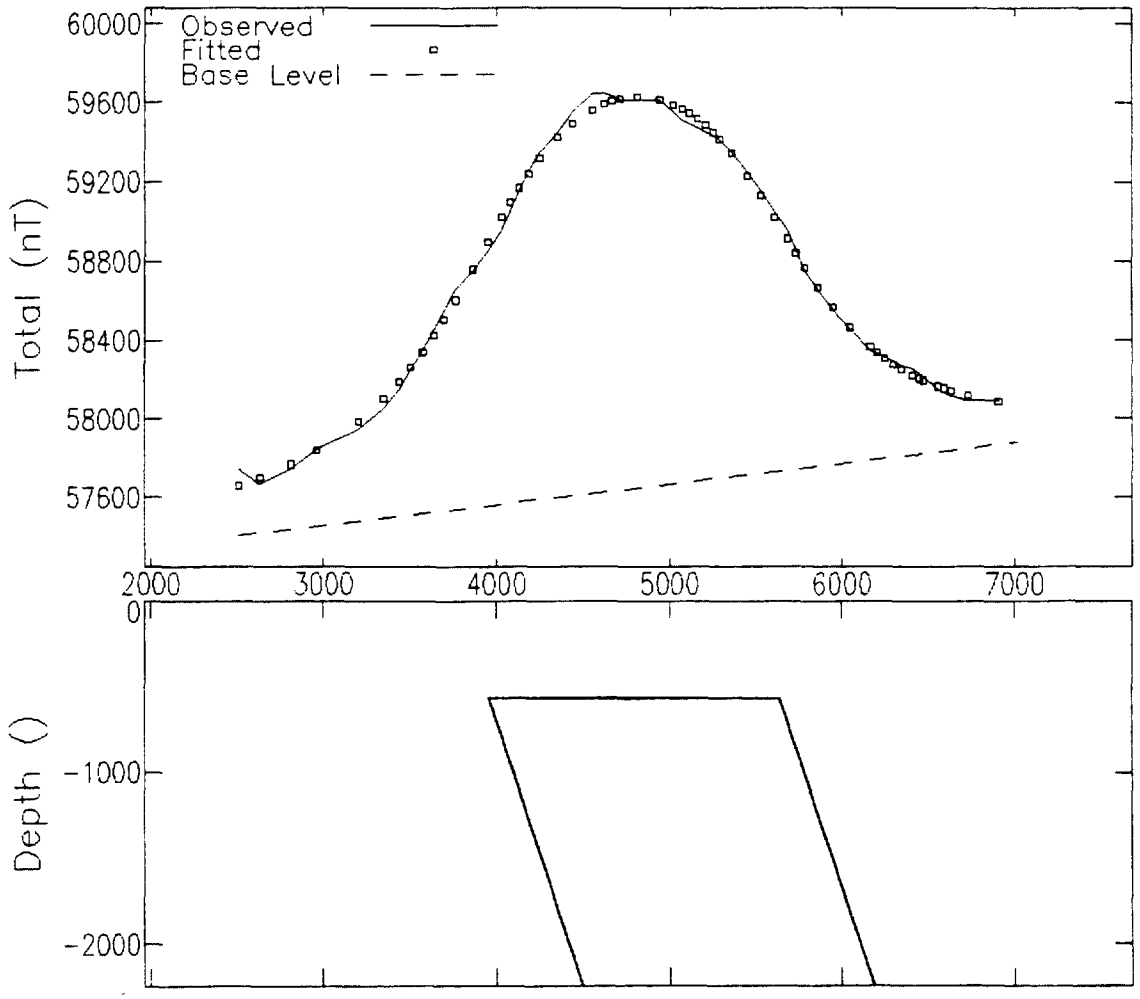
Field Strength	57000 nT
Inclination	75 deg
Declination	-23 deg

COORDINATES:

Sensor Height	45
Strike Perp	26 deg
Line Direction	30 deg
Main Direction	30 deg
Main Offset	
Cross Direction	
Cross Offset	

Tabular model

Depth originally set to 1000m



MODEL PARAMETERS:

Model Type		Tabular
Depth	F	565
Half Width	F	843
Dip	F	72 deg
Susceptibility	F	0.0101 emu
Remnance Ratio	X	0
Remnance Incl	X	0 deg
Remnance Decl	X	0 deg
Main Position	F	4798.062
Cross Position	X	10470
Base Level	F	57644.78 nT
Base Slope	F	.1041434 nT/

(F-fitted, X-fixed, L-limit)

GEOMAGNETIC FIELD:

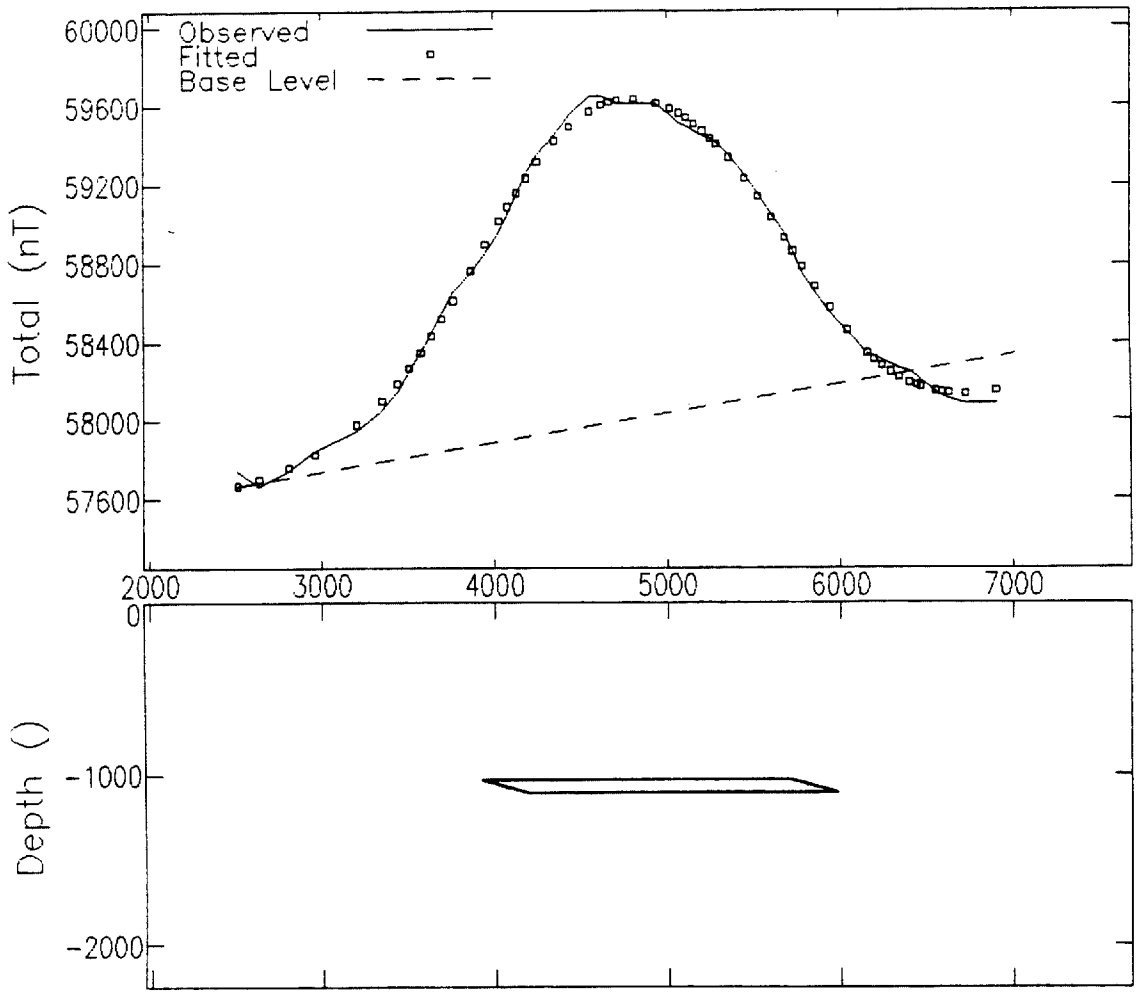
Field Strength	57000 nT
Inclination	75 deg
Declination	-23 deg

COORDINATES:

Sensor Height	45
Strike Perp	26 deg
Line Direction	30 deg
Main Direction	30 deg
Main Offset	
Cross Direction	
Cross Offset	

Tabular2 model

Depth originally 1000m, SL 1200m



MODEL PARAMETERS:

Model Type		Tabular2
Depth	F	1034
Half Width	F	894
Half Length	X	1200
Offset	X	0
Dip	F	16 deg
Thickness	L	73.5
Susceptibility	F	0.213 emu
Remnance Ratio	X	0
Remnance Incl	X	0 deg
Remnance Decl	X	0 deg
Main Position	F	4818.876
Cross Position	X	10470
Base Level	F	58012.57 nT
Base Slope	F	.1491197 nT/

GEOMAGNETIC FIELD:

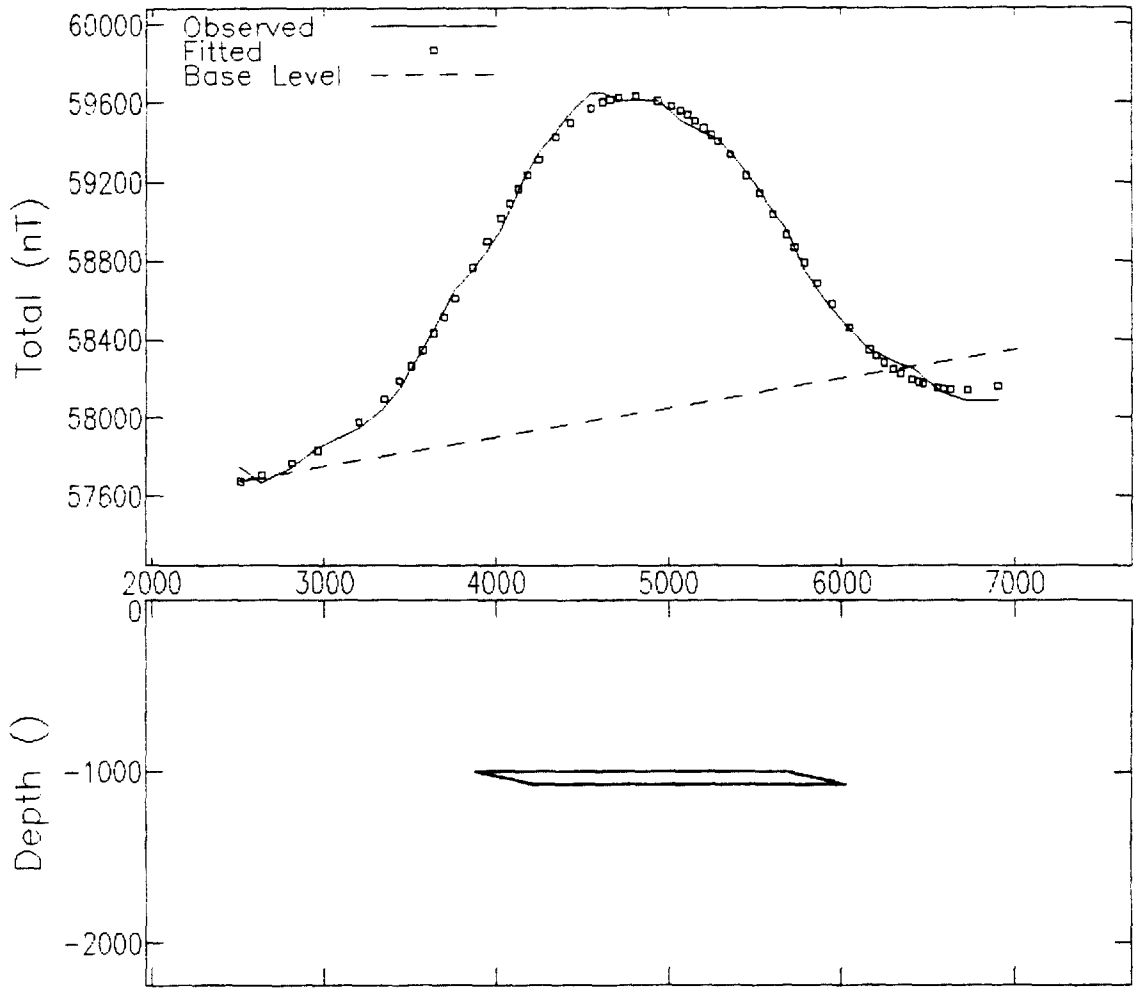
Field Strength	57000 nT
Inclination	75 deg
Declination	-23 deg

COORDINATES:

Sensor Height	45
Strike Perp	26 deg
Line Direction	30 deg
Main Direction	30 deg
Main Offset	
Cross Direction	
Cross Offset	

Tabular2 model

Depth fixed at 1000m, SL 1200m



MODEL PARAMETERS:

Model Type		Tabular2
Depth	X	1000
Half Width	F	902
Half Length	X	1200
Offset	X	0
Dip	F	12 deg
Thickness	L	73.5
Susceptibility	F	0.202 emu
Remnance Ratio	X	0
Remnance Incl	X	0 deg
Remnance Decl	X	0 deg
Main Position	F	4783.064
Cross Position	X	10470
Base Level	F	58017.34 nT
Base Slope	F	.1487397 nT/

GEOMAGNETIC FIELD:

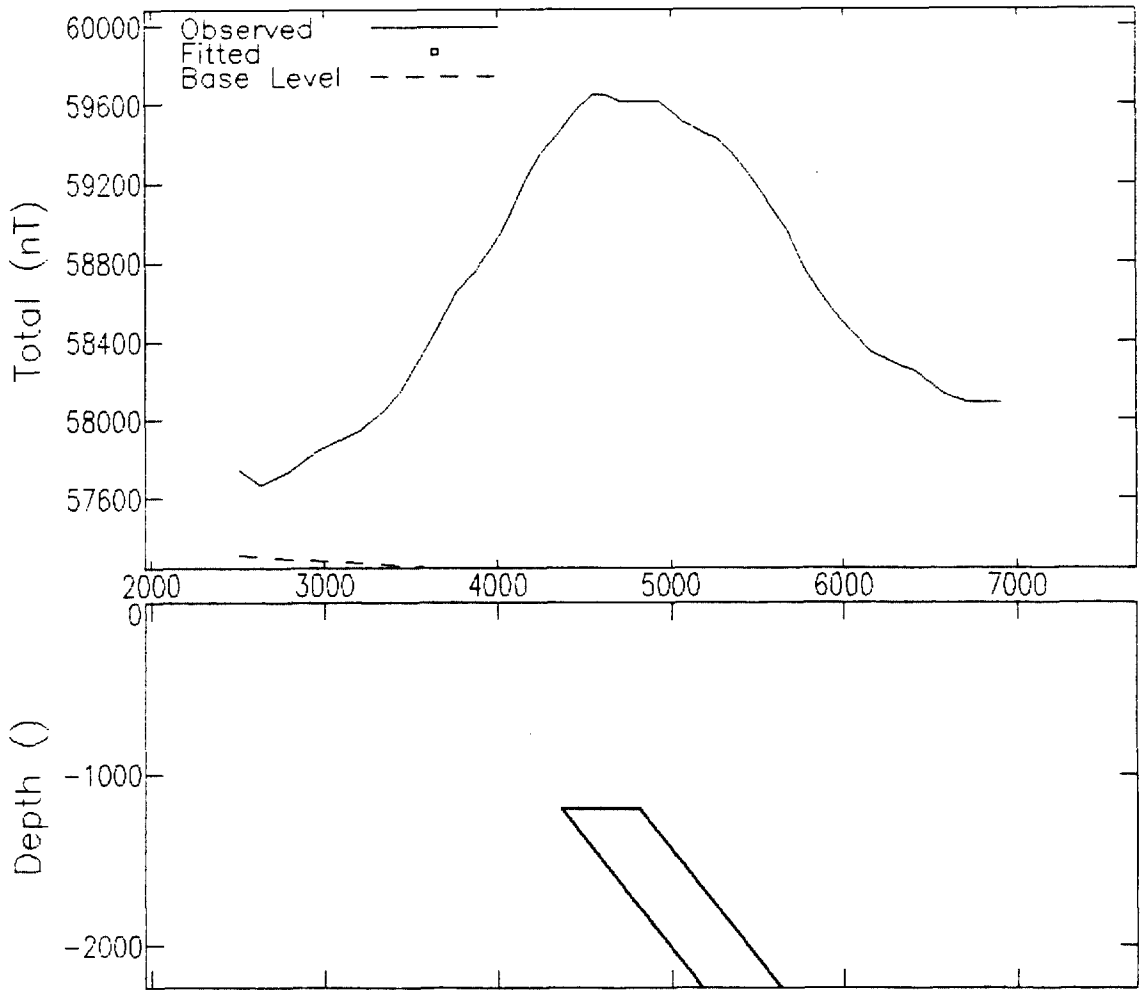
Field Strength	57000 nT
Inclination	75 deg
Declination	-23 deg

COORDINATES:

Sensor Height	45
Strike Perp	26 deg
Line Direction	30 deg
Main Direction	30 deg
Main Offset	
Cross Direction	
Cross Offset	

Tabular model

Depth fixed at 1200m



MODEL PARAMETERS:

Model Type		Tabular
Depth	X	1200
Half Width	F	225
Dip	F	52 deg
Susceptibility	F	0.0826 emu
Remnance Ratio	X	0
Remnance Incl	X	0 deg
Remnance Decl	X	0 deg
Main Position	F	4587.46
Cross Position	X	10470
Base Level	F	57195.63 nT
Base Slope	F	-.0559293 nT/

(F-fitted, X-fixed, L-limit)

GEOMAGNETIC FIELD:

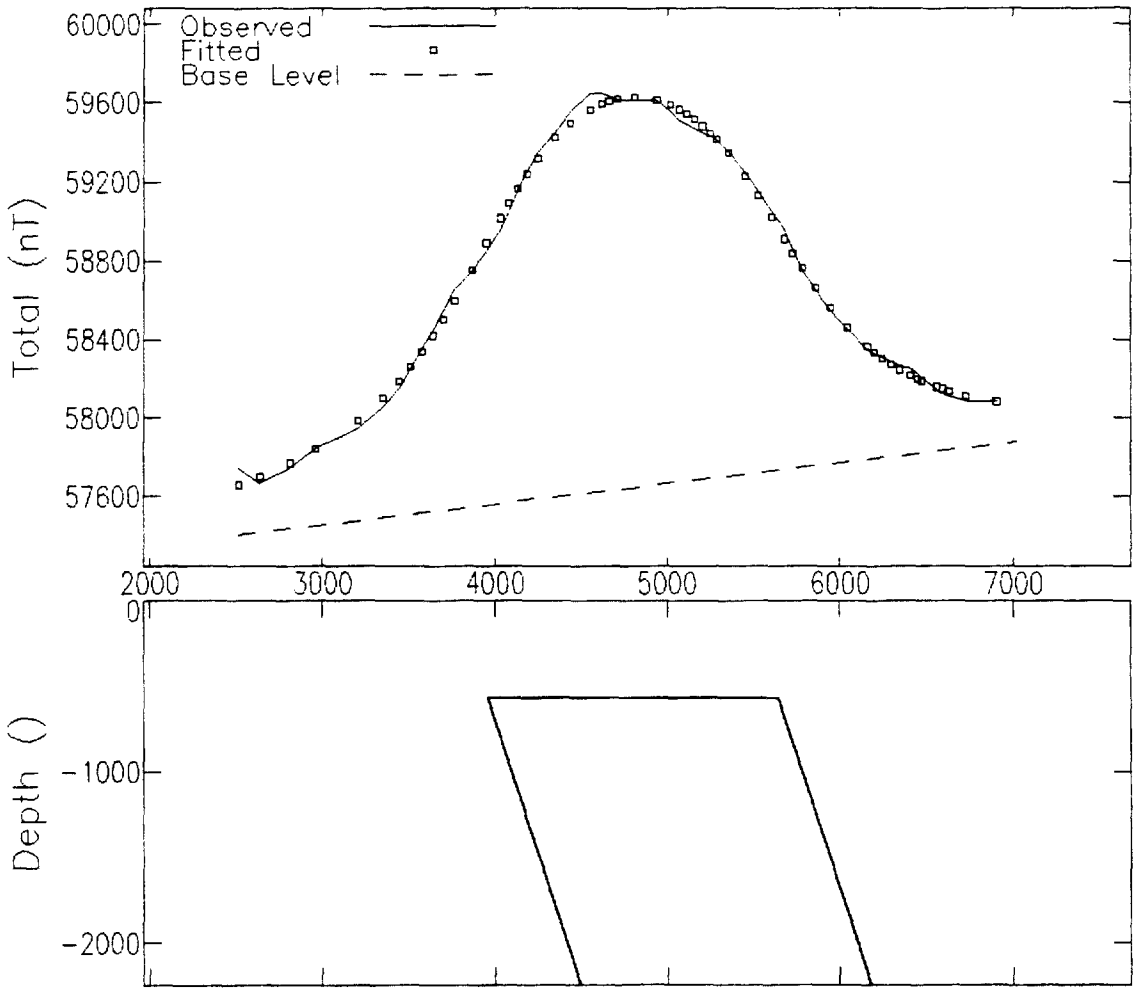
Field Strength	57000 nT
Inclination	75 deg
Declination	-23 deg

COORDINATES:

Sensor Height	45
Strike Perp	26 deg
Line Direction	30 deg
Main Direction	30 deg
Main Offset	
Cross Direction	
Cross Offset	

Tabular model

Depth originally at 1200m



MODEL PARAMETERS:

Model Type		Tabular
Depth	F	564
Half Width	F	843
Dip	F	72 deg
Susceptibility	F	0.0101 emu
Remnance Ratio	X	0
Remnance Incl	X	0 deg
Remnance Decl	X	0 deg
Main Position	F	4799.234
Cross Position	X	10470
Base Level	F	57645.58 nT
Base Slope	F	.1049322 nT/

(F-fitted, X-fixed, L-limit)

GEOMAGNETIC FIELD:

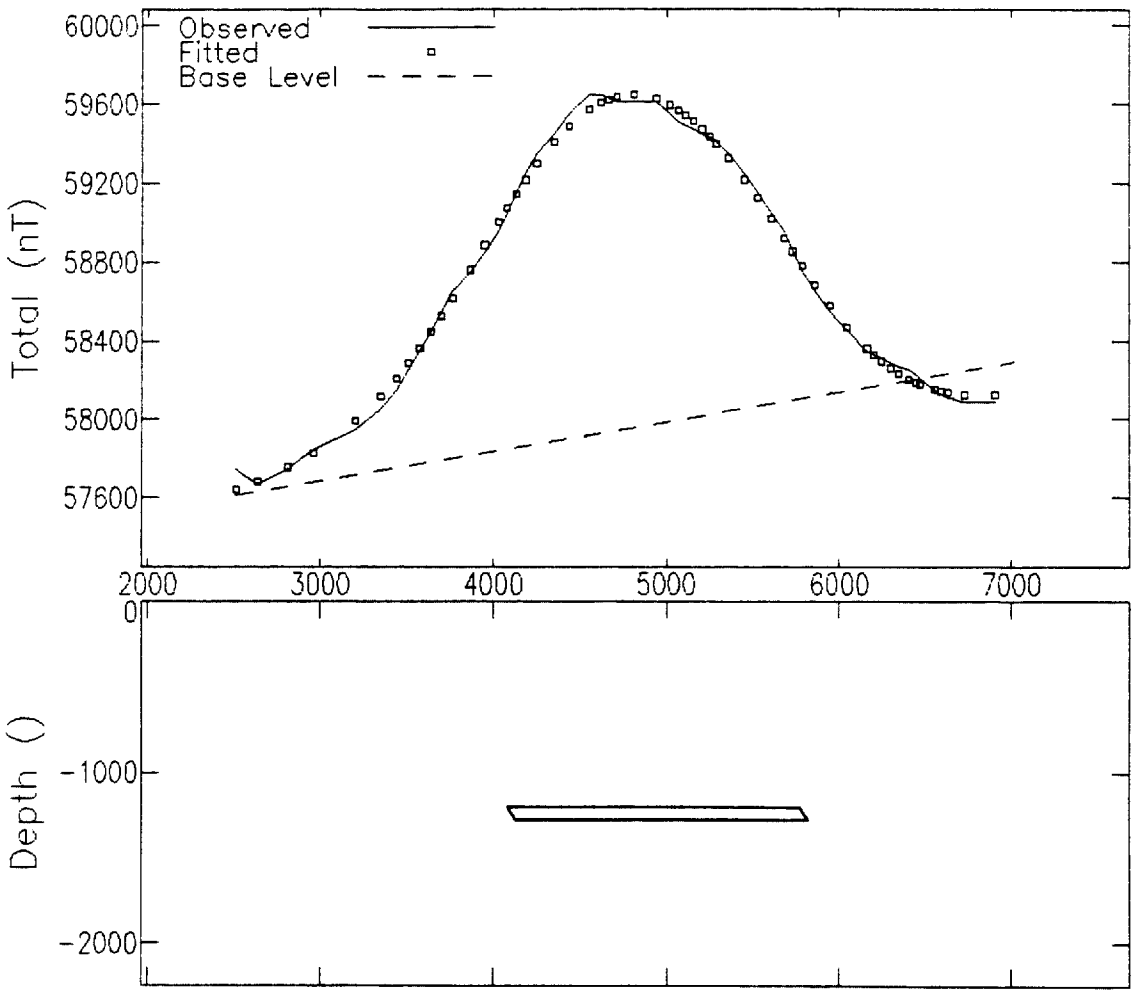
Field Strength	57000 nT
Inclination	75 deg
Declination	-23 deg

COORDINATES:

Sensor Height	45
Strike Perp	26 deg
Line Direction	30 deg
Main Direction	30 deg
Main Offset	
Cross Direction	
Cross Offset	

Tabular2 model

Depth fixed at 1200m, SL 1200m



MODEL PARAMETERS:

Model Type		Tabular2	
Depth	X	1200	
Half Width	F	843	
Half Length	X	1200	
Offset	X	0	
Dip	F	59	deg
Thickness	F	76.5	
Susceptibility	F	0.271	emu
Remnance Ratio	X	0	
Remnance Incl	X	0	deg
Remnance Decl	X	0	deg
Main Position	F	4927.115	
Cross Position	X	10470	
Base Level	F	57975.54	nT
Base Slope	F	.1505626	nT/

GEOMAGNETIC FIELD:

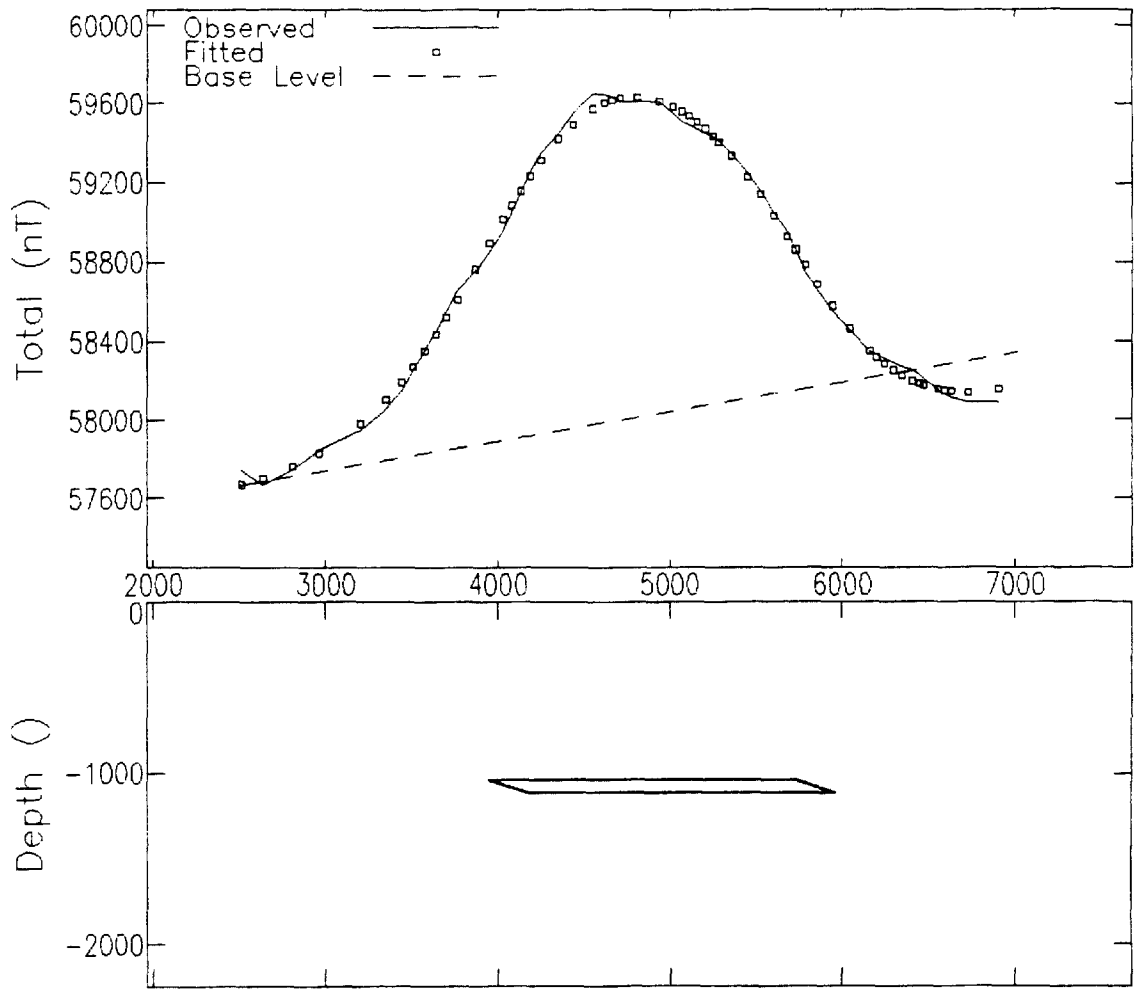
Field Strength	57000 nT
Inclination	75 deg
Declination	-23 deg

COORDINATES:

Sensor Height	45
Strike Perp	26 deg
Line Direction	30 deg
Main Direction	30 deg
Main Offset	
Cross Direction	
Cross Offset	

Tabular2 model

Depth originally 1400m, SL 1200m



MODEL PARAMETERS:

Model Type		Tabular2	
Depth	F	1038	
Half Width	F	894	
Half Length	X	1200	
Offset	X	0	
Dip	F	18	deg
Thickness	L	73.5	
Susceptibility	F	0.214	emu
Remnance Ratio	X	0	
Remnance Incl	X	0	deg
Remnance Decl	X	0	deg
Main Position	F	4837.198	
Cross Position	X	10470	
Base Level	F	58014.88	nT
Base Slope	F	.1492597	nT/

GEOMAGNETIC FIELD:

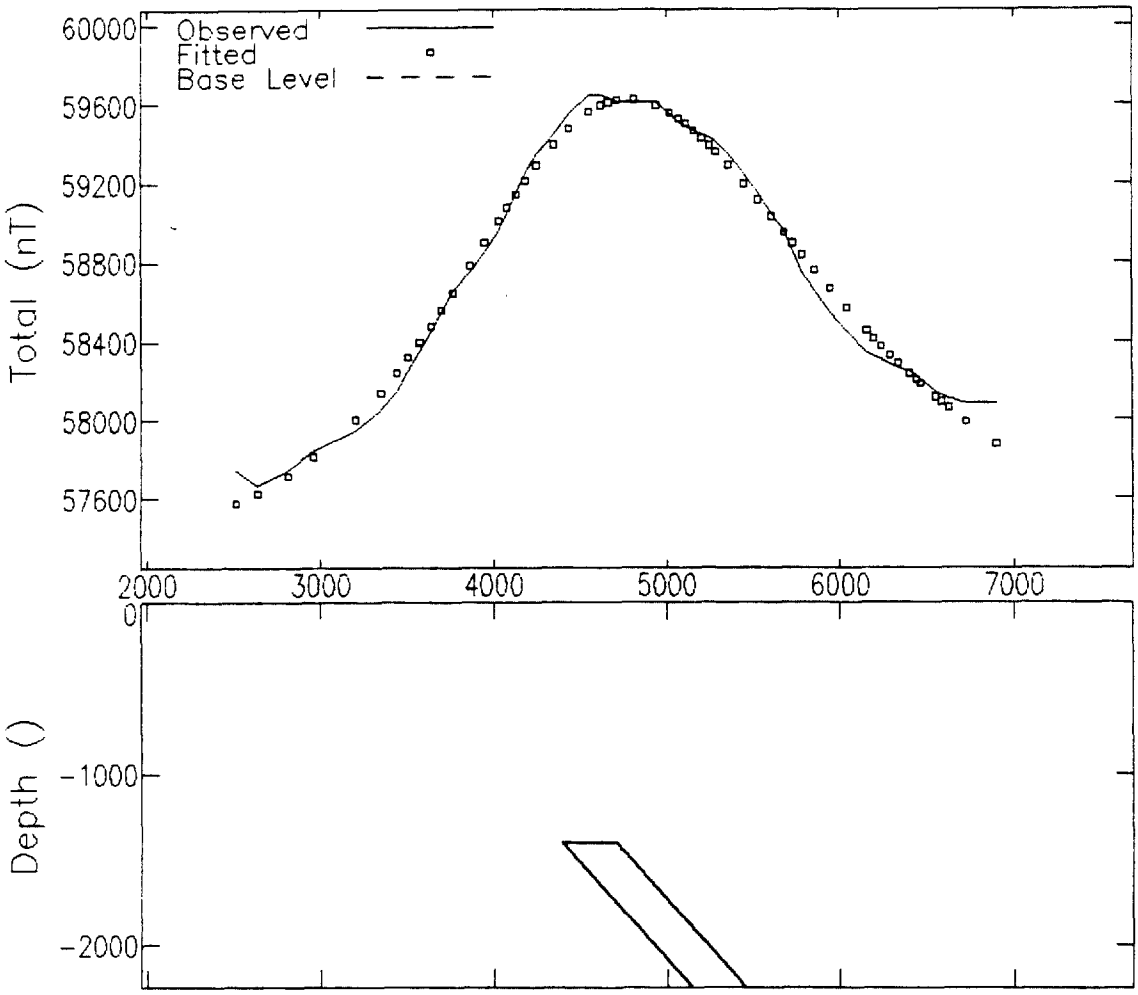
Field Strength	57000 nT
Inclination	75 deg
Declination	-23 deg

COORDINATES:

Sensor Height	45
Strike Perp	26 deg
Line Direction	30 deg
Main Direction	30 deg
Main Offset	
Cross Direction	
Cross Offset	

Tabular model

Depth fixed at 1400m



MODEL PARAMETERS:

Model Type		Tabular
Depth	X	1400
Half Width	F	156
Dip	F	48 deg
Susceptibility	F	0.159 emu
Remnance Ratio	X	0
Remnance Incl	X	0 deg
Remnance Decl	X	0 deg
Main Position	F	4548.703
Cross Position	X	10470
Base Level	F	56958.46 nT
Base Slope	F	-.1045915 nT/

(F-fitted, X-fixed, L-limit)

GEOMAGNETIC FIELD:

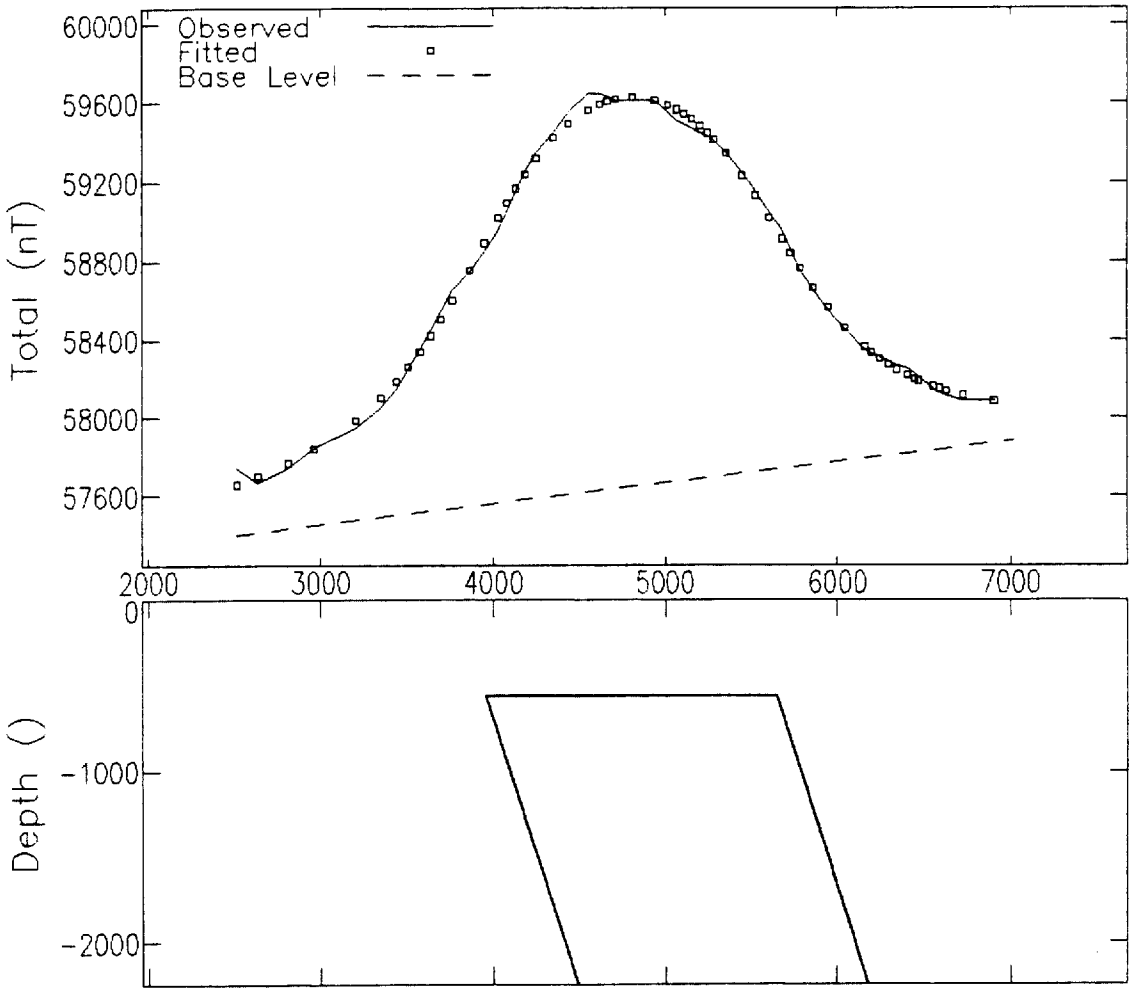
Field Strength	57000 nT
Inclination	75 deg
Declination	-23 deg

COORDINATES:

Sensor Height	45
Strike Perp	26 deg
Line Direction	30 deg
Main Direction	30 deg
Main Offset	
Cross Direction	
Cross Offset	

Tabular model 22

Depth originally 1400m



MODEL PARAMETERS:

Model Type		Tabular
Depth	F	563
Half Width	F	843
Dip	F	72 deg
Susceptibility	F	0.0100 emu
Remnance Ratio	X	0
Remnance Incl	X	0 deg
Remnance Decl	X	0 deg
Main Position	F	4801.73
Cross Position	X	10470
Base Level	F	57647.5 nT
Base Slope	F	.1064382 nT/

(F-fitted, X-fixed, L-limit)

GEOMAGNETIC FIELD:

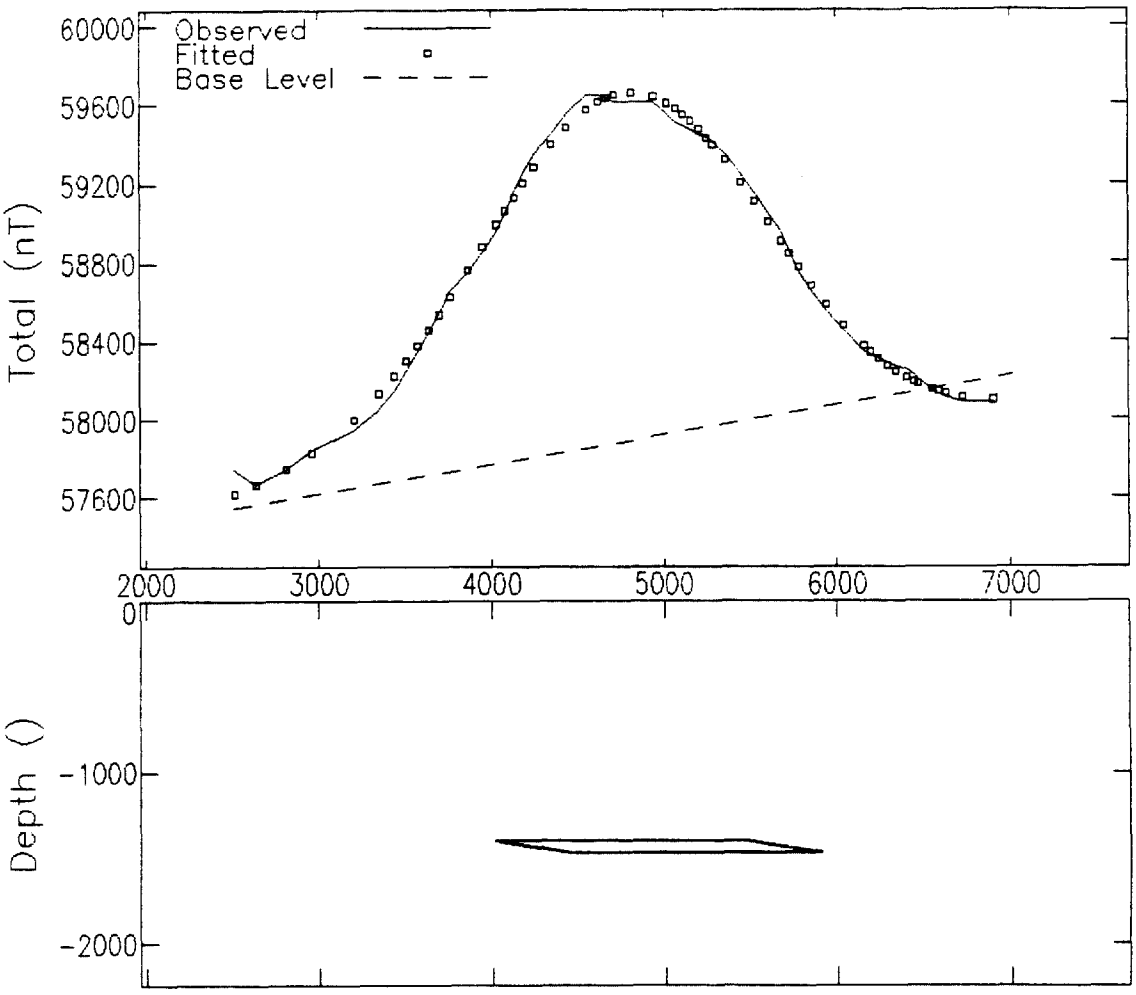
Field Strength	57000 nT
Inclination	75 deg
Declination	-23 deg

COORDINATES:

Sensor Height	45
Strike Perp	26 deg
Line Direction	30 deg
Main Direction	30 deg
Main Offset	
Cross Direction	
Cross Offset	

Tabular2 model

Depth fixed at 1400



MODEL PARAMETERS:

Model Type		Tabular2	
Depth	X	1400	
Half Width	F	725	
Half Length	X	1200	
Offset	X	0	
Dip	L	10	deg
Thickness	L	74.3	
Susceptibility	F	0.418	emu
Remnance Ratio	X	0	
Remnance Incl	X	0	deg
Remnance Decl	X	0	deg
Main Position	F	4737.234	
Cross Position	X	10470	
Base Level	F	57882.59	nT
Base Slope	F	.1508896	nT/

GEOMAGNETIC FIELD:

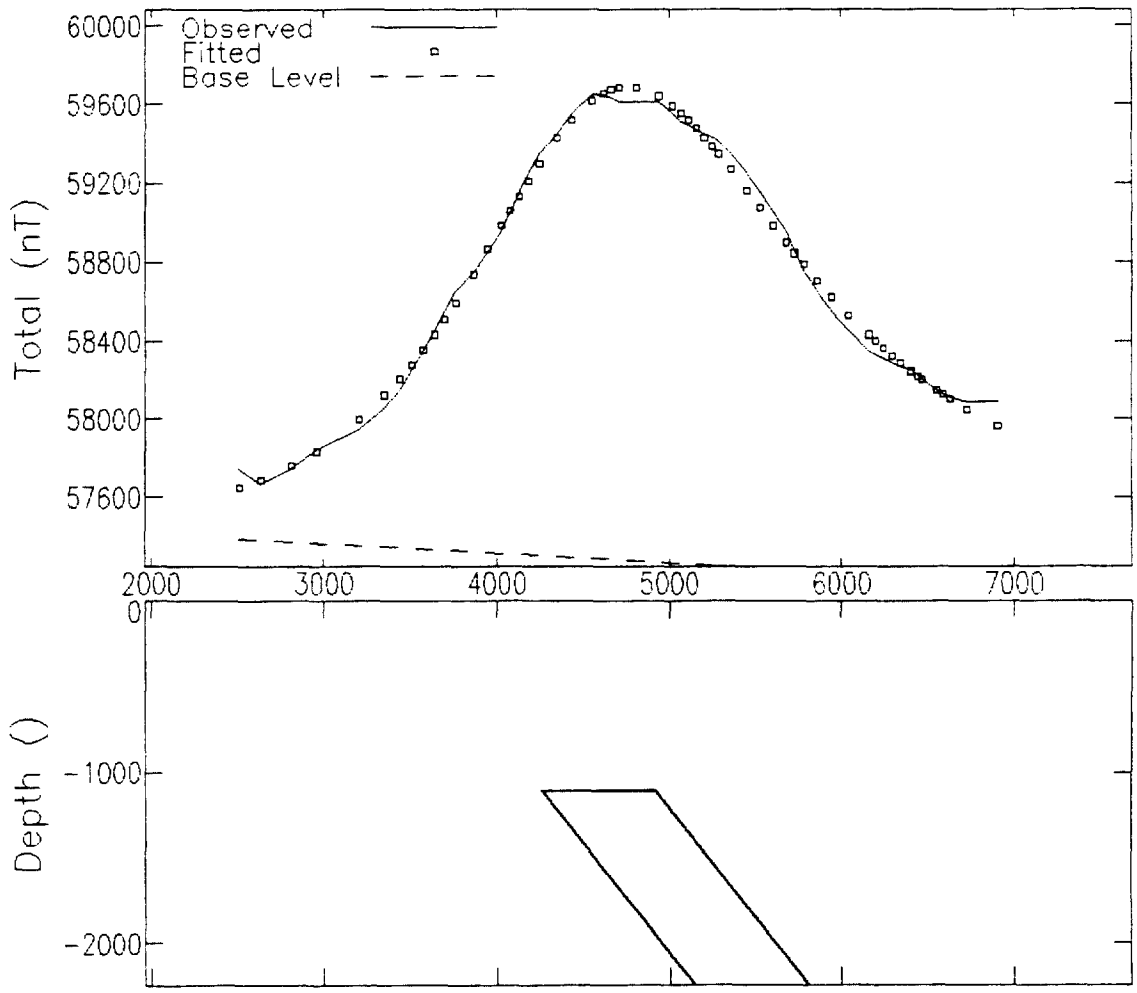
Field Strength	57000 nT
Inclination	75 deg
Declination	-23 deg

COORDINATES:

Sensor Height	45
Strike Perp	26 deg
Line Direction	30 deg
Main Direction	30 deg
Main Offset	
Cross Direction	
Cross Offset	

Tabular model

Depth originally at 2000m



MODEL PARAMETERS:

Model Type		Tabular
Depth	F	1110
Half Width	F	330
Dip	F	52 deg
Susceptibility	F	0.0512 emu
Remnance Ratio	X	0
Remnance Incl	X	0 deg
Remnance Decl	X	0 deg
Main Position	F	4588.115
Cross Position	X	10470
Base Level	F	57287.26 nT
Base Slope	F	-.0493673 nT/

(F-fitted, X-fixed, L-limit)

GEOMAGNETIC FIELD:

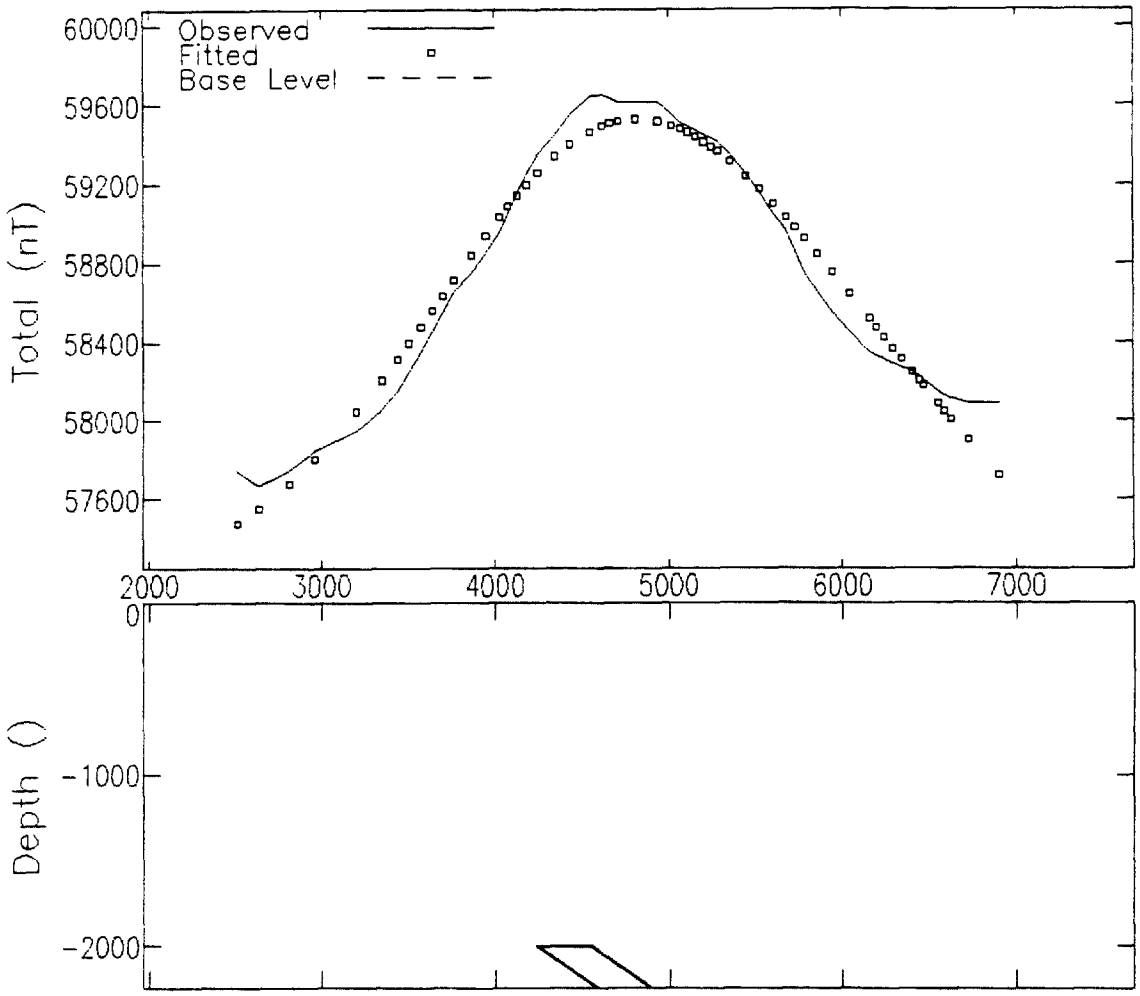
Field Strength	57000 nT
Inclination	75 deg
Declination	-23 deg

COORDINATES:

Sensor Height	45
Strike Perp	26 deg
Line Direction	30 deg
Main Direction	30 deg
Main Offset	
Cross Direction	
Cross Offset	

Tabular model

Depth fixed at 2000m



MODEL PARAMETERS:

Model Type		Tabular
Depth	X	2000
Half Width	F	155
Dip	F	36 deg
Susceptibility	F	0.392 emu
Remnance Ratio	X	0
Remnance Incl	X	0 deg
Remnance Decl	X	0 deg
Main Position	F	4394
Cross Position	X	10470
Base Level	F	56218.03 nT
Base Slope	F	-.3152916 nT/

(F-fitted, X-fixed, L-limit)

GEOMAGNETIC FIELD:

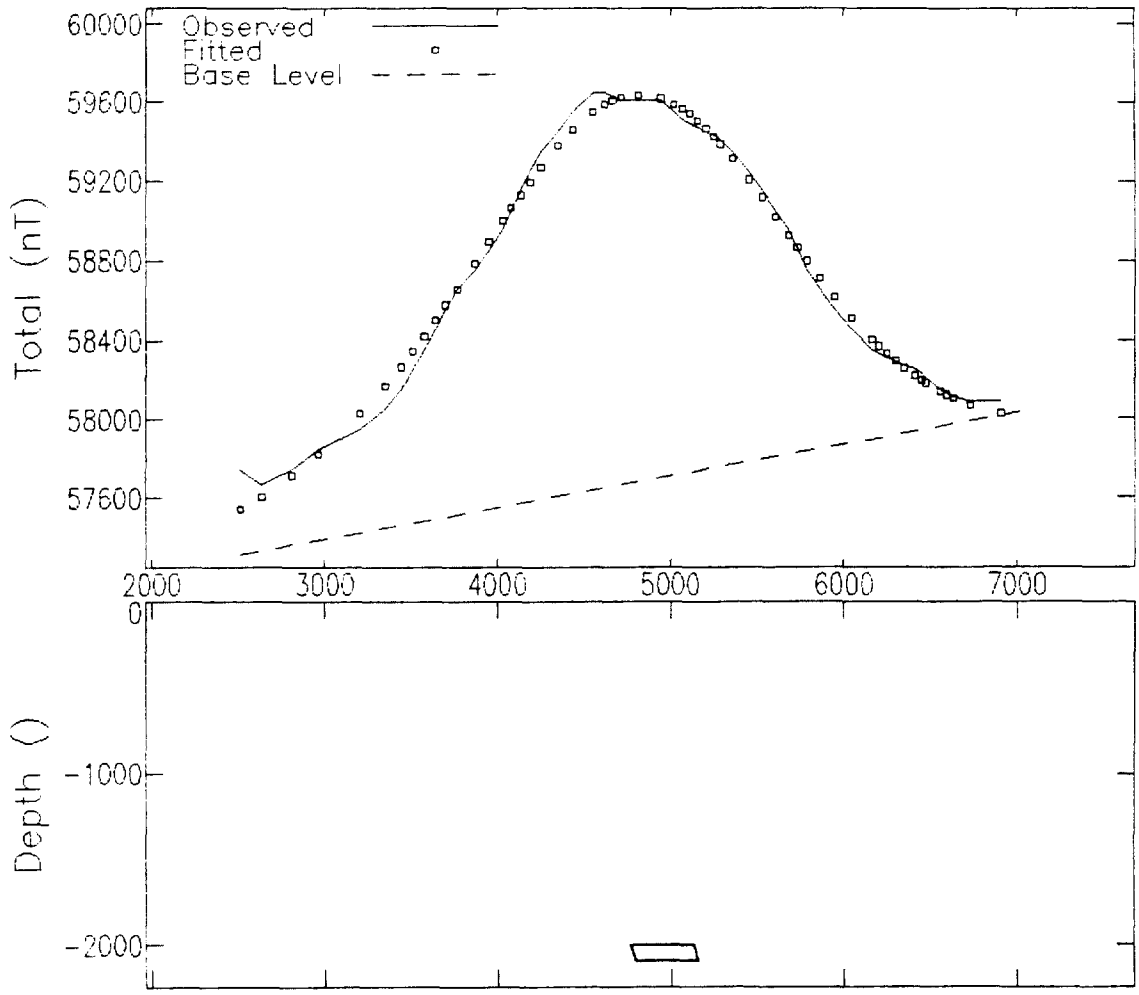
Field Strength	57000 nT
Inclination	75 deg
Declination	-23 deg

COORDINATES:

Sensor Height	45
Strike Perp	26 deg
Line Direction	30 deg
Main Direction	30 deg
Main Offset	
Cross Direction	
Cross Offset	

Tabular2 model

Depth fixed at 2000m



MODEL PARAMETERS:

Model Type		Tabular2
Depth	X	2000
Half Width	F	181
Half Length	X	1200
Offset	X	0
Dip	F	73 deg
Thickness	F	95.5
Susceptibility	F	2.74 emu
Remnance Ratio	X	0
Remnance Incl	X	0 deg
Remnance Decl	X	0 deg
Main Position	F	4947.123
Cross Position	X	10470
Base Level	F	57702.05 nT
Base Slope	F	.1597891 nT/

GEOMAGNETIC FIELD:

Field Strength	57000 nT
Inclination	75 deg
Declination	-23 deg

COORDINATES:

Sensor Height	45
Strike Perp	26 deg
Line Direction	30 deg
Main Direction	30 deg
Main Offset	
Cross Direction	
Cross Offset	

ANNEXE V.D

Schultz, P. H., 1992. Communication on his assessment of the Manicouagan Property.

BROWN UNIVERSITY *Providence, Rhode Island • 02912*

DEPARTMENT OF GEOLOGICAL SCIENCES
401 863-2526, 2417, 3338

September 28, 1992

CONFIDENTIAL

Ms. Lauri Boivin
Mineraux Manic, Inc.
103-B, Rue Tremoy
Quebec, J9X 1W5
CANADA

Dear Lauri:

Thanks for your letter. We were also happy to have a chance to meet you and discuss your bold project. Over the last two weeks Dave and I have been reviewing the literature, exploring modeling alternatives, and putting the mag anomalies in the context of crater-scaling relations inferred from my recent work (as reported at the Sudbury conference). Our goal was to find a simplified or direct way to recognize criteria for distinguishing a shock-generated remnant field from an inductive field, to establish some sensible scaling relation for observed impact-related fields, and to establish additional tests/approaches for resolving the origin of these signatures. As you are aware, considerable work has been done to measure field strengths and to model its structure to first order. Relatively little work has been done to design field experiments that would allow more unique solutions through modern data-processing techniques. And virtually no studies have been done to place the observed fields in the context of crater-scaling relations.

Let me give you a brief summary of our assessment thus far. The bottom line is that we feel we can show that impact-generated magnetic anomalies (i.e., the amount of magnetized material) may depend simply on impactor size. Unfortunately, we cannot yet uniquely establish the role of susceptibility (i.e., unique composition). This information requires further constraints on the depth of the source region. Nevertheless, our approach could prove useful for placing Manicouagan in the framework of Sudbury and Vredefort, other impact sites yielding mineable ores.

Without going into the details, consider the dependence of both anomaly diameter (Figure 1) and magnetic intensity (Figure 2) as a function of the original crater diameter. Figure 1a clearly shows that the size of the anomaly increases essentially linearly with size with Vredefort and Sudbury anomalies being enormous. The size of the Manicouagan anomaly, however, seems small relative to crater diameter in this representation, even though the magnetic flux (magnetic field strength times anomaly area) at Manicouagan falls on the same line as Vredefort and Sudbury (Figure 2). Scaling relations (relation between crater diameter and impactor energy) indicate that crater diameter also increases approximately with impactor size. Consequently, referencing crater diameter to either impactor size or the mag anomaly should produce a straight line unless other variables enter the problem (e.g., impactor density or velocity). Figure 1b shows that this seems to be the case for most of the data with the obvious exceptions of Manicouagan and Haughton. One simple and logical explanation is that the impactor forming Manicouagan (and Haughton) was either smaller or faster. In the former case, it would also have to be more dense, i.e., a smaller denser object would create a larger crater even though the size of the magnetic anomaly remains about the same (see the arrows in Figure 1).

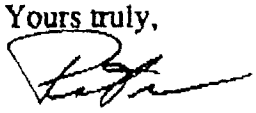
As encouraging as Figure 1 might be, the magnetic flux of the anomaly at the surface nevertheless appears to be quite normal. This inconsistency with the working hypothesis could be dismissed if the physical structure of the anomaly is different. For example, the source rock modeled as a thin plate would require increased magnetization for Manicouagan relative to other impacts in order to account for the non-anomalous magnetic flux (Figure 2). There will be a trade-off, however, between the susceptibility of region and its thickness in order to maintain the observed magnetic flux. Key inputs would be a more unique model of the anomaly (depth and thickness), better constraints on the magnetic carriers (i.e., susceptibility from the drill cores), and independent assessment of the source depth (e.g., seismic profiles).

We offer this insight to add at least credibility to the hypothesis. It can't yet be used as a proof; this may only come from your drilling program. We have actually looked into the problem in greater detail than what is described here, but much of the discussion becomes quite obtuse. You may use what's offered here to bolster your case, but I ask that it be done sparingly since our approach is the kernel of an interesting paper.

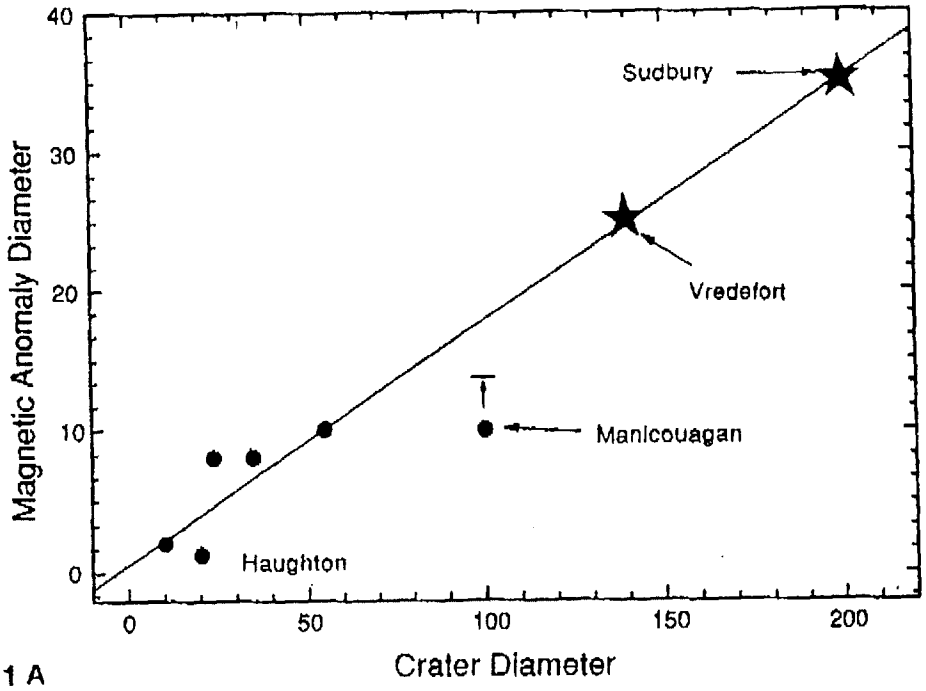
Now in answer to your other questions. I will pass on a note to Dietz reinforcing his ideas as a worthy hypothesis. And, I would be happy to talk with some of your contacts. My approach, however, would be to emphasize that this is a viable idea, particularly in light of what we don't know and in light of your geophysical data. I think a much stronger statement could be made, however, with further constraints on the structure. In terms of matching money from scientific funding, I feel it is premature since government agencies are conservative and tight. A better way would be to put a student or post-doc on the problem. The only caveat would be to protect them from any possible perception by the rest of the community as doing "fringe science." This can be done with the proper goals.

In terms of publicity, this could help your cause but could hurt ours. I have learned that you can advance more quickly scientifically when you are allowed to be wrong; this isn't possible in a public forum. Nevertheless, I (we) are excited about the project and look forward to collaborating on the committee. My instincts tell me that Manicouagan will surprise us and I want to be there.

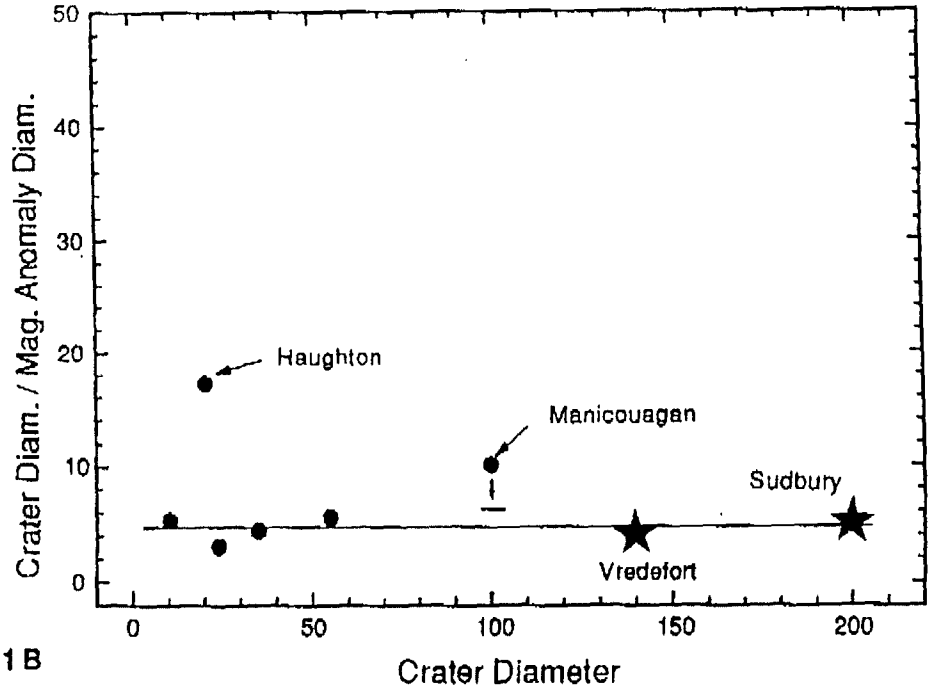
Yours truly,



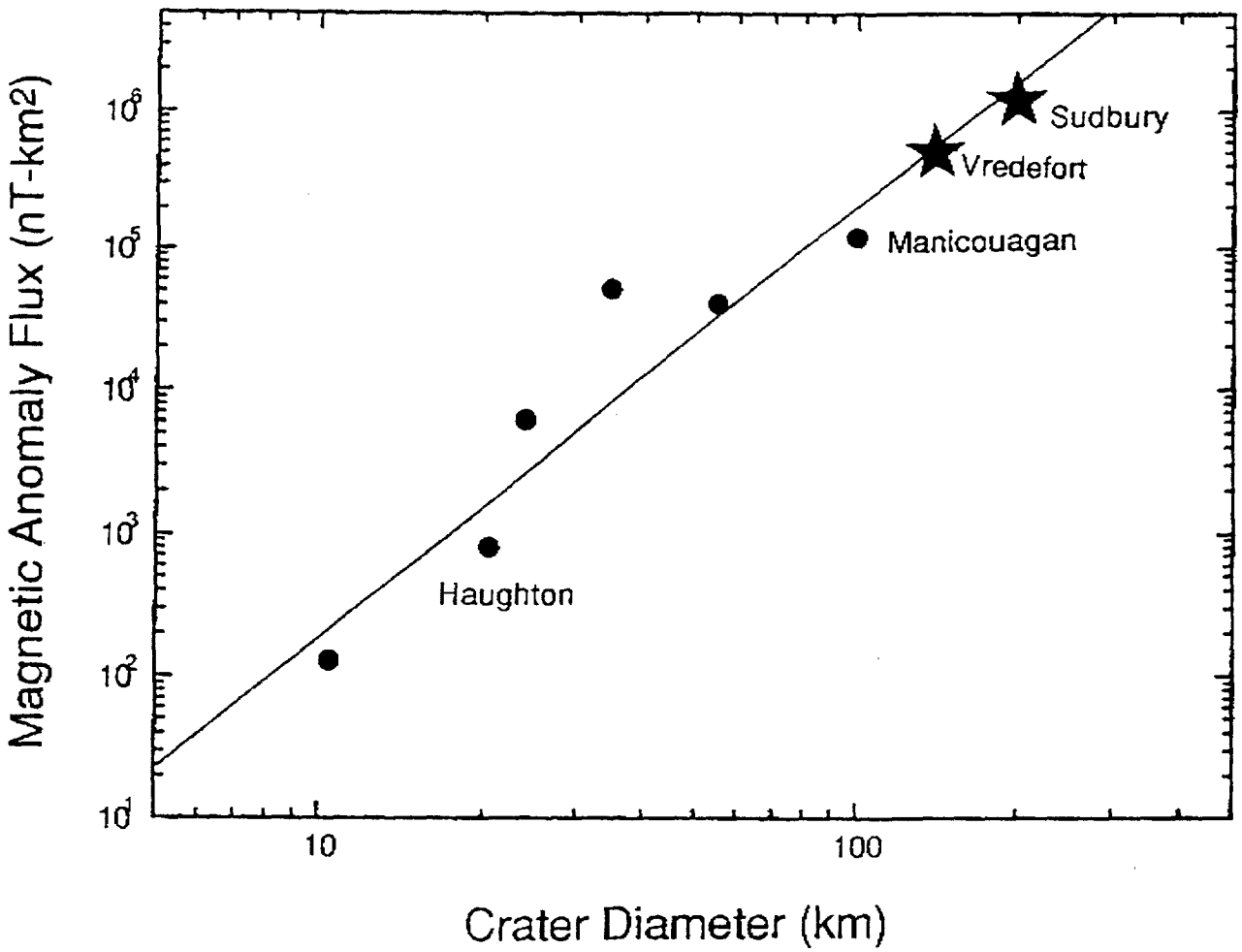
Peter H. Schultz


Magnetic Anomaly Diameter
Crater Diameter
Sudbury
Vredefort
Manicouagan
Haughton
0
10
20
30
40
0
50
100
150
200

1 A


Crater Diam. / Mag. Anomaly Diam.
Crater Diameter
Haughton
Manicouagan
Sudbury
Vredefort
0
10
20
30
40
50
0
50
100
150
200

1 B



2

Sep. 29 '92 11:18 0000 [illegible] PLAN.SEC. TEL 4018533978 P. 5

ANNEXE VI

INFORMATION ON THE MELIS METHOD

SAGAX GEOPHYSIQUE

Siège social.
6700, avenue du Parc, bur. 110
Montréal, QC, Canada H2V 4H9
Tél.: (514) 271-3150
Fax: (514) 271-4679

Bureau d'exploration:
200 Landry, Val d'Or
QC, Canada J9P 5N6
Tél.: (819) 874-5163
Fax: (819) 874-5264

M E L I S

March 1993

(Magneto ELectric Induction System)

1. Description of the method

   - Transmitting system
   - Receiving system

2. Field operations

   - Equipment description
   - Logistics
   - Operating costs

3. Interpretation principles

   - Qualitative description of MELIS anomalies
   - Theoretical models

4. Depth of investigation

5. Case histories

   - Géant Dormant (Sleeping Giant)
   - Louvicourt
   - Lac Yasinski (Lake Yasinski)
   - Masa Valverde

SAGAX GEOPHYSIQUE

M E L I S

(Magneto ELectric Induction System)

Despite all the technical developments of the last decade, we must acknowledge that surface geophysics reaches its limits when trying to locate vertical conductive bodies deeper than 150m in an environment such as the Canadian Shield. Until now, this problem had not been addressed adequately and cost-effectively. Fortunately, a new technique called "MELIS in LOOP ρ' mode" has recently been introduced by the BRGM and it promises to fill this gap. This method has most of the advantages of traditional EM systems but without their major weaknesses. Before going into more details on this original and proven technique, here is a list of its major characteristics:

* Uses a fixed source similar to a vertical magnetic dipole which produces a magnetic moment approximately 2000 times greater than MaxMin;
* The primary field is dipolar, allowing maximum coupling in almost all of the investigated volume;
* Depth of investigation is four times that of MaxMin and twice that of DEEPEM;
* Operates in frequency domain for a better signal to noise ratio;
* Good sensitivity to poor conductors, such as sphalerite lenses;
* Uses the out-of-phase component of the H_r/H_z ratio to compute a purely inductive apparent resistivity, exempt of static shifts and topographic effects;
* The data is presented as pseudosections of resistivity versus frequency;
* Two dimensional software modelling using finite elements can simulate conductive overburden and multiple conductors;
* The geophysical signature of a surface effect is quite different from that of a vertical thin plate.

1. *DESCRIPTION OF THE METHOD*

As is the case for all electromagnetic techniques, the MELIS method consists of an EM field transmitting system and a receiving system. The latter measures the primary field as well as secondary fields induced by the presence of conductors in the ground (figure 1).

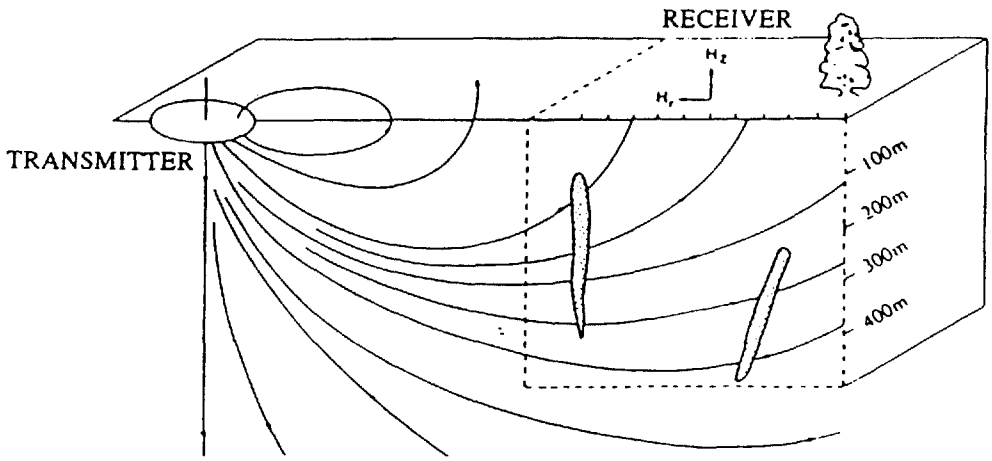


Figure 1: The MELIS in loop ρ' method.

TRANSMITTING SYSTEM

The MELIS primary field is created by an alternating current flowing in a loop of wire. The dimensions of this loop should be small compared to the distance to measuring points. The field source can therefore be considered as a vertical magnetic dipole such as is the case for horizontal loop EM (MAXMIN). In order to obtain investigation depths of 500 m or more, the spacing between the transmitter and receiver should be much larger than in HLEM, of the order of 1 to 1.5 kilometers. Such a spacing, together with the anticipated investigation depth, requires a very strong magnetic moment.

We should recall that $M \alpha A \cdot n \cdot I$

where M is the magnetic moment
A the surface of the loop
n the number of turns in the loop
I the current flowing in the loop

Using a 200 m x 200 m loop with two turns, a magnetic field 2 000 times stronger than one created by a MAXMIN transmitter can be generated, while respecting dipolar field parameters. Contrary to MAXMIN, this source must be in a fixed location for cost reasons.

The dipolar nature of a MELIS primary field is one of the technique advantages. Figure 2 shows the direction of the primary field created by a MELIS transmitter in much the same fashion as TEM (Pulse EM for example). The length of the arrows indicates the relative amplitude of this field. Several observations can be made:

1°) The primary field always has an important horizontal component capable of generating eddy currents (therefore a secondary field) in any subvertical conductor located in the survey zone illustrated in figure 2.

2°) In the case of investigating for deep subhorizontal conductors, it might be preferable to place the loop far enough from the survey zone in order to maximize the vertical component of the primary field.

3°) In the case of a subvertical conductor, the deeper it is, the better the coupling (figure 3). At surface the MELIS primary field being vertical, coupling is virtually nil. Filtering of subsurface conductors that are already known is then accomplished automatically. Therefore detection of deeper conductors is favoured.

4°) The coupling being good in the entire survey area, a single loop should be necessary in order to detect any subvertical conductor, which is not the case for PULSE EM for example (figure 4). As we shall see later on MELIS may sometimes require a second loop in order to better define a good conductor.

Finally we must point out that a magnetic field source such as is encountered in MELIS, PULSE EM, and HLEM is less sensitive to lateral inhomogeneities than an electric field source such as is encountered in magnetotellurics such as CSAMT. Moreover, the use of a small loop gives a better resolution and less sensitivity towards conductive overburden than TEM.

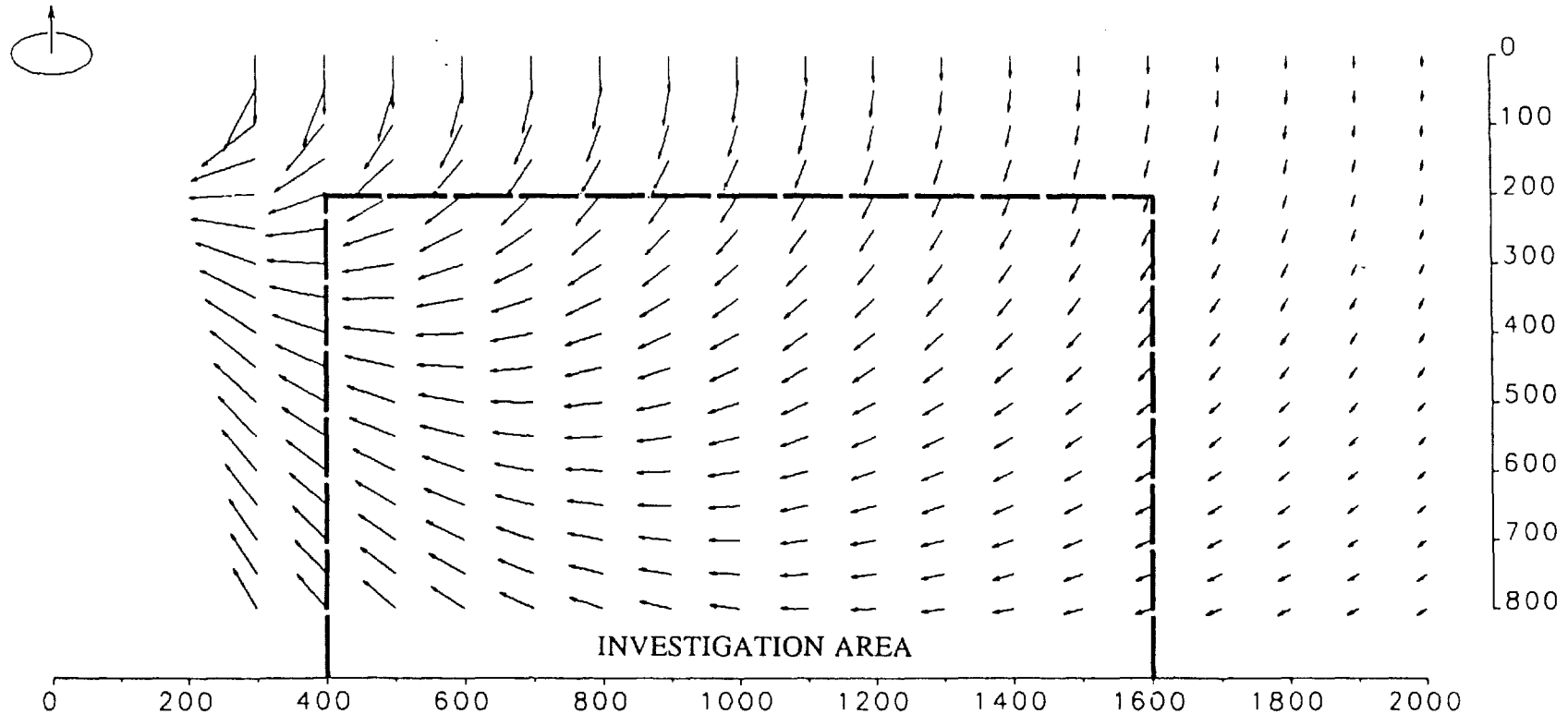


Figure 2: Direction and relative strength of MELIS primary field.

SAGAX GEOPHYSIQUE

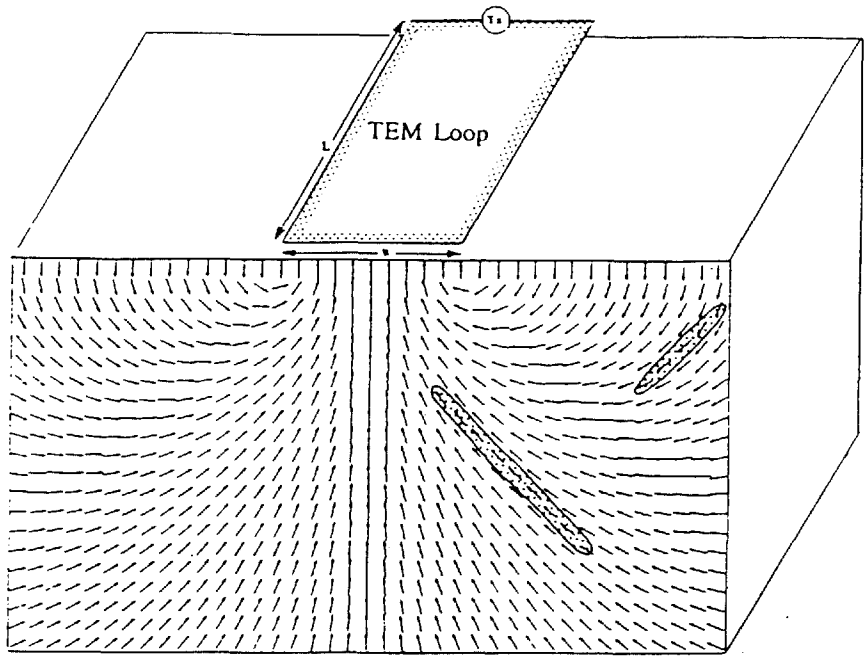


Figure 4: Examples of non-coupled conductors that would require a second loop in TEM.

RECEIVING SYSTEM

Two orthogonal magnetic coils connected to a MELIS receiver measure the in-phase (real) and out-of-phase (imaginary) components of the radial horizontal field H_r with respect to the vertical field H_z. In the absence of conductors, the latter represents the primary field whereas H_r exists only when the ground is conductive. Measurements are then taken at about ten frequencies that are chosen according to surrounding resistivity as well as the investigation depth.

Figure 5 illustrates the real and imaginary parts of the H_r/H_z ratio as a function of the induction number $|kr| = r(\omega\mu\sigma)^{1/2}$. This function increases in a monotonous fashion, therefore one to one, and can consequently be inverted. The induction number and the corresponding apparent resistivity can be calculated from the field ratio by the following equations:

$$\rho_a = \frac{1}{\sigma} = \frac{\omega\mu r^2}{|kr|^2}$$

where $|kr|$ = induction number
ω = $2\pi x$ (frequency)
μ = magnetic permeability
r = transmitter receiver distance

Therefore as a general rule: $\rho_a \alpha \left(\frac{H_r}{H_z}\right)^{-1}$

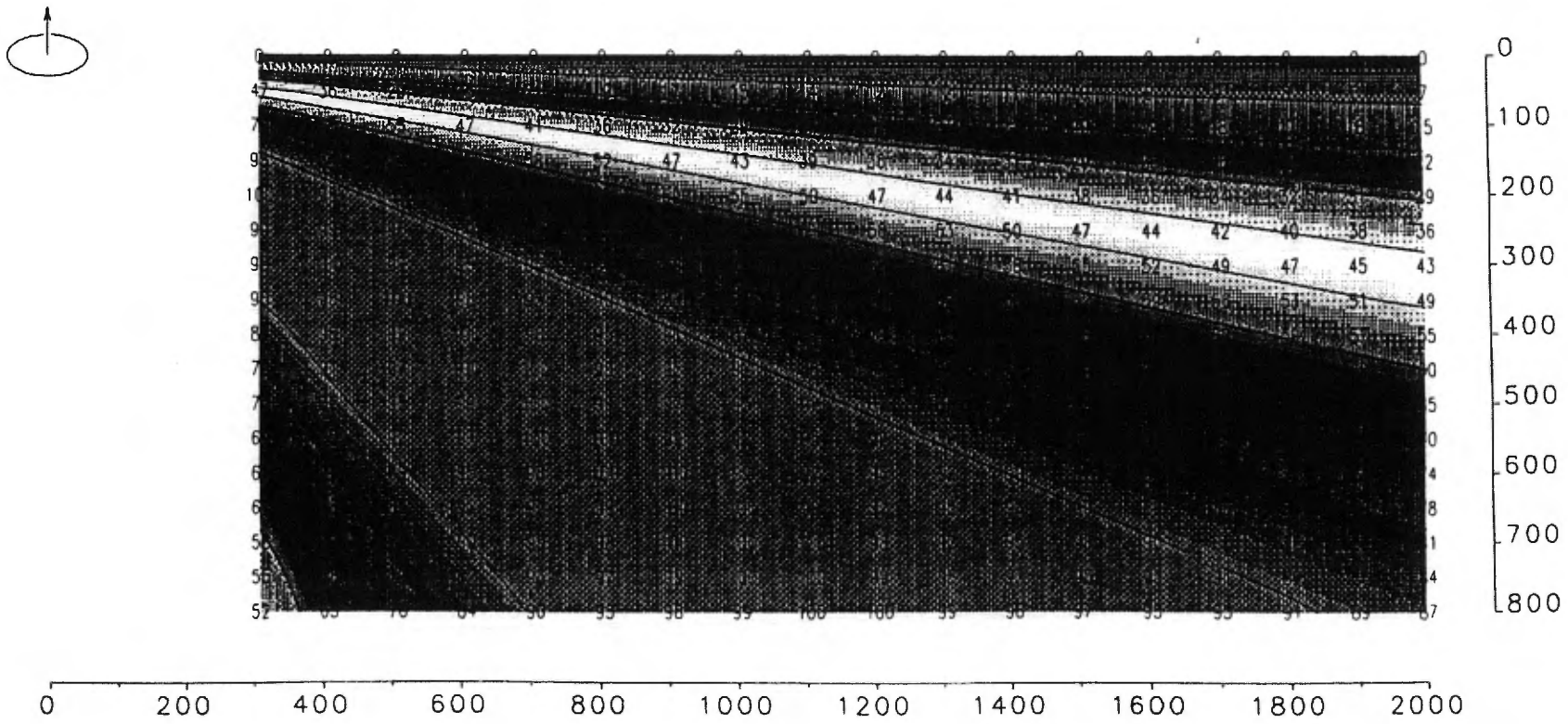


Figure 3: Coupling (in %) of the MELIS primary field with subvertical conductors.

SAGAX GEOPHYSIQUE

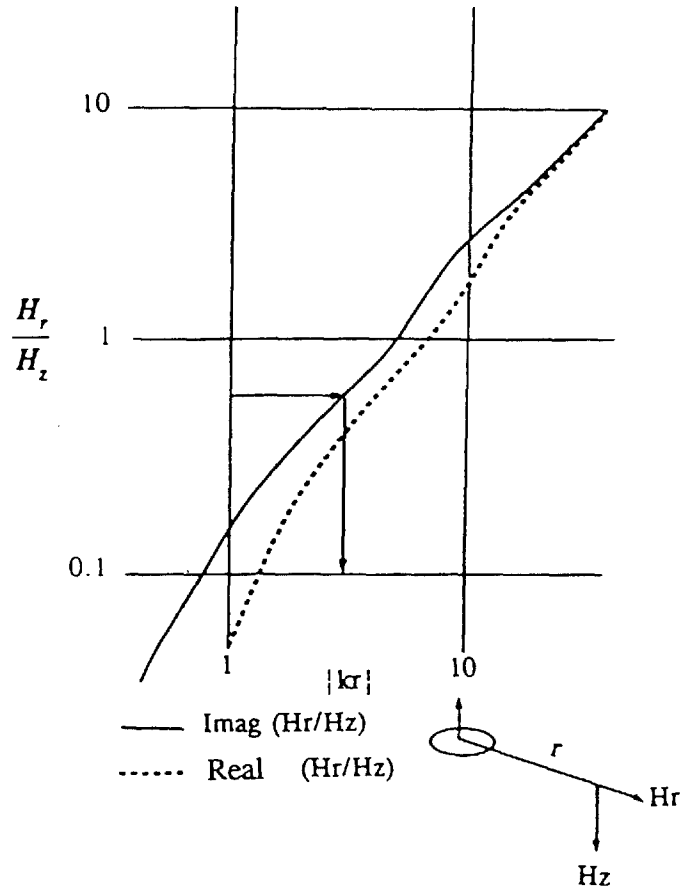


Figure 5: Real and imaginary parts of the field ratios for the MELIS method.

One of the advantages of MELIS is to rid itself of the dependency upon the transmitter dipole moment for the determination of apparent resistivity thanks to the use of a magnetic field ratio. Even if the amount of current flowing in a loop can easily be determined, the determination of the area can sometimes be fastidious in certain field conditions. Apparent resistivity determined by MELIS is then purely inductive, without static shifts which appear in magnetotellurics where one of the components is electric.

Due to topography in the survey area, measurements could be taken in a surface plane which is not that of the transmitting loop (figure 6). These topographic effects are not important at high and medium induction, but this is not the case for low induction in particular for the determination of H_r, the horizontal component of the magnetic field. This component is weak at low induction numbers and, if the coils are below or above the surface plane of the loop, it will contain, along with the horizontal field, the horizontal component of the primary field. This horizontal component appears as the primary field is tilted when it leaves the surface plane of the loop.

These topographic effects could generate false conductors and therefore be a serious setback if the field amplitude ratio was measured only.

To eliminate these difficulties, MELIS measures not only the field amplitude ratio but also the real and imaginary parts of the transfer function between H_r and H_z. At low induction, the horizontal magnetic field is out-of-phase with the primary field and the vertical magnetic field is mostly in phase. The horizontal component of the primary field out of the loop surface plane does not affect the measurement if the out-of-phase horizontal component is taken only. Topographic effects become negligible in this case.

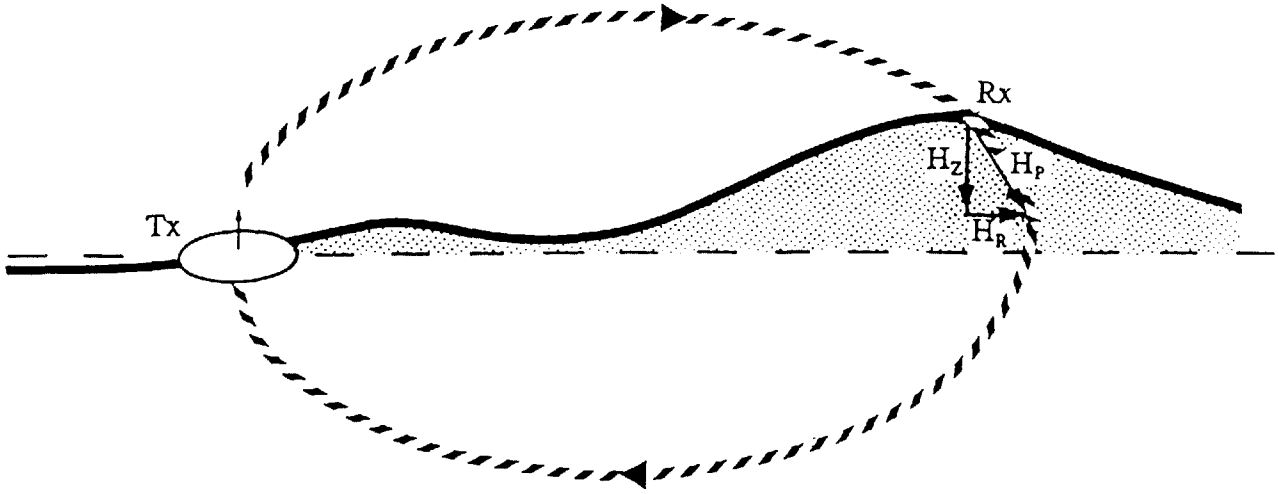


Figure 6: *Undesirable contribution of the primary field H_p to the in-phase component of H_r when the receiver is not in the same surface plane as the transmitting loop. This contribution becomes negligible if the out-of-phase component of H_r is measured.*

Using the measured values of $im(H_r/H_z)$, the MELIS receiver determines the value of $| kr |^2$ by second-order interpolation from a precomputed table of values stored in the instrument memory (table 1). The computed apparent resistivities are then presented in pseudosections versus frequency.

If there are no good electrical conductors in the area, these pseudosections will look like geoelectrical cross-sections where the overburden layer and geological contact between resistivity contrasted units should be easily mapped. The introduction of a good conductor will however distort the primary field to a point where the apparent resistivity values may be meaningless unless they are interpreted with the help of numerical models, as with HLEM for example.

$\|kr\|^2$	$Im[H_r/H_z]$	$\|kr\|^2$	$Im[H_r/H_z]$
0.0E+00	0.000000E+00	4.0E+01	1.390959E+00
1.0E-04	2.499952E-05	4.5E+01	1.522129E+00
1.0E-02	2.494612E-03	5.0E+01	1.656719E+00
1.0E-01	2.437226E-02	6.0E+01	1.934392E+00
3.0E-01	6.890542E-02	7.0E+01	2.214313E+00
5.0E-01	1.079896E-01	8.5E+01	2.592954E+00
7.0E-01	1.423075E-01	1.0E+02	2.853255E+00
8.5E-01	1.653671E-01	1.1E+02	2.949570E+00
1.0E+00	1.864506E-01	1.2E+02	3.001829E+00
1.2E+00	2.119185E-01	1.3E+02	3.032691E+00
1.5E+00	2.454491E-01	1.5E+02	3.094022E+00
2.0E+00	2.919453E-01	1.7E+02	3.193594E+00
2.5E+00	3.301523E-01	2.0E+02	3.405798E+00
3.0E+00	3.626513E-01	2.5E+02	3.807130E+00
4.0E+00	4.165088E-01	3.0E+02	4.186408E+00
5.0E+00	4.610834E-01	4.0E+02	4.808417E+00
6.0E+00	5.000198E-01	5.0E+02	5.350321E+00
7.5E+00	5.518932E-01	7.5E+02	6.520136E+00
1.0E+01	6.283679E-01	1.0E+03	7.509670E+00
1.2E+01	6.844887E-01	2.0E+03	1.057985E+01
1.5E+01	7.640718E-01	4.0E+03	1.493308E+01
2.0E+01	8.905538E-01	1.0E+04	2.358048E+01
2.5E+01	1.014167E+00	3.0E+04	4.079851E+01
3.0E+01	1.137783E+00	1.0E+05	7.453560E+01
3.5E+01	1.263040E+00		

Table 1: *Imaginary parts of the field ratios used in the computation of apparent resistivities for MELIS.*

2. *FIELD OPERATIONS*

Before going into the details of data interpretation, we will take a look into some practical aspects of the MELIS method.

EQUIPMENT DESCRIPTION

The transmitting apparatus is composed of a IRIS Instruments Tx1000 transmitter (21 Kg) powered by a 220 Volts, 50/60 Hz commercial motor generator of at least 1500 watts. This combination allows to inject at low and medium frequencies a 12 amps square wave in a 200 m square loop. This loop is made of 2 to 3 turns of 10 gage wire and has a resistance of about 8 ohms. The injected current is lower at higher frequencies due to the loop inductance. Since the current is injected at a discrete frequency, all the available energy is concentrated at this frequency (and its harmonics) which is not the case with time-domain EM methods, such as PULSE EM.

The MELIS receiver is in fact a 2 channel spectral analyzer which can simultaneously measure H_r and H_z between 0.1 and 8 000 Hz. During the readings, the receiver displays in real time the out-of-phase component of H_r and the reference signal amplitude (H_z).

The receiver also measures the signal to noise ratio by comparing the signal amplitude to the amplitude of adjacent frequencies (figure 7). The signal-to-noise ratio is then used as a weighing factor in order to determine the contribution of each measure to the final reading which is obtained by averaging.

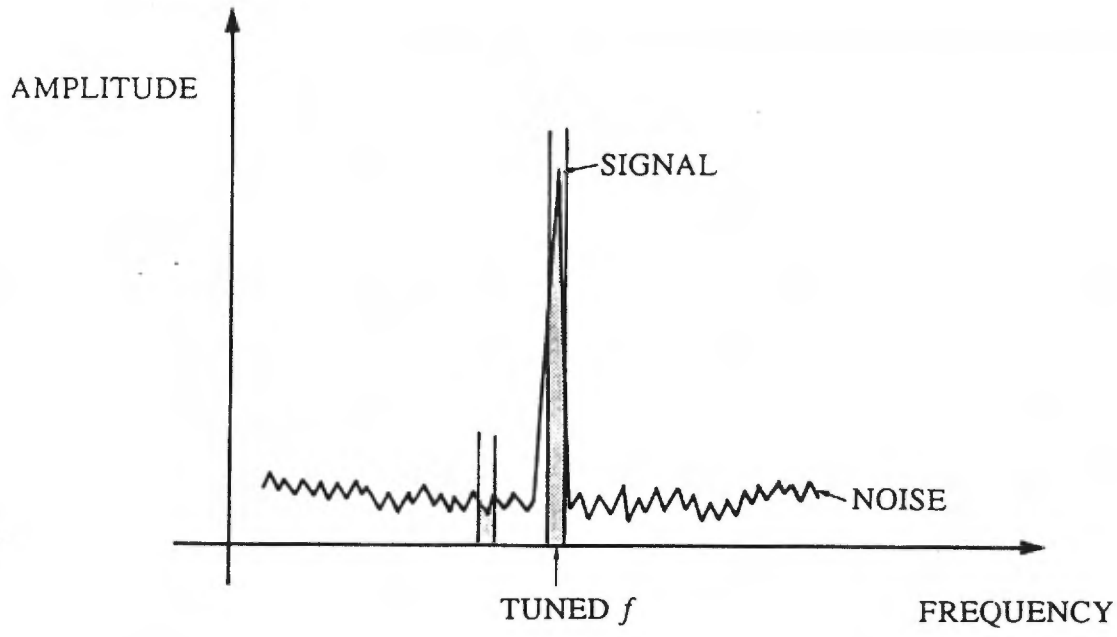


Figure 7: Simultanious noise and signal reading by the MELIS receiver.

LOGISTICS

For the search of a deeply buried (>200 m) subvertical body, a 200 x 300 m loop should cover a 0.8 km^2 zone centered on the horizon to be investigated (figure 8). The distance between the loop and the horizon should be at least 1.5 times the expected depth of investigation. Obviously, the loop should not be placed directly over a good conductor.

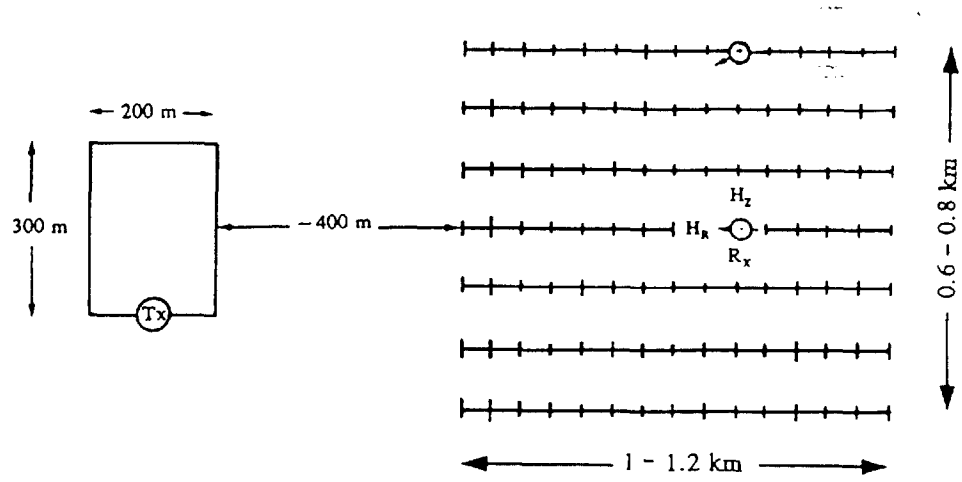


Figure 8: Typical layout of a MELIS loop in respect to a deeply buried target.

The reading density depends on the target depth and geometry. Usually a 200 m x 50 m mesh is considered sufficient for the search of subvertical bodies. Since the investigated volume has a conical shape, the mesh can be enlarged to 300 m x 75 m if the bodies are deep and have a certain longitudinal extension. For subhorizontal bodies, the mesh can be of 400 m x 100 m, which has a direct influence on survey costs.

In a 1000 $\Omega \cdot$m (or more) environment, 10 to 12 frequencies in the 15 to 7600 Hz are sufficient to insure that the technique maximal depth of investigation has been reached.

OPERATING COSTS

Unlike MAG, VLF or HLEM, MELIS in loop ρ' mode is not a systematic exploration tool. It is rather reserved for the investigation of favorable targets identified by the geological context, geochemistry or other geophysical methods.

Three days work would be necessary to cover a 1000m by 600m target with a 200m by 50m grid mesh, with 10 frequencies read at every station. The cost for this survey would be about 1260$/km, including the transmitting loop set up and removal. This is about the same as for a DEEPEM survey when two loops are required or twice the cost if only one loop is used. However, depth of investigation and the quality of the information delivered is superior with MELIS.

Table 2 on next page shows the unit cost for different ground EM techniques and the total survey cost for a 2 km by 1 km target for each techniques. It can be seen that the cost per cubic km of investigated ground is about the same as for VLF and HLEM but much less than DEEPEM.

MELIS having a larger depth of investigation than these techniques, cost comparison by cubic km is more appropriate than a comparison based on linear km.

Depending on the target dimensions, the survey mesh is between 200m by 50m and 400m by 100m. If one is interested in the 300m to 600m depth range, a 300m by 75m mesh should be adequate. The lateral sensibility of MELIS being about half the investigation depth, a 300m spacing between survey lines is adequate for the search of targets buried at 300m or more. Furthermore, the MELIS anomaly generated by such a conductor would have a wavelength greater than 450m for which a station spacing of 75m is sufficient. In this case the MELIS survey cost would be half of VLF and two-thirds of HLEM.

Table 2: COST COMPARISON BY CUBIC KM BETWEEN MELIS AND OTHER EM TECHNIQUES

Method	Line spacing	Station spacing	cost/km	Investigation range	Example: target of 2 km X 1 km			Cost/km³
					Nb of km	Survey cost	Investigated volume	
VLF (one station)	100 m	12.5 m	70 $	0 - 50 m	21 km	1 470 $	0.10 km³	14 700 $
HLEM (T_x-R_x spacing = 100m)	100 m	25 m	150 $	0 - 150 m	21 km	3 150 $	0.30 km³	10 500 $
TDEM (DEEPEM, EM-37)								
one loop	200 m	50 m	500 $	150 - 300 m	11 km	5 500 $	0.30 km³	18 350 $
two loops	200 m	50 m	500 $	150 - 300 m	22 km	11 000 $	0.30 km³	36 700 $
MELIS								
detail survey	200 m	50 m	1200 $	150 - 600 m	11 km	13 200 $	0.90 km³	14 700 $
reconnaissance survey	300 m	75 m	900 $	150 - 600 m	7 km	6 300 $	0.90 km³	7 000 $

3. *INTERPRETATION PRINCIPLES*

Even though apparent resistivities allow a qualitative interpretation, they should nonetheless be considered as part of a data normalization process. As with electrical resistivity methods (dipole-dipole for instance), their behaviour is not always intuitively guessed and theoretical models are more often necessary. Before examining those theoretical models, we will try to understand the behaviour of the H_r/H_z ratio in the vicinity of a conductor.

QUALITATIVE DESCRIPTION OF MELIS ANOMALIES

Figure 9 lower part shows in red the secondary field (H_s) inducted by the primary field (H_p, in black) in the presence of a vertical conductor.

If the secondary field is decomposed in its horizontal and vertical components, it can be seen that:

1°) H_s horizontal component is maximum directly over the conductor and it fades out to zero far from the conductor. A graph of H_r/H_z (normalized by the distance) would then have a symmetrical bell shape, as illustrated by figure 9a.

2°) H_s vertical component has the same orientation as H_p between the loop and the conductor and is opposed to H_p on the conductor's other side. This generates an asymmetrical signature similar to VLEM (figure 9b).

When those two effects are added, we obtain an asymmetrical H_r/H_z anomaly with a decrease of the ratio between the conductor and the loop and a H_r/H_z high on the side opposite to the loop (figure 9c).

Since $\rho_a \propto \left(\frac{H_r}{H_z}\right)^{-1}$, the ρ_a profile should be the mirror image of the H_r/H_z profile.

Other phenomenons will affect the anomaly shape, although to a lesser degree. For instance, the attenuation of the primary field by the conductor will appear as a larger decrease of ρ_a (increase of the H_r/H_z ratio) on the side opposite to the loop. The investigation depth and induction number being a function of the frequency, its variations will globally affect the MELIS response.

As is the case for DC resistivity surveys, a conductor signature is not limited to a resistivity decrease over the conductor, hence the importance of numerical modelling.

THEORITICAL MODELS

We shall present eight pertinent models which will greatly facilitate the analysis of field examples to be presented. These 2D models were calculated using the B.R.G.M.'s BIEFEM modelling software.

The first three models are vertical plates located at different depths (50, 100 and 200m) from surface (figure 10). The hostrock has a resistivity of 5000 Ω • m and is covered by an overburden (200 Ω • m) of moderate thickness (20 m). The vertical extension of the plate is 500 m. The computations were done for a moderate conductor (3,33 siemens, figure 11) with the transmitting loop located 700 m from the vertical location of the conductor.

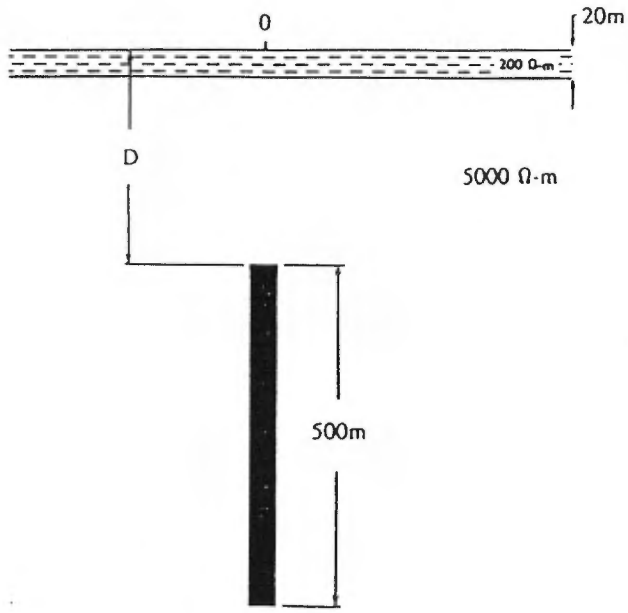


Figure 10: The vertical plate model.

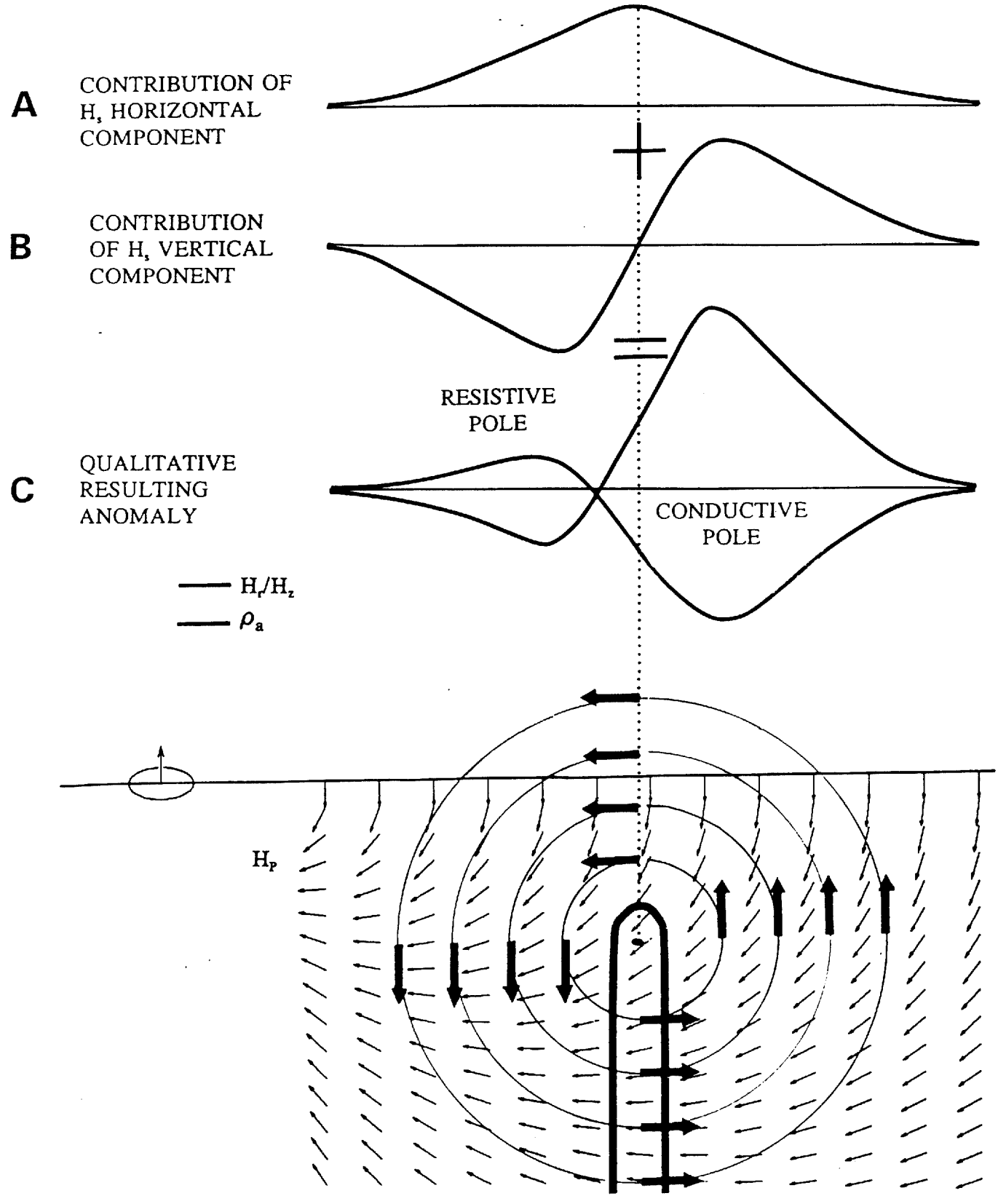


Figure 9: *Qualitative contribution of the horizontal (A) and vertical (B) components of the secondary field H_s to the resulting H_s/H_z anomaly (blue curve on C). The ρ_a response (orange curve on C) is qualitatively the opposite because ρ_a is inversely proportional to (H_s/H_z).*

SAGAX GEOPHYSIQUE

On the apparent resistivity pseudosections of figure 11, the vertical plate is characterized by a conductive anomaly at low frequencies and by a resistive anomaly at high frequencies, with an alternating anomaly of bipolar type at medium frequencies. This phenomenon is particularly obvious for the deepest conductor. For shallower sources, the anomaly remains bipolar even at high frequencies, the purely resistive response probably appearing at even higher frequencies which are not measured in the field. The resistive pole is an artifact whose derivation has been explained in section 3.

The horizontal location of the source is usually done at low frequencies where the conductive anomaly is best centered over the conductor. However, for a deeply seated poor conductor, the anomaly may not be pronounced enough to allow an exact location.

Two complementary models are presented to illustrate the effect of geological noise and of an equivalent geoelectrical structure.

The first model is represented by an overburden trough. To accentuate the trough effect, the overburden thickness was limited to 10 m with a 30 m deep trough 50 m in width. The results obtained (figure 12) delineated a very weak and narrow anomaly which is characteristic of a superficial effect. Such an anomaly would not mask the presence of a bedrock conductor nor could it be interpreted as such a conductor. Lower resistivities are observed for all frequencies close to the transmitting loop. They correspond to a smaller depth of penetration caused by the proximity of the transmitting loop. The limit values obtained close to the loop are identical to the overburden resistivity. These effects are not present in our field examples because the survey area starts at over 400 m from the loop.

The equivalent geoelectric structure is that of a thick (100 m @ 100 $\Omega \cdot m$ = 1 siemens), poorly conductive zone in a resistive hostrock. This could represent a fault zone which has been intensely altered. The results (figure 13) are very similar to those obtained with shallow plates, taking into account the conductance ratios. Therefore, this model is in fact geoelectrically equivalent to the previous models and could only be discriminated by criteria independent of an electromagnetic survey. We must point out the vertical behaviour of the bipolar anomaly, which is characteristic of a shallow source.

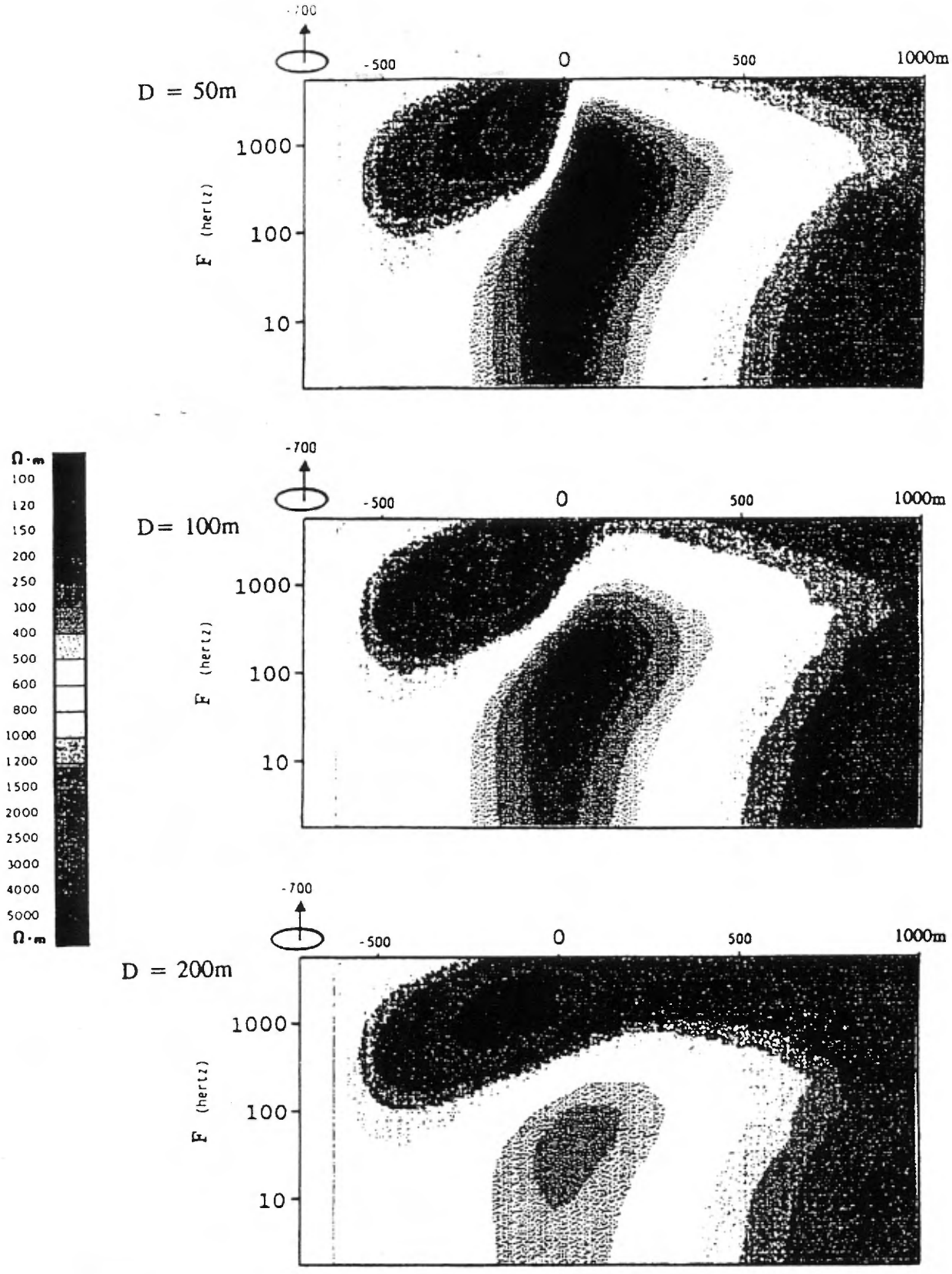


Figure 11: *MELIS apparent resistivity pseudosections for a vertical dyke of conductance 3,33 siemens.*

SAGAX GEOPHYSIQUE

The next three models (figure 14) represent a horizontal slab extending 400m within slightly resistive hostrock (500 $\Omega \cdot m$). The modelling was performed for three depths of conductors (100, 200 and 400m) and for a transmitter-receiver separation of 1000m.

As was the case in the previous models, these anomalies are also bipolar: the horizontal nature of the conductor is illustrated in the pseudosections by a *subhorizontal* limit between the resistive and conductive poles. At low frequency, the conductive anomaly is best centered over the slab. For slightly higher frequencies, the conductive anomaly is slightly off center of the conductor. For high frequencies the resistive anomaly for a shallow source tends to separate with an apparent resistivity maximum on the edge of the conductor, the side of the conductor farthest from the loop producing the strongest anomaly.

A 1D inversion was performed at station 0 (centered on the conductor). An overestimation of 15 to 33% on the depth (Table 3) is observed. This is still quite acceptable. As expected, the modelled conductance deviated from the true conductance (50 S) as the conductor gets deeper. The reason for this is that as the conductor gets deeper, it behaves less and less as a 1D model.

Table 3: 1D inversion of a 2D horizontal model having a conductance of 50S.

Depth to conductor	1D Inversion results	
	Depth	Conductance
100 m	115 m	39 S
200 m	266 m	29 S
400 m	495 m	27 S

These latter models are very interesting because they show that even for a subhorizontal body (poorly coupled with the primary field) which is also located in slightly conductive hostrock, a distinct bipolar anomaly is still observed for a conductor located at a depth of 400 m. In a resistive hostrock environment such as the Canadian Shield, a subvertical conductor should therefore be easily delineated with MELIS. From figures 11 and 14 sets of models, such a conductor would produce a subvertical bipolar anomaly having a wide conductive pole. This resistivity low would not be centered over the true position of the conductor, but shifted away from the loop.

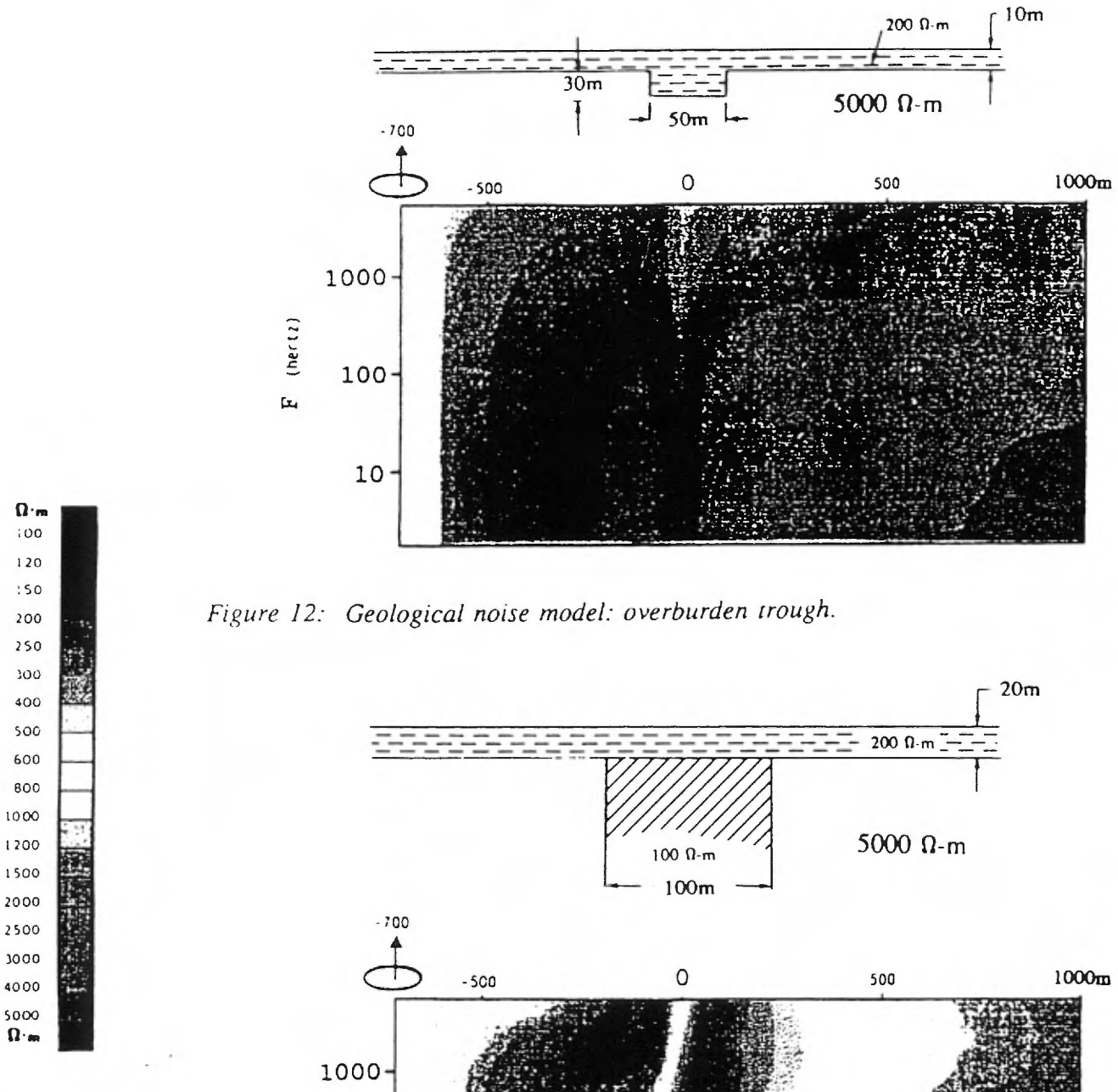


Figure 12: Geological noise model: overburden trough.

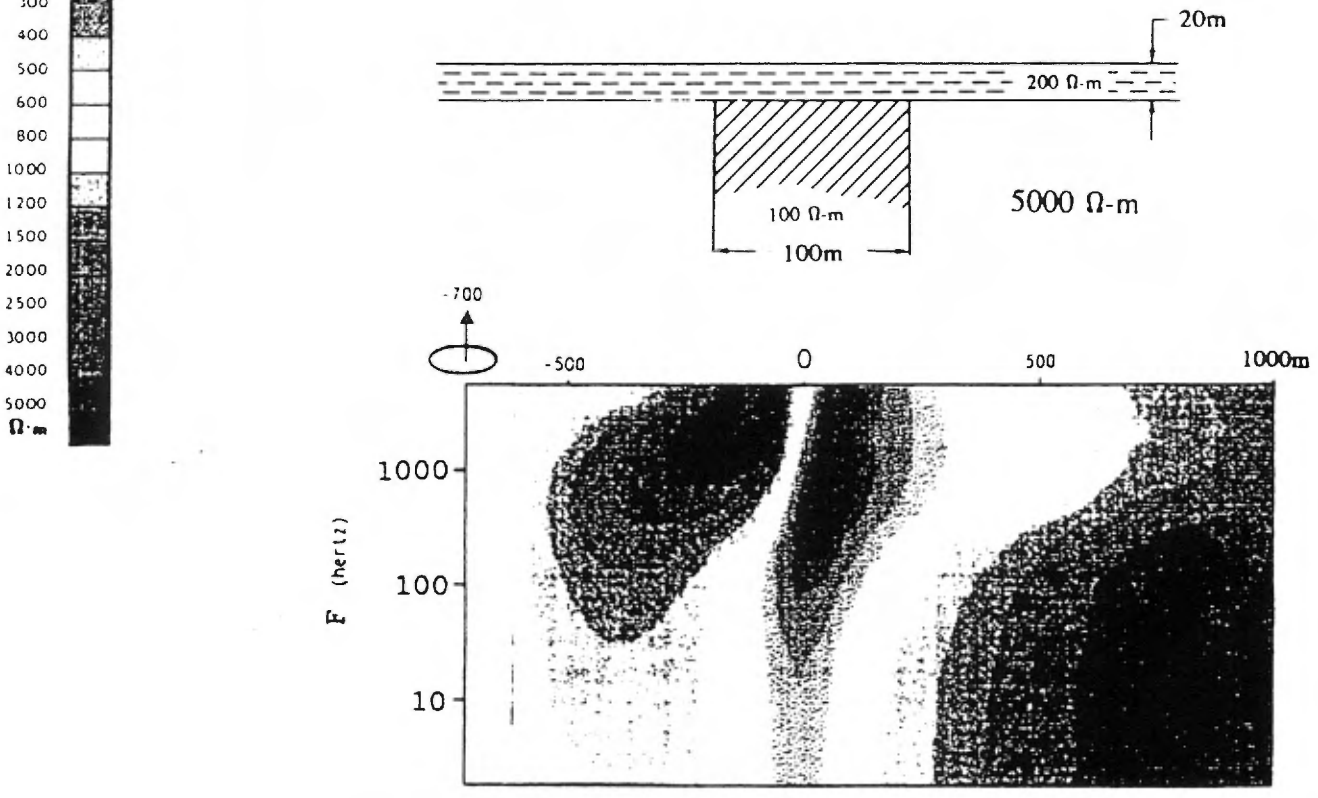
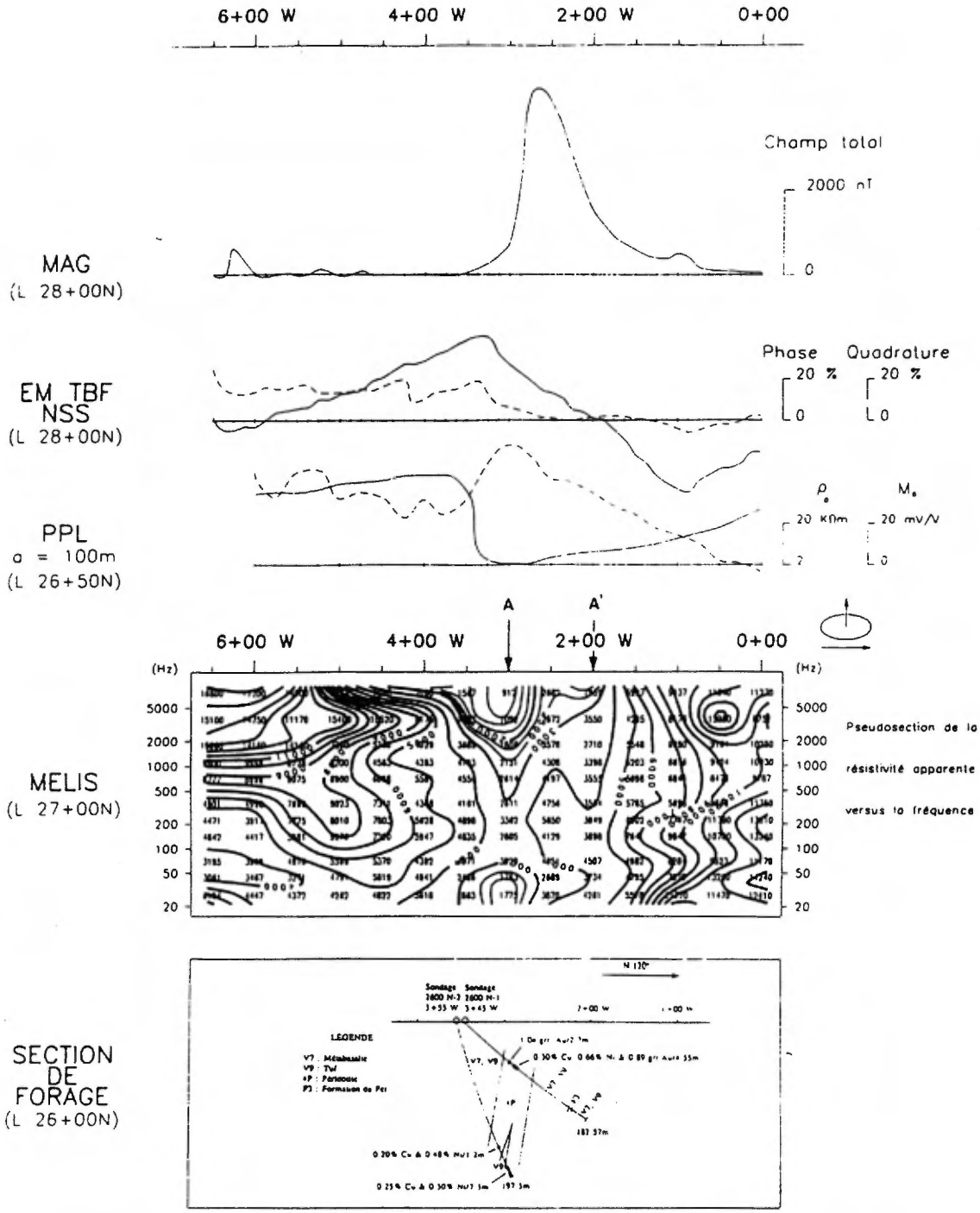


Figure 13: Vertical alteration zone located in resistive hostrock overlain by conductive overburden.

SAGAX GEOPHYSIQUE

LIGNE 27+00N



RESS. MIN. PLATINOR inc. et RESS. MIN. AUGYVA inc.
PROPRIETE DU LAC YASINSKI

Levés par SAGAX Géophysique inc

Date: Sept 1990 à déc 1991

50 0 50 100 150 200
(metres)

SAGAX GEOPHYSIQUE

Figure Y-1

On the other hand, MELIS anomaly A is increasing in amplitude towards the south (see pseudosection of L-26+00N on figure Y-3). However, the presence of the power line prevented the survey from taking place more to the south. Drillholes 2600N-1 and 2600N-2 which targeted the MELIS anomaly have been very encouraging as shown by the mineral intersections presented on figure Y-1. A drillhole implanted 50m to the south (2550N-1) intersects significant values in Cu-Ni and chrome:

1.42% Cu & 0.89% Ni for 0.9m @ 92.6m
0.58% Cu & 0.79% Ni for 0.4m @ 95.9m
0.53% Cu & 0.84% Ni for 0.45m @ 97.0m

this being inside a zone having an average of 0.39% Cu and 0.41% Ni for 4.85m from 92.6m to 97.45m. The drillhole also intersected an average of 4.58% Cr_2O_3 for 2.85m from 110.15m to 113m (Borduas, 1992).

It should be noted that the MELIS signature of conductor A (sections 26+00N and 27+00N) shows that it's conductance increases with depth. This justifies further drilling not only to the south but in priority at depth, between 250 and 500m.

---

(1) Borduas, Bernard: Rapport des sondages de octobre à décembre 1991, Propriété du lac Yasinski, février 1992.

MELIS FIELD EXAMPLE

YASINSKI LAKE Ni-Cu SHOWING

(PLATINOR & AUGYVA)

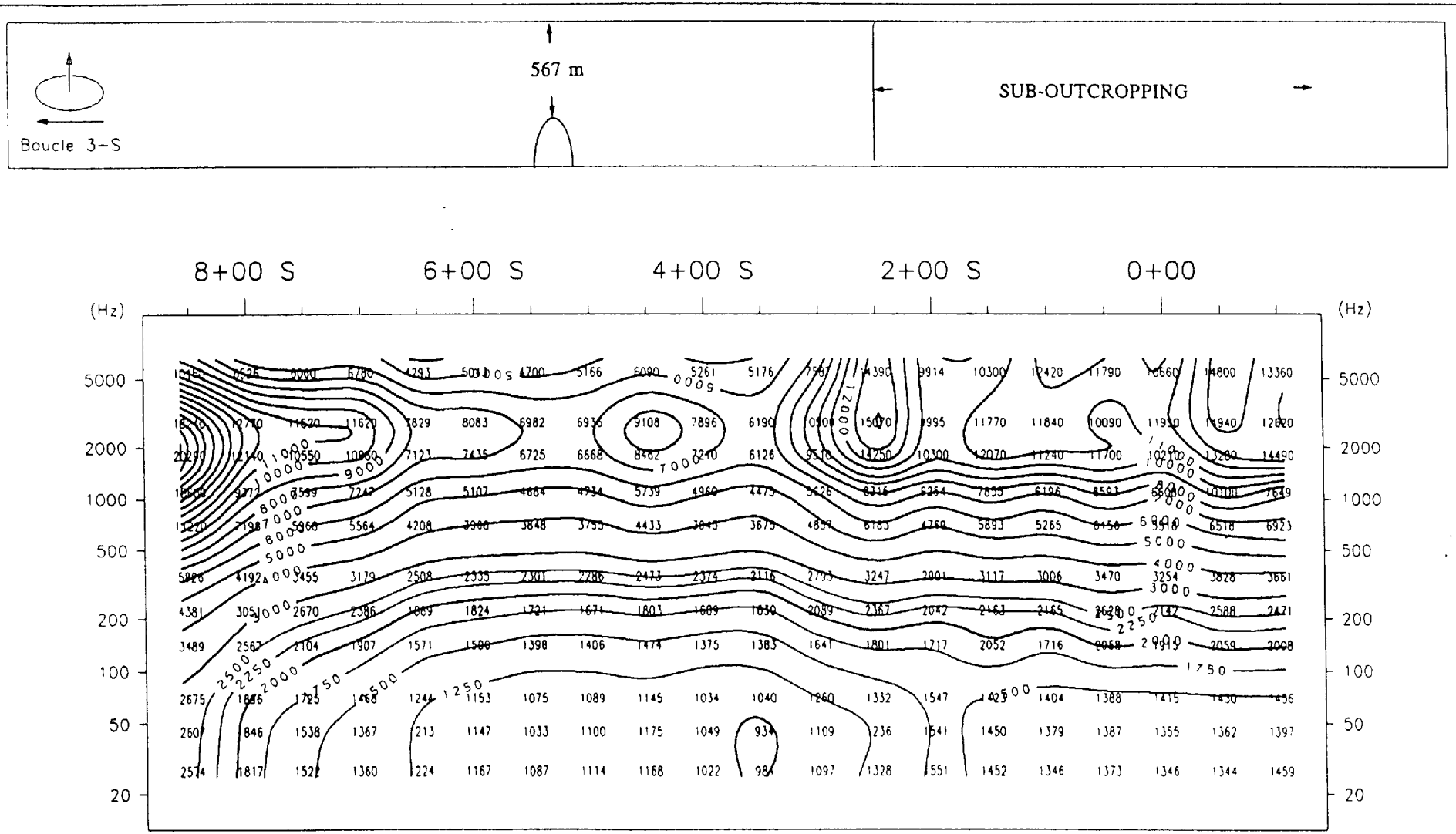
MARCH 1992

Since 1990, Platinor Mineral Ressources Inc. (in joint venture with Augyva Mineral Ressources Inc.) has conducted numerous geophysical surveys (MAG, VLF-EM, IP and MELIS) and drilled 62 exploration holes on the Yasinski Lake property located in the James Bay area, Quebec.

The aim of this case history is to relate the contribution of MELIS to the positionning of drillholes on "a Ni-Cu showing of economical interest and a chrome showing discovered in hole 2700N-1 drilled in February 1990"[1]. Figure Y-1 presents a compilation of the geophysical surveys conducted over those showings. It should be noted that those profiles are not all from the same line. This is due to the presence of a power line which affected some surveys. We chose to present only the profiles that were the least affected. The only drill section built from two DDHs, section 26+00N, is also presented.

The MAG and VLF-EM both show the presence of a magnetite bearing iron formation located around station 2+00W. The IP anomaly is caused by ultramafic rocks and can be observed for several kilometres. It is not possible to detect the presence of sulfides since the peridotite is both conductive and polarizable. The anomaly is monotonous over all of its extension.

The goal of the MELIS survey was to try to distinguish between the sulfides from the peridotite and to evaluate the extension at depth of the Cu-Ni showing. The MELIS pseudosection for line 27+00N shows two conductors: one at 2+00W (conductor A') and the other at 3+00W (conductor A). The first seems to correspond to the VLF anomaly (iron formation) while the other coincides with the Cu-Ni showing. For comparison, the MELIS anomaly on line 28+00N (figure Y-2) is related by its position and amplitude to anomaly A' of line 27+00N (iron formation). A drillhole on section 28+00N did not intersect any value in Cu or Ni, although it intersected some gold values and significant values in chrome (Borduas, 1992).



Instrumentation: MELIS de IRIS

Intervalles de contour: 50, 250, 1000 Ωm

Ligne 84+00 W

Echelle 1:5000

50 0 50 100 150 200

(metres)

Levé no: SAGAX

Date: Août 1991

Plan no 84WB3

SAGAX GEOPHYSIQUE

LEVE MELIS EN MODE LOOP ρ'

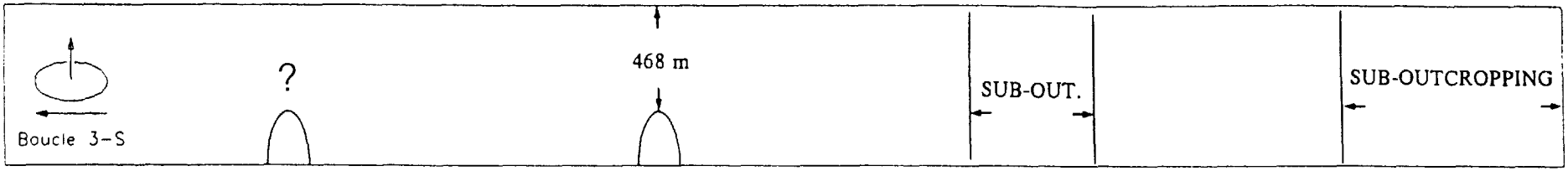
PSEUDOSECTION DE LA

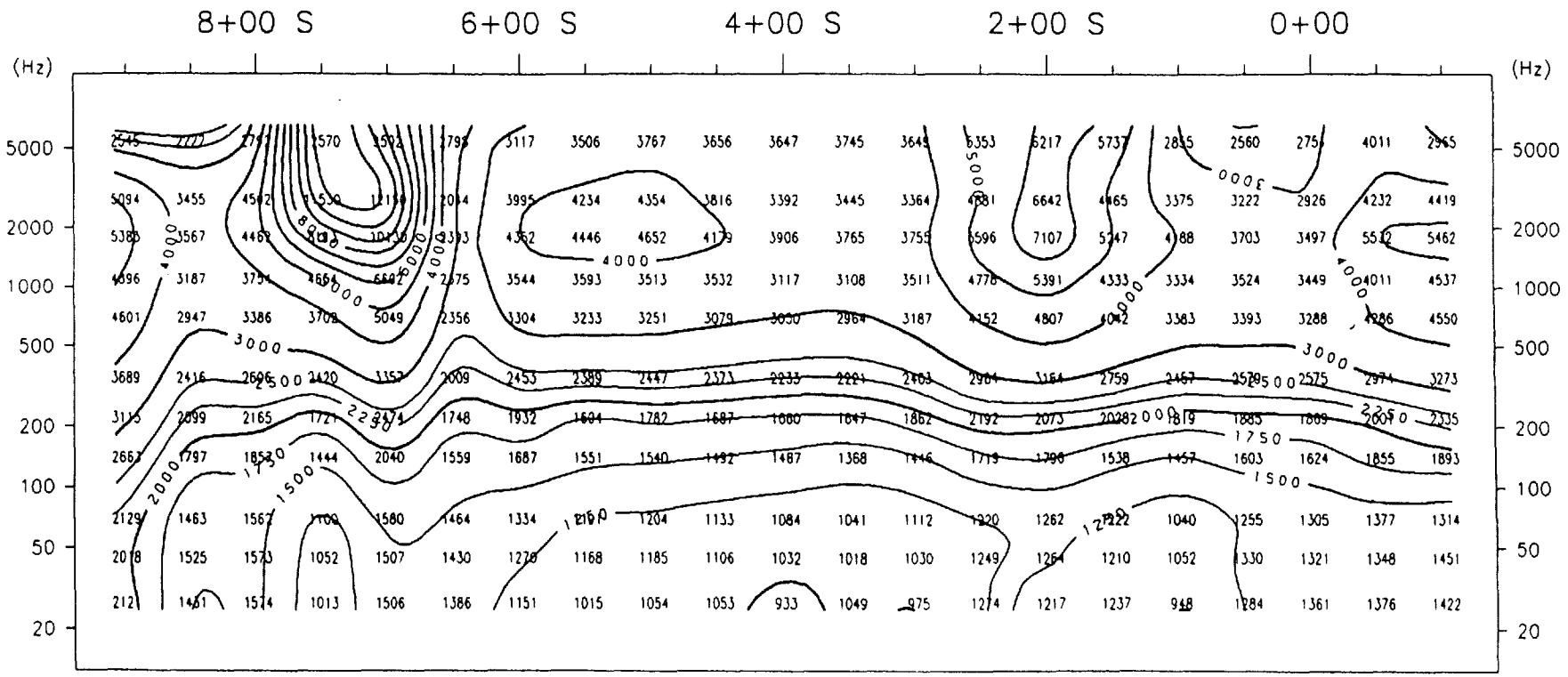
RESISTIVITE APPARENTE

RESSOURCES AUR INC.

PROPRIETE LOUVICOURT

CANTON LOUVICOURT





Instrumentation: MELIS de IRIS
Intervalles de contour: 50, 250, 1000 Ωm

Ligne 66+00 W

Echelle 1:5000
50 0 50 100 150 200
(metres)

Levé par: SAGAX
Date: Août 1991
Plan no 66WR3

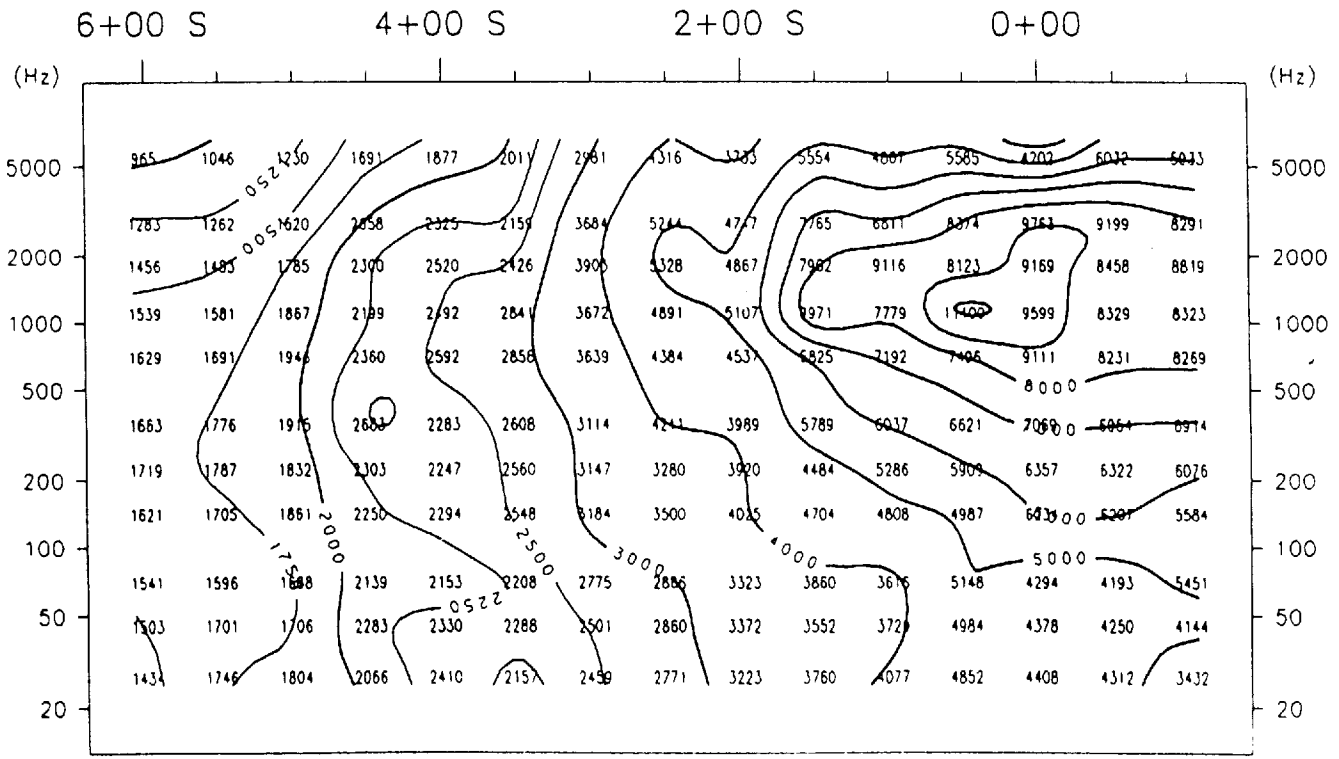
SAGAX GEOPHYSIQUE

LEVE MELIS EN MODE LOOP ρ'
PSEUDOSECTION DE LA
RESISTIVITE APPARENTE

RESSOURCES AUR INC.
PROPRIETE LOUVICOURT
CANTON LOUVICOURT

Boucle 2-S

← SUB-OUTCROPPING →



Instrumentation: MELIS de IRIS

Courbes de contour: 50, 250, 1000 Ωm

Ligne 84+00 W

Echelle 1:5000

50 0 50 100 150 200

(metres)

SAGAX GEOPHYSIQUE

Levé par: SAGAX

Date: Août 1991

Plan no 84WB2

SAGAX GEOPHYSIQUE

LEVE MELIS EN MODE LOOP ρ'_a

PSEUDOSECTION DE LA

RESISTIVITE APPARENTE

RESSOURCES AUR INC.

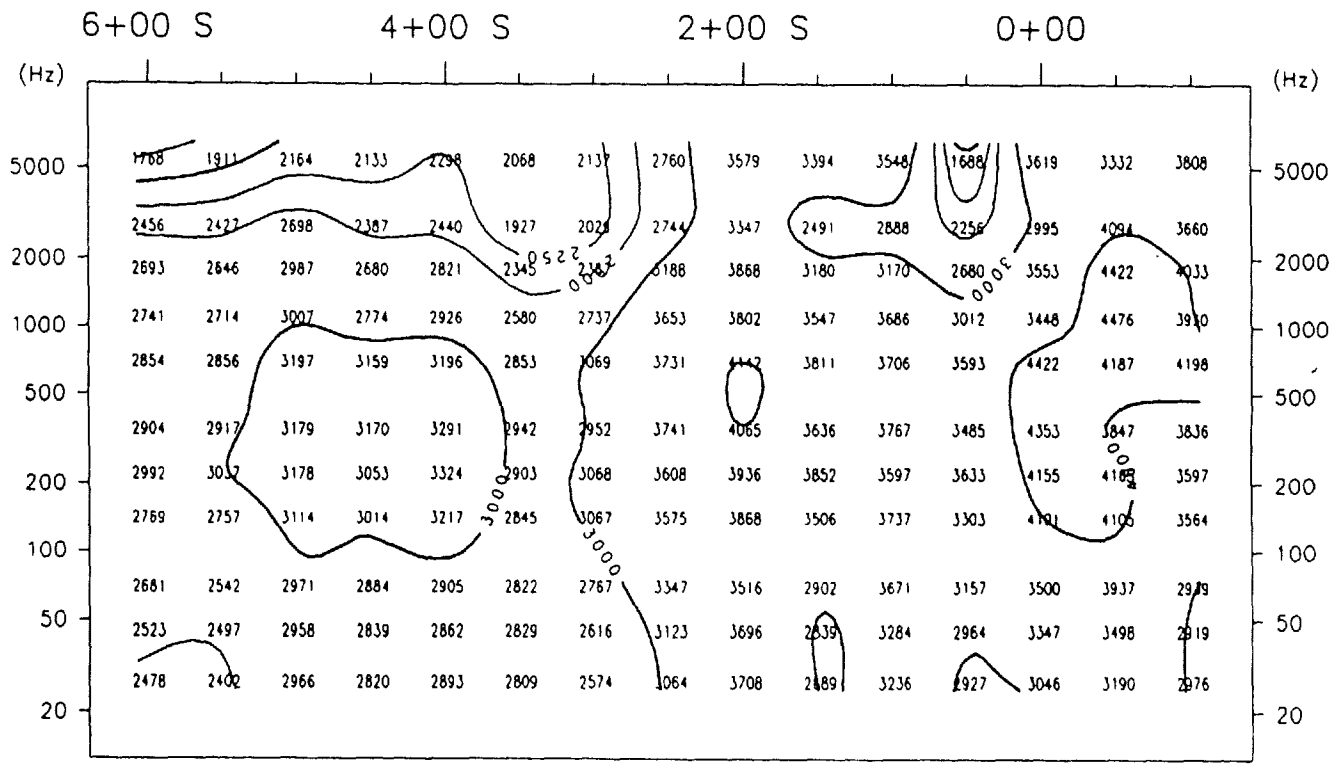
PROPRIETE LOUVICOURT

CANTON LOUVICOURT

Boucle 2-S

← SUB-OUT. →

← SUB-OUTCROPPING →



Instrumentation: MELIS de IRIS

Intervalles de contour: 50, 250, 1000 Ωm

Ligne 66+00 W

Echelle 1:5000

50 0 50 100 150 200

(metres)

Levé par: SAGAX

Date: Août 1991

Plan no 66WB2

SAGAX GEOPHYSIQUE

LEVE MELIS EN MODE LOOP ρ'

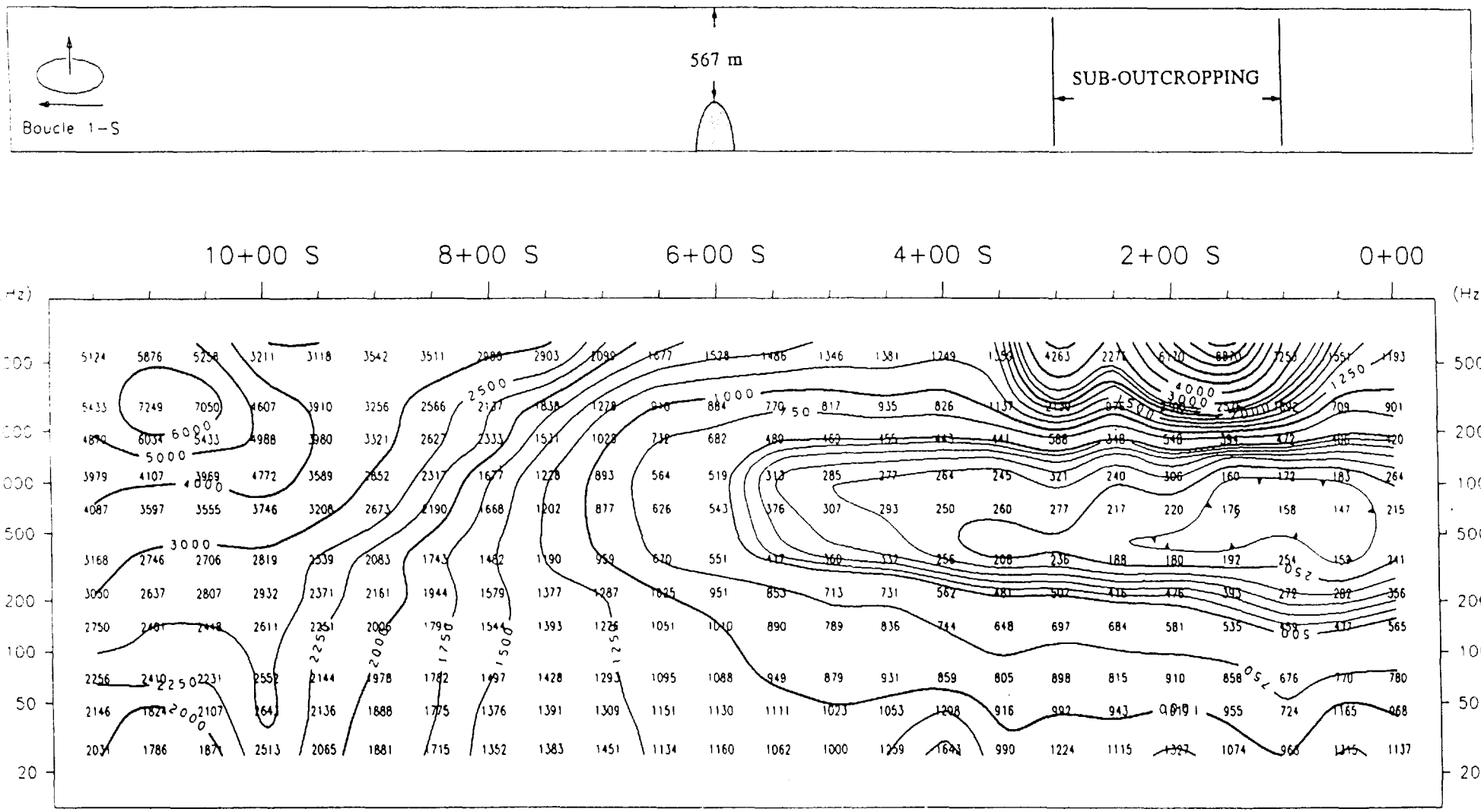
PSEUDOSECTION DE LA

RESISTIVITE APPARENTE

RESSOURCES AUR INC.

PROPRIETE LOUVICOURT

CANTON LOUVICOURT



Instrumentation: MELIS de IRIS

Intervalle de contour: 50, 250, 1000 Ωm

Ligne 84+00 W

Echelle 1 5000

50 0 50 100 150 200

(metres)

Levé par: SAGAX

Date: Août 1991

Plan no 84WB1

SAGAX GEOPHYSIQUE

LEVE MELIS EN MODE LOOP ρ'

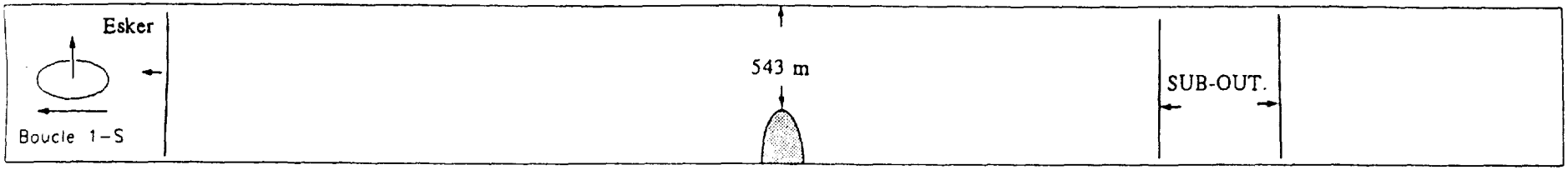
PSEUDOSECTION DE LA

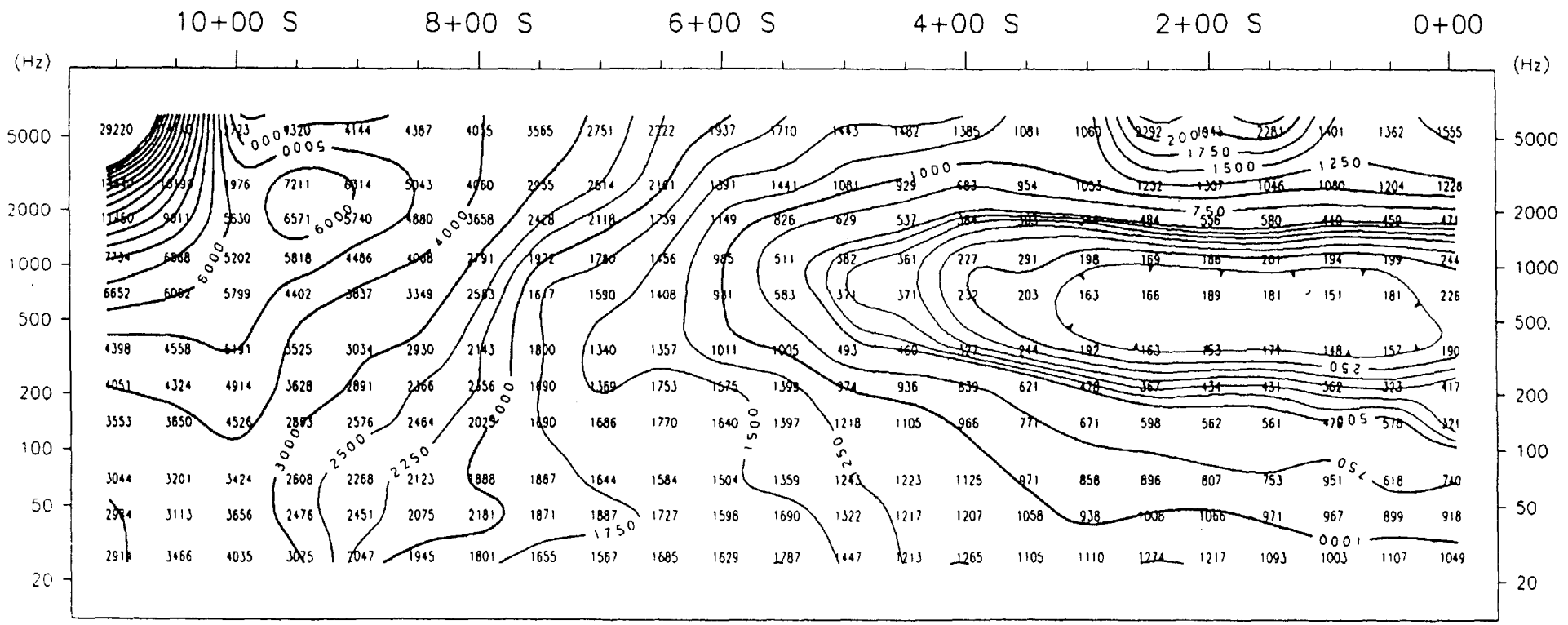
RESISTIVITE APPARENTE

RESSOURCES AUR INC.

PROPRIETE LOUVICOURT

CANTON LOUVICOURT





Instrumentation: MELIS de IRIS

Intervalles de contour 50, 250, 1000 Ωm

Ligne 72+00 W

Echelle 1:5000

50 0 50 100 150 200

(metres)

Levé par: SAGAX

Date: Août 1991

SAGAX GEOPHYSIQUE

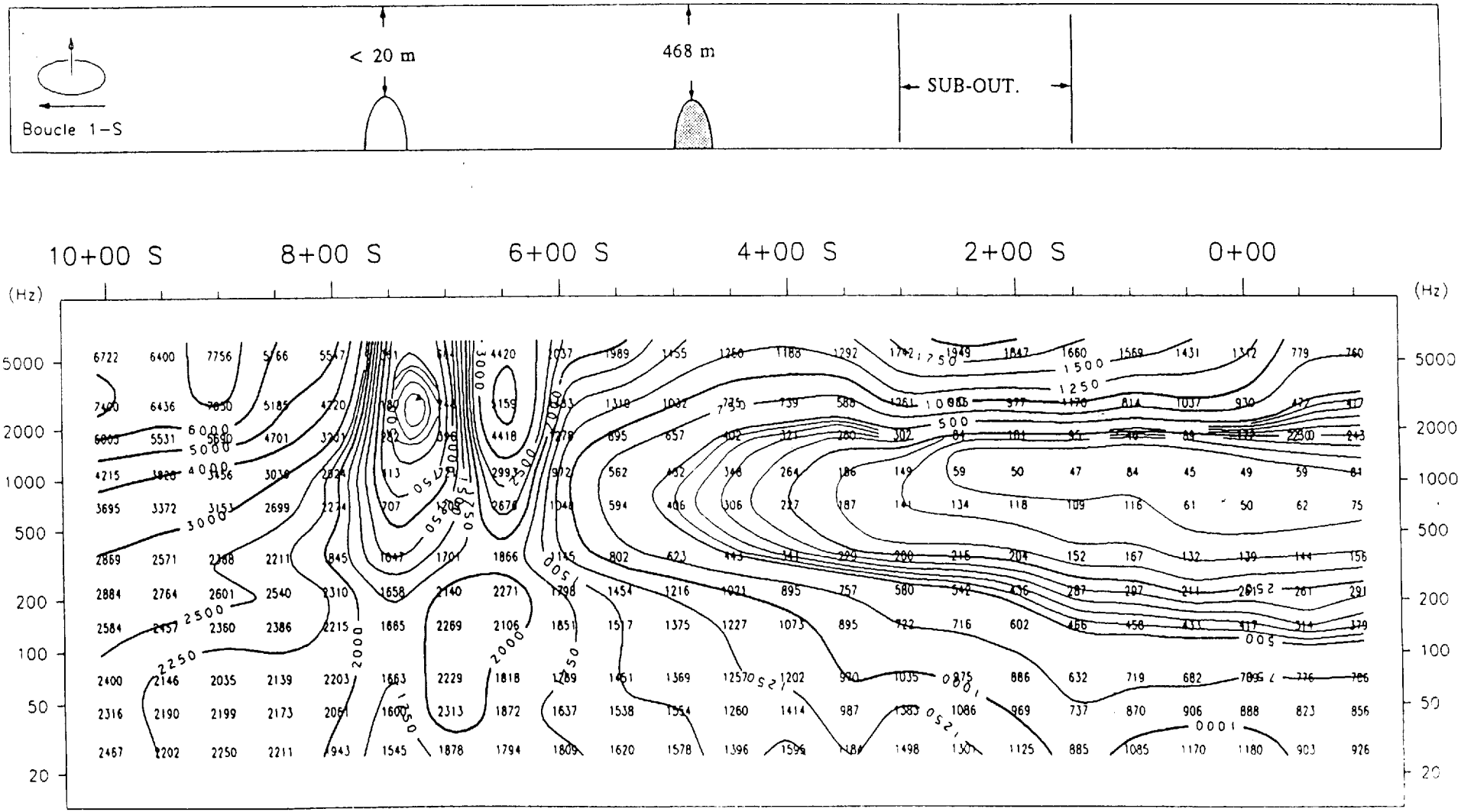
LEVE MELIS EN MODE LOOP ρ'

PSEUDOSECTION DE LA

RESISTIVITE APPARENTE

RESSOURCES AUR INC.

PROPRIETE LOUVICOURT



Instrumentation: MELIS de IRIS

Intervalles de contour 50, 250, 1000 Ωm

Ligne 66+00 W

Echelle 1:5000

50 0 50 100 150 200

(metres)

SAGAX GEOPHYSIQUE

Levé par: SAGAX

Date: Août 1991

Plan no 66WB1

SAGAX GEOPHYSIQUE

LEVE MELIS EN MODE LOOP ρ'

PSEUDOSECTION DE LA

RESISTIVITE APPARENTE

RESSOURCES AUR INC.

PROPRIETE LOUVICOURT

CANTON LOUVICOURT

AUR RESOURCES INC.

1 Adelaide Street East
Suite 2501
Toronto, Ontario M5C 2V9
(416) 362-2614
FAX (416) 367-0427

November 22, 1991

Mr. Pierre Bérubé
President
Sagax Geophysique Inc.
Suite 110,
6700 Avenue du Parc
Montréal, Québec
H2V 4H9

Dear Pierre:

RE: RELEASE OF LOUVICOURT PROJECT MELIS-EM TEST SURVEY DATA

This is to confirm that the partners in the Louvicourt Joint Venture have no objection to the release of the Melis EM test survey data for the Louvicourt deposit.

We are impressed with the results and concur that the method has great potential for detecting new deep-seated conductive ore deposits.

As previously mentioned, we would appreciate having an English version of the report documenting the test results (even if it's just a short resumé) for the benefit of our anglophone staff.

Yours very truly,

AUR RESOURCES INC.

Donald S. Bubar
Vice-President, Exploration

/vyw

cc: C.N. Britt
H.R. Stockford

Dip

For a shallow conductor, the circulation of the eddy currents at the edge of the conductor allow the determination of the dip for most of the EM methods. However, at depth, the dip cannot be determined. Furthermore, MELIS generates asymmetric anomalies which render dip determination difficult even for shallow sources.

Part IV: Comparison with geological data

Figure L-3 shows a representative N-S geological cross-section through the Louvicourt deposit. The optimal drill target, as determined by the quantitative interpretation of the MELIS results, has been superimposed on this section, showing an excellent correlation with the main mass of the deposit (lenses A-4 and A-5). The inferred depth to the top of the conductor (505m) is also in very good agreement with the true depth of the deposit (490m).

Contours of the massive sulphides lenses at level -610m have been reported on figure L-2 along with the inferred MELIS conductor. Each of these sulphide lenses is oriented E-W, but the MELIS conductor shows a N70° direction because MELIS cannot resolves each of these conductors and only sees the overall EM response. The MELIS conductor also appears to be shifted to the north with respect to zones A-4 and A-5 (at level -610m) but again, the geophysical anomaly represents the overall effect of all the conductors, including their extension at depth. In fact, the MELIS conductor would coincide well with zones A-4 and A-5 contours at level -690m because these lenses dip 70°N.

Finally, the inferred conductor strike length west of L-66W agrees quite well with the known extension of the body according to figure L-2. In conclusion, we can state that MELIS is not only able to detect conductor as deep as 600m, but also to provide high quality geometrical information about the source of the anomaly for drilling purposes.

Two other findings allow us to validate this choice:

- the anomaly is perceptible when the transmitter-conductor separation is 700m, indicating that the conductor depth is between 350 and 700m;

- the numerical modelling (figure L-4) for a depth of 450m gives a reasonable fit with the field results. One should note that since MELIS numerical modelling is very time consuming, quantitative interpretation by model fitting becomes very expensive. Its use is only justifiable before the drilling of the promising anomaly of unknown source.

Strike length

The great source depth hampers the determination of the conductor lateral extension. As shown on the L-84W pseudosection, a conductor generating a secondary field powerful enough to be detected on a line centered over the source will also be detected at a distance from its border equal to at least its depth.

We should note that the relative amplitude of the anomalies is a good indicator for the implantation of a first DDH. In our case, the better response is on 66W. However, since we do not have any other survey line east of this one, it would be safer to position the first DDH between lines 66W and 72W. On the basis of all the information we have gathered from the MELIS survey, the best DDH target would be 70+00'W, 5+10mS, -660m.

Assuming that line 84W is off the western edge of the conductor, we may determine its strike length west of line 66W, as shown in figure L-5. This extension is 300m but the conductor probably extends farther east of line 66W.

Vertical extension

The vertical extension of a source only has a relatively minor influence on its geophysical signature, especially if the body is at depth. This is true, of course, as long as the vertical extension is not negligible in respect to the dimensions of the system. MELIS is no exception to this rule and only DDHs in conjunction with borehole EM would allow to determine the vertical extension of the conductor.

Depth of the body

Two thumb rules can be applied to determine the minimum depth to the top of the conductor. The results have been compiled in table 3.

1°) Frequency

This method consists in determining at which frequency the resistive pole reaches its maximum. The body shouldn't be deeper than half the skin depth at that frequency.

2°) Wavelength

This second technique consists in taking the half distance between the surface projection of the resistive and conductive poles of the anomaly. This technique only works for non outcropping, subvertical bodies.

Table 3 shows the results obtained for the present case. Results for the wavelength method are about 20% less than those obtained by the frequency method. This can partly be explained by the difficulty in determining the north extremity of the conductive pole.

Table 3: Compilation of depths determining with the different techniques.

Line	Frequency (Loop 1-SOUTH)	Frequency (Loop 3-SOUTH)	Wavelength	Average
66W	490m	490m	425m	468m
72W	660m	---	425m	543m
84W	600m	600m	500m	567m

The distance seems to increase towards the west, which would confirm the observation made in part II. For drilling purposes, we would recommend a target depth of 130% the average depth obtained on lines 72W and 66W (505m), that is 660m.

Table 2: *Compilation of results obtained from the interpretation of the surface projection of the conductor.*

Line	Graphical method Loop 1-SOUTH	Estimation according to Loop 3-SOUTH	Numerical modelling Loop 1-SOUTH	Average
66W	4+75mS	5+00mS	4+00mS	4+58mS
72W	5+50mS	---	5+00mS	5+25mS
84W	6+00mS	5+25mS	5+50mS	5+58mS

According to table 2, the MELIS conductor seems to be oriented at ~ 070° (see figure L-5). However, the presence of a superficial conductor on line 66W distorts the pseudosections, making the interpretation less reliable on that line and our conclusion about the azimuth of the conductor possibly erroneous.

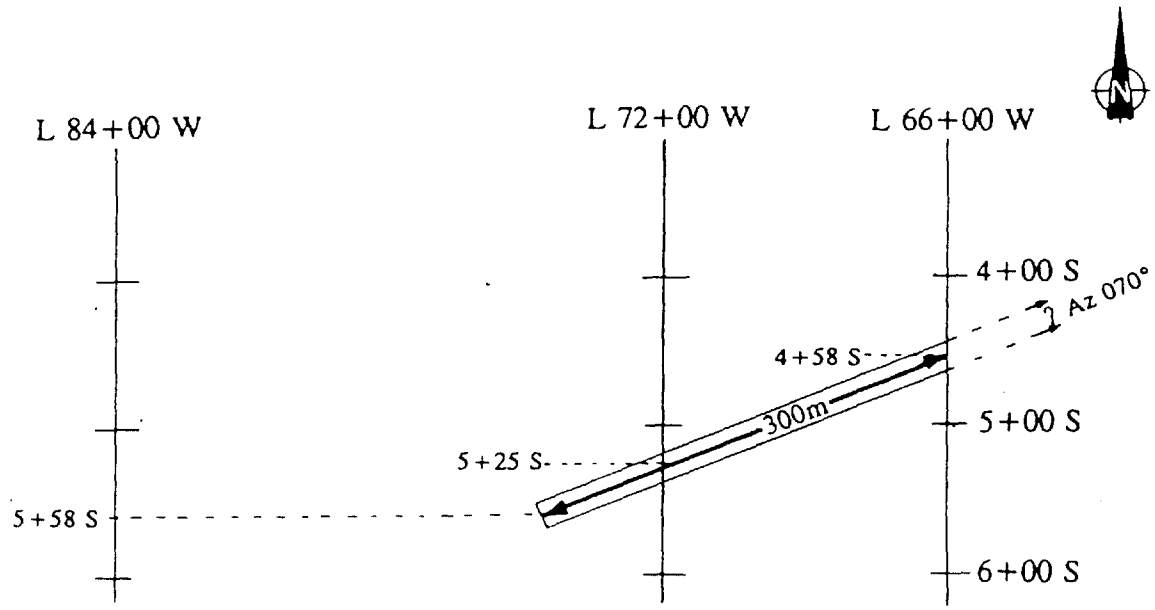


Figure L-5: *Surface projection of the average interpreted MELIS conductor.*

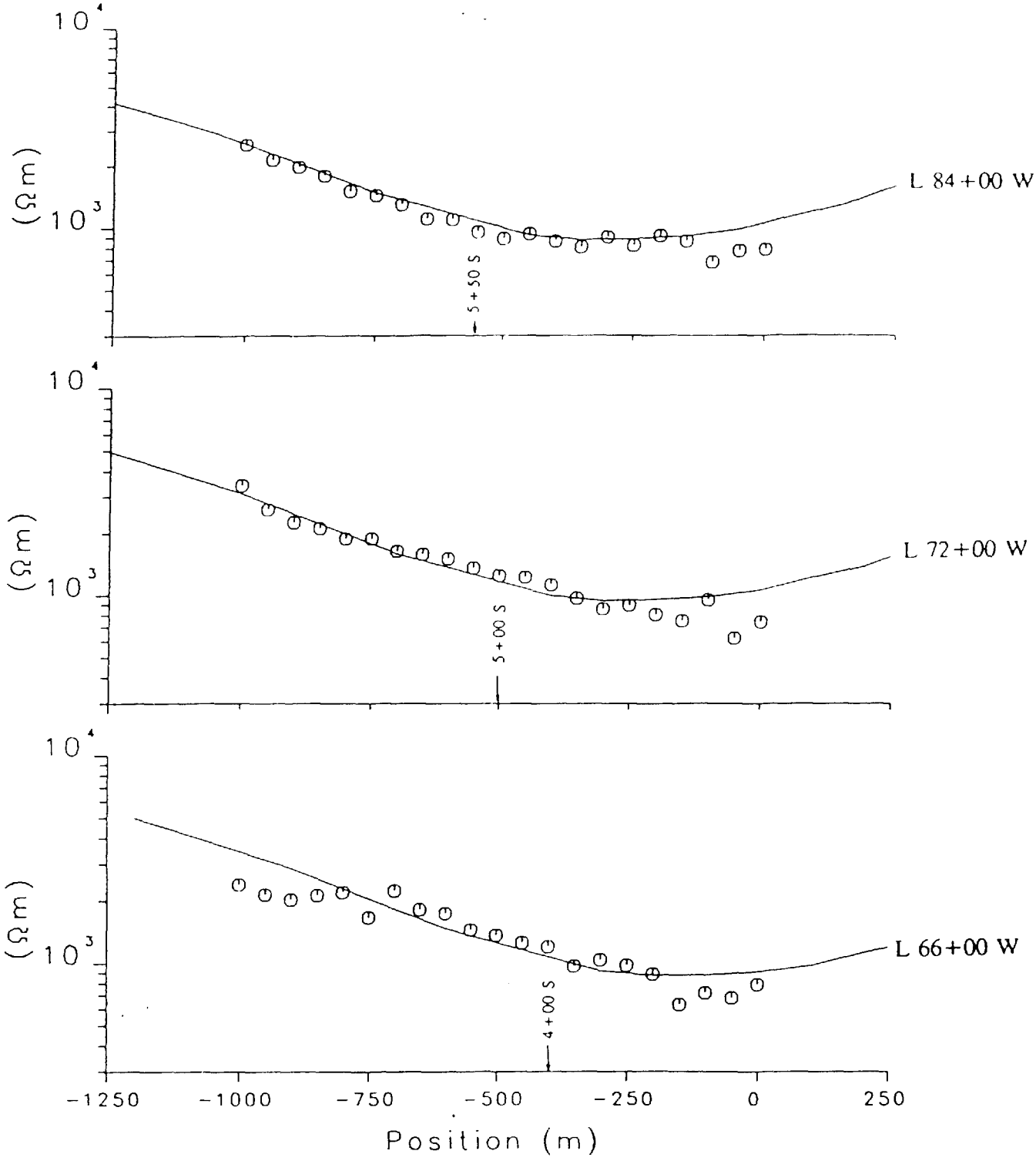


Figure L-4: Superposition of MELIS field data to a 2D numerical model approximating "a priori" the LOUVICOURT deposit.

SAGAX GEOPHYSIQUE

Part III: Qualitative interpretation of the MELIS results

Surface projection

Spatial location of the conductive body is hampered by the long wavelength of the anomaly. Three methods can be used to determine the position of the body (these estimates are compiled in table 2).

1°) Graphical method

For a subvertical body, it is possible to graphically determine the position of the body. The transmitter must be far from the conductor and we must have the complete bipolar signature. In that case, the body is at the intersection between the line segment joining the two anomaly poles and the beginning of the conductive pole.

2°) Variation of the distance between the conductor and the loop

When the loop is moved towards the conductive body, the anomaly moves towards the lower frequencies and tends to migrate towards the real position of the conductor. This is the case when we go from loop 1-S to loop 3-S.

3°) Numerical modelling

Numerical modelling allows to simulate the ground response and to compare the results with the field data. By trial and error, a reasonable fit between the theoretical and field values can be reached and the conductor location thus obtained. The following parameters have been assumed in the case of the Louvicourt orebody:

Shape:	2D vertical dyke
Depth:	450m (underestimated)
Conductance:	40m @ 0.5 Ωm = 80 siemens
Hostrock:	10000 Ωm (overestimated)
Transmitter-conductor distance:	1000m

Figure L-4 shows the superposition of the field results at 70 Hz and the theoretical response at 50 Hz. The fit is very good even though the conductor is in reality a 3D body dipping 70°N.

The main features of line 84W are essentially the same as for line 72W, although there is a decrease of the anomaly intensity and an increase of its wavelength, indicating that the center of the conductor is getting further away. Even though according to Aur Resources line 84W is not situated directly over the orebody, we still get a definite anomaly since the distance to the source is only increased by about 14% when we move from line 66W to line 84W.

The anomaly shape that can be seen on these three pseudosections falls between the one of a subvertical body at an average depth (figure 8 of the MELIS brochure) and the one of a subhorizontal deep conductive body (figure 11 of the brochure). Results from a numerical simulation for a model resembling the Louvicourt orebody will be shown in part II. The aim of this qualitative description was simply to recognize the MELIS anomalous signature of such a good and deep conductor. It also reminds us that a MELIS survey profile should extend at least twice as long as the depth of the conductor.

Loop 2-SOUTH

This loop was set-up at a small distance (around 400m) from the center of the profiles. The pseudosections of lines 66W and 84W are characterized by the total disappearance of the anomaly that was obtained on those same lines with loop 1-SOUTH. Any doubts on the large depth of the conductive body were dissipated with this loop.

Loop 3-SOUTH

This loop was set-up halfway between 1-S and 2-S, about 700m from the center of the survey lines. Here also the pseudosections of lines 66W and 84W show similar results. There is a bipolar anomaly analogous to the one of figures 11 and 12 of the MELIS brochure: a resistive pole covers a conductive pole from 3+00mS to 6+50mS. The source of the anomaly is the same that the one revealed by loop 1-S. However, the loop proximity moves the anomaly towards the real position of the source, as shown by figures 11 and 12 of the brochure.

This third loop shows that for a conductor located at the same depth that the Louvicourt orebody, the ideal location for the loop is at least 800m from the target.

At the time of the MELIS test survey, workers were busy on various projects preparing for the green light to go underground: installation of air compressor, pouring of foundations for powerline substation and warehouse and construction of a 1.5km powerline from Highway 117. However, grounds and conductors for that line were not in place during the MELIS operations and therefore could not have introduced cultural effects.

A diesel generator was providing electrical power to the construction crews. In order to check the influence of this possible source of noise and of all the other operations on the MELIS measurement, south half of lines 66W, 72W and 84W (using loop 1-SOUTH) were redone during workers week-end off-time. Standard deviation of apparent resistivity did decrease, but anomaly shape and amplitude remained the same.

Next is a qualitative description of the MELIS profiles followed by a quantitative interpretation of these results and a comparison with the known geological picture of the deposit, as provided by Aur Resources inc.

Part II: Qualitative description of the MELIS pseudo-sections

Loop 1-SOUTH

The first was set-up around 1km south from the center of the proposed survey lines in order to obtain an investigation depth greater than 500m. Lines 66W, 72W and 84W were surveyed with soundings every 50m.

Line 66W shows two anomalous zones:

- The first one is a shallow conductor of limited extent, centered at 7+50mS. Might be an artificial effect.

- The second one is characterized by a bipolar (resistive pole at 9+00mS and conductive pole at 1+00mS) of long wavelength. This is the signature of a good conductor situated at depth between the two poles. Although the complete signature seems to exceed the extent of the profile (both in length and in frequency), we have enough information to localize the conductor since we have the complete transition zone between the two poles.

The main anomaly of line 72W is similar to the one of line 66W. However, we have a much better image of the transition zone between the resistive and conductive poles of the anomaly since there is no superficial conductor. This will facilitate the quantitative interpretation of the source geometry. The apparent resistivity contrast is slightly less on line 72W than on line 66W, indicating either that line 72W is closer to the conductor's western edge than line 66W is, or that the conductive part of the orebody is deeper under line 72W than under line 66W.

LOUVICOURT deposit

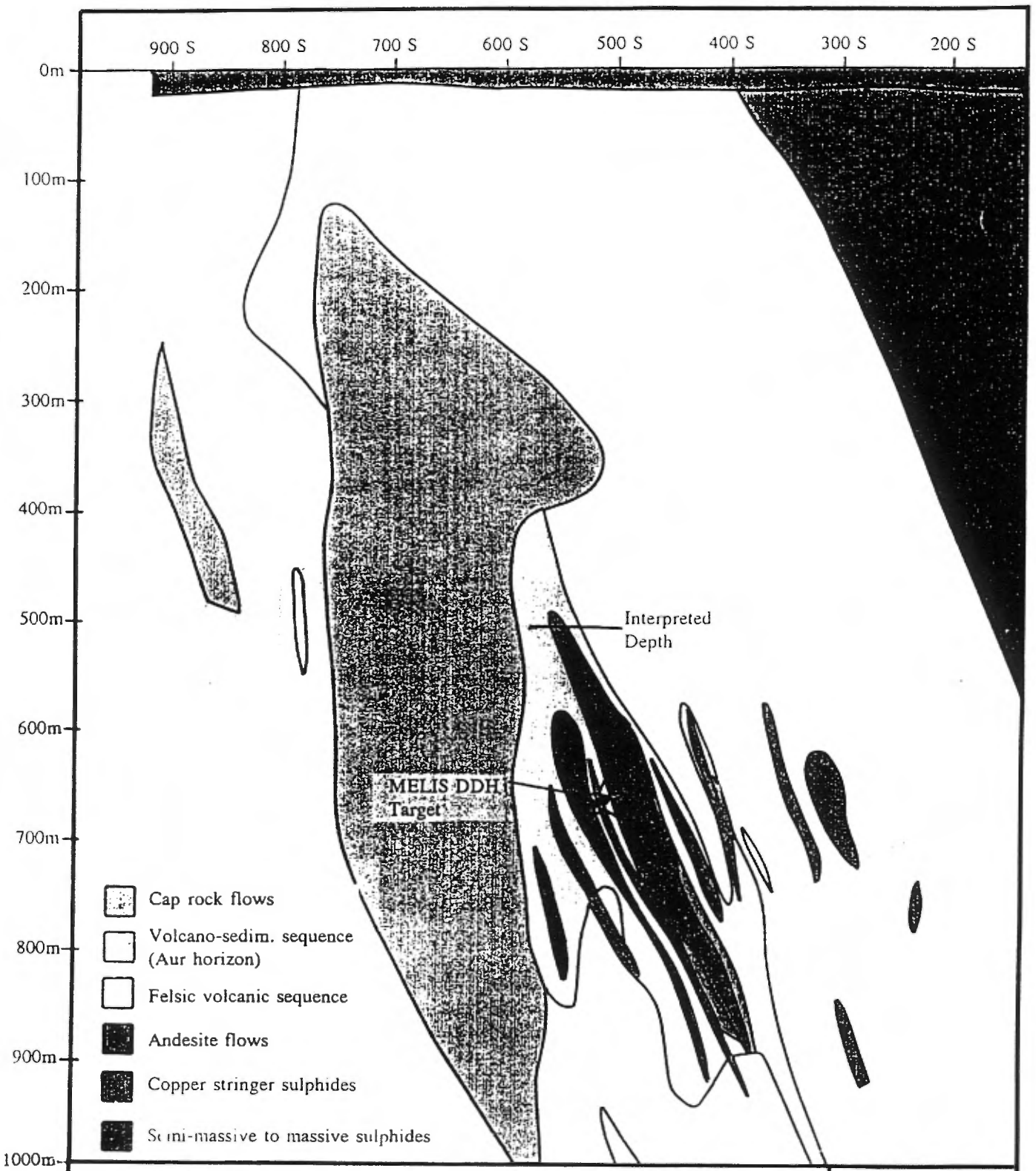


Figure L-3: **Section 66+00' W (30750m E)**
(Looking west)

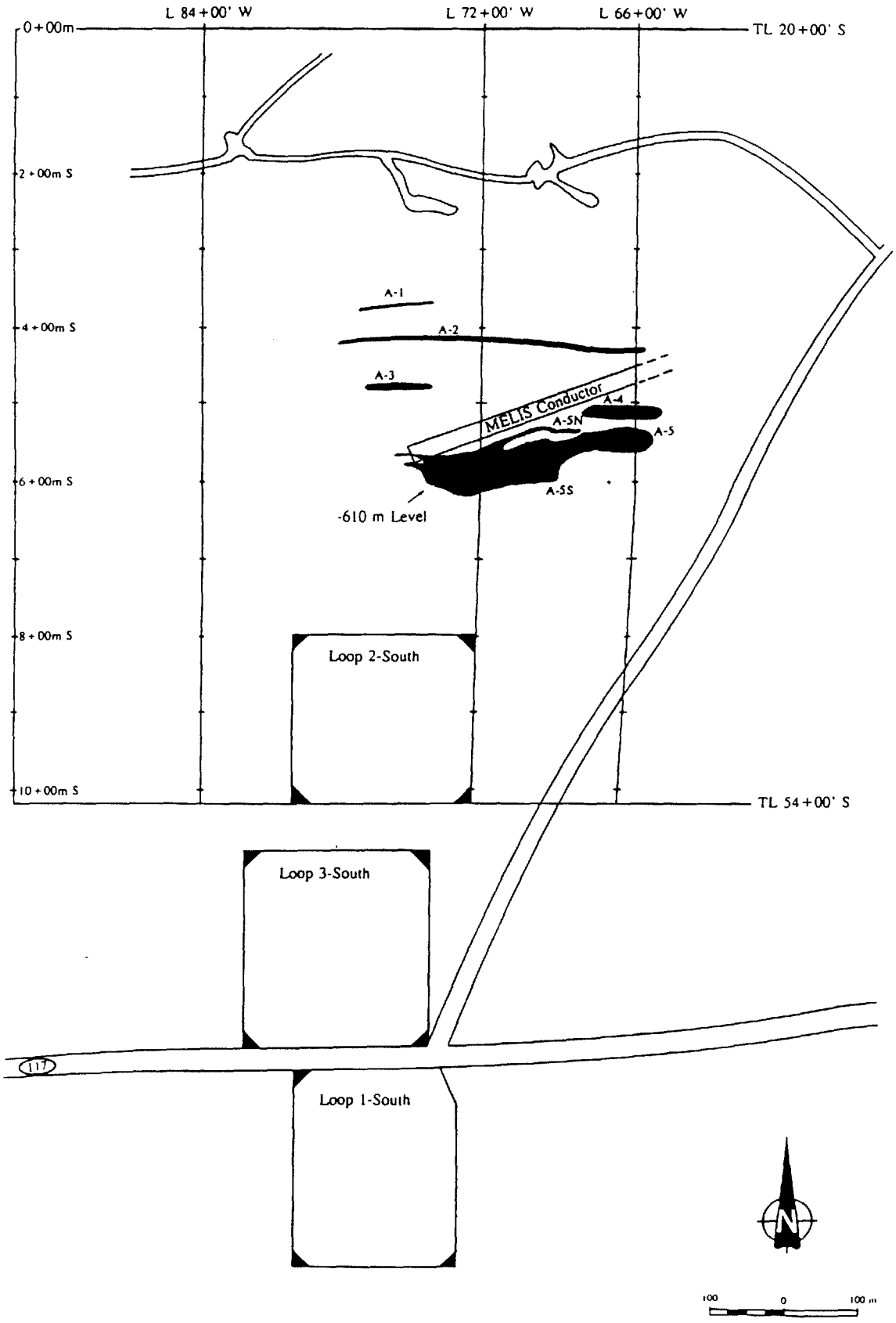
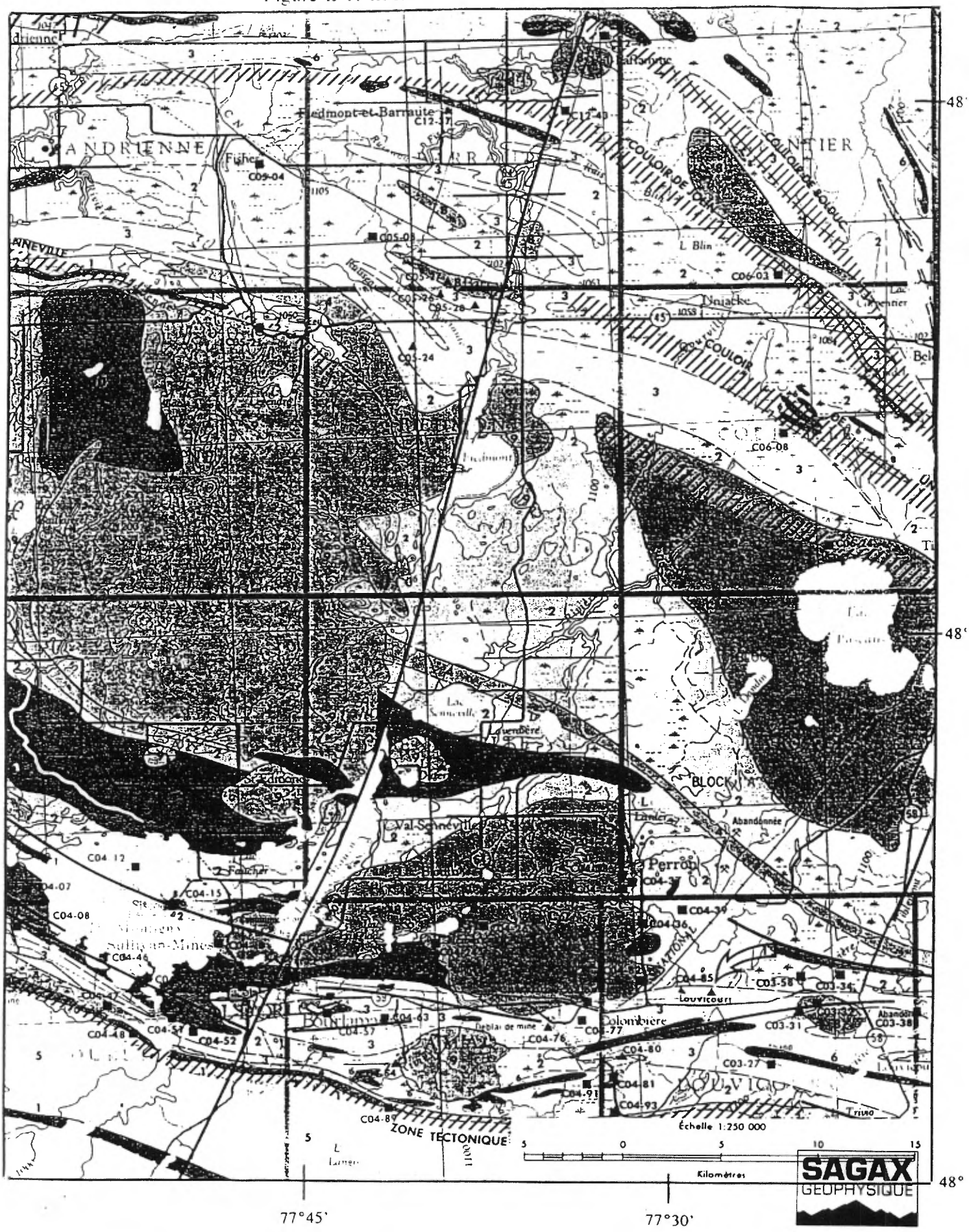


Figure L-2: Location of the MELIS conductor with respect to the massive sulphides zones of the Louvicourt deposit at the -610 m level.

SAGAX
GEOPHYSIQUE

Figure L-1: Location of the LOUVICOURT deposit



Part I: Context of the field test

The Louvicourt copper-zinc massive sulphides deposit was discovered in June 1989 through a program of deep drilling to test the depth extension of the past-producing Louvem mine horizon on the Louvicourt property, held 55% by Aur Resources and 45% by La Société Minière Louvem. The deposit occurs near the base of the Val d'Or formation, in a geological setting which is typical in many ways of classical Noranda-type volcanogenic massive sulphides deposits. A representative geological cross-section is shown on figure L-3. Diluted minable reserves have been established to 22.8 million tonnes grading 4.0% copper, 2.0% zinc, 0.04 oz. gold and 1.00 oz. silver per tonne.

This document describes the results of the MELIS blind test conducted by SAGAX Geophysics inc. over that deposit until then recognized as geophysically blind from the surface (except for gravity). The reader should refer to the MELIS technical brochure published by SAGAX (MELIS - DECEMBER 1991) for a complete description of the method and of the interpretation principles, particularly regarding the meaning of apparent resistivity in the loop ρ' mode.

A first loop was set-up ~ 1km south of the target. It was then brought at ~ 400m (loop 2) and then at 700m (loop 3) from that target in order to confirm the great depth of the conductor identified with the first loop. Loop locations and dimensions are listed in table 1.

Readings have been taken along an old N-S imperial grid that was rechained in meters prior to the MELIS field work. Station 0+00m of the MELIS profiles coincide with tie-line 20+00'S of the old grid. Apparent resistivities were measured at 10 frequencies over the 28-5450Hz bandwidth and every 50m along survey lines. Figure L-2 shows the loop and profile locations on the Louvicourt test site.

Loop	Center	Size	Distance to the target
1-SOUTH	76+50'W, 69+70'S	212m X 266m	~ 1000m south
2-SOUTH	76+00'W, 50+50'S	227m X 237m	~ 400m south
3-SOUTH	77+80'W, 60+40'S	243m X 263m	~ 700m south

Table 1: Description of the three loops used for the demonstration over the LOUVICOURT deposit.

MELIS FIELD EXAMPLE

LOUVICOURT DEPOSIT
(AUR-LOUVEM)

OCTOBER 1991

ABSTRACT

In collaboration with Aur Resources inc., SAGAX Geophysics inc. conducted a MELIS in loop ρ' mode EM field test at the beginning of November 1991 on the Louvicourt massive sulphides deposit property located 22km east of Val d'Or in Abitibi (figure L-1).

Field results recorded on three survey lines using three different loop locations indicate undoubtedly that a very sharp MELIS anomaly associated with the deposit is obtained if the loop is moved away from the conductor at least 1.5 times its depth.

Besides allowing the detection of the Louvicourt deposit, quantitative analysis of the MELIS field data led to a rather good definition of its physical characteristics as shown below:

PARAMETER	MELIS CONDUCTOR	LOUVICOURT DEPOSIT
Surface projection	see figure L-2	see figure L-2
Depth	505 $\pm$ 50m	490m (figure L-3)
Strike length *	300m	300m
Conductance (σt)	~ 80 siemens	unknown

* part west of L-66W only

The depth extension and dip of the orebody cannot however be determined from the surface with MELIS. The MELIS in loop ρ' mode nevertheless becomes the first electrical or electromagnetic technique to respond to a deposit deeper than 300m in the Canadian Shield.

SAGAX Geophysics inc. wishes to thank Aur Resources' team for their precious help during the field work. We are also most grateful to all the partners in the Louvicourt Joint Venture for their consent to release the MELIS test survey results along with the relevant geological data.

Figure G-3 : MELIS - GÉANT DORMANT - CAMBIOR & MINES AURIZON

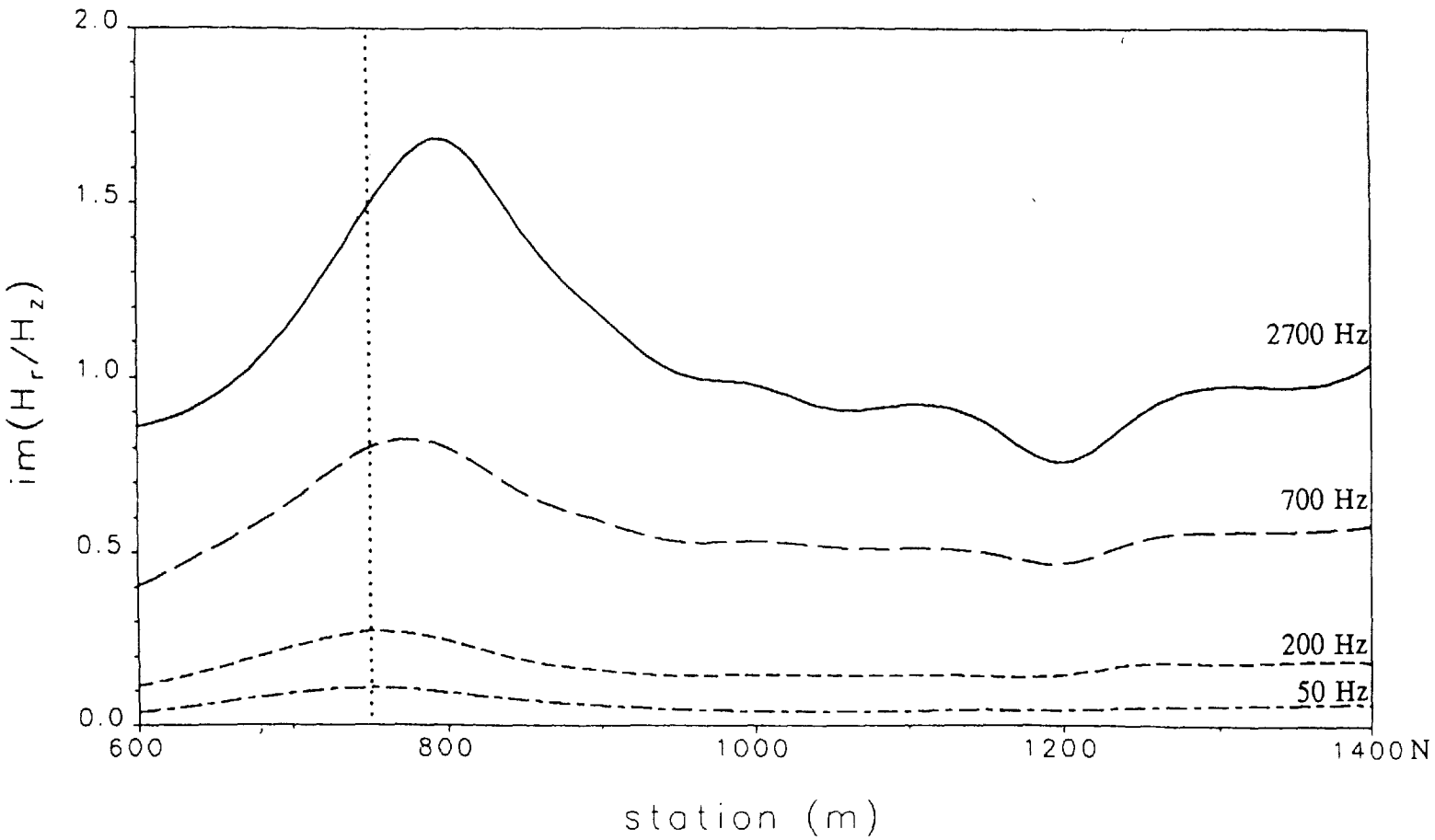
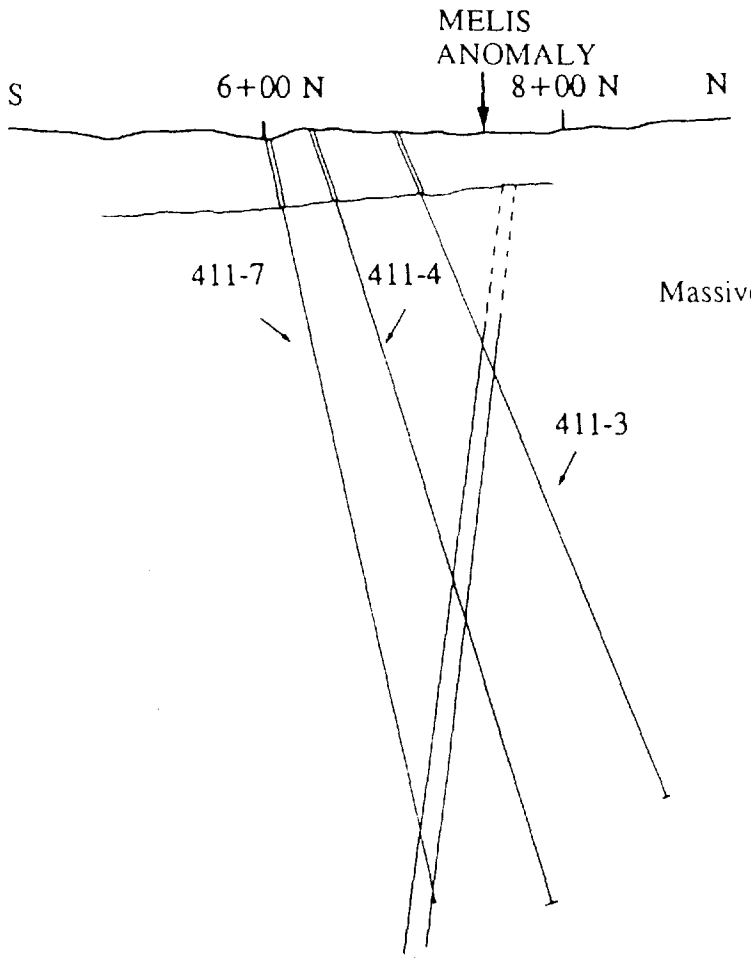


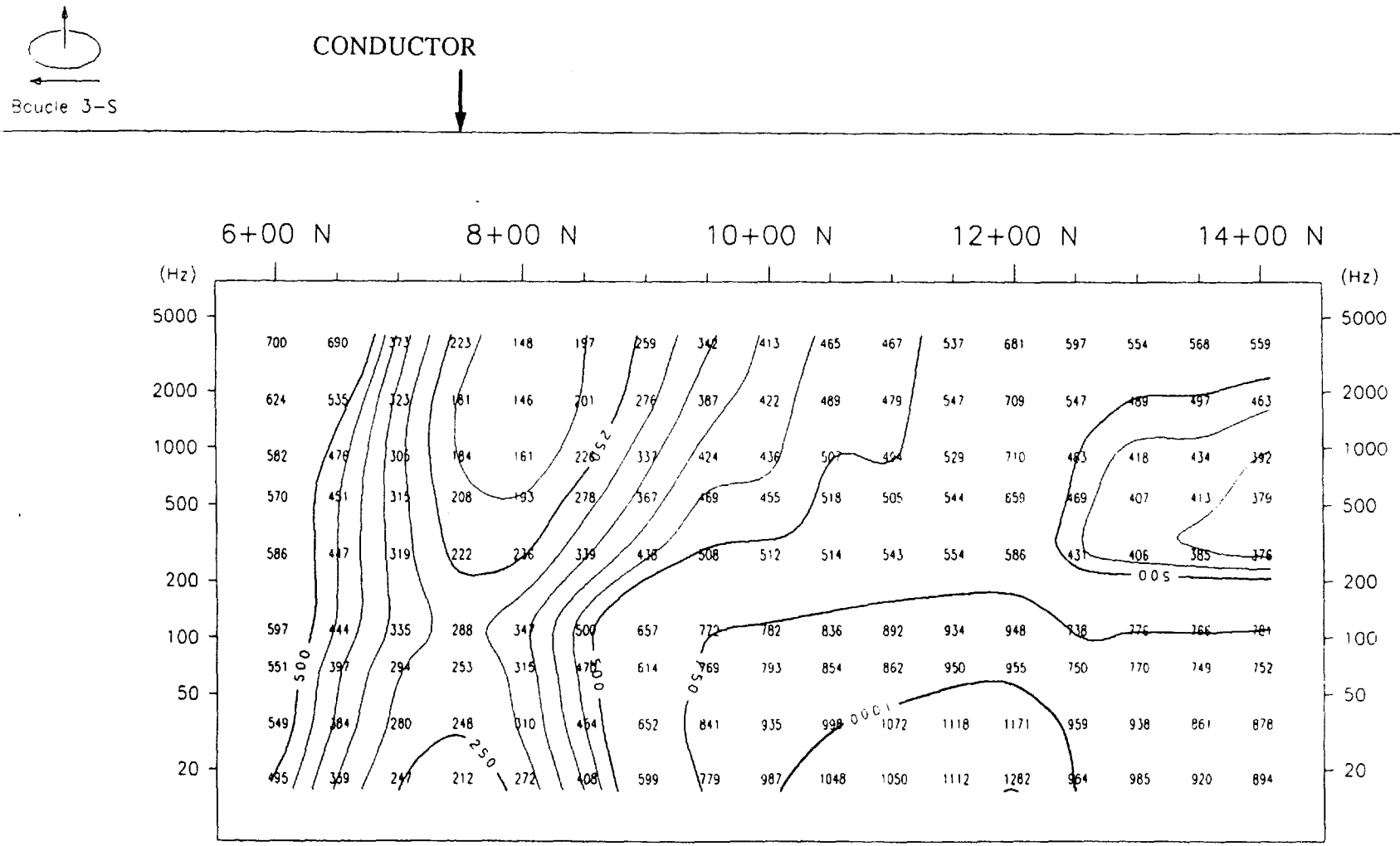
Figure G-2



CAMBIOR-AURIZON
GÉANT DORMANT
SECTION 9+60 E

SAGAX GEOPHYSIQUE

Figure G-1



Instrumentation: MELIS de IRIS
Intervalles de contour: 50, 250, 1000 Ωm

Ligne 9+60 E

Echelle 1:5000

50 0 50 100 150 200
(metres)

Levé par: SAGAX Date: Août 1991 Plan no 91395-9	SAGAX GEOPHYSIQUE	LEVE MELIS EN MODE LOOP ρ' PSEUDOSECTION DE LA RESISTIVITE APPARENTE	CAMBIOR INC. PROPRIETE GEANT DORMANT CANTON CHASTE

MELIS FIELD EXAMPLE

GÉANT DORMANT PROPERTY

(CAMBIOR & MINES AURIZON)

MAY 1992

This example is aimed at showing the MELIS response of a shallow deep conductor. This survey has been carried out at the request of CAMBIOR INC. on the eastern extension of the geological horizon containing the Géant Dormant auriferous deposit. Two weak input anomalies (2 and 3 channels) were observed around stations 9+00N to 10+00N. The MELIS survey, which took place on three lines 120 m apart, showed the presence of a bedrock conductor at around 7+50N.

The pseudosection of line 9+60E (figure G-1) shows a two-layer ground model (overburden and bedrock) with a subvertical conductor near the southern edge of the profile. As mentioned in the previous section discussing theoretical models, the conductor is positioned under the conductive pole obtained at low frequency, which in our case is around 7+50N. The resistive pole normally observed between the conductive pole and the loop cannot be seen here because the profile southern extension is too short. The profiles had been centered on the INPUT anomalies. MELIS shows the presence of a conductor only at 7+50N, suggesting that the INPUT anomalies were poorly localised.

A mineralized zone, similar to those exploited at the Géant Dormant mine (but non-economical), had already been discovered by drilling. This laminated zone (figure G-2) is interpreted as a shear zone and contains auriferous quartz veins and subsidiary sulfides (Py, Cp, Sp, Po) with iron formations, chert and magnetite. This mineralized zone coincides precisely with the interpreted position of the MELIS conductor. It should be noted that the conductor dip slightly increases the anomaly asymmetry.

The H_r/H_z profiles (figure G-3) show a sharp decrease of the response at lower frequencies, confirming the poor conductivity of this conductor. The large difference between background levels at high and low frequencies indicates a thick overburden (45 to 50 m according to drilling results).

This example illustrates the type of MELIS response associated to a subvertical conductor. It also shows that even poor conductors can be easily identified under thick overburden and that their positioning and depth can be accurately interpreted.

SAGAX Géophysique inc. wishes to thank Cambior inc. and Les Mines Aurizon ltée for their assistance in preparing this case-history and for their permission to distribute it.

6°) Data presentation on pseudosection is better suited than profiles for the identification of deep conductors.

With its 600 m investigation depth, MELIS can be used to thoroughly search base metal prospects, eliminating ambiguities caused by overburden through.

4. *DEPTH OF INVESTIGATION*

Investigation depth for EM methods cannot be precisely determined. For MELIS, investigation depth depends on:

- transmitter - receiver distance
- frequency
- hostrock resistivity
- target's geometry and conductivity

According to the BRGM, the investigation depth of MELIS is about:

200 m in a 10 Ω·m hostrock
500 m in a 100 Ω·m hostrock
1000 m in a 1000 Ω·m (or more) hostrock.

However, in practice the wavelength of an anomaly produced by a conductor buried at 1000 m would exceed the maximum length of a profile carried out with a single loop. Its identification would then be unlikely. According to the numerical models and to field test-cases, we believe that a thick conductor should produce a clear signature to a depth up to 600 m. Obviously, a source of lesser conductance will decrease the effective investigation depth, producing a filtering of anomalies.

For the same subvertical target, MELIS offers an investigation depth four times larger that HLEM and at least twice that of TEM (Pulse EM for example). Although Pulse EM can detect excellent two-dimensional conductors (such as graphite) up to 400 - 500 m, its effective investigation depth is about 200 m for three-dimensional bodies (massive sulfides), which is the investigation radius observed in the field of borehole Pulse EM. (Winston Lake case is different since it has a large lateral extension compared to its depth, here a 2D model).

In the end, why is MELIS a better method that time domain EM (Pulse EM for instance)?

1°) For subvertical conductors, coupling with the primary field increases with depth (it's almost zero at surface level) and is generally more favorable along all of the conductor surface.

2°) The primary field, being concentrated at one frequency, is more intense and produces a stronger secondary field.

3°) The H_r/H_z ratio is twice as sensitive (H_r increases and H_z decreases) as opposed to TEM which takes its readings without the primary field being present.

4°) MELIS has a wider frequency spectrum.

5°) Signal to noise ratio is higher in frequency domain.

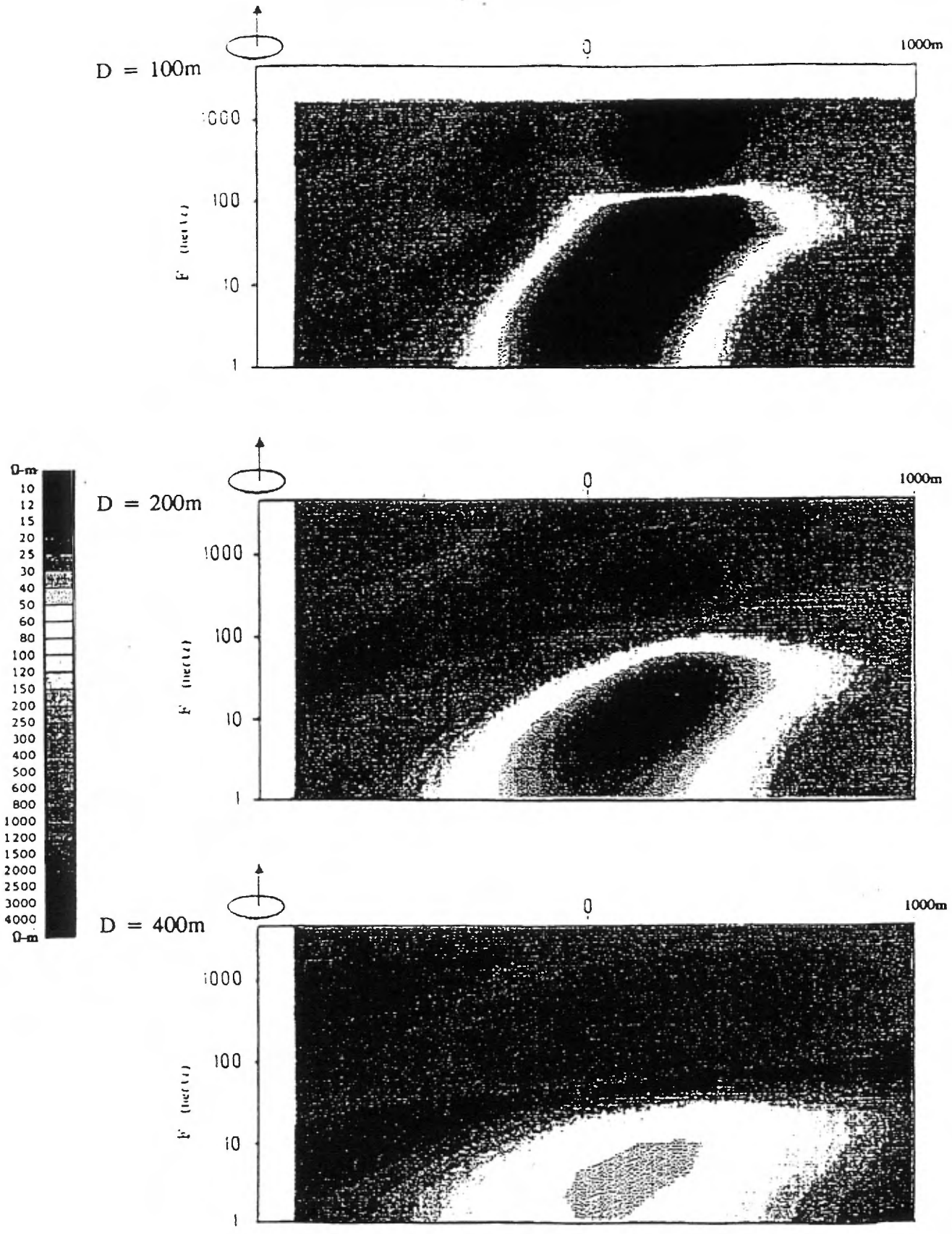


Figure 14: MELIS apparent resistivity pseudosections for a horizontal slab of 50 siemens of conductance.

SAGAX GEOPHYSIQUE

Of the previous models, we should mainly retain that:

- the apparent resistivity pseudosection anomalies due to bedrock conductors are bipolar with a resistive high on the loop side (especially at high frequencies). This resistivity high can be very useful in determining the depth of the source and in distinguishing between an overburden trough and a subvertical bedrock conductor;

- the horizontal location of a conductor is closer to the resistivity low at low frequencies, if it can be observed;

- in the case of a deep conductor, moving the transmitter closer to the source will tend to center the conductive pole over the true location of the conductor (if the depth of investigation is sufficient to produce a clear anomaly);

- superficial effects have characteristic signatures that should not introduce any ambiguities in the interpretation;

- the depth of investigation will be maximised if the hostrock is resistive, the conductor subvertical, the transmitter far away and the frequency is low;

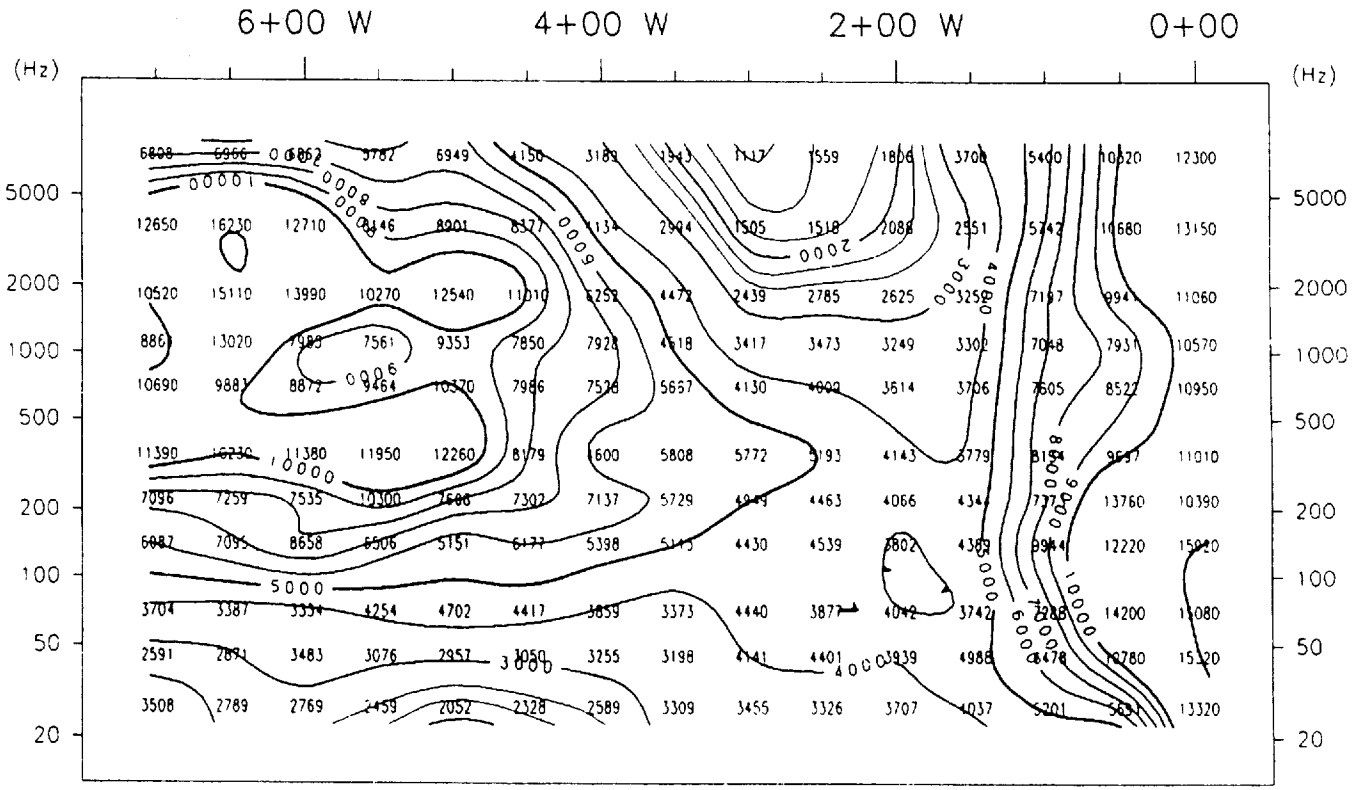
- because of anomaly asymmetry, the dip of deep sources cannot usually be determined;

- as for all electromagnetic methods, the difference between an ionic conductor (fault) and a metallic one (sulfides or graphite) is not possible on the basis of MELIS data only.

For a deeply burried conductor, the apparent resistivity contrast being stronger on the vertical axis (frequency) than on the horizontal axis, data presentation on pseudosection format will be clearly more pertinent for MELIS than the conventional profile format which is better suited for shallow investigation tools.

A'

Boucle 1-E



Instrumentation: MELIS de IRIS

Intervalles de contour: 250, 1000, 5000 Ωm

Ligne 28+00 N

Echelle 1:5000

50 0 50 100 150 200

(metres)

Levé par: SAGAX

Date: décembre 1991

Plan no Y-2

SAGAX GEOPHYSIQUE

LEVE MELIS EN MODE LOOP ρ'

PSEUDOSECTION DE LA

RESISTIVITE APPARENTE

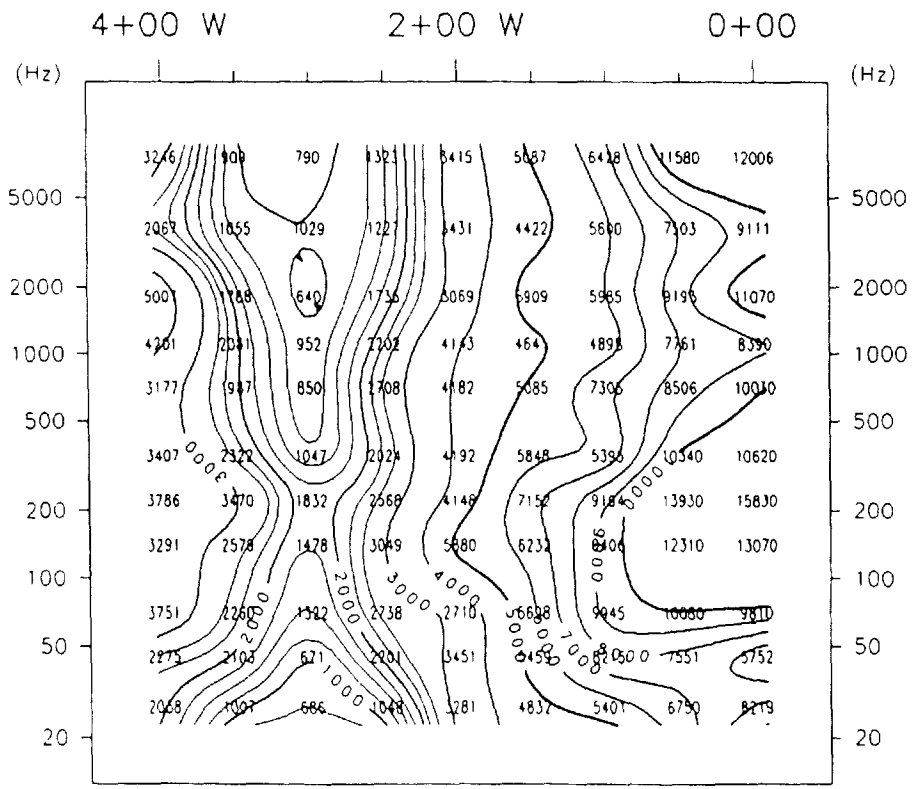
AUGYVA-PLATINOR, J.V.

Propriété du Lac Yasinski (Grille Nord)

Canton 3114, Baie James Qc

A

Boucle 1-E



Instrumentation: MELIS de IRIS

Intervalles de contour 250, 1000, 5000 Ωm

Ligne 26+00 N

Echelle 1:5000

50 0 50 100 150 200

(metres)

Levé par: SAGAX
Date: Décembre 1991
Plan no Y-3

SAGAX GEOPHYSIQUE

LEVE MELIS EN MODE LOOP ρ'
PSEUDOSECTION DE LA
RESISTIVITE APPARENTE

AUGYVA-PLATINOR, J.V.
Propriété du Lac Yasinski (Grille Nord)
Canton 3114, Baie James Qc

MELIS FIELD EXAMPLE

THE MASA VALVERDE PROSPECT, SPAIN[1]

(HUELVA, ESPAGNE)

OCTOBER 1991

EXPLORATION HISTORY

A mining J.V. was formed in 1982 by ADARO and PENARROYA for the systematic exploration of block 25 of the "state reserves" as well as the Autonomia prospect in Spain. Most of the area is located within the Culm formation which overlies the volcano-sedimentary complex at the base of the Carboniferous (figure M-1).

All the deposits of the south-iberian pyritic belt are located within these volcanic sediments; however, the small deposits located in the outcropping and slightly eroded part of the volcanic series are of limited interest. The exploration program was therefore focused on searching for areas where the thickness of the Culm sediments was no more than a few hundred meters.

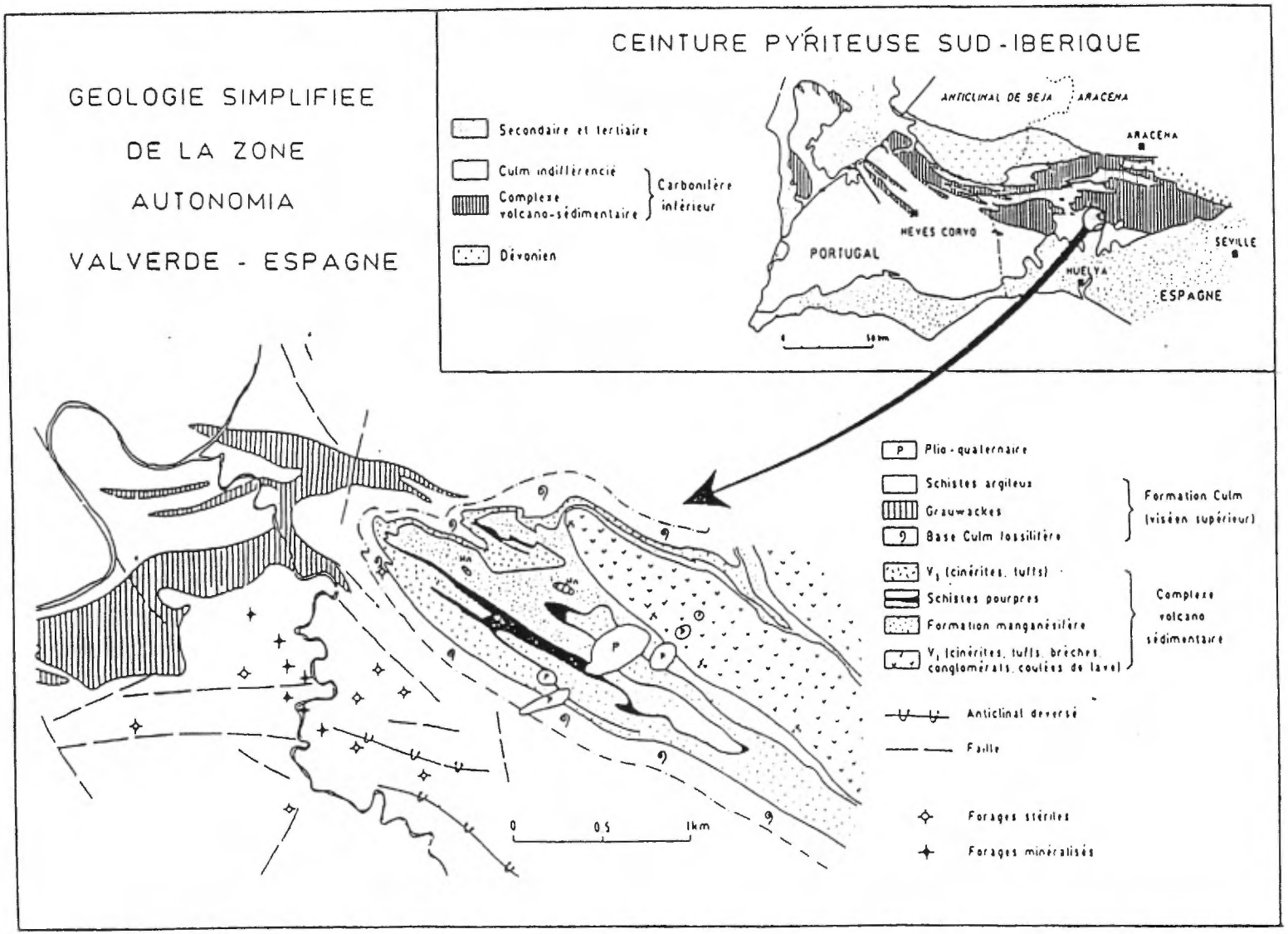
A first phase consisted of stratigraphic and structural analysis of the Culm sediments. On the selected areas where the volcano-sedimentary complex was potentially not very deep, a systematic gravity survey was performed on a 100m by 100m grid. A significant gravity anomaly (figure M-2) was delineated at the junction of block 25 and the Autonomia prospect southwest of the town of Valverde del Camino (Huelva). The first drillhole intersected 96m in length of sulfides at a depth of 434 meters.

Up to July 1989, eighteen drillholes were done on this area and ten of them intersected mineralization zones. At the same time, follow-up gravity surveys were performed as well as magnetic profiles, electrical soundings (in order to better define the regional setting), TEM surveys (SIROTEM), audio-magnetotelluric, mise-à-la-masse, density logs (γ - γ), γ - ray logs and resistivity surveys.

(1) Taken in large part from VALLA, P., (1991) and BERNARD, J., BOURGEOIS, B., and VALLA, P. (1989).

SAGAX GEOPHYSIQUE

Figure M-1: Simplified geological map of the Masa Valverde area (Autonomia prospect).



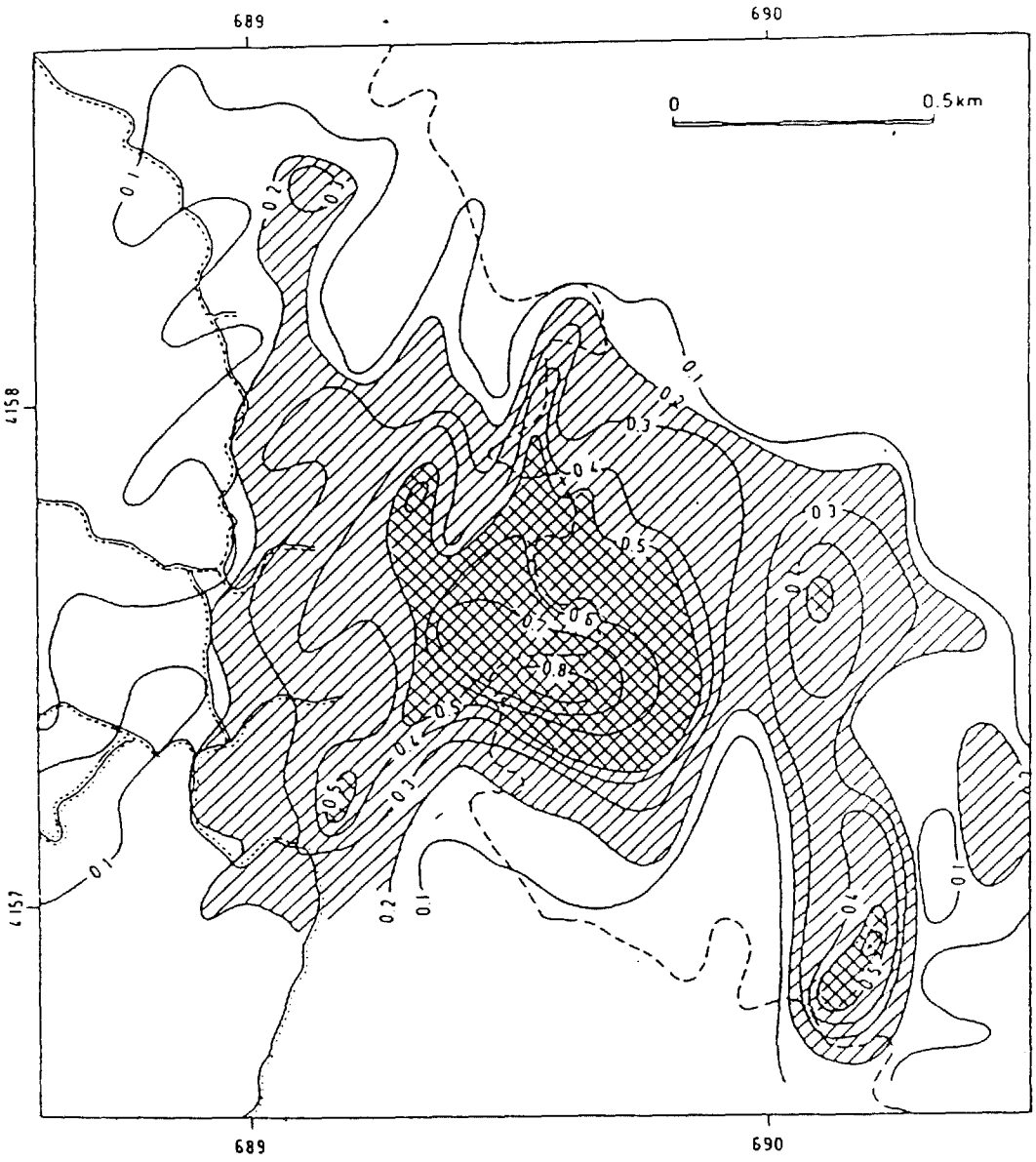


Figure M-2: Residual gravity (mgal) map of the Masa Valverde area.

GEOLOGICAL SETTING AND GEOELECTRIC PROPERTIES

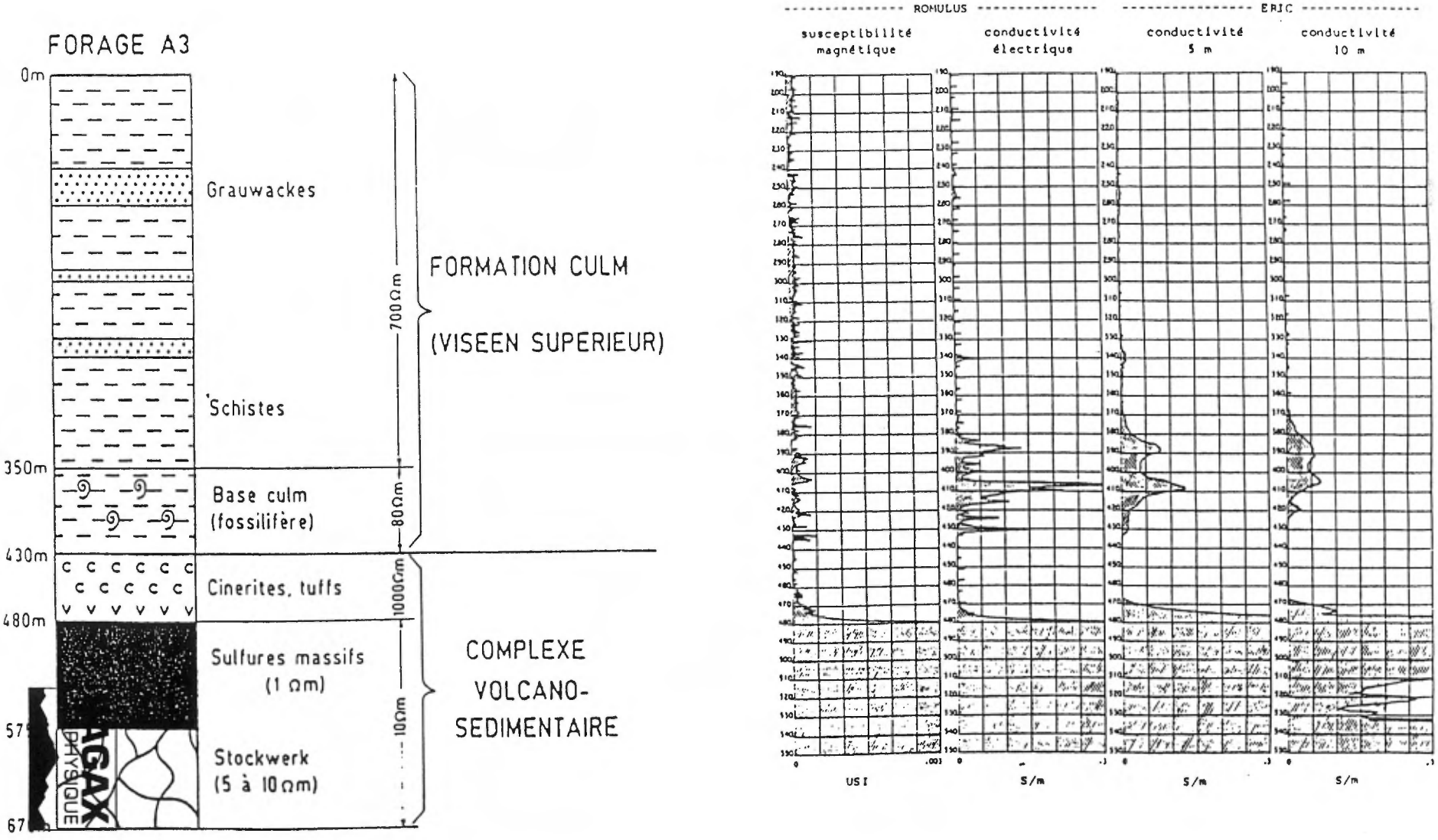
The Valverde body is located in the volcano-sedimentary complex at the base of the Carboniferous (Tournaisian, Upper Visean) which is characteristic of the sub-Iberian peninsula. This set of rocks is overlain by a series of slates of the Culm formation (Upper Visean) which is characterized at its base by fossil-bearing and graphitic units several tens of meters thick.

As illustrated on figure M-1, the general structural trend of the area, where the mineralized zones were intersected on the flank of a gravity anomaly, is NW-SE. This area seems to be on the southern flank of an anticline.

The electrical properties of the different formations were obtained by electrical and electromagnetic logs (figure M-3). The Culm is relatively resistive (approx. 700 Ω-m) below the superficial alteration zone (50 to 200m) of variable resistivity. This setting is favorable for EM penetration; the graphitic base is nonetheless more conductive (10 to 80 Ω-m over a few tens of meters).

The non-mineralized volcanic episodes are equally resistive (approx. 100 Ω-m). The massive mineralisation is very conductive (< 1 Ω-m) as well as the stockwork associated with it (< 10 Ω-m).

Figure M-3: Lithological section and electromagnetic log, Masa Valverde prospect.



MELIS SURVEY

A 200m square loop (B2) was layed out at approximately one kilometer south of the known location of the deposit. Three profiles perpendicular to the long axis of the conductive body were performed at 300m intervals with readings every 100m (figure M-4). Apparent resistivity pseudosections of the three profiles (P2, P3, P4) in radial mode are illustrated in figure M-5.

These pseudosections are qualitatively quite similar. The similarity at low frequencies is even excellent for profiles P2 and P4: the spatial wavelengths for the conductive anomaly at 6.2 Hz is identical. This wavelength increases on profile P3 which means either an increase in conductivity or depth of the conductor. Drillhole A12 (figure M-4) was implemented to test the mineralization extension suggested by MELIS. The mineralization was intersected at a depth of 680m!

If we do not take into account the existence of a superficial conductive structure near stations 9 and 10 of profile P2, then these pseudosections present a signature quite similar to that of a subhorizontal deeply buried body (figure 11 of the MELIS brochure, D=400m). Given the low frequency profiles, the conductive body appears to be centered at station 7 of profile P4, station 8 of profile P2 and between stations 8 and 9 of profile P3. However, if the frequency considered was not low enough, then the conductor would have to be shifted towards the south (towards loop B2). The width of the conductor appears to be of the order of 300 to 400 meters, but this approximation is not very significant given the great depth of the source.

A 1D inversion of profile P2 has delineated an 8 siemens conductive layer below stations 7 and 8 at a depth of over 640m (figure M-6). The body is in fact at a depth of 480m at this location but an overestimation of depth is to be expected with a 1D inversion.

A complete 2D model allowing for the analysis of a deeply buried body at 500m in hostrocks representative of the Valverde area (figure M-7) shows a distinct qualitative and quantitative analogy with the pseudosections on figure M-5, in particular profile P4. The bipolar anomaly is obviously more complete on figure M-7 because of the profile length and the computations: down to 1 Hz, versus 6.2 Hz for field data. In a more resistive hostrock environment such as the Canadian Shield, the penetration of EM waves is greater and the conductive pole of anomalies appears at higher frequencies (100 to 1000 Hz). We must note that the anomaly wavelength is twice the depth of the conductor. Stations spaced every 100m are then most sufficient with detail stations every 50m for superficial sources.

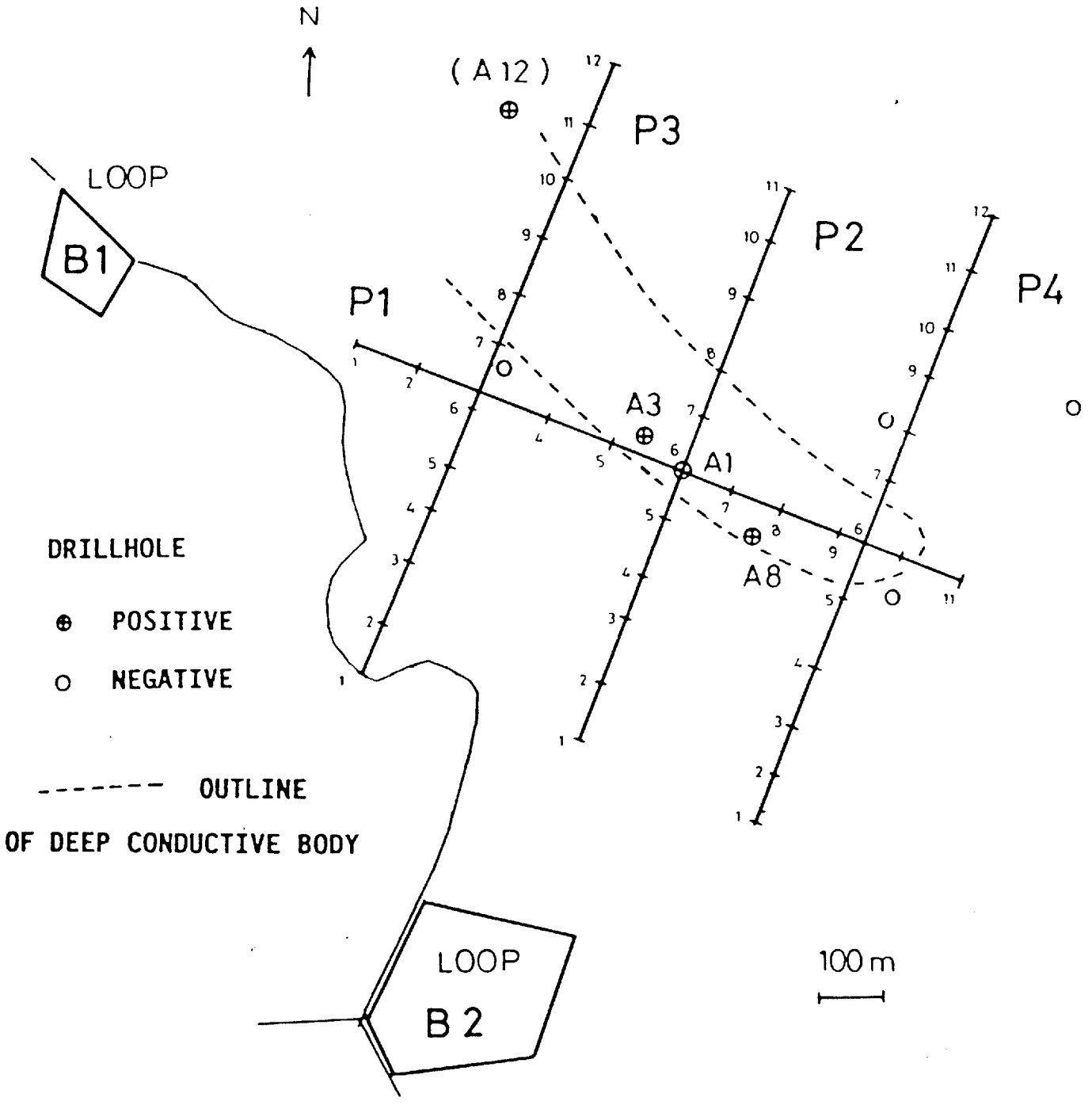


Figure M-4: Location of profiles and loops at Masa Valverde.

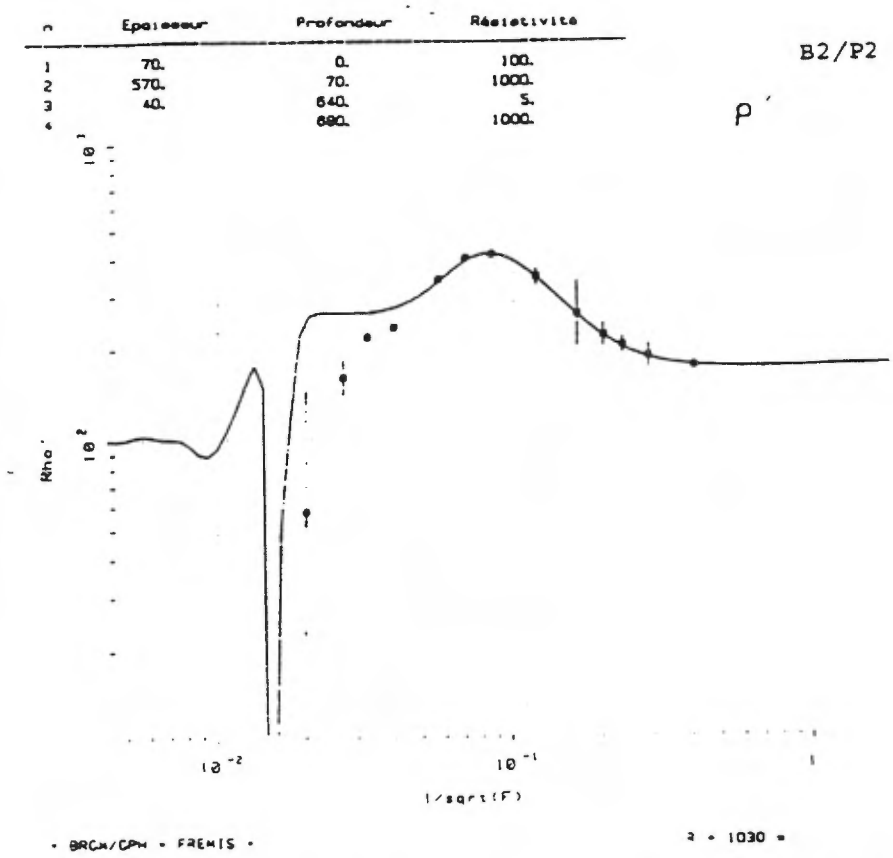


Figure M-6: 1D inversion for station 8 of profile P2.

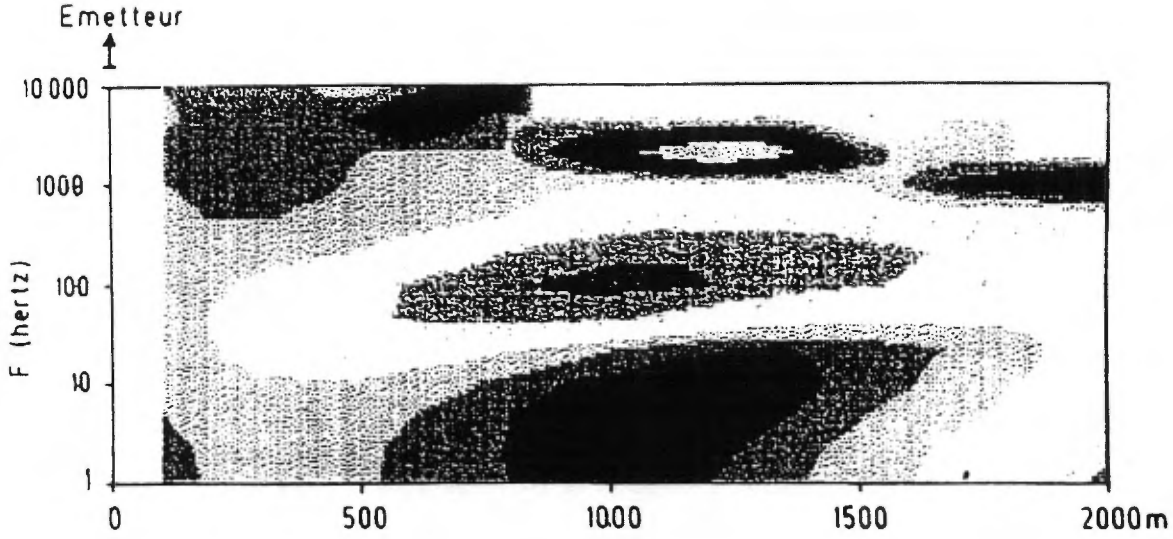
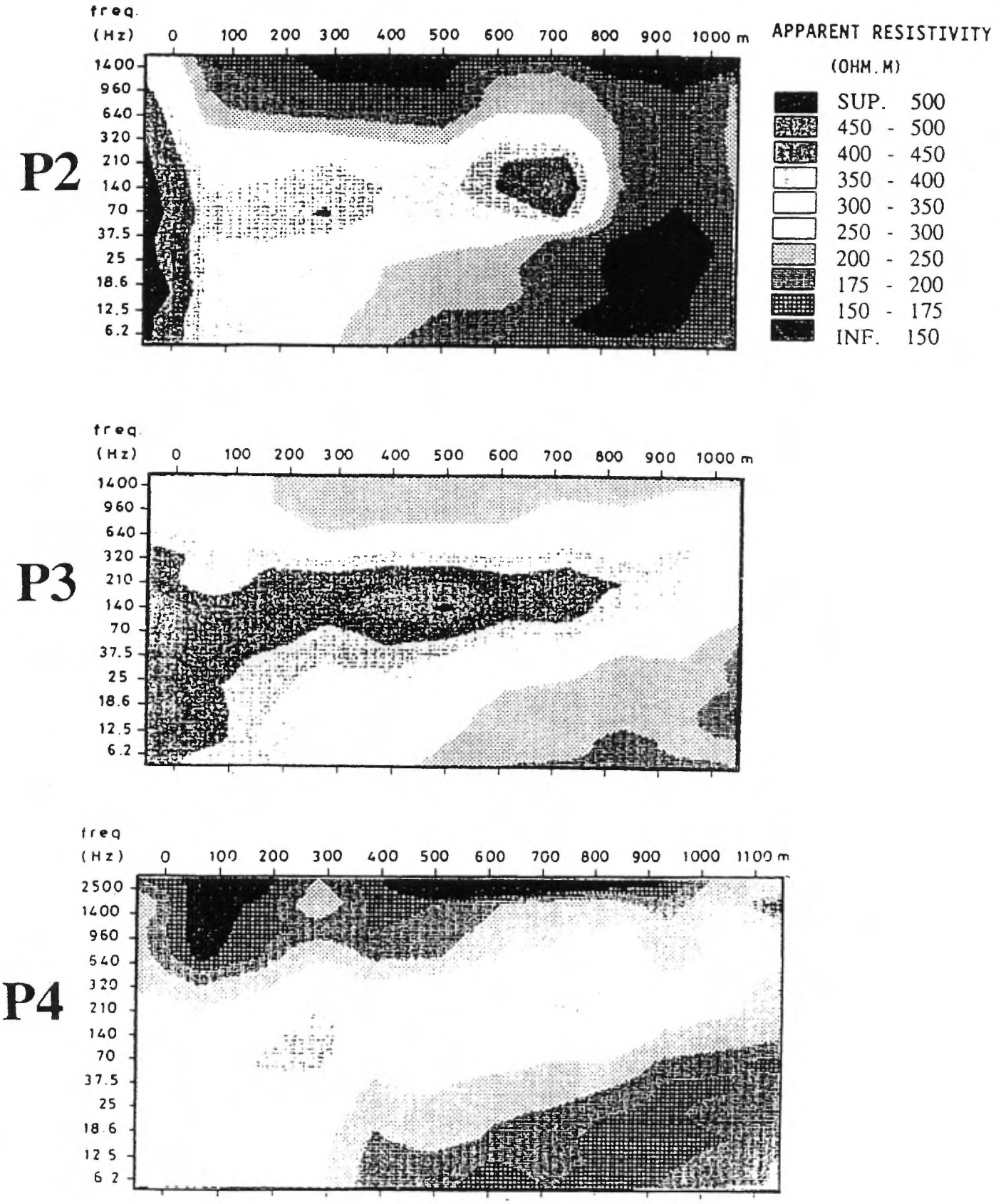


Figure M-7: Apparent resistivity pseudosection for a deeply seated body (500m) at the Valverde site.

SAGAX GEOPHYSIQUE

Figure M-5: Apparent resistivity versus frequency pseudosections for the Masa Valverde deposit obtained with MELIS in LOOP ρ' mode.



REFERENCES

BERNARD J. (1985) - Note sur l'utilisation et l'interprétation de la méthode MÉLIS. Rapport du B.R.G.M. : 85 SGN 036 GPH.

BERNARD J., BOURGEOIS B. & VALLA P. (1989) - Application of a Loop Source Multi Frequency EM Method in the Detection of a Deep Massive Sulphide Orebody (Spain). 59th SEG annual meeting (Dallas) expanded abstracts, pp. 395-397.

KELLER G.V. & FRISCHNECHT (1966) - Electrical methods in Geophysical prospecting. Pergamon Press, 524 p.

SPIES B.R. & EGGERS D.E. (1986) - The use and misuse of apparent resistivity in electromagnetic methods. Geophysics, vol. 51, n° 7, pp. 1462-1471.

VALLA P. (1991) - Applications de la modélisation numérique aux méthodes d'électromagnétisme fréquentiel en prospection géophysique. Rapport BRGM : R 32 119 GPH SGN 91, 472 p., 105 fig., 2 annexes.

SAGAX GEOPHYSIQUE

PM 97216 015

PROJET MANICOUAGAN

RAPPORT GÉOLOGIQUE

RES...
BUREA...
'97 AUG -4 14:23
BUREAU DU REGISTRAIRE
RECU AU BUREAU
'97 AOU 5 AM 10 42

MAI 1994

IMPACT MANICOUGAN
RAPPORT GÉOLOGIQUE
PARTIE I

TABLE DES MATIÈRES

1 INTRODUCTION

1.1 Description du mandat
1.2 Organisation du document

2 PHYSIOGRAPHIE GÉNÉRALE

3 DOCUMENTS CARTOGRAPHIQUES

4 RÉFÉRENCES

ANNEXES

Annexe a Emplacement de la zone étudiée et localisation des feuillets topographiques au 1:5 000. **(1:50 000)**

Annexe b Topographie et géologie de la roche de fond **(1:50 000)**

Annexe c Géologie des dépôts de surface **(1:50 000)**

Annexe d Emplacement des coupes de lignes feuillet 1 **(1:5 000)**

Annexe e Emplacement des coupes de lignes feuillet 2 **(1:5 000)**

Annexe f Emplacement des coupes de lignes feuillet 5 **(1:5 000)**

Annexe g Emplacement des coupes de lignes feuillet 6 **(1:5 000)**

Annexe h Emplacement des coupes de lignes feuillet 7 **(1:5 000)**

Annexe i Emplacement des coupes de lignes feuillet 9 **(1:5 000)**

Annexe j Emplacement des coupes de lignes feuillet 10 **(1:5 000)**

Annexe k Emplacement des coupes de lignes feuillet 13 **(1:5 000)**

Annexe l Emplacement des coupes de lignes feuillet 14 **(1:5 000)**

Annexe m Disquettes des fichiers numérisées

Annexe n Photographies aériennes interprétées (fourni dans une enveloppe jointe au document)

1 INTRODUCTION

1.1 Description du mandat

Le 15 janvier 1994, **Amadeus Resources** a mandaté la firme **Géovision International** pour réaliser les travaux suivants:

- Interprétation photogéologique d'un secteur du feuillet topographique 22 N7 entre les latitudes 51° 13' à 51° 30' et les longitudes 68° 50' à 68° 25';

- Numérisation du feuillet topographique de ce même secteur (planimétrie et isocontours topographiques principaux).

- Transfert des limites géologiques interprétées sur le feuillet 1:50 000 numérisé;

- Transfert des lignes coupées (localisation déjà établie) sur des feuillets 1:5 000 générés à partir du feuillet numérisé au 1:50 000 (déjà remis);

- Rédaction d'un court rapport (ci-joint).

1.2 Organisation du rapport

Ce document est présenté en deux parties distinctes. La Partie I introduit la région à l'étude et décrit les techniques adoptées pour réaliser les différentes cartes. La Partie II est écrite en anglais et discute la méthode de travail et les résultats obtenus suite à l'interprétation des photographies aériennes.

Les documents cartographiques sont présentés en annexes. Ils sont pliés et insérés dans une pochette. Les fichiers numériques sont fournis sur disquettes de type Macintosh et présentés à l'annexe m. Les photographies aériennes interprétées sont fournies à l'annexe n.

2 PHYSIOGRAPHIE GÉNÉRALE

L'impact de Manicouagan est localisé sur le Bouclier Canadien dans la province de Grenville, au centre du Québec (51° 23'N, 68° 42' O). Généralement circulaire, cette structure possède un diamètre de 65 km et correspond à un des plus grands et des mieux préservés des impacts terrestres existants.

Suite aux travaux qui ont menés à la réalisation du réservoir Manicougan, le niveau d'eau a été augmenté à un point tel que la partie centrale du cratère est maintenant isolée et accessible uniquement par avion ou par bâteau. Cette île se nomme "Île René-Levasseur" et correspond à la zone d'étude de ce mandat.

À partir des travaux antérieurs réalisés dans la région de Manicougan (Murtaugh, 1976, Bérard, 1962, Grieve et al., 1978, Orphal et al., 1978, Orphal et al.,1978,), les points suivants ont été retenus:

• *De toutes évidences, la structure de Manicougan est le résultats d'un impact météoritique important.*

•*L'âge de l'impact remonte au Triassique, soit a environ 210 millions d'années a.a., calculé par K-ar.*

• *La partie centrale de la structure (Ile René-Levasseur) se caractérise d'abord par les reliefs élevés des Monts de Babel, d'une zone appelée le Plateau annulaire, composé essentiellement de roches ignées du Triassique et d'une zone de Basse-Terre intérieure composée de gneiss fissurés, vestiges de l'énergie générée lors de l'impact.*

• *Selon les relevés magnétiques disponibles dans la région, une portion "Plateau annulaire", celle située au sud des Monts de Babel, se caractérise par une forte anomalie. La profondeur de celle-ci est difficile à évaluer, mais la modélisation mathématique des données a montré que cette zone anomalique se situe à au moins 560 m de profondeur et provient probablement d'un massif minéralisé imposant* [1]

• *Cette région est déglacée depuis seulement 7500 ans et est recouverte d'une importante couche de dépôts meubles (glaciaires / fluvioglaciaires) (voir*

[1] Plan d'affaire Geovest Inc.

Partie II). Mise à part la région immédiate des Monts de Babel, peu d'affleurements ont été identifiés.

3 DOCUMENTS CARTOGRAPHIQUES

Les 12 documents (3 documents présentés dans ce rapport et 9 documents déjà remis) cartographiques présentés dans ce rapport ont été conçus à partir de la numérisation du fichier topographique 22 N7 à l'échelle du 1:50 000. La numérisation s'est faite à l'aide d'un ordinateur de type Macintosh IIx, d'une tablette graphique et du logiciel Freehand 4.0. Les imprimés laser ont été tirés d'une imprimante à jets d'encre de grand format.

Les documents numérisés sont disponibles en format de type Macintosh Freehand et sont fournis sur disquettes à l'annexe m.

4 RÉFÉRENCES

Bérard, J., 1962. Summary geological investigation of the area bordering Manicougan-Mouchalagan lakes, Saguenay County: Quebec Dept. Nat. Resources, Prelim. Rept. no. 494, 14p.

Grieve, R.A.F., 1978. Manicougan Impact melt, Quebec 2. Chemical interrelations with basement and formational processes. Journal of Geophysical research. Vol. 83, no. B6. pp.2761-2771.

Murtaugh,J.G., 1976. Manicougan impact structure. Ministèere des Richesses Naturelles, DPV-432. 180p..

Onorato, P.J.K. and Uhlmann, D.R., 1978. The termal history of Manicougan impact melt sheet, Quebec. Journal of Geophysical research. Vol. 83, no. B6. pp.2789-2798.

Orphal, D.L. and Schultz, P.H., 1978. An alternative model for the Manicougan impact structure. Proc. Lunar Planet Sci. Conf. 9th. pp 2695-2712.

REPORT ON MANICOUGAN STRUCTURE
PART II

REPORT ON MANICOUGAN STRUCTURE
PART II
SURFICIAL GEOLOGY
TABLE OF CONTENTS

CONCLUSIONS & RECOMMENDATIONS 1
Environmental Geology 1
Economic Geology — 1
- Location and distribution of bedrock outcrops & near-surface occurrences 1
- Surficial deposits as a prospecting medium 2
- Use of Satellite imagery 2

1 INTRODUCTION
1.1 General statement 3
1.2 Approach and Scope 3
1.3 Previous Studies 4

2 PHYSIOGRAPHY
2.1 Terrain features (divisions) 5

3 SURFICIAL MATERIALS
Pre-Quaternary
•Bedrock - map code "R" 6
Quaternary—Wisconsinan—Morainal sediments
•Lodgment till - map code 1 7
•Drumlinized till - map code 2 8
•Ablation till - map code 3 9
•Ribbed moraine - map code 4 10
•Reworked till - map code 5 11
Quaternary—Wisconsinan—Glaciofluvial sediments
•Outwash - map code W 12
•Ice-contact kame complex - map code K 13
•Ice-contact eskers - map code E 14

Quaternary—Late Wisconsinan
•Lacustrine sediments - map code L 15
Quaternary—Holocene
•Organic sediments - map code N 16
•Rock slides - map code S 17
•Colluvial sediments - map code C 18

4 REFERENCES 19

CONCLUSIONS & RECOMMENDATIONS

Environmental Geology

The surficial deposits shown on the interpreted photos emphasize the mosaic of unconsolidated materials interspersed with rocky substrates and reflect the main differences in texture and thickness of deposits that are pertinent to a variety of land-based activities.

Another report could be produced which would relate the characteristics, capabilities and limitations of each of the mapped units to a number of engineering and construction problems that should be considered early in a planning process, before a site development is initiated.

The issues of development that could be discussed would be as follows:

- road construction
- construction materials
- excavation
- foundations
- slope stability
- solid waste disposal
- sewage disposal

Economic Geology —

• Location and distribution of bedrock outcrops & near-surface occurrences

Murtaugh, 1976, p.13, mentioned as one of the significant impediments to geological mapping in this area "...the abundant glacial & vegetative cover and consequent scarcity of good outcrops and exposures of contacts."

The pattern of bedrock outcrop and veneer overburden bedrock occurrences revealed by this mapping now provides a sound basis for the design of any further field mapping program.

- **Surficial deposits as a prospecting medium**

Taking into consideration the fact that most of the interior of Manicougan structure is a sheet of grossly homogenous impact melt about 230m thick (a pseudo lava with the overall composition of a monzonite) and if the mineralization of interest is thought to reside in the underlying country rock, then geochemical sampling or boulder tracing of the surficial deposits may not be appropriate exploration techniques.

- **Use of satellite imagery**

The remote sensing sensor system aboard Landsat TM, the most generally used satellite imagery currently available, records the intensity of solar energy reflected from earth surface covers occurring within 900 m^2 sampling pixels in the visible and near infrared electro-magnetic spectral wavelength bands—i.e. **the data are strictly surficial and are non-penetrative.**

As shown on the forestry image, Figure 1, there are three surface cover types in the study area: **forest**, covering about 85%± of the ground; **water surface**, 10%±; and **bare rock**, 5%±, this last all located on the Monts de Babel.

Given such target terrain conditions, there is, in our opinion, little potential involved in an investment to use such imagery for lithological or structural investigation purposes. As indicated on the Figure, the only spectral or spatial image content having previously unmapped structural implications in the various (multitemporal high and low sun angles and azimuths) local images we have seen are two sub-parallel lineaments following the monsonite-latite contact escarpment southeast of Lac Observation.

Finally, unlike stereoscopic air photography, most satellite images are monoscopic; a fact which seriously constrains their use for lithological mapping in densely vegetated and moderate to low relief areas.

1 INTRODUCTION

1.1 General statement

The work reported here was undertaken following discussions with Lauri Boivin (Amadeus Resouces).

It was agreed that mapping at 1:50,000 scale of the nature, extent and thickness of surficial deposits occurring in the vicinity of the Manic Project area would provide information useful both for the planning of further exploration activity and any subsequent property development.

1.2 Approach and Scope

Satellite images of terrestrial impact craters in cratonic areas are now widely disseminated. Views of the Manicougan structure, as the largest of its kind in North America, are quite familiar. However, the spatial and spectral resolutions of the sensor systems tend to limit the photogeologic utility of such scenes to their initial discovery and their general structural characterization. The mapping of surficial geology at larger scales utilizing this type of imagery is no more feasible within such structures than it is in adjacent terrain.

Larger scale, high spatial resolution airborne photography remains the most practical data base for such mapping. Therefore, this mapping task was undertaken utilizing 1:50,000 scale airphotos taken in 1976. At that photo scale, sixteen stereo photos cover the 644 km^2 study area.

Two types of geologic information were interpreted from the stereo sets:

1 The location, nature and extent of occurring surficial deposits

2 The estimated thickness of the deposits over local bedrock subcrops

Twelve types of surficial deposits and four depth classes have been mapped and are characterized in section 3.

These results are presented on nine annotated airphotos and the interpretations are to be transferred to a 1:50,000 digitized planimetric map base.

1.3 Previous Studies

The only quaternary geology mapping known to have been carried out in the area is the map produced by Klassen et al., published in 1992 as G.S.C. Map 1814A, scale 1:1,000,000, depicting seven classes of landforms and deposits. Observations by Kish (1968) referred to glacial striae directions in the Manicougan Uplands adjacent to our study area.

2 PHYSIOGRAPHY

2.1 Terrain features

Four groups of terrain features are apparent at airphoto scale:

1 The Monts de Babel
2 Outcrop areas south of the Monts de Babel
3 Drumlinized till zones
4 Disordered till and glaciofluvial deposit areas

These features may be correlated to Murtaugh's division of terrain inside the Manic structure (p.10-11) as follows:

Group 1	The Monts de Babel are his "central mountain"
Group 2	The Outcrop areas south correspond to his "annular plateau" of Triassic rocks
Groups 3 & 4	are located in his "inner lowland"

3 Surficial Materials
Pre-Quaternary

Map Unit - Name: *Bedrock* **Code:** R

Observable photogeologic characteristics

- **Topographic site**
  Local topographic highs

- **Elevation range (meters)**
  430 - 950

- **Local relief (meters)**
  10-300

Inferred geologic characteristics

- **Genetic**
  With the exception of the anorthosites of the Monts de Babel, vegetation cover and the limited discontinuous extent of individual interpreted outcrops do not permit a distinction of the lithology or composition of the bedrock.

3 Surficial Materials
Quaternary—Wisconsinan—Morainal Sediments

Map Unit - Name: *Lodgment Till* **Code:** 1

Observable photogeologic characteristics

- **Topographic site**
  footslopes - sideslopes - upland basins - ridge crests

- **Elevation range (meters)**
  360 - 850

- **Local relief (meters)**
  0.5 - 150

Inferred geologic characteristics

- **Genetic**
  Originates subglacially - at and from the base of a moving glacier. Pressure melting of flowing ice frees drift particles which are plastered on to the subglacial floor. Crushing and abrasion of particles is intense and the till is compact (overconsolidated).

- **Textural**
  Unsorted and unstratified heterogeneous mixture of clay, sand, silt, gravel and boulders; finer sizes comprising the matrix. Stones tend to lodge with their long axis parallel to the direction of flow.

- **Hydrologic**
  Generally well-drained
  Materials tend to have low permeabilities and low moisture contents.

3 Surficial Materials
Quaternary—Wisconsinan—Morainal Sediments

Map Unit - Name: *Drumlinized till*
Code: 2

Observable photogeologic characteristics

- **Topographic site**
  Broad low relief areas, vicinity Lac Observation and Lac Deporte and on higher ground around eastern lakes.

- **Elevation range (meters)**
  410 - 670

- **Local relief (meters)**
  Streamlined low linear hills, long axes oriented in direction of ice movement.
  Height most common between 15 and 25 m.

Inferred geologic characteristics

- **Genetic**
  Subglacial molding of saturated till originating in same manner as Unit #1.
  Crag and tail symbol is associated with occurrence of a rock boss at upstream end of the unit.

- **Textural**
  Same as for Unit #1. Some higher occurrences may have a bedrock core.

- **Hydrologic**
  Poor internal drainage, but active surface run off.

3 Surficial Materials
Quaternary—Wisconsinan—Morainal Sediments

Map Unit - Name: *Ablation till* Code: 3

Observable photogeologic characteristics

- **Topographic site**
  Frequently marginal to re-worked till deposits (Unit 5) and on plateaux often above or near Lodgment till areas.

- **Elevation range (meters)**
  460 - 670

- **Local relief (meters)**
  Chaotic topography of low sharp ridges, hummocks and depressions. Range 5 - 10 m heights.

Inferred geologic characteristics

- **Genetic**
  Subglacial sediments, subglacial in origin, exposed on glacier surface as result of pattern of ice flow. Bodies of ice become buried in sedimentary sequence. Ice bodies subsequently melt down and disturb overlying strata.

- **Textural**
  Loose, non-compact, non-stratified till. Fines are washed away selectively; more granular than Lodgment till.

- **Hydrologic**
  Disordered surface drainage, with many semi-stagnant pools. Internal drainage highly variable, but generally good.

3 Surficial Materials
Quaternary—Wisconsinan—Morainal Sediments

Map Unit - Name: *Ribbed moraine*
Code: 4

Observable photogeologic characteristics

- **Topographic site**
  In valleys and along valley sides.

- **Elevation range (meters)**
  365 - 580

- **Local relief (meters)**
  To 10 m— succession of discrete irregular to sinuous ridges with rounded crests and generally steep sides. Lie transverse to former local ice flow directions.

Inferred geologic characteristics

- **Genetic**
  Englacially formed by the stacking and piling-up of thick basal debris sequence. The upper surface of the transverse bed obstacle is then smoothed by clean ice moving overhead.

- **Textural**
  Generally bouldery till of the Lodgment type.

- **Hydrologic**
  Similar to drumlinized till, Unit 2.

3 Surficial Materials
Quaternary—Wisconsinan—Morainal Sediments

Map Unit - Name: *Reworked till* **Code:** 5

Observable photogeologic characteristics

- **Topographic site**
  Topographic lows and intermont valleys acting as spillway channels.

- **Elevation range (meters)**
  400 - 640

- **Local relief (meters)**
  Similar to Ablation till—hummocky terrain with local water or organic-filled small depressions.

Inferred geologic characteristics

- **Genetic**
  Lodgment or Ablation till which has been subjected by washing action of channeled or sheet glacial melt water flows.

- **Textural**
  As Lodgment till, but most fine fractions removed leaving coarse sand, gravel, boulders and local boulder "field" concentrations.

- **Hydrologic**
  Generally well-drained.

3 Surficial Materials
Quaternary—Wisconsinan—Glaciofluvial Sediments

Map Unit - Name: *Outwash* Code: W

Observable photogeologic characteristics

- **Topographic site**
  Associated with re-worked till areas and other glaciofluvial sediments in topographic lows.

- **Elevation range (meters)**
  400 - 580

- **Local relief (meters)**
  Flat, nearly level surface locally fitted with sharply depressed "kettle holes".

Inferred geologic characteristics

- **Genetic**
  Drift washed out from a glacier by its meltwaters and deposited at and beyond (proglacial) the margin of the glacier.

- **Textural**
  Mainly stratified and well sorted sands and gravels with some local muck-filled lenses.

- **Hydrologic**
  High infiltration of rainfall results in lack of surface drainage. Very good internal drainage, vertically and horizontally.

3 Surficial Materials
Quaternary—Wisconsinan—Glaciofluvial Sediments

Map Unit - Name: *Ice-Contact Kame Complex*
Code: K

Observable photogeologic characteristics

- **Topographic site**
  In valley at foot of Mont de Babel

- **Elevation range (meters)**
  535 - 560

- **Local relief (meters)**
  Knob and kettle topography, irregular terrain with many slumping features.

Inferred geologic characteristics

- **Genetic**
  Deposited by meltwater flowing between a glacier margin and the nearby valley wall. One side was supported by the ice face. After the ice body melted away this support was removed and the inward side of the deposit slumped.

- **Textural**
  Material often poorly sorted with granulars, silts and some till pockets mixed. Granulars usually dirty. Often slumped, causing abrupt changes in material. Stratification is irregular.

- **Hydrologic**

  Groundwater liable to be varied. but usually good internal drainage.

3 Surficial Materials
Quaternary—Wisconsinan—Glaciofluvial Sediments

Map Unit - Name: *Ice-contact Eskers*
Code: ~~E~~

Observable photogeologic characteristics

- **Topographic site**
  In valleys and lowlands with reworked till and other glaciofluvial deposits.

- **Elevation range (meters)**
  400 -475

- **Local relief (meters)**
  Elongated, sinuous, continuous and discontinuous ridges with knife-edged crests. Side slopes are at angle of repose (approx 35°) others modified to gentler. Height 20-40M.

Inferred geologic characteristics

- **Genetic**
  Deposited by subglacial meltwater streams material slumped down to angle of repose when supporting ice melted.

- **Textural**
  Irregularly stratified sand and gravel, may grade into silt lenses locally.

- **Hydrologic**
  Good drainage, due to deposit geometry and composition.

3 Surficial Materials
Quaternary—Late Wisconsinan

Map Unit - Name: *Lacustrine sediments*
Code: LX-LZ

Observable photogeologic characteristics

- **Topographic site**
  On low ground at eastern foot of Mont de Babel. Near reservoir.

- **Elevation range (meters)**
  365-400

- **Local relief (meters)**
  Terrain is smooth and level.

Inferred geologic characteristics

- **Genetic**
  Material deposited from suspension in lakes resulting directly or indirectly from presence of a glacier (ice dam or tilting due to isostatic depression).

- **Textural**
  Stratified, silts, fine sands, some clay moderately to well-sorted.
  Local deposits may not be very thick over till. LX units may be sandier than LZ.

- **Hydrologic**
  Water tables expected to be generally higher than in other deposit types (excepting organic).
  Integrated surface drainage visible.

3 Surficial Materials
Quaternary—Holocene

Map Unit - Name: *Organic sediments*
Code: N

Observable photogeologic characteristics

- **Topographic site**
  Ubiquitous in poorly or un-drained depressions.

- **Elevation range (meters)**
  390 - 820

- **Local relief (meters)**
  nil

Inferred geologic characteristics

- **Genetic**
  Accumulation of decomposing vegetative matter in anaerobic environment of stagnant drainage site.

- **Textural**
  Typical section might comprise fibrous organic material followed by amorphous organic and soft clayey subsoil or glacial till.

- **Hydrologic**
  Stagnant drainage; water table at or near surface throughout growing season.

3 Surficial Materials
Quaternary—Holocene

Map Unit - Name: *Rockslides* **Code:** S

Observable photogeologic characteristics

- **Topographic site**
  At monzonite-latite upslope contact, southeast of Lac Observation.

- **Elevation range (meters)**
  440-670

- **Local relief (meters)**
  230 from unit headwall to downslope toe; displaced mass at base is ridged and hummocky.

Inferred geologic characteristics

- **Genetic**
  Materials deposited downslope by large scale mass movement - rapid movement of detached segments of the bedrock sliding on plane of separation and along downslope surface.

- **Textural**
  Blocks and rubble in finer matrix of crushed rock.

- **Hydrologic**
  Good internal drainage.

3 Surficial Materials
Quaternary—Holocene

Map Unit - Name: *Colluvial sediments* Code: C

Observable photogeologic characteristics

- **Topographic site**
  Along face and at foot of steep rock slopes or escarpments.

- **Elevation range (meters)**
  365-850

- **Local relief (meters)**
  Mimics slope on which it occurs, or may be local talus cone.

Inferred geologic characteristics

- **Genetic**
  Weathered and disintegrated local bedrock moved downslope by gravity, solifluction or rainwash.

- **Textural**
  Heterogeneous material of all particle sizes but fines probably removed. Can be massive to moderately stratified.

- **Hydrologic**
  Well drained.

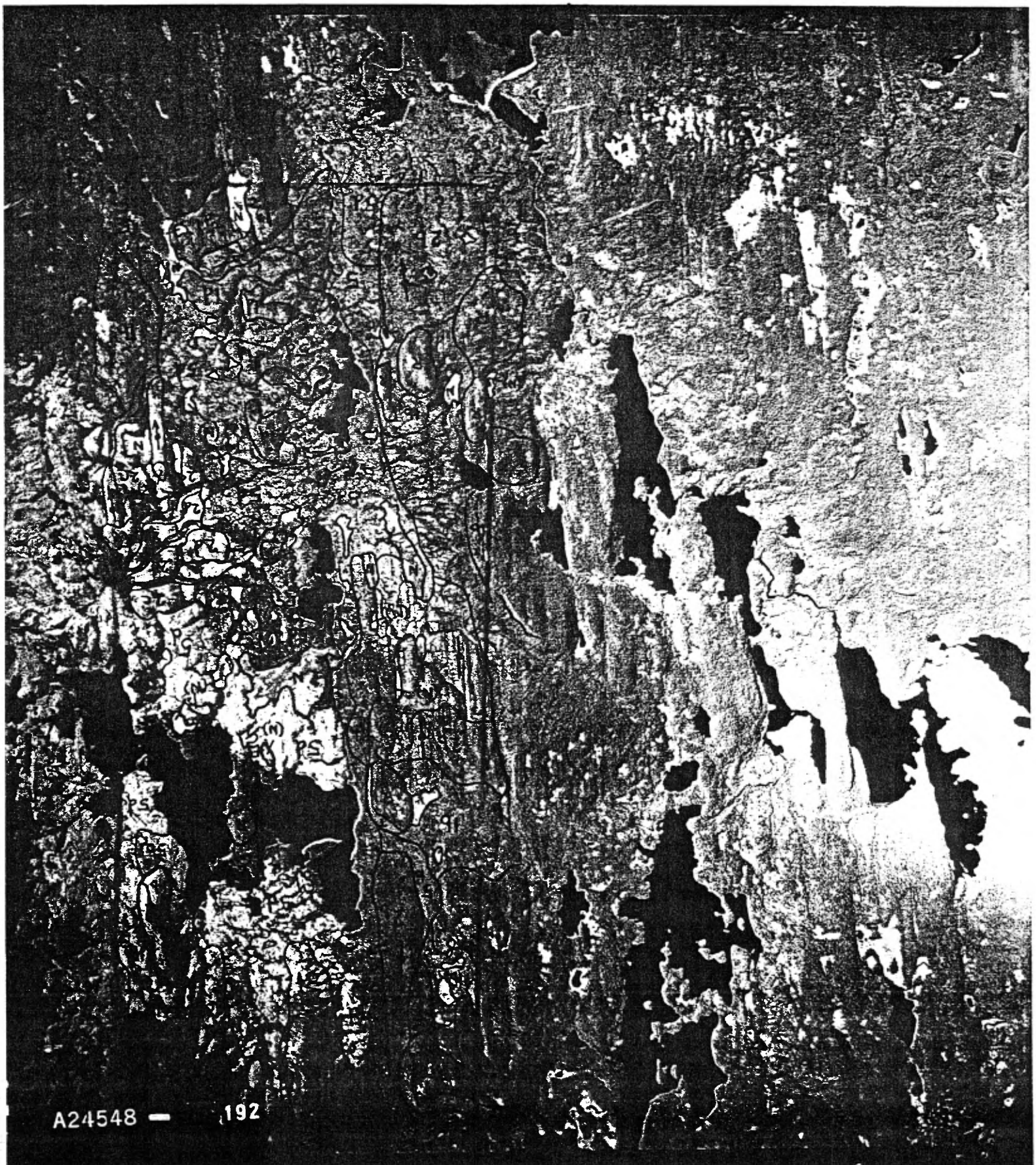
4 REFERENCES

- Kish, L. 1968. *Hart-Jaune River area, Saguenay County:* Québec Natural Resources Geological Report 132.

- Klassen, R.A. et al, 1992. *Glacial Landforms & Deposits, Labrador, Newfoundland & Eastern Québec.*. Geological Survey of Canada, Map 1814A, scale 1:1,000,000.

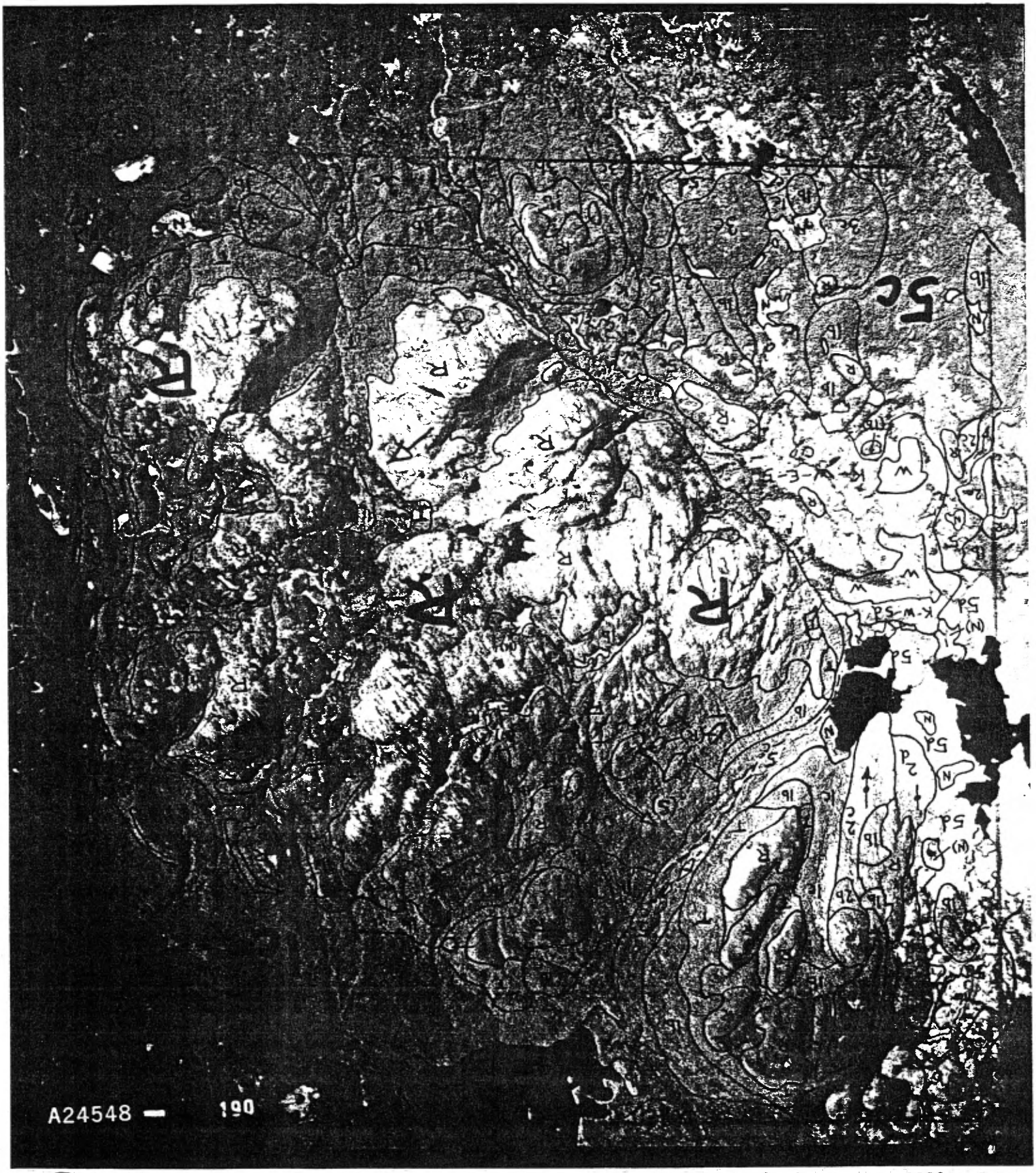
- Murtaugh, J.G. 1976. *Manicougan Impact Structure*. Ministère des Richesses Naturelles, Québec, Report DPV-432.

© SA MAJESTE LA REINE DU CHEF DU CANADA, MINISTERE DE L'ENERGIE, DES MINES ET DES RESSOURCES.



© HER MAJESTY THE QUEEN IN RIGHT OF CANADA, DEPARTMENT OF ENERGY, MINES AND RESOURCES.

© SA MAJESTE LA REINE DU CHEF DU CANADA, MINISTERE DE L'ENERGIE, DES MINES ET DES RESSOURCES.



© HER MAJESTY THE QUEEN IN RIGHT OF CANADA, DEPARTMENT OF ENERGY, MINES AND RESOURCES.

© SA MAJESTE LA REINE DU CHEF DU CANADA, MINISTERE DE L'ENERGIE, DES MINES ET DES RESSOURCES.



© HER MAJESTY THE QUEEN IN RIGHT OF CANADA, DEPARTMENT OF ENERGY, MINES AND RESOURCES.

SA MAJESTE LA REINE DU CHEF DU CANADA, MINISTERE DE L'ENERGIE, DES MINES ET DES RESSOURCES.

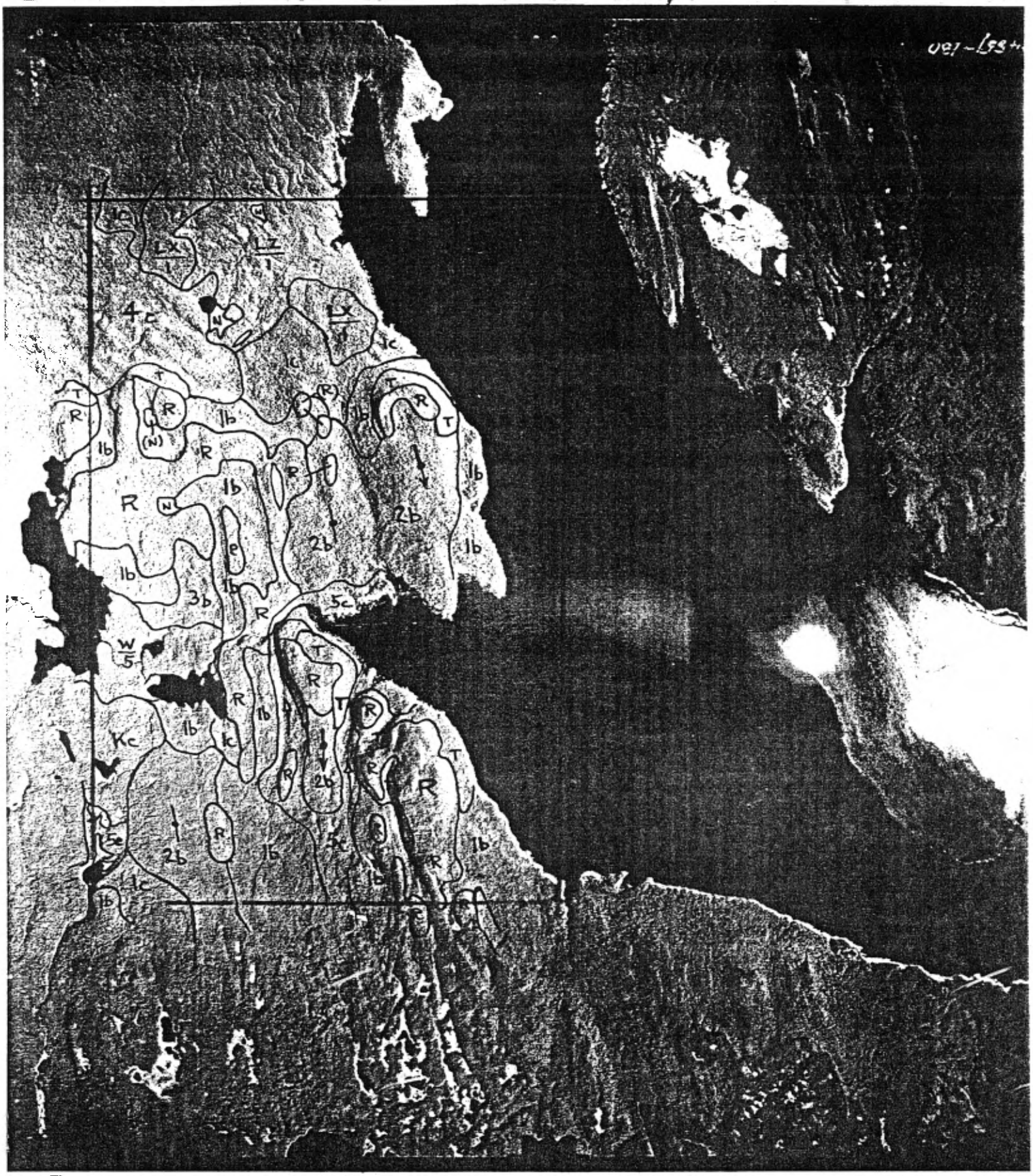


HER MAJESTY THE QUEEN IN RIGHT OF CANADA, DEPARTMENT OF ENERGY, MINES AND RESOURCES.

Photo 4

photo 5

© SA MAJESTE LA REINE DU CHEF DU CANADA, MINISTERE DE L'ENERGIE, DES MINES ET DES RESSOURCES. 1



© HER MAJESTY THE QUEEN IN RIGHT OF CANADA, DEPARTMENT OF ENERGY, MINES AND RESOURCES. 1

Photo 6


A25563

HER MAJESTY THE QUEEN IN RIGHT OF CANADA, DEPARTMENT OF ENERGY, MINES AND RESOURCES.

SA MAJESTE LA REINE DU CHEF DU CANADA, MINISTERE DE L'ENERGIE, DES MINES ET DES RESSOURCES.

Photo 8

SA MAJESTE LA REINE DU CHEF DU CANADA, MINISTERE DE L'ENERGIE, DES MINES ET DES RESSOURCES.



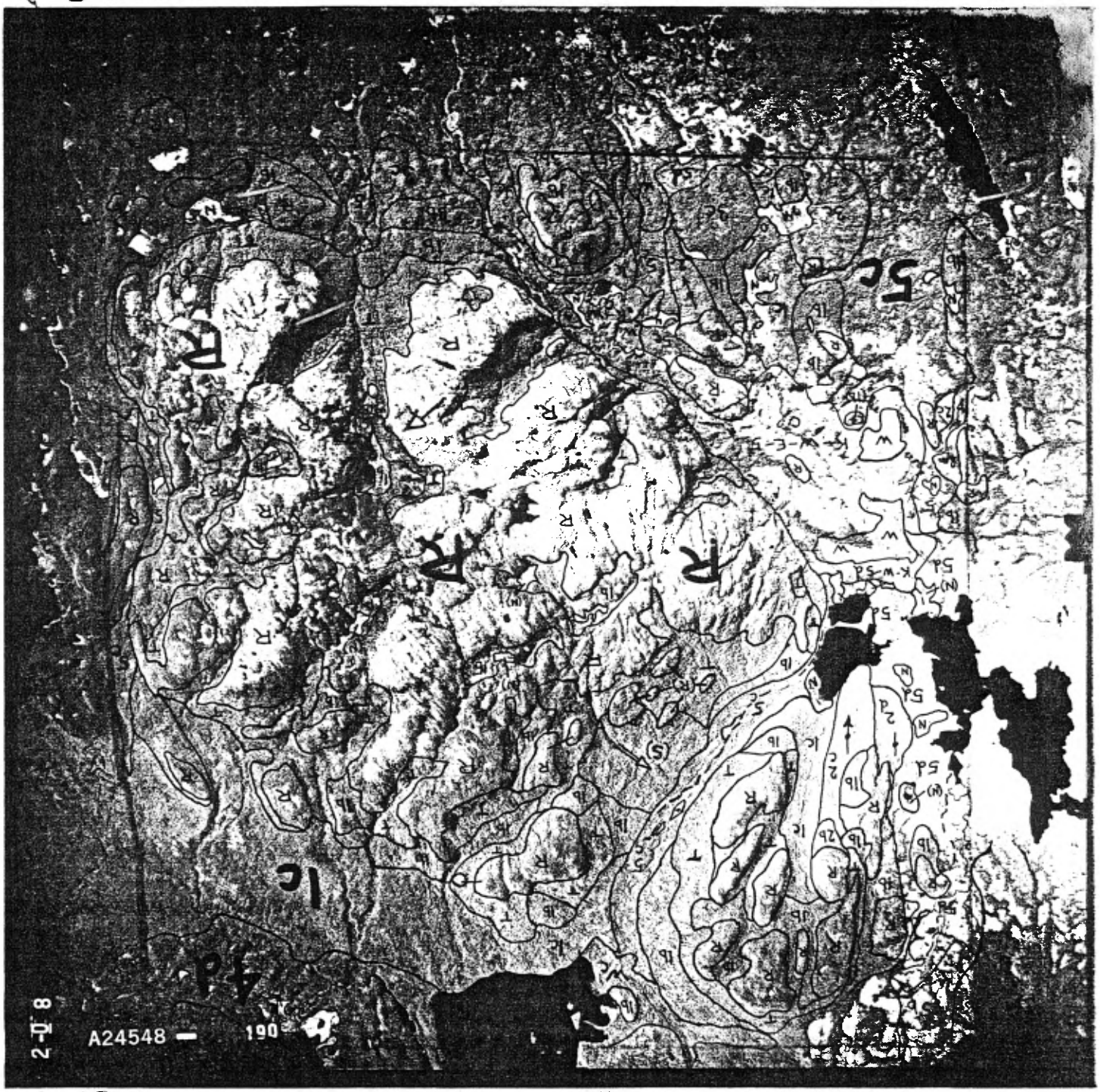
HER MAJESTY THE QUEEN IN RIGHT OF CANADA, DEPARTMENT OF ENERGY, MINES AND RESOURCES.

© SA MAJESTE LA REINE DU CHEF DU CANADA, MINISTERE DE L'ENERGIE, DES MINES ET DES RESSOURCES. 1



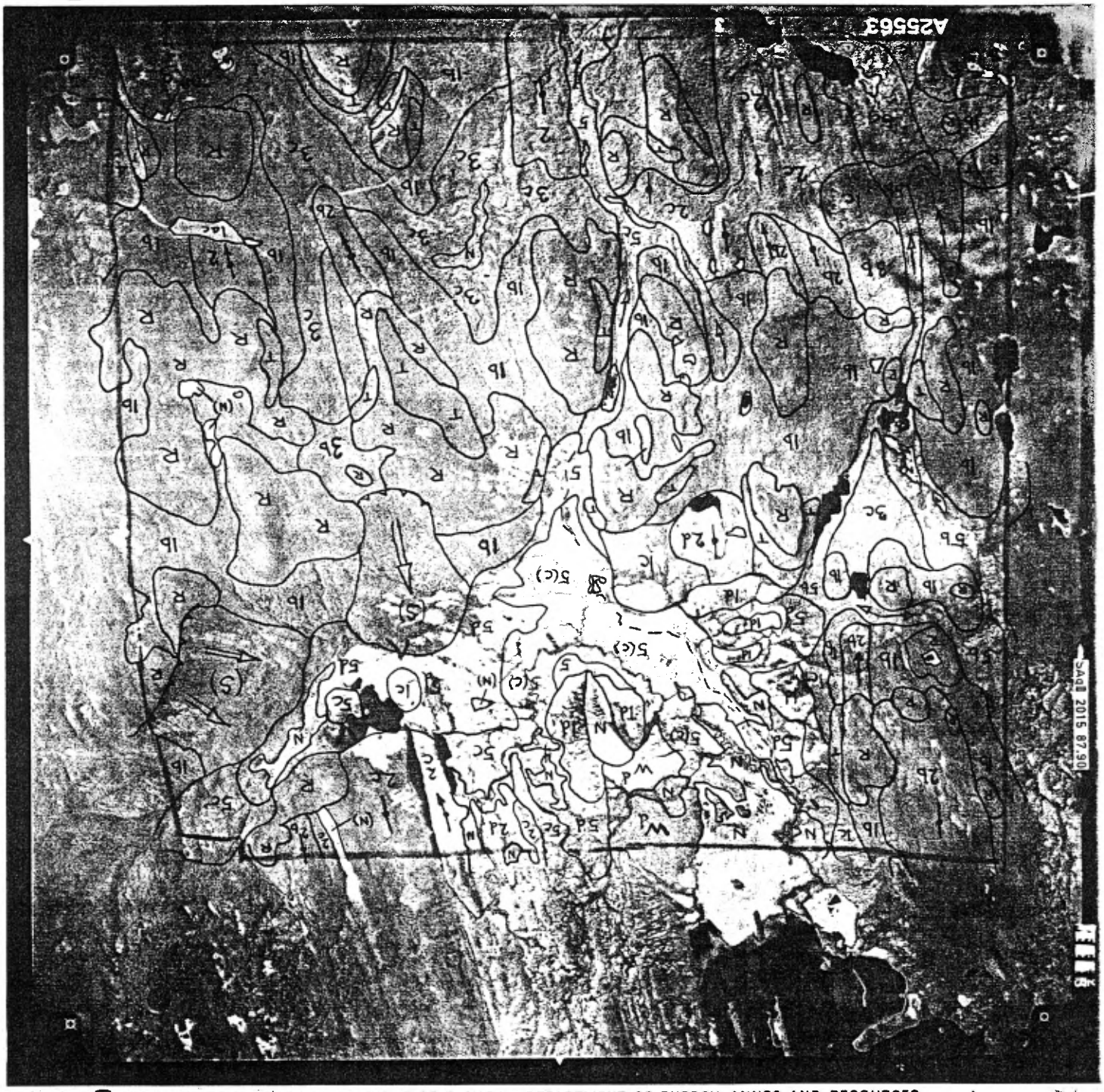
© HER MAJESTY THE QUEEN IN RIGHT OF CANADA, DEPARTMENT OF ENERGY, MINES AND RESOURCES. 1

© SA MAJESTE LA REINE DU CHEF DU CANADA, MINISTERE DE L'ENERGIE, DES MINES ET DES RESSOURCES.



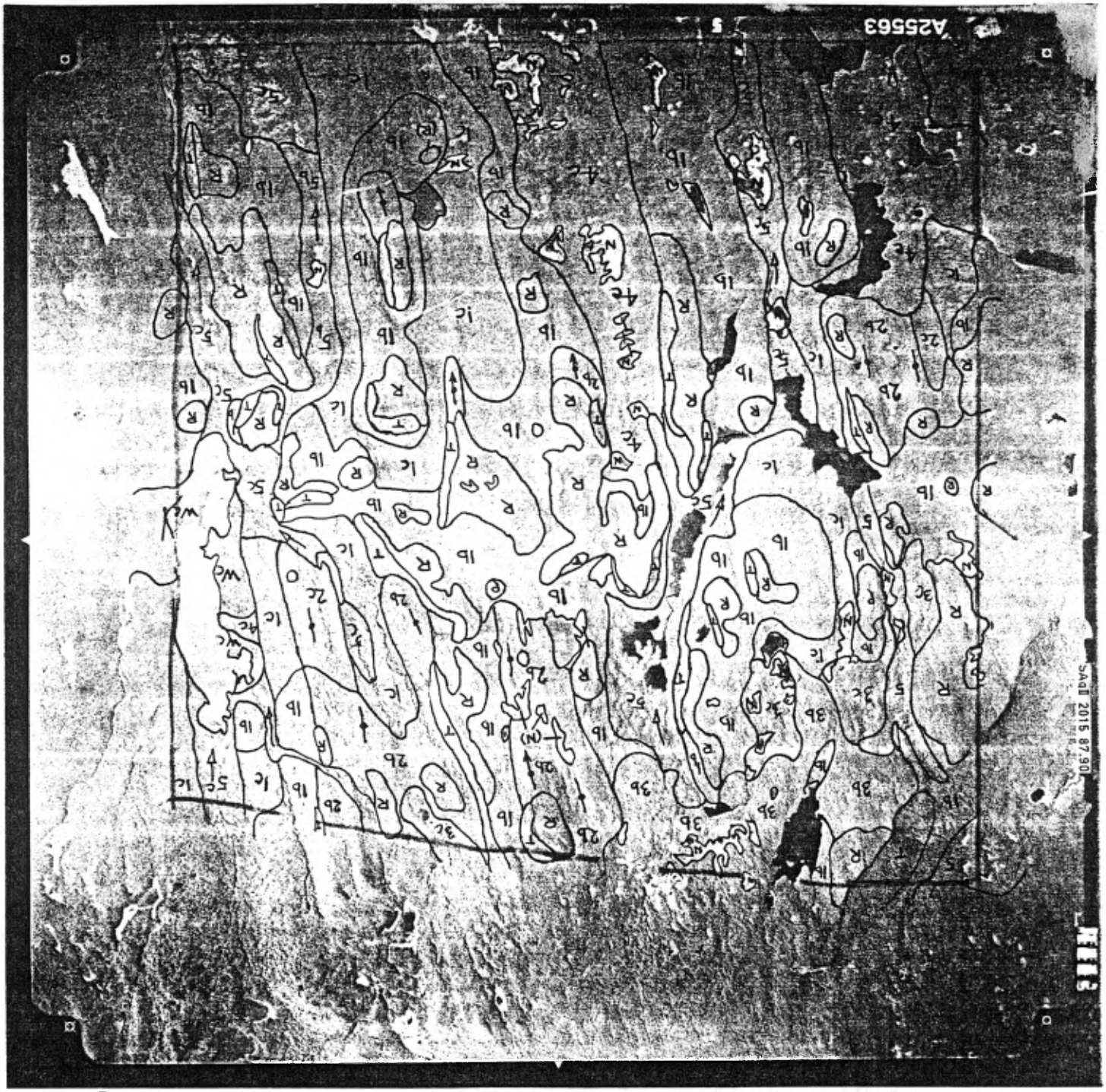
© HER MAJESTY THE QUEEN IN RIGHT OF CANADA, DEPARTMENT OF ENERGY, MINES AND RESOURCES.

© SA MAJESTE LA REINE DU CHEF DU CANADA, MINISTERE DE L'ENERGIE, DES MINES ET DES RESSOURCES.



© HER MAJESTY THE QUEEN IN RIGHT OF CANADA, DEPARTMENT OF ENERGY, MINES AND RESOURCES.

© SA MAJESTE LA REINE DU CHEF DU CANADA, MINISTERE DE L'ENERGIE, DES MINES ET DES RESSOURCES.



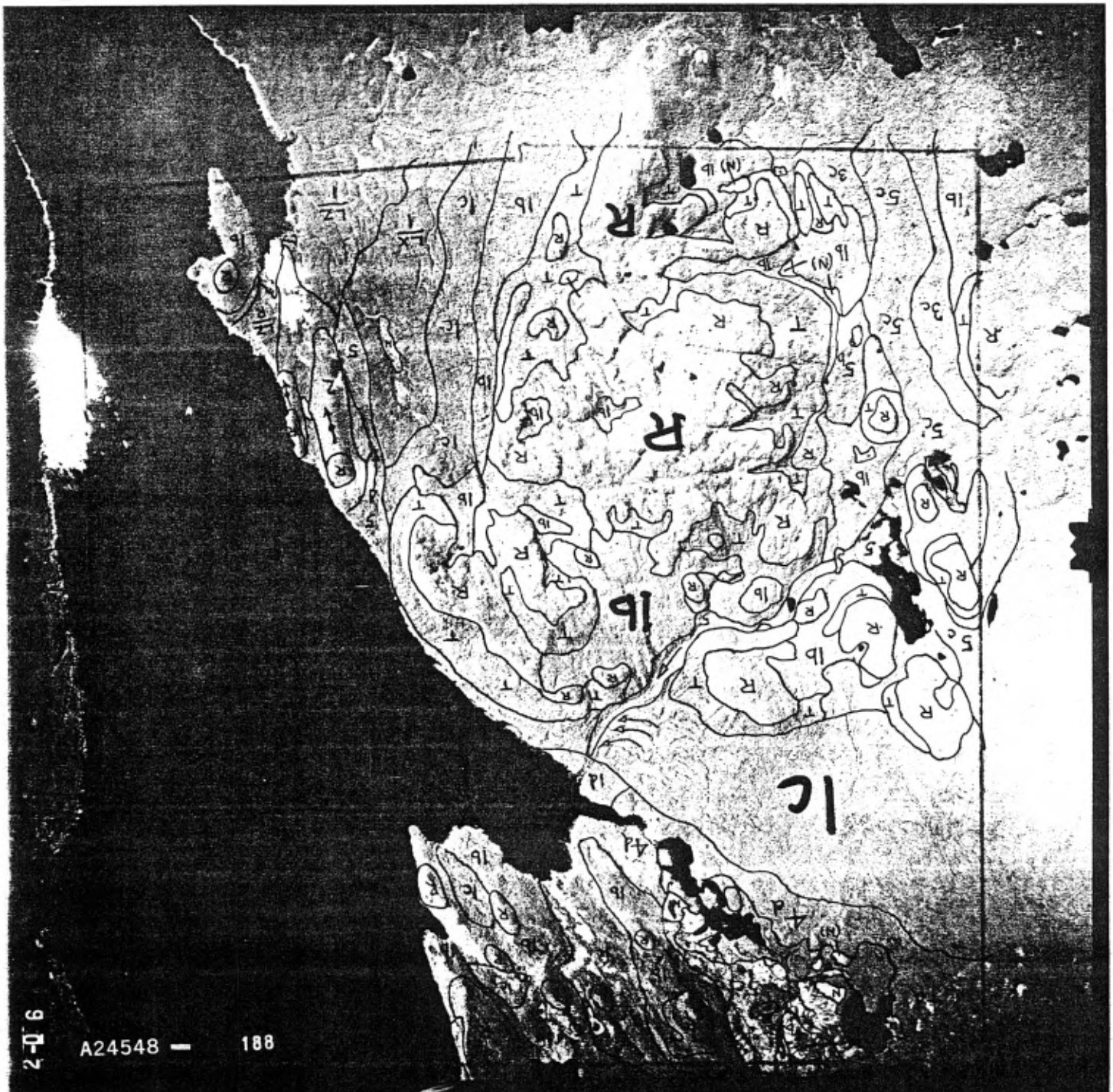
© HER MAJESTY THE QUEEN IN RIGHT OF CANADA, DEPARTMENT OF ENERGY, MINES AND RESOURCES.

© SA MAJESTE LA REINE DU CHEF DU CANADA, MINISTERE DE L'ENERGIE, DES MINES ET DES RESSOURCES.



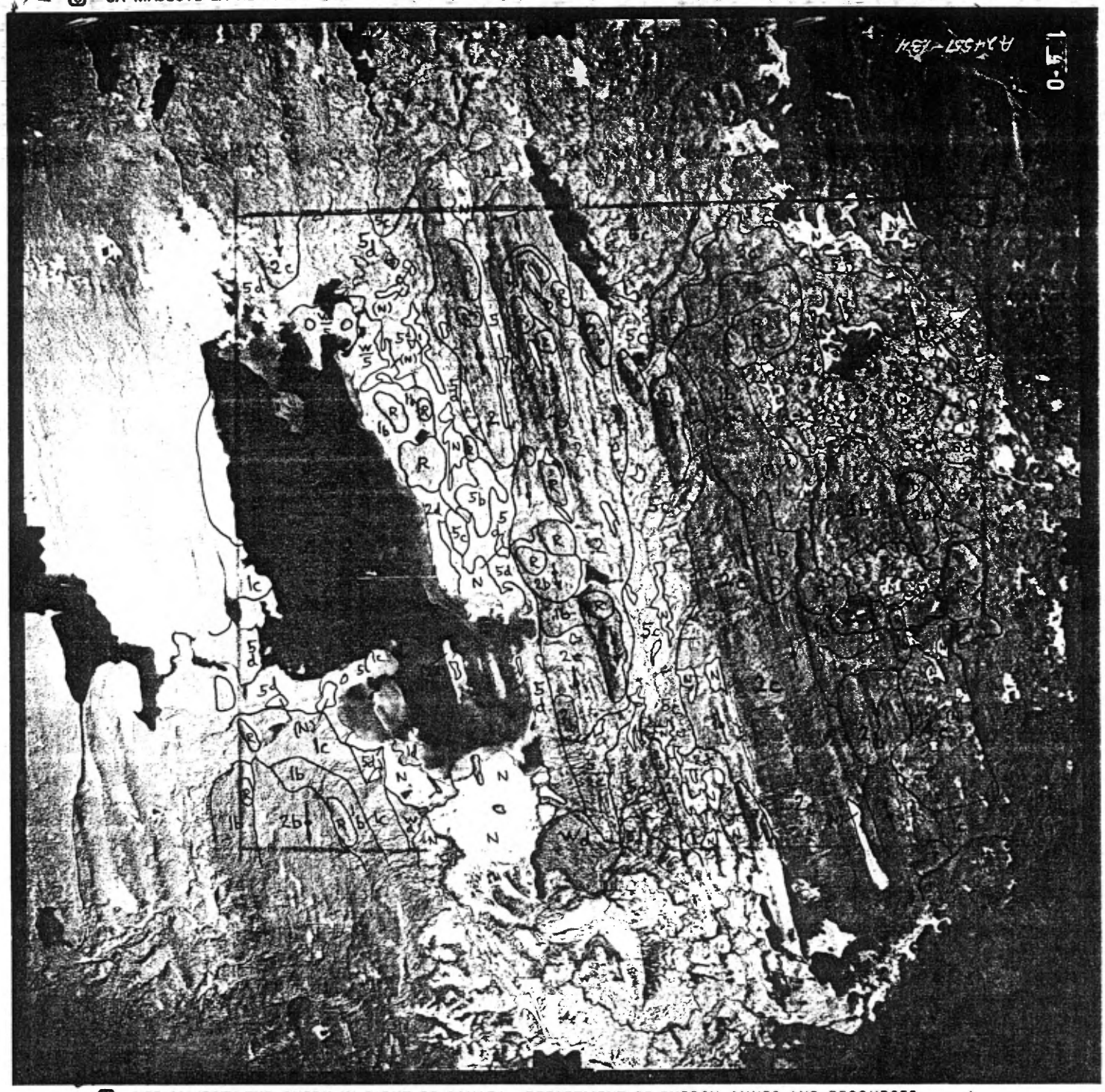
© HER MAJESTY THE QUEEN IN RIGHT OF CANADA, DEPARTMENT OF ENERGY, MINES AND RESOURCES.

© SA MAJESTE LA REINE DU CHEF DU CANADA, MINISTERE DE L'ENERGIE, DES MINES ET DES RESSOURCES.



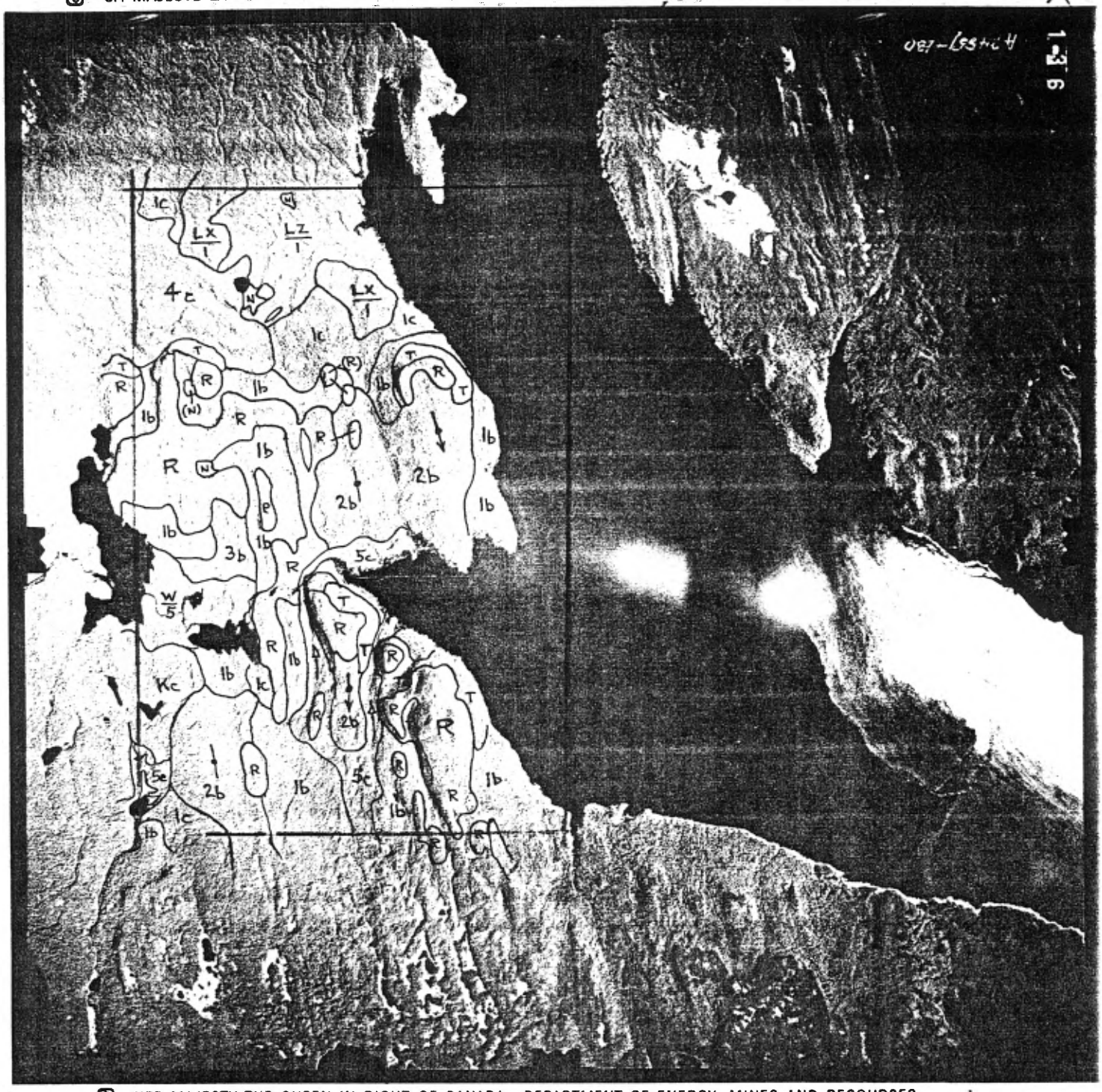
© HER MAJESTY THE QUEEN IN RIGHT OF CANADA, DEPARTMENT OF ENERGY, MINES AND RESOURCES.

© SA MAJESTÉ LA REINE DU CHEF DU CANADA, MINISTÈRE DE L'ÉNERGIE, DES MINES ET DES RESSOURCES.



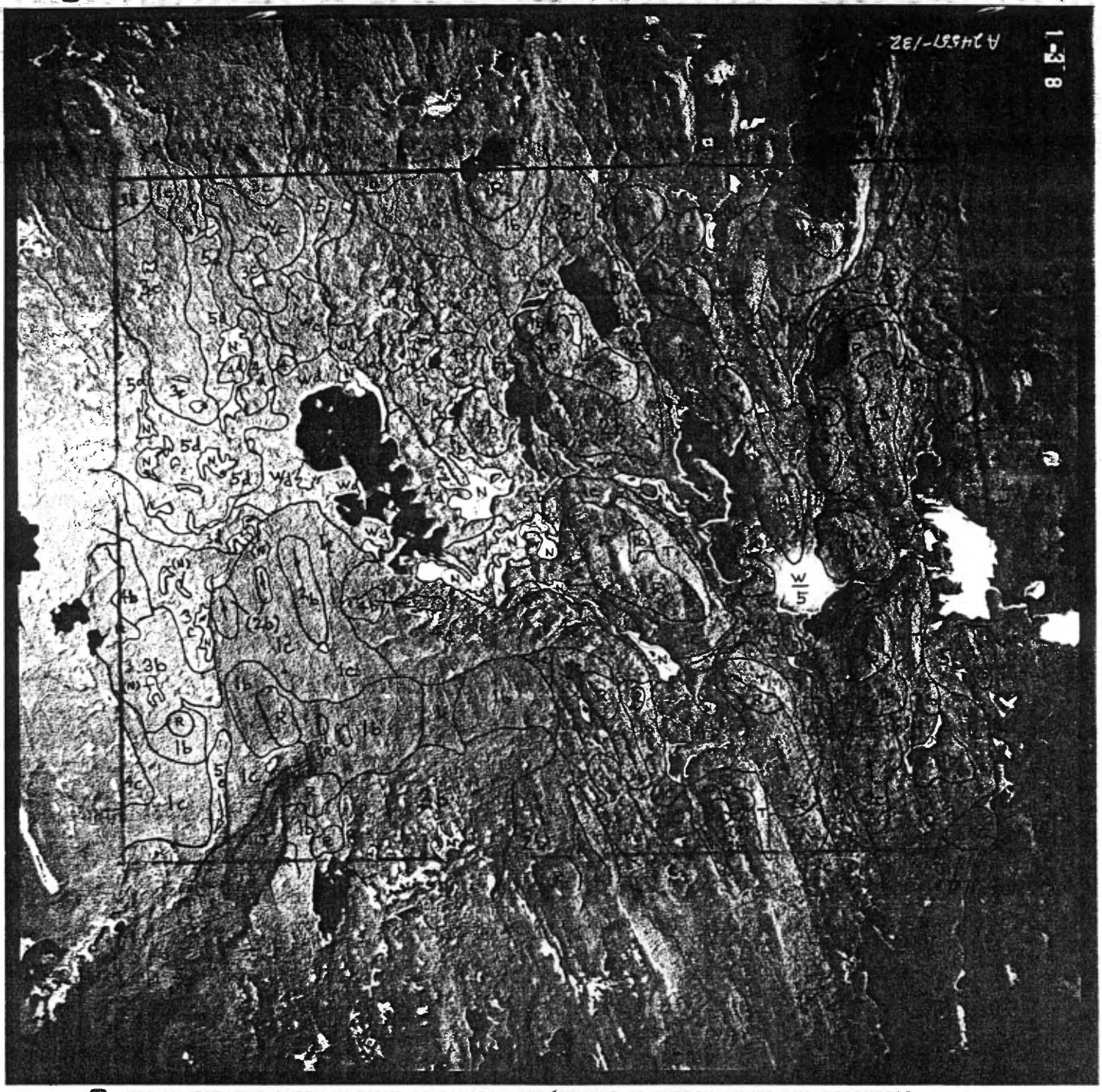
© HER MAJESTY THE QUEEN IN RIGHT OF CANADA, DEPARTMENT OF ENERGY, MINES AND RESOURCES.

© SA MAJESTE LA REINE DU CHEF DU CANADA, MINISTERE DE L'ENERGIE, DES MINES ET DES RESSOURCES.



© HER MAJESTY THE QUEEN IN RIGHT OF CANADA, DEPARTMENT OF ENERGY, MINES AND RESOURCES.

© SA MAJESTE LA REINE DU CHEF DU CANADA, MINISTERE DE L'ENERGIE, DES MINES ET DES RESSOURCES. 1



© HER MAJESTY THE QUEEN IN RIGHT OF CANADA, DEPARTMENT OF ENERGY, MINES AND RESOURCES. 1

Gouvernement du Québec
Ministère des Ressources naturelles
Service de la comptabilité forestière

SPATIOCARTE FORESTIÈRE SYNTHÈSE

GUIDE D'INTERPRÉTATION DE L'IMAGE

TYPE DE COUVERT FORESTIER

Résineux mûr .....
Résineux mûr ouvert .....
Résineux jeune .....
Résineux en régénération ...

Mélangé mûr .....
Mélangé jeune .....
Mélangé en régénération ...

Feuillu mûr .....
Feuillu jeune .....
Feuillu en régénération ...

PERTURBATION

Coupe par bandes .....
Épidémie légère .....

ORIGINE

Brûlis total .....
Chablis total .....
Coupe totale .....
Épidémie sévère .....

AUTRE TERRAIN

Agricole .....
Urbain et industriel .....
Dénudé sec .....
Tourbière .....

d'après données Landsat TM du 29 juillet 1986

REPORT ON MANICOUGAN STRUCTURE
PART II
SURFICIAL GEOLOGY
TABLE OF CONTENTS

CONCLUSIONS & RECOMMENDATIONS 1
Environmental Geology 1
Economic Geology — 1
- Location and distribution of bedrock outcrops & near-surface occurrences 1
- Surficial deposits as a prospecting medium 2
- Use of Satellite imagery 2

1 INTRODUCTION
- 1.1 General statement 3
- 1.2 Approach and Scope 3
- 1.3 Previous Studies 4

2 PHYSIOGRAPHY
- 2.1 Terrain features (divisions) 5

3 SURFICIAL MATERIALS

Pre-Quaternary
- •Bedrock - map code "R" 6

Quaternary—Wisconsinan—Morainal sediments
- •Lodgment till - map code 1 7
- •Drumlinized till - map code 2 8
- •Ablation till - map code 3 9
- •Ribbed moraine - map code 4 10
- •Reworked till - map code 5 11

Quaternary—Wisconsinan—Glaciofluvial sediments
- •Outwash - map code W 12
- •Ice-contact kame complex - map code K 13
- •Ice-contact eskers - map code E 14

Quaternary—Late Wisconsinan
•Lacustrine sediments - map code L 15
Quaternary—Holocene
•Organic sediments - map code N 16
•Rock slides - map code S 17
•Colluvial sediments - map code C 18

4 REFERENCES 19

CONCLUSIONS & RECOMMENDATIONS

Environmental Geology

The surficial deposits shown on the interpreted photos emphasize the mosaic of unconsolidated materials interspersed with rocky substrates and reflect the main differences in texture and thickness of deposits that are pertinent to a variety of land-based activities.

Another report could be produced which would relate the characteristics, capabilities and limitations of each of the mapped units to a number of engineering and construction problems that should be considered early in a planning process, before a site development is initiated.

The issues of development that could be discussed would be as follows:

- road construction
- construction materials
- excavation
- foundations
- slope stability
- solid waste disposal
- sewage disposal

Economic Geology —

• Location and distribution of bedrock outcrops & near-surface occurrences

Murtaugh, 1976, p.13, mentioned as one of the significant impediments to geological mapping in this area "...the abundant glacial & vegetative cover and consequent scarcity of good outcrops and exposures of contacts."

The pattern of bedrock outcrop and veneer overburden bedrock occurrences revealed by this mapping now provides a sound basis for the design of any further field mapping program.

• **Surficial deposits as a prospecting medium**

Taking into consideration the fact that most of the interior of Manicougan structure is a sheet of grossly homogenous impact melt about 230m thick (a pseudo lava with the overall composition of a monzonite) and if the mineralization of interest is thought to reside in the underlying country rock, then geochemical sampling or boulder tracing of the surficial deposits may not be appropriate exploration techniques.

• **Use of satellite imagery**

The remote sensing sensor system aboard Landsat TM, the most generally used satellite imagery currently available, records the intensity of solar energy reflected from earth surface covers occurring within 900 m^2 sampling pixels in the visible and near infrared electro-magnetic spectral wavelength bands—i.e. **the data are strictly surficial and are non-penetrative**.

As shown on the forestry image, Figure 1, there are three surface cover types in the study area: **forest**, covering about 85%± of the ground; **water surface**, 10%±; and **bare rock**, 5%±, this last all located on the Monts de Babel.

Given such target terrain conditions, there is, in our opinion, little potential involved in an investment to use such imagery for lithological or structural investigation purposes. As indicated on the Figure, the only spectral or spatial image content having previously unmapped structural implications in the various (multitemporal high and low sun angles and azimuths) local images we have seen are two sub-parallel lineaments following the monsonite-latite contact escarpment southeast of Lac Observation.

Finally, unlike stereoscopic air photography, most satellite images are monoscopic; a fact which seriously constrains their use for lithological mapping in densely vegetated and moderate to low relief areas.

1 INTRODUCTION

1.1 General statement

The work reported here was undertaken following discussions with Lauri Boivin.

It was agreed that mapping at 1:50,000 scale of the nature, extent and thickness of surficial deposits occurring in the vicinity of the Manic Project area would provide information useful both for the planning of further exploration activity and any subsequent property development.

1.2 Approach and Scope

Satellite images of terrestrial impact craters in cratonic areas are now widely disseminated. Views of the Manicougan structure, as the largest of its kind in North America, are quite familiar. However, the spatial and spectral resolutions of the sensor systems tend to limit the photogeologic utility of such scenes to their initial discovery and their general structural characterization. The mapping of surficial geology at larger scales utilizing this type of imagery is no more feasible within such structures than it is in adjacent terrain.

Larger scale, high spatial resolution airborne photography remains the most practical data base for such mapping. Therefore, this mapping task was undertaken utilizing 1:50,000 scale airphotos taken in 1976. At that photo scale, sixteen stereo photos cover the 644 km^2 study area.

Two types of geologic information were interpreted from the stereo sets:

1 The location, nature and extent of occurring surficial deposits

2 The estimated thickness of the deposits over local bedrock subcrops

Twelve types of surficial deposits and four depth classes have been mapped and are characterized in section 3.

3 Surficial Materials
Pre-Quaternary

Map Unit - Name: *Bedrock*	Code: R

Observable photogeologic characteristics

- **Topographic site**
  Local topographic highs

- **Elevation range (meters)**
  430 - 950

- **Local relief (meters)**
  10-300

Inferred geologic characteristics

- **Genetic**
  With the exception of the anorthosites of the Monts de Babel, vegetation cover and the limited discontinuous extent of individual interpreted outcrops do not permit a distinction of the lithology or composition of the bedrock.

3 Surficial Materials
Quaternary—Wisconsinan—Morainal Sediments

Map Unit - Name: *Lodgment Till* **Code: 1**

Observable photogeologic characteristics

- **Topographic site**
  footslopes - sideslopes - upland basins - ridge crests

- **Elevation range (meters)**
  360 - 850

- **Local relief (meters)**
  0.5 - 150

Inferred geologic characteristics

- **Genetic**
  Originates subglacially - at and from the base of a moving glacier. Pressure melting of flowing ice frees drift particles which are plastered on to the subglacial floor. Crushing and abrasion of particles is intense and the till is compact (overconsolidated).

- **Textural**
  Unsorted and unstratified heterogeneous mixture of clay, sand, silt, gravel and boulders; finer sizes comprising the matrix. Stones tend to lodge with their long axis parallel to the direction of flow.

- **Hydrologic**
  Generally well-drained
  Materials tend to have low permeabilities and low moisture contents.

3 **Surficial Materials**
Quaternary—Wisconsinan—Morainal Sediments

Map Unit - Name: *Drumlinized till* Code: 2

Observable photogeologic characteristics

- **Topographic site**
  Broad low relief areas, vicinity Lac Observation and Lac Deporte and on higher ground around eastern lakes.

- **Elevation range (meters)**
  410 - 670

- **Local relief (meters)**
  Streamlined low linear hills, long axes oriented in direction of ice movement.
  Height most common between 15 and 25 m.

Inferred geologic characteristics

- **Genetic**
  Subglacial molding of saturated till originating in same manner as Unit #1.
  Crag and tail symbol is associated with occurrence of a rock boss at upstream end of the unit.

- **Textural**
  Same as for Unit #1. Some higher occurrences may have a bedrock core.

- **Hydrologic**
  Poor internal drainage, but active surface run off.

3 **Surficial Materials**
Quaternary—Wisconsinan—Morainal Sediments

Map Unit - Name: *Ablation till* Code: 3

Observable photogeologic characteristics

- **Topographic site**
  Frequently marginal to re-worked till deposits (Unit 5) and on plateaux often above or near Lodgment till areas.

- **Elevation range (meters)**
  460 - 670

- **Local relief (meters)**
  Chaotic topography of low sharp ridges, hummocks and depressions. Range 5 - 10 m heights.

Inferred geologic characteristics

- **Genetic**
  Subglacial sediments, subglacial in origin, exposed on glacier surface as result of pattern of ice flow. Bodies of ice become buried in sedimentary sequence. Ice bodies subsequently melt down and disturb overlying strata.

- **Textural**
  Loose, non-compact, non-stratified till. Fines are washed away selectively; more granular than Lodgment till.

- **Hydrologic**
  Disordered surface drainage, with many semi-stagnant pools. Internal drainage highly variable, but generally good.

3 **Surficial Materials**
Quaternary—Wisconsinan—Morainal Sediments

Map Unit - Name: *Ribbed moraine* Code: 4

Observable photogeologic characteristics

- **Topographic site**
  In valleys and along valley sides.

- **Elevation range (meters)**
  365 - 580

- **Local relief (meters)**
  To 10 m— succession of discrete irregular to sinuous ridges with rounded crests and generally steep sides. Lie transverse to former local ice flow directions.

Inferred geologic characteristics

- **Genetic**
  Englacially formed by the stacking and piling-up of thick basal debris sequence. The upper surface of the transverse bed obstacle is then smoothed by clean ice moving overhead.

- **Textural**
  Generally bouldery till of the Lodgment type.

- **Hydrologic**
  Similar to drumlinized till, Unit 2.

3 **Surficial Materials**
Quaternary—Wisconsinan—Morainal Sediments

Map Unit - Name: *Reworked till* Code: 5

Observable photogeologic characteristics

- **Topographic site**
  Topographic lows and intermont valleys acting as spillway channels.

- **Elevation range (meters)**
  400 - 640

- **Local relief (meters)**
  Similar to Ablation till—hummocky terrain with local water or organic-filled small depressions.

Inferred geologic characteristics

- **Genetic**
  Lodgment or Ablation till which has been subjected by washing action of channeled or sheet glacial melt water flows.

- **Textural**
  As Lodgment till, but most fine fractions removed leaving coarse sand, gravel, boulders and local boulder "field" concentrations.

- **Hydrologic**
  Generally well-drained.

3 **Surficial Materials**
Quaternary—Wisconsinan—Glaciofluvial Sediments

Map Unit - Name: *Outwash* Code: W

Observable photogeologic characteristics

- **Topographic site**
  Associated with re-worked till areas and other glaciofluvial sediments in topographic lows.

- **Elevation range (meters)**
  400 - 580

- **Local relief (meters)**
  Flat, nearly level surface locally fitted with sharply depressed "kettle holes".

Inferred geologic characteristics

- **Genetic**
  Drift washed out from a glacier by its meltwaters and deposited at and beyond (proglacial) the margin of the glacier.

- **Textural**
  Mainly stratified and well sorted sands and gravels with some local muck-filled lenses.

- **Hydrologic**
  High infiltration of rainfall results in lack of surface drainage. Very good internal drainage, vertically and horizontally.

3 **Surficial Materials**

Quaternary—Wisconsinan—Glaciofluvial Sediments

Map Unit - Name: *Ice-Contact Kame Complex* Code: K

Observable photogeologic characteristics

- **Topographic site**
  In valley at foot of Mont de Babel

- **Elevation range (meters)**
  535 - 560

- **Local relief (meters)**
  Knob and kettle topography, irregular terrain with many slumping features.

Inferred geologic characteristics

- **Genetic**
  Deposited by meltwater flowing between a glacier margin and the nearby valley wall. One side was supported by the ice face. After the ice body melted away this support was removed and the inward side of the deposit slumped.

- **Textural**
  Material often poorly sorted with granulars, silts and some till pockets mixed. Granulars usually dirty. Often slumped, causing abrupt changes in material. Stratification is irregular.

- **Hydrologic**

  Groundwater liable to be varied. but usually good internal drainage.

3 **Surficial Materials**

Quaternary—Wisconsinan—Glaciofluvial Sediments

Map Unit - Name: *Ice-contact Eskers* Code: ~~E~~

Observable photogeologic characteristics

- **Topographic site**

  In valleys and lowlands with reworked till and other glaciofluvial deposits.

- **Elevation range (meters)**

  400 -475

- **Local relief (meters)**

  Elongated, sinuous, continuous and discontinuous ridges with knife-edged crests. Side slopes are at angle of repose (approx 35°) others modified to gentler. Height 20-40M.

Inferred geologic characteristics

- **Genetic**

  Deposited by subglacial meltwater streams material slumped down to angle of repose when supporting ice melted.

- **Textural**

  Irregularly stratified sand and gravel, may grade into silt lenses locally.

- **Hydrologic**

  Good drainage, due to deposit geometry and composition.

3 **Surficial Materials**
Quaternary—Late Wisconsinan

Map Unit - Name: *Lacustrine sediments* Code: LX-LZ

Observable photogeologic characteristics

- **Topographic site**
  On low ground at eastern foot of Mont de Babel. Near reservoir.

- **Elevation range (meters)**
  365-400

- **Local relief (meters)**
  Terrain is smooth and level.

Inferred geologic characteristics

- **Genetic**
  Material deposited from suspension in lakes resulting directly or indirectly from presence of a glacier (ice dam or tilting due to isostatic depression).

- **Textural**
  Stratified, silts, fine sands, some clay moderately to well-sorted.
  Local deposits may not be very thick over till. LX units may be sandier than LZ.

- **Hydrologic**
  Water tables expected to be generally higher than in other deposit types (excepting organic).
  Integrated surface drainage visible.

3 **Surficial Materials**
Quaternary—Holocene

Map Unit - Name: *Organic sediments* Code: N

Observable photogeologic characteristics

- **Topographic site**
  Ubiquitous in poorly or un-drained depressions.

- **Elevation range (meters)**
  390 - 820

- **Local relief (meters)**
  nil

Inferred geologic characteristics

- **Genetic**
  Accumulation of decomposing vegetative matter in anaerobic environment of stagnant drainage site.

- **Textural**
  Typical section might comprise fibrous organic material followed by amorphous organic and soft clayey subsoil or glacial till.

- **Hydrologic**
  Stagnant drainage; water table at or near surface throughout growing season.

3 **Surficial Materials**
Quaternary—Holocene

Map Unit - Name: *Rockslides* **Code: S**

Observable photogeologic characteristics

- **Topographic site**
  At monzonite-latite upslope contact, southeast of Lac Observation.

- **Elevation range (meters)**
  440-670

- **Local relief (meters)**
  230 from unit headwall to downslope toe; displaced mass at base is ridged and hummocky.

Inferred geologic characteristics

- **Genetic**
  Materials deposited downslope by large scale mass movement - rapid movement of detached segments of the bedrock sliding on plane of separation and along downslope surface.

- **Textural**
  Blocks and rubble in finer matrix of crushed rock.

- **Hydrologic**
  Good internal drainage.

3 **Surficial Materials**
Quaternary—Holocene

Map Unit - Name: *Colluvial sediments* **Code: C**

Observable photogeologic characteristics

- **Topographic site**
  Along face and at foot of steep rock slopes or escarpments.

- **Elevation range (meters)**
  365-850

- **Local relief (meters)**
  Mimics slope on which it occurs, or may be local talus cone.

Inferred geologic characteristics

- **Genetic**
  Weathered and disintegrated local bedrock moved downslope by gravity, solifluction or rainwash.

- **Textural**
  Heterogeneous material of all particle sizes but fines probably removed. Can be massive to moderately stratified.

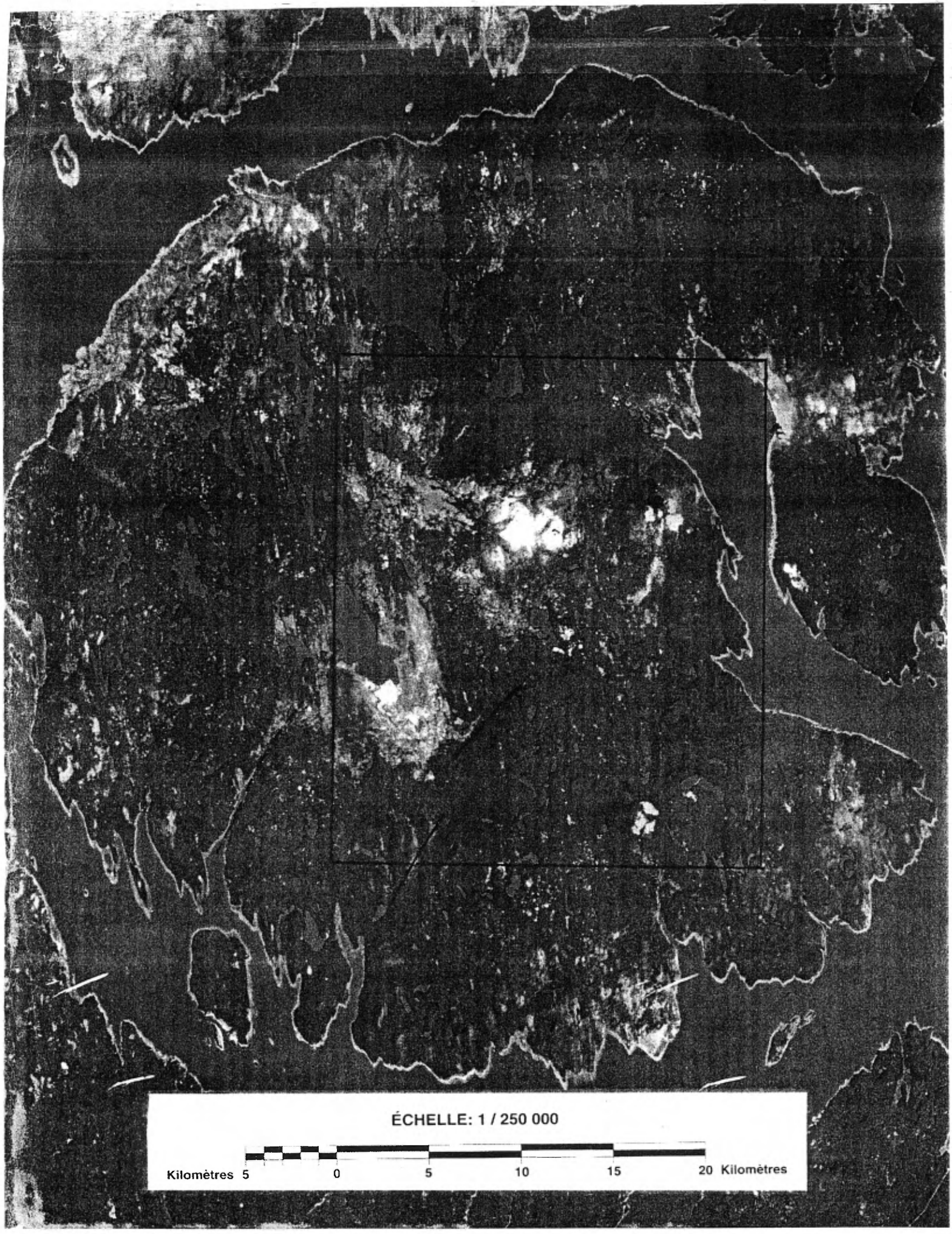
- **Hydrologic**
  Well drained.

4 REFERENCES

- Kish, L. 1968. *Hart-Jaune River area, Saguenay County:* Québec Natural Resources Geological Report 132.

- Klassen, R.A. et al, 1992. *Glacial Landforms & Deposits, Labrador, Newfoundland & Eastern Québec.*. Geological Survey of Canada, Map 1814A, scale 1:1,000,000.

- Murtaugh, J.G. 1976. *Manicougan Impact Structure.* Ministère des Richesses Naturelles, Québec, Report DPV-432.


ÉCHELLE: 1 / 250 000
Kilomètres 5
0
5
10
15
20 Kilomètres